



**HAL**  
open science

# Development of a multiscale composite platform for delivery of natural active compounds: applications of curcumin toward skin

Rosa Calderon-Jacinto

## ► To cite this version:

Rosa Calderon-Jacinto. Development of a multiscale composite platform for delivery of natural active compounds: applications of curcumin toward skin. Cellular Biology. CY Cergy Paris Université, 2022. English. NNT: 2022CYUN1115 . tel-03979549

**HAL Id: tel-03979549**

**<https://theses.hal.science/tel-03979549v1>**

Submitted on 8 Feb 2023

**HAL** is a multi-disciplinary open access archive for the deposit and dissemination of scientific research documents, whether they are published or not. The documents may come from teaching and research institutions in France or abroad, or from public or private research centers.

L'archive ouverte pluridisciplinaire **HAL**, est destinée au dépôt et à la diffusion de documents scientifiques de niveau recherche, publiés ou non, émanant des établissements d'enseignement et de recherche français ou étrangers, des laboratoires publics ou privés.

## Doctoral Thesis

To obtain the title of PhD of the Cergy Paris Université

Speciality: Life and Health Sciences

Doctoral School n° 417, Sciences and Engineering

# Development of a multiscale composite platform for delivery of natural active compounds: applications of curcumin toward skin.

Prepared at the Equipe de Recherche sur les Relations Matrice Extracellulaire-Cellule Laboratory

Presented at Neuville-sur-Oise,

On the 20/06/2022, by:

**Rosa CALDERON-JACINTO**

Jury composed of:

Pr. Catherine LE VISAGE	University of Nantes, France	President of the jury
Pr. Silvia ARPICCO	University of Turin, Italy	Reviewer
Pr. Ana VALLÉS-LLUCH	Universitat Politècnica de València, Spain	Reviewer
Dr. Simona MURA	Université Paris-Saclay, France	Examiner
Pr. Pietro MATRICARDI	Sapienza University of Rome, Italy	Examiner
Dr. Violeta RODRIGUEZ-RUIZ	CY Cergy-Paris Université, France	Supervisor
Pr. Emmanuel PAUTHE	CY Cergy-Paris Université, France	Thesis Director



## **Foreword**

This work was funded by the Ministry of Higher Education and Research, through the Doctoral School n° 417, Sciences and Engineering of CY Cergy-Paris Université. It was carried out through a scientific collaboration between ERRMECe Laboratory (Équipe de Recherche sur les Relations Matrice Extracellulaire-Cellules), CY Cergy-Paris Université, France; the Department of Drug Chemistry and Technologies of Sapienza University of Rome, Italy; and the Cardiovascular Bioengineering Group of the INSERM U1148 - LVTS Laboratory (Laboratory for Vascular Translational Science), Université Sorbonne Paris Nord, France. This collaboration allowed a total of five months of research stay in the Italian Laboratory of Pr. Matricardi (in 2019 and in 2021-2022). In order to recognize the European dimension of this research, this doctoral project aims to be rewarded with the European doctorate label.



## Acknowledgements

Tout d'abord, je tiens à remercier le Ministère de l'Education nationale, de l'Enseignement et de la Recherche Français pour la bourse qui m'a permis d'effectuer cette thèse.

Je remercie également l'ensemble des membres du jury d'avoir accepté d'évaluer ce travail et toutes les discussions qui en ont écoulé. Merci au Pr. Catherine Le Visage pour avoir présidé le jury, thanks to the Pr. Ana Vallès-Lluch and Pr. Silvia Arpico for reviewing my work, to Pr. Pietro Matricardi for evaluating my work, et au Dr. Simona Mura pour avoir examiné ce travail et avoir participé aux comités de suivi de thèse depuis la deuxième année.

Un remerciement spécial pour Emmanuel and Violeta, mes encadrants. Grace à vous deux, chacun avec un style différent, la fille qui a commencé cette thèse n'est pas la même qui a réussi à finir ce manuscrit. Manu, merci pour ta bonne humeur, sincérité et optimisme lors de nos échanges. Que ce soit pour l'avenir du projet ou préparer un orale, discuter avec toi éclairait les idées et calmait l'esprit. Tu as été un exemple de leadership pendant ces années.

Violeta, cela a été une belle expérience d'être ta première thésarde....sur une longue liste, j'en suis sûre. Merci d'avoir forgé mon caractère de chercheuse. Ces années ont compris même une pandémie, mais on a réussi à avancer sur ce projet. Je ne te remercierai jamais assez pour les encouragements dans les moments où j'en avais besoin et pour te soucier non seulement de moi en tant que doctorante, mais aussi en tant que personne. Gracias Violeta. Te echaré de menos.

Pietro, my "Italian" supervisor. Pietro, you have always been there for me despite the distance. Thanks for believing in me since we first met, for all the discussions...even beyond science and for hosting me twice during my PhD at your lab in Rome. Five and a half months where I had the chance to meet great people, feel part of your research group and learn a lot! (science and Italian). Your excellent science is only a reflection of the excellent person you are. Grazie per tutti!

Graciela et Virginie, j'aurais voulu partager de plus près la recherche avec vous. Mais cela a été un énorme plaisir d'avoir collaboré avec vous. Malgré la distance, j'ai apprécié vos conseils, vos suggestions, vos critiques et toute votre aide. Vous êtes des exemples des chercheuses.

A Véronique Rosilio et Florence Agnely, responsables du master Pharmacotechnie et Biopharmacie de l'Université Paris-Saclay. Je ne vous remercierai jamais assez de m'avoir soutenue lors de ma candidature à la bourse qui m'a permis de venir en France faire mes études de master dans un premier temps. Sachez que les connaissances que j'ai pu acquérir pendant les deux années de master ont été clés pour la réalisation de cette thèse.

To Ana Isabel Torres-Suárez, researcher at the Department of Pharmaceutics and Food Technology- Faculty of Pharmacy at Complutense University of Madrid, for initiating me in the world of drug delivery. Thanks for giving the chance to a third-year pharmacy student to make an internship in your lab and start her desire to know more about nanoparticles. You opened my mind to a research field that was far from me in Peru. Gracias por ello.

Aux membres du « grand » bureaux des doctorants/post-docs, avec qui 18h était l'heure de «décompresser » tout l'stress de la journée: Maxime, Solène, Anamar, Carla, Phoung Anh et Chahrazed. Merci pour tous ces fous rires, les pauses midi et les moments passés au tour d'une raclette, un verre ou encore un Dixit!. Maxime et Solène, que des beaux souvenirs avec vous en congrès, au labo et en soirée! Les photos et vidéos en témoignent. Merci de votre accueil quand je venais toute juste d'arriver à Cergy. En trois années et quelque...on a transformé le bureau ! Chahrazed, merci pour les discussions sur la culture cellulaire et surtout pour tes mots d'encouragement !

Aux autres doctorants du labo : Audrey, Mathilde, Sahil, Amel pour la bonne humeur dans les couloirs...ou le sas de la salle de culture cellulaire. Du même aux « anciennes » doctorantes du labo : Amel H et Carine. Merci de votre accueil dès mon arrivée à ERRMECe. Amel H, « la boss » merci pour ton soutien pendant cette dernière ligne droite. Parler avec toi fait toujours bien au cœur!

Carla, merci de ton amitié dès que j'étais stagiaire à Lille et ton soutien dans et dehors le laboratoire. Tu sola presencia en el laboratorio hizo más llevaderos los momentos más difíciles de este doctorado, incluyendo la pandemia. Espero podamos seguir riéndonos, aunque a veces nadie entienda nuestro humor peruano. Merci Carlita!

Aux autres membres de l'équipe Biosan...Adeline, cela a été un plaisir travailler avec toi pendant les cours d'enzymologie auxquels j'ai eu l'occasion de participer pendant ma première année. Michel, merci de ta bonne humeur au labo. Échanger avec toi éclairait mes démarches scientifiques et apaisait l'esprit.

Damien, merci de ta bonne humeur. On pouvait avoir une mauvaise journée, mais tes blagues aidaient à mieux tenir pendant les pires moments de stress.

Agnès, même si on s'est rapprochées qu'à la fin de ma thèse, merci de ton sourire ! J'ai hâte de connaître tes aventures avec les phages et les NLCs!

Rémy et Lamia, merci pour être toujours présents quand j'avais besoin. Vous êtes une partie clé du fonctionnement du laboratoire. Isabelle, merci pour toutes les démarches que tu as fait pour mes séjours en Italie. Que ce soit des choses administratives ou même l'envoi de mes produits.

Johanne, Sabrina, Cédric, Franck et Gilles, on se croissait de temps en temps, mais vous avez été toujours gentils et prêts à échanger pendant les animations scientifiques du laboratoire.

Un grand merci à Severine Alfonsi, ingénieur d'études au LPPI, merci d'avoir été toujours disponible pour me réserver des créneaux pour utiliser la DLS.

Du même à Ana-Andreea Arteni, ingénieur de recherche de la plateforme Cryo-EM de I2BC, pour ses explications et son aide lors des analyses TEM.

A mis padres, Armida y Edwin. Gracias por el apoyo y los sacrificios que hicieron para que yo pueda seguir todo este camino. Me hicieron falta estos años, pero gracias por estar ahí siempre que los necesitaba. Gracias mami por haber hecho el esfuerzo de venir y darme la tranquilidad que necesitaba en la recta final de la redacción. Papi, ya nos tocará disfrutar en Europa.

A mis hermanos, José, Rubí y Francisco, por ser mi fuente de motivación, mi inspiración de esfuerzo y porque ustedes pueden alegrarme los días, aunque sea a distancia. Los quiero.

A Angela, mi mejor amiga, porque a pesar del océano que tenemos de por medio, tus palabras de ánimo me ayudan muchísimo.

Et finalement, merci William, pour ta présence à mes côtés dans les bons et les « moins bons » moments ainsi que pour ta compréhension pendant la dernière ligne droite de ce travail de thèse.





# Table of Contents

<b>List of Figures</b> .....	<b>V</b>
<b>List of Tables</b> .....	<b>IX</b>
<b>Abbreviations</b> .....	<b>XI</b>
<b>Abstract</b> .....	<b>XV</b>
<b>General Introduction and Objectives</b> .....	<b>1</b>
<b>Chapter 1: State of art</b> .....	<b>5</b>
1.1.Skin and physio-pathological skin conditions.....	7
1.1.1.Structure and physiology of the skin .....	7
1.1.1.1.Structure.....	7
1.1.1.2.Functions of the skin .....	9
1.1.2.Inflammatory physio-pathological skin conditions .....	10
1.1.2.1.Acute wounds .....	10
1.1.2.2.Chronic wounds .....	11
1.1.2.3.Hypertrophic scars and keloids .....	12
1.1.2.4.Psoriasis.....	14
1.1.2.5.Atopic dermatitis .....	15
1.1.3.Skin mechanisms to fight ROS and inflammation .....	15
1.1.3.1.Sources of ROS and inflammation.....	16
1.1.3.2.Detoxification mechanisms .....	18
1.2.Topical drug delivery to the skin .....	18
1.2.1.Skin drug-delivery: biopharmaceutical aspects .....	18
1.2.1.1.Passive diffusion: Fick's 1 <sup>st</sup> Law .....	20
1.2.1.2.The partition coefficient.....	21
1.2.1.3.Permeability coefficient.....	21
1.2.2.Formulation technologies for skin delivery .....	22
1.2.2.1.Common pharmaceutical forms .....	22
1.2.2.2.Physical and chemical enhancement techniques .....	23
1.3.Natural compounds to fight ROS and inflammation.....	24
1.3.1.Curcumin .....	25
1.3.1.1.Sources .....	25
1.3.1.2.Uses.....	26
1.3.1.3.Physico-chemical properties .....	26
1.3.1.4.Interaction with cells .....	31
1.3.1.5.Potential in inflammatory skin disorders .....	33
1.4.Combining formulation technologies for curcumin delivery to the skin.....	39
1.4.1.Lipid nanocarriers.....	39

1.4.1.1.Nanostructured Lipid Carriers (NLCs).....	41
1.4.2.Hydrogels.....	53
1.4.2.1.Hydrogels as topical therapeutic materials.....	54
1.4.2.2.Hydrogels in pharmaceutical and cosmetic formulations.....	57
<b>Chapter 2: Materials and Methods .....</b>	<b>69</b>
1.1.CUR-NLCs/gel components.....	71
1.1.1.Excipients.....	71
1.1.1.1.The solid lipid: Precirol ®ATO 5.....	71
1.1.1.2.The oil: Labrafac ® lipophile WL 1349.....	71
1.1.1.3.The surfactant: Poloxamer 407.....	72
1.1.1.4.The co-surfactant: Tween® 80.....	72
1.1.1.5.The hydrogel matrix polymer: Carbopol ® 980.....	73
1.1.1.6.The neutralizing agent: TEA.....	73
1.1.2.The active ingredient: curcumin.....	74
1.2.Formulation procedures.....	75
1.2.1.CUR-NLCs formulation development.....	75
1.2.1.1.General Hot Homogenization Method procedure.....	75
1.2.1.2.Change of method parameters in general procedure.....	75
1.2.1.3.Change of formulation parameters in general procedure.....	76
1.2.1.4.Optimized preparation protocol for CUR-NLCs/gel.....	77
1.2.1.5.Purification by SEC.....	78
1.2.2.CUR-NLCs/gel formulation development.....	79
1.2.2.1.Choice of CUR-NLCs incorporation and neutralization procedure.....	79
1.2.2.2.Optimized preparation protocol for CUR-NLCs/gel.....	80
1.3.Physico-chemical characterization of CUR-NLCs.....	81
1.3.1.Particle size and zeta-potential.....	81
1.3.2.Morphology.....	82
1.3.2.1.Negative Staining-Transmission Electron Microscopy (Negative staining-TEM).....	82
1.3.2.2.Cryo-Transmission Electron Microscopy (Cryo-TEM).....	82
1.3.3.Mass quantification.....	83
1.3.4.Entrapment efficiency.....	83
1.3.4.1.Direct Method.....	84
1.3.4.2.Indirect Method.....	84
1.3.5.Antioxidant activity: ABTS assay.....	85
1.3.6.Stability at different pH.....	87
1.3.7 Freeze-drying.....	87
1.3.8.CUR release in different biological media.....	88
1.3.9.Permeation and penetration studies on Strat-M ® membrane.....	89
1.3.9.1.Permeation studies on Strat-M ® membrane.....	90

1.3.9.2. Penetration studies on Strat-M ® membrane .....	90
1.4. Physico-chemical characterization of CUR-NLCs/gel .....	91
1.4.1. Swelling properties of the Carbopol ® matrix .....	91
1.4.2. Rheological characterization .....	91
1.4.3. Penetration studies on Strat-M ® membrane .....	92
1.5. Biological tests for CUR-NLCs .....	93
1.5.1. Studied cell lines .....	93
1.5.1.1. BJ-Fibroblasts .....	93
1.5.1.2. HEK293T .....	93
1.5.1.3. Biological reagents .....	93
1.5.1.4. Preparation of CUR and NLCs samples for biological tests .....	94
1.5.2. Cytotoxicity studies .....	94
1.5.2.1. MTT .....	94
1.5.2.2. Trypan Blue .....	95
1.5.3. Curcumin uptake preliminary studies .....	96
1.5.4. Migration/proliferation test .....	97
1.5.5. Establishment of an oxidative-stress model .....	98
1.5.5.1. Metabolic activity of cells exposed to oxidative-stress inducer: Luperox ® .....	98
1.5.5.2. ROS detection for oxidative stress verification .....	98
1.5.6. Effect of NLCs on BJ-Fibroblasts under oxidative stress .....	99
1.6. Supporting information .....	100
<b>Chapter 3: Development of CUR-NLCs .....</b>	<b>101</b>
1.1. Introduction .....	103
1.2. Results and discussion .....	103
1.2.1. Optimization of CUR-NLCs preparation .....	103
1.2.1.1. Impact of changing method parameters .....	103
1.2.1.2. Impact of changing formulation parameters .....	105
1.2.1.3. Impact of the loading technique .....	108
1.2.2. CUR-NLCs physico-chemical characterization .....	110
1.2.2.1. Drug loading and Entrapment efficiency .....	110
1.2.2.2. Particle size and zeta-potential .....	113
1.2.2.3. NLCs purification by permeation through SEC column: impact on particle size and zeta potential .....	115
1.2.2.4. Morphology .....	119
1.2.2.5. Antioxidant activity .....	122
1.2.2.6. Behaviour at different pH .....	126
1.2.2.7. Impact of freeze-drying on NLCs size distribution .....	129
1.2.2.8. CUR release in different biological media .....	131
1.2.3. CUR-NLCs biological characterization .....	132

1.2.3.1.Cytotoxicity studies.....	132
1.2.3.2.Curcumin uptake: preliminary studies.....	137
1.3.Supporting information.....	142
1.4.Conclusions .....	144
<b>Chapter 4: Potential of CUR-NLCs and CUR-NLCs/gel delivery systems for topical applications ....</b>	<b>145</b>
1.1.Introduction .....	147
1.2.Results and discussion .....	147
1.2.1.Effects of CUR-NLCs on dermal cells.....	147
1.2.1.1.Impact of CUR-NLCs on the migration/proliferation of healthy cells .....	147
1.2.1.2.Development of a model of oxidatively stressed cells .....	153
1.2.1.3.Impact of CUR-NLCs on the viability of oxidatively stressed cells.....	157
1.2.2.Incorporation of CUR-NLCs into a carbopol hydrogel matrix.....	159
1.2.2.1.Impact of neutralizing agent in the formulation of CUR-NLCs/gel.....	159
1.2.2.2.Swelling properties of Carbopol® 980 hydrogel .....	161
1.2.2.3.Rheological characterization of CUR-NLCs/gel.....	163
1.2.2.4.Permeation and penetration studies of CUR-NLCs and CUR-NLCs/gel.....	168
1.3.Supporting information.....	172
1.4.Conclusions .....	172
<b>Chapter 5: Conclusions and perspectives .....</b>	<b>173</b>
<b>References .....</b>	<b>179</b>
<b>List of communications and publications.....</b>	<b>205</b>

## List of Figures

---

Figure 1.- Schematic representation of the developed hydrogel containing curcumin-loaded NLCs (CUR-NLCs/gel).....	2
Figure 2.- Schematic representation of main skin layers and skin appendages.....	7
Figure 3.- Principal components of the Epidermis and Dermis.....	9
Figure 4.- Wound healing process in acute wounds.....	10
Figure 5.- Pathological skin conditions examples.....	13
Figure 6.- Psoriatic lesions.....	14
Figure 7.- Atopic dermatitis to isothiazolinones lesions.....	15
Figure 8.- Drug transport across skin layers.....	19
Figure 9.- Cellular permeation routes across the SC.....	20
Figure 10.- Curcumin obtention from <i>Curcuma longa</i> L.....	25
Figure 11.- Chemical structure of the main curcuminoids.....	27
Figure 12.- Keto-enol equilibrium, deprotonation and degradation of Curcumin in aqueous media.....	28
Figure 13.- pH dependent changes of curcumin in aqueous solutions.....	29
Figure 14.- Tautomerism keto-enol of curcumin.....	30
Figure 15.- Probable sites for free radical reaction with curcumin in its two tautomeric forms.....	31
Figure 16.- Different type of NLCs according to the state of the lipidic matrix.....	42
Figure 17.- Drug distribution on the lipidic matrix of NLCs.....	42
Figure 18.- High energy approaches for NLCs preparation.....	44
Figure 19.- Equipment used for size reduction during Hot-Homogenization.....	45
Figure 20.- Low energy approaches for NLCs preparation.....	47
Figure 21.- General structures of the network in (A) a physical gel and (B) a chemical gel.....	54
Figure 22.- Delivery mechanisms in hydrogels.....	56
Figure 23.- General composition of carbomers.....	60
Figure 24.- Images of Carbopol® 934 and Carbopol® 974 particles in their dry state.....	62
Figure 25.- Optical microscopy images of the progressive hydration of Carbopol® Ultrez 30 particles in aqueous media.....	62
Figure 26.- Formation of a carbomer gel.....	63
Figure 27.- Carbomer gel formation by hydrogen bonding.....	64
Figure 28.- Hydrogels with same viscosity and different yield value.....	65
Figure 29.- Effect of crosslinking on the suspending properties of carbomer (Carbopol ®) gels.....	66
Figure 30.- Flow properties of neutralized carbomer polymer dispersions.....	66
Figure 31.- Graphical representation of macroviscosities and microviscosities in a carbomer gel.....	67
Figure 32.- Chemical structure of the major component in Precirol ® ATO 5.....	71
Figure 33.- Chemical structure of the major component in Labrafac ® Lipophile WL 1349.....	72
Figure 34.- Chemical structure of Poloxamer 407 <sup>83</sup> .....	72
Figure 35.- Chemical structure of Tween® 80.....	72
Figure 36.- Schematic representation of Carbopol ® 980 structure.....	73
Figure 37.- Structure and dissociation of TEA.....	74
Figure 38.- Chemical structure of the three curcuminoids present in CUR.....	74
Figure 39. NLCs general preparation by the Hot Homogenization Method.....	75
Figure 40.- Optimized preparation of CUR-NLCs.....	78
Figure 41.- Diagram of the purification process of NLCs by SEC.....	79
Figure 42.- Diagram showing the optimized preparation protocol for gel, CUR-NLCs/gel and Blank-NLCs/gel.....	80
Figure 43.- Model of the electric double layer (EDL) around a particle during a ZP measurement.....	81
Figure 44.- Diagram showing the general steps in the quantification of loaded-CUR in CUR-NLCs by the	

direct method and the indirect method.....	83
Figure 45.- ABTS Assay for determination of antioxidant activity.....	87
Figure 46.- Diagram showing the method for the assessment of CUR release from CUR-NLCs.....	89
Figure 47.- Permeation and penetration studies on Strat-M® membrane.....	89
Figure 48.- Transformation of MTT to a formazan product in viable cells. ....	94
Figure 49.- Diagram showing the main steps in MTT test.....	95
Figure 50.-Diagram showing the main steps in the migration/proliferation test.....	98
Figure 51.- Use of fluorogenic probe DCFH-DA for ROS detection.....	99
Figure 52.- In vitro model for ROS generation and confirmation.....	99
Figure 53.- In vitro model for the evaluation of of the effect of NLCs on BJ-Fibroblasts metabolic activity after undergoing oxidative stress.....	100
Figure 53.- Size distribution (expressed in % intensity) of NLCs prepared by the Hot Homogenization Method at different temperatures and times of homogenization.....	105
Figure 54.- Size distribution (expressed in % intensity) of NLCs prepared by the Hot Homogenization Method at different temperatures and times of homogenization.....	106
Figure 55.-Thermograms of lipids used for NLCs preparation.....	108
Figure 56.- Determination of CUR solubility in four different oils.....	109
Figure 57.- Obtained calibration curves for curcumin determination by Direct Method and Indirect Method.....	111
Figure 58.- Variation of the amount of curcumin loaded into CUR-NLCs over 45 days after preparation.....	112
Figure 59.- Aspect and particle size of Blank-NLCs and CUR-NLCs at day 1 after preparation.....	113
Figure 60.-Particle size and zeta potential of Blank-NLCs and CUR-NLCs over 45 days after preparation.....	114
Figure 61.- NLCs separation using SEC column (Bio-Gel P10).....	117
Figure 62.- Aspect and particle size of pooled fractions 3-5 of Blank-NLCs and CUR-NLCs after permeation through SEC column.....	118
Figure 63.- Morphological characterization of Blank-NLCs and CUR-NLCs suspensions before passing through the SEC column.....	121
Figure 64.- Morphological characterization of Blank-NLCs and CUR-NLCs suspensions after passing through the SEC column.....	122
Figure 65.- Inhibition of ABTS <sup>+</sup> in NLCs formulations and no entrapped antioxidant compounds.....	124
Figure 66.- pH variation for Blank-NLCs and CUR-NLCs suspensions over 45 days after preparation.....	127
Figure 67.- Blank-NLCs and CUR-NLCs stability at different pH.....	128
Figure 68.- CUR release from CUR-NLCs in different biological media.....	132
Figure 69.- Cell viability assays on BJ-Fibroblasts in basal conditions after 24h treatment with CUR, CUR-NLCs or Blank-NLCs.....	133
Figure 70.- Phase contrast images of BJ-Fibroblasts after 24h treatment with DMEM 10%FBS, Control; CUR at 20 µM; Blank-NLCs at 1.1 g/L or CUR-NLCs at 1.10 g/L containing 20 µM of Loaded CUR.....	134
Figure 71.-MTT assay on BJ-Fibroblasts after 24h treatment with CUR (20 µM), CUR-NLCs (20 µM of CUR entrapped in 1.10 g/L CUR-NLCs) or Blank-NLCs + CUR (1.10 g/L Blank-NLCs added to 20 µM of CUR non entrapped).....	135
Figure 72.- Cell viability assays on HEKn in basal conditions after 24h treatment with CUR, CUR-NLCs or Blank-NLCs.....	135
Figure 73.- Phase contrast images of HEKn after 24h treatment with DMEM 10%FBS, Control; CUR at 20µM; Blank-NLCs at 1.1 g/L or CUR-NLCs at 1.10 g/L containing 20µM of Loaded CUR.....	136
Figure 74.- Impact of CUR-NLCs on HaCaT keratinocytes.....	139
Figure 75.- Curcumin (C) determination by UPLC-DAD/MS.....	140
Figure 76.- Chromatogram for the sample.....	141
Figure 77.-Reduction in the gap area during the migration/proliferation essay.....	149
Figure 78.-Phase-contrast images of the gap during the migration/proliferation assay on BJ-Fibroblasts.....	150
Figure 79.- Phase-contrast images of the gap during the migration/proliferation assay on HEKn.....	151

Figure 80.- Phase contrast images of BJ Fibroblasts and HEK293 cells after treatment with different Luperon concentrations and subsequently incubation with MTT.....	155
Figure 81.-Evaluation of oxidative stress induced by different concentrations of Luperon on BJ-Fibroblasts. ....	156
Figure 82.-Effect of NLCs on BJ-Fibroblasts under oxidative stress. ....	158
Figure 83.- Impact of the addition step of CUR-NLCs and employed neutralizing agent into the final appearance of CUR-NLCs/gel.....	160
Figure 84.- Aspect of Gel, Blank-NLCs/gel and CUR-NLCs/gel. ....	161
Figure 85.-Swelling and deconstruction behaviour of Carbopol ® 980 NF 0.5 % w/v unloaded gel in water and in PBS. ....	162
Figure 86.- Strain ( $\gamma$ ) sweep for Carbopol ® 980 NF 0.5% w/v unloaded and loaded gels. ....	164
Figure 87 .- Frequency sweep for Carbopol ® 980 NF 0.5% w/v unloaded and loaded gels.....	164
Figure 88.- Flow curves for Carbopol ® 980 NF 0.5% w/v unloaded and loaded gels.....	165
Figure 89.- Evaluation of time dependent flow behavior (Recovery Test) for Carbopol ® 980 NF 0.5% w/v unloaded and loaded gels.....	166
Figure 90.- CUR-NLCs permeation through Strat-M ® membrane .....	168
Figure 91.- CUR penetration studies into Strat-M ® membrane .....	169





## List of Tables

---

Table 1.- ROS free radicals and non-radicals.....	16
Table 2.-Examples of some jellifying agents according to their origin. ....	23
Table 3.- Physico-chemical characteristics of curcuminoids.....	27
Table 4.- Observed and excluded intracellular localization of native curcumin (non-entrapped curcumin) reported in previous studies.....	32
Table 5.- Examples of studies assessing the curcumin potential in cases of acute and abnormal wound-healing.....	34
Table 6.- Examples of studies assessing the curcumin potential in psoriasis topical treatment.....	36
Table 7.- Examples of studies assessing the curcumin potential in dermatitis topical treatment.....	38
Table 8.- Most common excipients used in the formulation of NLCs .....	50
Table 9.- NLCs systems formulated for CUR entrapment and delivery to the skin .....	51
Table 10.- Thickening/gelling agents for the formulation of fluid gels in pharmaceutical and cosmetic formulations.....	58
Table 11.- Carbomer types according to the composition of polymer chains and cross-linker used between them.....	61
Table 12.- Recommended substitutes for benzene grade carbomers based on viscosity criteria.....	61
Table 13.-Size distribution parameters and pH of NLCs prepared by the Hot Homogenization Method at different temperatures and times of homogenization. ....	105
Table 14.- Size distribution parameters of NLCs prepared by the Hot Homogenization Method by varying the solid lipid/oil ratio (% w/w). ....	107
Table 15.- Size distribution parameters of NLCs prepared by the Hot Homogenization Method, using 3 different oils. ....	107
Table 16.- Thermal properties of precirol and its mixtures with Sunflower oil and Labrafac at solid lipid:oil ratio 82:18 % w:w. ....	108
Table 17.-Amount of CUR entrapped in NLCs by employing different techniques .....	109
Table 18.- Curcumin loading into NLCs before passing through SEC column .....	112
Table 19.- Sizes, PDI and Zeta Potential of CUR- and Blank-NLCs before and after permeation through SEC column .....	119
Table 20.- Antioxidant activity measured by lipophilic ABTS assay.....	124
Table 21.- Size distribution (% intensity) of Blank-NLCs and CUR-NLCs before and after freeze-drying and using different cryoprotectants.....	130
Table 22.- Metabolic activity of BJ-Fibroblasts and HEK293 after 1h exposition to stressor (Luperox). (n=2). .....	154
Table 23.- Amount entrapped of CUR per unit area ( $D_e$ ) and accumulation ( $A_c$ ) on Strat-M <sup>®</sup> membranes. .....	169



## Abbreviations

---

% DL	: Drug loading
% EE	: Encapsulation efficiency
A.U.	: Arbitrary units
ABTS	: 2,2'-Azino-bis (3-ethylbenzothiazoline-6-sulfonic acid) diammonium salt
$A_c$	: accumulation
ACN	: Acetonitrile
ADP	: Adenosine diphosphate
ARE	: Antioxidant response element
ATCC	: American Type Culture Collection
ATP	: Adenosine triphosphate
BBB	: Blood-brain barrier
BDMC	: Bisdemethoxycurcumin
C	: Curcumin
C10	: Capric acid
C16	: Palmitic acid
C18	: Stearic acid
C8	: Caprylic acid
CI	: Crystallinity index
cmc	: Critical micelle concentration
COX	: Cyclooxygenase
cP	: Centipoise
Cryo-TEM	: Cryo-Transmission Electron Microscopy
CUR	: Total of curcuminoids (C + DMC + BDMC)
CXCR3	: C-X-C Motif Chemokine Receptor 3
DAD	: diode array detector
DBM	: Dermal basal medium
DCM	: Dichloromethane
$D_e$	: drug entrapped per unit area
Dh	: Hydrodynamic diameter
DLS	: Dynamic Light Scattering
DMC	: Demethoxycurcumin
DMEM	: Dulbecco's Modified Eagle Medium
DNCB	: Dinitrochlorobenzene
Dt	: Diffusion coefficient
e-	: Electrons
e.g.	: example given
ECM	: Extracellular matrix
EMA	: European Medicines Agency
EP	: European Pharmacopoeia
ER	: Endoplasmic reticulum
ET	: Electron transfer
EtOH	: Ethanol
EU	: European Union

FACS	: Fluorescence Activated Cell Sorting
FBS	: Foetal bovine serum
FDA	: Food and Drug Administration
GMS	: Gatan Microscopy Suite
GPx	: Glutathione peroxidase
GSH	: Glutathione
GSR	: Glutathione reductase
GSSG	: Oxidized glutathione
HAT	: Hydrogen atom transfer
HEK <sub>n</sub>	: Human Epidermal Keratinocytes neonatal
HLB	: Hydrophilic–lipophilic balance
HPLC	: high pressure liquid chromatography
IFN- $\gamma$	: Interferon gamma
Ig	: Immunoglobulin
IL-1	: Interleukin-1
IMQ	: Imiquimod
INCI	: International Nomenclature of Cosmetic Ingredients
INCI	: International Nomenclature of Cosmetic Ingredients
K <sub>2</sub> S <sub>2</sub> O <sub>8</sub>	: Potassium Persulfate
kcps	: Kilocounts per second
Keap1	: Kelch-like ECH-associated protein 1
LDCs	: Lipid-drug conjugates
LNP	: Lipid nanoparticle
LOX	: Lipoxygenase
LVE	: Linear Viscoelastic Region
MEs	: Microemulsions
MPEG-PCL	: Methoxy poly(ethylene glycol)-block-poly ( $\epsilon$ -caprolactone)
MS	: mass spectrometry
MTT	: Methylthiazolyldiphenyl-tetrazolium bromide
$\eta$	: Viscosity
NEs	: Nanoemulsions
NF- $\kappa$ B	: Nuclear factor kappa B
NLCs	: Nanostructured Lipid Carriers
NOX	: NADPH Oxidases
NPs	: Nanoparticles
Nrf2	: Nuclear factor erythroid 2-related factor 2
O/W	: Oil in water
PBS	: Phosphate buffered saline
PEG	: Polyethylene glycol
PIT	: Phase inversion temperature
pKa	: Acidic dissociation constant
PLGA	: Poly(lactic-co-glycolic acid)
PVA	: Polyvinyl alcohol
px	: Pixel
Ref.	: Reference
Rh	: Hydrodynamic radius
ROS	: Reactive oxygen species
RT	: Room temperature

s	: Second
SC	: <i>stratum corneum</i>
SEC	: Size exclusion chromatography
SLNs	: Solid Lipid Nanoparticles
SOD	: Superoxide dismutases
TEA	: Triethanolamine
TEM	: Transmission Electron Microscopy
TEWL	: Transepidermal water loss
TFA	: Trifluoroacetic acid
TGF- $\beta$	: Transforming Growth Factor $\beta$
TNCB	: Trinitrochlorobenzene
TNF	: Tumour necrosis factor
TNF- $\alpha$	: Tumour necrosis factor alpha
TPA	: Tetradecanoylphorbol acetate
UPLC	: ultra performance liquid chromatography
UPLC-MS/DAD	: ultra performance liquid chromatography coupled to a diode array detector and a mass spectrometry detector
USP	: United States Pharmacopoeia
UVA	: Ultraviolet A
VEGF	: Vascular Endothelial Growth Factor
W/O	: Water in oil
W/O/W	: Water in oil in water
XDR	: X-ray Diffraction
ZP	: Zeta potential
$\alpha$ -CD	: Alpha cyclodextrin
$\lambda_{\max}$	: Wavelength of maximal absorption



## Abstract

---

From acute wounds to diseases -such as psoriasis or dermatitis- skin is submitted to numerous biological and physio-pathological situations where prooxidant and antioxidant reactions must be finely controlled. Particularly, the excess of reactive oxygen species (ROS), which is often related to inflammatory processes. Natural exogenous antioxidant molecules -like curcumin- represent pertinent candidates to favour this prooxidant-antioxidant balance; especially due to their capacity to control the toxicity of radicals and to activate cytoprotective signalling pathways in dermal cells.

However, due to their hydrophobic nature, the formulation of such compounds remains a challenge. It is thus necessary, especially with curcumin, to develop strategies able to deliver it at the site of action, while preserving its antioxidant properties and with adjustment of its capacity of penetration into the dermis through an appropriate application to the skin surface.

The overall objective of this work was on one hand, to develop a multiscale composite delivery platform, based on a hydrogel matrix containing a curcumin-loaded nanoparticulated reservoir, On the other hand, to evaluate it in order to explore its potential for topical dermal uses.

First, this work has been focused on the design, preparation, as well as physico-chemical and biological characterization of curcumin-loaded Nanostructured Lipid Carriers (CUR-NLCs). Second, the incorporation of these curcumin reservoirs in a carbomer hydrogel have been studied. The applicability for a topical dermal use was studied at the cell level by assessing CUR-NLCs impact on migration/proliferation as well as their influence in cells undergoing oxidative stress. Moreover, CUR-NLCs incorporated in the hydrogel (CUR-NLCs/gel) were evaluated in terms of their ability to control curcumin penetration into synthetic membranes mimicking the human skin.

The main results show that it is possible to obtain, with an encapsulation efficiency of 85%, stable and reproducible NLCs formulation mostly composed of negatively charged nanoparticles of two size populations (P1, 70-85 nm and P2, 280-360 nm). These NLCs are able to preserve curcumin antioxidant properties. The developed carriers were found to reduce the proliferation/migration of both human fibroblasts and keratinocytes cells *in vitro*. Moreover, they did not affect their metabolic activity even when assessed in an *in vitro* oxidative stress model (for CUR concentrations up to 10  $\mu$ M). CUR-NLCs are less likely to cross synthetic membranes mimicking intact human skin, but they could contribute to curcumin accumulation into them. This effect is modulated by their incorporation into the hydrogel.

These results showed the feasibility of using CUR-NLCs/gel as a platform for curcumin delivery to the skin. The fact that CUR-NLCs do not affect cellular viability ( $[CUR] \leq 10 \mu M$ ), even during oxidative stress conditions, makes them good candidates for the development of topical treatments where protection from oxidative stress and a controlled cell migration are needed without compromising metabolic activity.

Keywords: antioxidants, curcumin, lipid nanoparticles, topical dermal drug delivery, oxidative stress





## General Introduction and Objectives

---

Skin is the largest organ in the body, with the main function to act as a barrier (physical and immune) for external aggressions. Its structure and function can be disrupted or altered in numerous biological situations like wounds and skin diseases: psoriasis, dermatitis, hypertrophic scars and keloids. In all of them **physio-pathological conditions origin from prolonged inflammatory processes and/or oxidative stress**. The consequences can impact not only the physiological, but also the psychological and social aspects of patients' life <sup>1</sup>. As result, skin diseases are considered as the fourth leading cause of non-fatal morbidity worldwide <sup>2,3</sup> affecting both, high and low income countries<sup>4</sup>.

Psoriasis and dermatitis are mainly uncontrolled inflammatory conditions. In **psoriasis, the main problem is the excessive proliferation of keratinocytes provoked by IFN- $\gamma$ , TNF- $\alpha$  and IL production** by lymphocytes. For **dermatitis, lesions are caused due to excessive IgE production after exposition to irritants or allergens**. During wound-healing, skin diseases can appear in two main cases. In one side, **chronic wounds can appear due to ROS excess during an uncontrolled inflammation phase**. In the other side, **keloids and hypertrophic scars appear due to uncontrolled migration and proliferation of dermal cells during the proliferation phase**, leading to the formation of granulation tissue in excess which is not able to disappear during the remodelling phase.

In chronic wounds as well as in keloids and hypertrophic scars, restoration of the structure and function of skin is hindered.

Treatments for these conditions tend to be expensive and long. However, by re-establishing the pro-oxidant /antioxidant balance which is often related to inflammatory processes, the evolution of these skin conditions can be improved. In this context, natural exogenous compounds appear as promising candidates to be used as adjuvant therapy. **Curcumin** is a polyphenol extracted from the rhizomes of *Curcuma longa*. It has demonstrated **capacity to both control the toxicity of radicals** (through electron or hydrogen transfer) and to **activate cytoprotective pathways in dermal cells**, (mainly through the activation of the Nrf2/ARE signalling pathway). Moreover, it has shown **ability to inhibit NF- $\kappa$ B, downregulate pro-inflammatory cytokines (as TNF- $\alpha$ ) and inhibit the activation of immunoglobulins (as IgE)**.

However, curcumin formulation remains a challenge due to its physico-chemical properties, in particular its hydrophobicity. Thus, there is a need to develop formulation strategies able to ensure the delivery of curcumin to the site of action through an efficient application on skin surface and tuning of its penetration,

while preserving its antioxidant properties.

Classical formulations such as ointments, creams and gels can be used to formulate curcumin for topical applications, yet they do not allow to have a moisturizing effect, promote adherence to the skin and have a good penetration of the active ingredient, all at the same time. Such properties are important, not only to allow the delivery of the active ingredient to its site of action, but also so that skin could regain its physical properties. Face to this, innovative drug delivery systems offer the possibility to formulate composite platforms, in order to obtain for example in one formulation: possibility of high penetration of the active, good moisturizing properties and preservation of its antioxidant properties.

Is in this context that works in this thesis were performed. The main objective of this work was to **develop a multiscale composite platform based on a hydrogel containing curcumin-loaded NLCs (CUR-NLCs) and to explore its potential in topical dermal applications.**

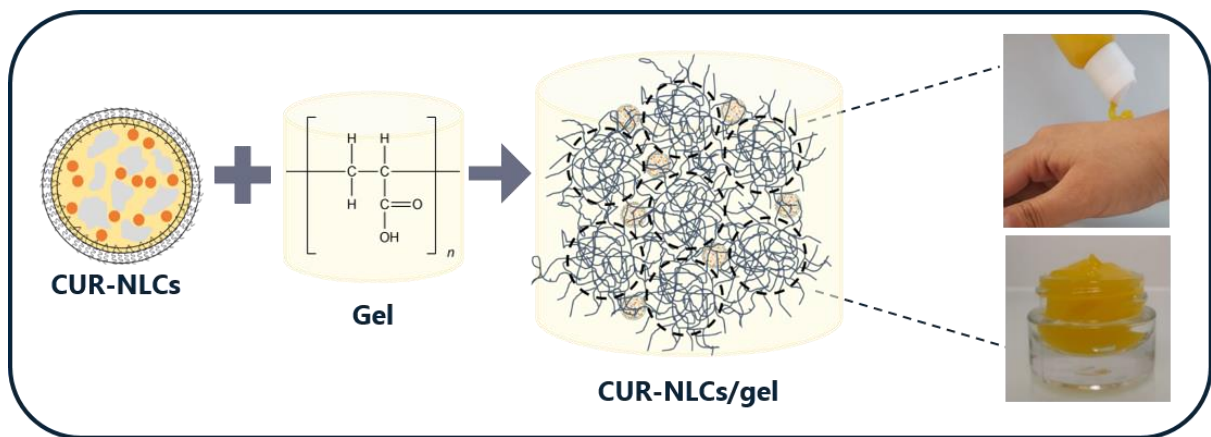


**Figure 1.- Schematic representation of the developed hydrogel containing curcumin-loaded NLCs (CUR-NLCs/gel).**

This manuscript is divided in 5 chapters.

In chapter 1, a bibliographic introduction is presented. It is further divided in four parts. A first part providing the background about skin structure and function, as well as some skin conditions in which oxidative stress and inflammation are involved and in which the developed formulation could be applied. The sources of ROS in the skin and the mechanisms that skin has to fight ROS and inflammation will be presented. A second part will be consecrated to the classical strategies for skin drug delivery. After explaining the key principles for drug delivery to the skin, the most common pharmaceutical forms and drug penetration techniques used for this administration route are reviewed. In a third part, the potential of natural bioactive compounds (NBC) for fighting oxidative stress and inflammation will be presented. Physico-chemical characteristics of curcumin and its interaction with cells will be described. A summary of the studies demonstrating its potential in conditions presenting inflammation or oxidative stress will be presented. In the fourth part of

the first chapter, NLCs and hydrogels will be introduced as innovative the tools to deliver curcumin topically. Emphasis will be given to their formulation as well as to their potential contribution to the preparation of a multiscale system, presenting their advantages compared the classical pharmaceutical forms.

In chapter 2, **materials and methods** employed for performing the works here presented are described. It is split in five sections. The first introduce the excipients and the active ingredient used for the composite formulation of CUR-NLCs/gel. The second part presents the experimental procedures followed for the development for CUR-NLCs and CUR-NLCs/gel formulations. For both of them, the approach for optimising the preparation procedure as well as the final formulation protocol are presented. Then, methods employed for physico-chemical characterization are depicted, in section three for CUR-NLCs, and in section four for CUR-NLCs/gel. Finally, the fifth part describes the biological tests performed with CUR-NLCs, as well as relevant information about studied cell lines, biological reagents and sample preparation for those tests.

Chapter 3 and Chapter 4 are dedicated to present the results of this research and to discuss them. Chapter 3 will be dedicated to the **development of CUR-NLCs**, presenting main results of the **optimisation procedure, and the characterisation of the formulation from the physico-chemical and biological point of view**.

Chapter 4 will present the **potential of CUR-NLCs to be applied in topical dermal situations**. First, **at a cellular level**, by assessing its impact on the migration/proliferation as well as its influence in cells undergoing oxidative stress. Second, **through the physico-chemical properties when NLCs are incorporated in the hydrogel matrix**. In particular, rheological characteristics and its capacity to control curcumin penetration into synthetic membranes mimicking human skin (Strat-M ® membranes).

The last part of this manuscript, Chapter 5, will highlight the main conclusions of this work and give perspectives for the continuation of this research topic.



**Chapter 1: State of art**

---



## 1.1. Skin and physio-pathological skin conditions

### 1.1.1. Structure and physiology of the skin

#### 1.1.1.1. Structure

Skin is a complex organ and the biggest of the body. In the adult, it represents near 16% of the body weight, it has a surface of 1.5 to 2 m<sup>2</sup> and an average thickness of around 2 mm in adults<sup>5,6</sup>. Skin can be divided in three main compartments: the epidermis, the dermis and the hypodermis (Figure 2). Hair follicles, sweat glands and sebaceous glands are skin appendages that make possible that the skin functions well in touch, excretion and temperature sensation and regulation, but that can also influence on drug absorption, although their contribution is minimal.

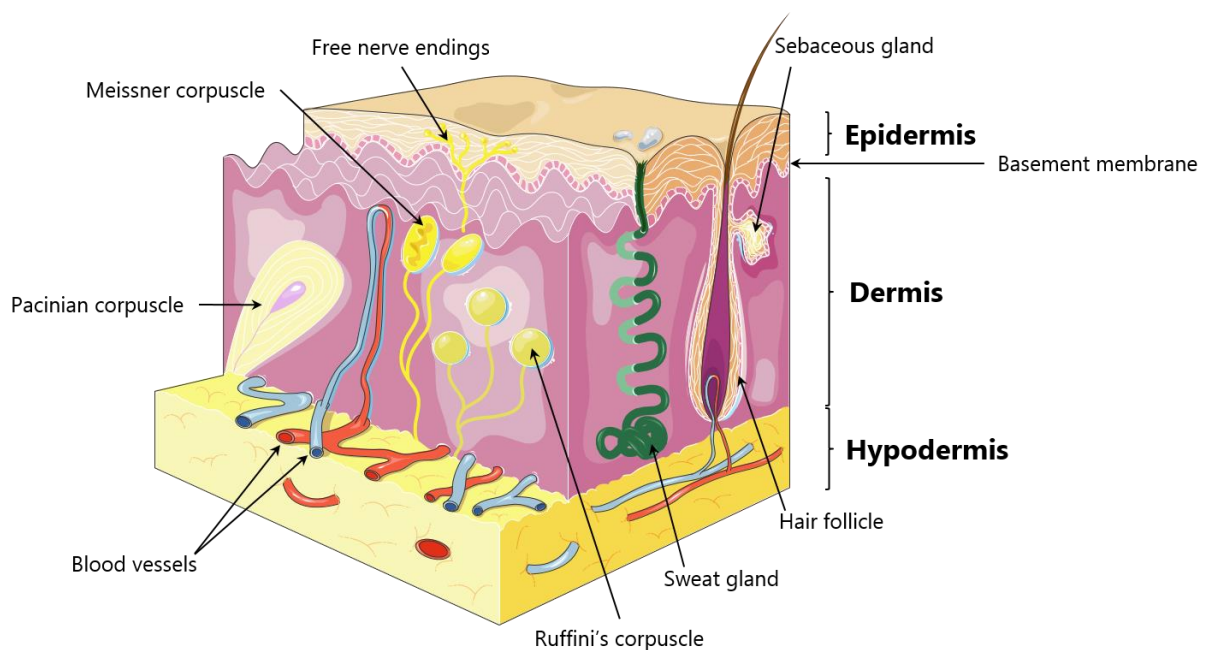


**Figure 2.- Schematic representation of main skin layers and skin appendages.**

This figure contains modified images from Servier Medical Art (<https://smart.servier.com>) licenced under a Creative Commons Attribution 3.0 Unported License.

**The epidermis** has multi-layered structure and is in constant renewal. It is not irrigated by blood, but with lymphatic fluid. Two main regions can be distinguished: the *stratum corneum* (no viable epidermis) and the living epidermis (Figure 3).

- **The *stratum corneum* (SC):** is the principal barrier to drug absorption through skin. Is in this part that most of physical and chemical ways of drug absorption enhancement act. SC is composed of corneocytes (anucleate, flattened and keratinized cells) immersed in a matrix of lipid bilayers (ceramides, free fatty acids, cholesterol) filling the intercellular spaces, a "brick and mortar" structure. From the inner to the external part, three under layers are present and correspond to the final stages of the differentiation of



the keratinocytes coming from the living epidermis: the *stratum lucidum*, the *stratum compactum*, and the *stratum disjonctum*. It desquamates naturally at the surface making possible its renewal<sup>7,8</sup>. In normal conditions, an hydrolipidic film composed of sweat and sebum is extended on the surface of the SC. The whole structure is impermeable to bacteria.

- **The living epidermis:** is the first skin layer containing living cells. It comprises the granular layer (*stratum granulosum*), the spinous layer (*stratum spinosum*) and the basal layer (*stratum germinativum*)<sup>8</sup>. Several types of cells can be found. Keratinocytes are the principal one (80%). By the production of keratin and the presence of desmosomes, keratinocytes help to accomplish the barrier and protective function of the skin. They produce vitamin D when exposed to UV rays. Also, they differentiate into corneocytes (keratinisation process). Langerhans cells (4%) are macrophages responsible of the immune response face to foreign substances. Melanocytes (13%) are responsible of skin's pigmentation and its protection face to solar ultraviolet rays through the secretion of melanin. Finally, Merkel cells (3%) provide the mechanoreceptor role to the skin<sup>9</sup>.

**The dermis** is the implantation site for skin appendages and contains blood and lymph vessels. It is separated from the epidermis thanks to the dermo-epidermal junction, principally constituted of the basal membrane, an important exchange surface and the place where keratinocytes proliferate and their migration starts<sup>9</sup>. Fibroblasts are the principal cell type in this layer (Figure 3). They synthesize tropocollagen, the basic monomer for the formation of collagen. Together with proteoglycans, collagen is a common site for drug binding in this part of the skin<sup>10</sup>. Other ECM (Extracellular matrix) components are elastine and glycosaminoglycans which make this part of the skin highly hydrophilic. Other less abundant cells like macrophages, lymphocytes and granulocytes are responsible of defence responses. Due to its composition, hydrophilic drugs will preferentially act in this layer of the skin. However, this type of drugs will encounter an obstacle while trying to pass through an intact SC in the epidermis due to its hydrophobic nature.

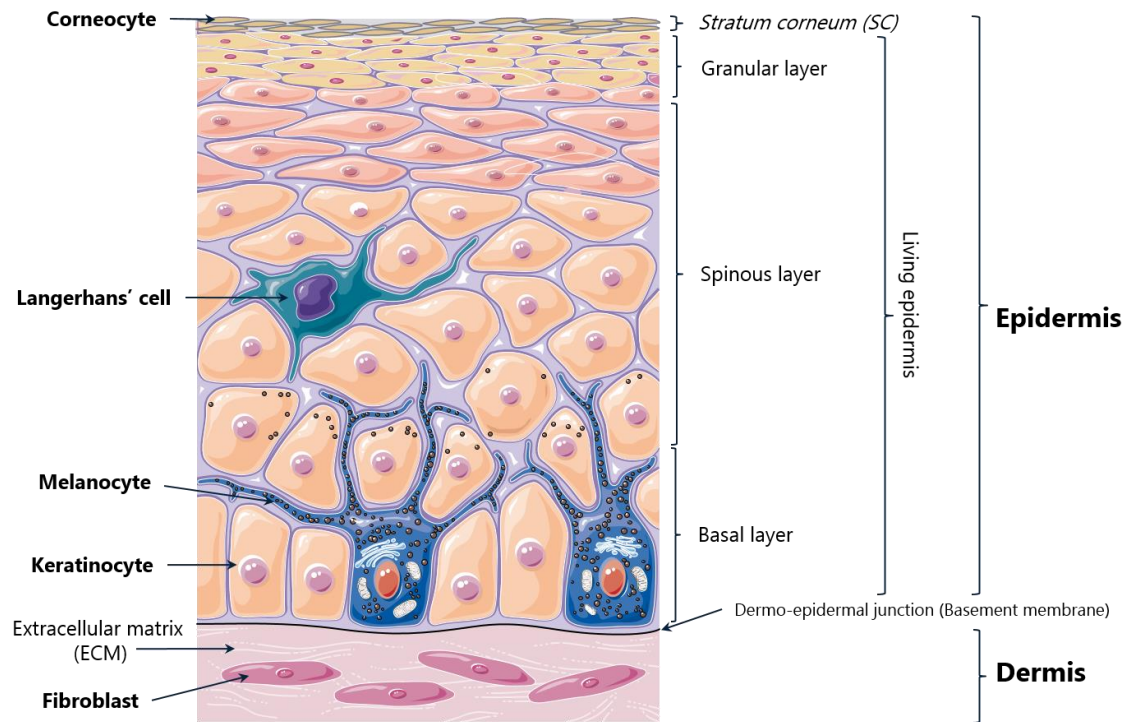


**Figure 3.- Principal components of the Epidermis and Dermis.**

This figure contains modified images from Servier Medical Art (<https://smart.servier.com>) licenced under a Creative Commons Attribution 3.0 Unported License.

**The hypodermis** is the deepest layer of skin and contains mainly adipocytes, vasculature, nerves and adipose stromal cells<sup>11</sup>. Its principal functions are to cushion shocks and to protect the body from the cold by an insulation mechanism. Adipocytes in this layer might be implicated in the migration of fibroblasts<sup>9,12</sup>.

### 1.1.1.2. Functions of the skin

**Physical and immunity barrier:** Skin protects organs and inner tissues from the external medium and from mechanical aggressions. In the SC, corneocytes immersed into a lipidic matrix represent a physical barrier to the penetration of pathogens. Due to its pigmentation (melanin produced by melanocytes), skin is able to protect itself by reflecting UV rays. Skin is the first line of defence face to microorganisms mainly due to the production of antimicrobial peptides<sup>13</sup>. Langerhans cells and keratinocytes can activate lymphocytes T. Moreover, keratinocytes produce pro-inflammatory cytokines which take part in the inflammatory reaction of the skin<sup>9</sup>.

**Thermoregulation:** Normal temperature of skin is around 32-33 °C<sup>14,15</sup>; However, when inner temperature (body's core) increases, it secretes sweat and through its evaporation at the surface it regulates body's core temperature and stabilises it in between 36-37.2°C<sup>16</sup>. Blood irrigation in the dermis and hypodermis also contribute to the liquid exchange required for thermoregulation.

**Mechano and thermoreceptor:** Nerve endings in skin allow the organism to perceive sensations like the touch, temperature, pressure or pain. This thanks to Merkel cells, Meissner's, Pacinian and Ruffini's corpuscles<sup>9</sup>.

Overall, the principal skin function can be described as to protect the organism from external aggressions: pathogens, heat, cold, mechanical shocks, etc, and to provide an appropriate reaction to them. This is why it is so important to maintain skin's integrity. Any disruption on it will also affect its protective barrier role.

## 1.1.2. Inflammatory physio-pathological skin conditions

### 1.1.2.1. Acute wounds

In a broad sense, a wound is a damage of any biological tissue: skin, mucous membranes and organ tissues. For skin, it implies the breakdown of its protective function. Acute wounds are usually due to some kind of trauma that can be blunt or penetrating<sup>17</sup>. For example: first degree burns, superficial cuts or abrasions, surgical incisions and animal bites. In most cases, they present just a loss of the epidermis and/or the upper layer of the dermis, leaving the basal membrane intact. In consequence, such wounds can go through the normal phases of wound healing and achieve a complete dermal restoration (integrity and function) in 3-4 weeks<sup>18</sup>. The healing process starts immediately when the wound is formed, occurs through the activation of many cellular signalling pathways and is composed of four temporarily and spatially overlapping phases: homeostasis, inflammation, proliferation and remodelling (Figure 4).

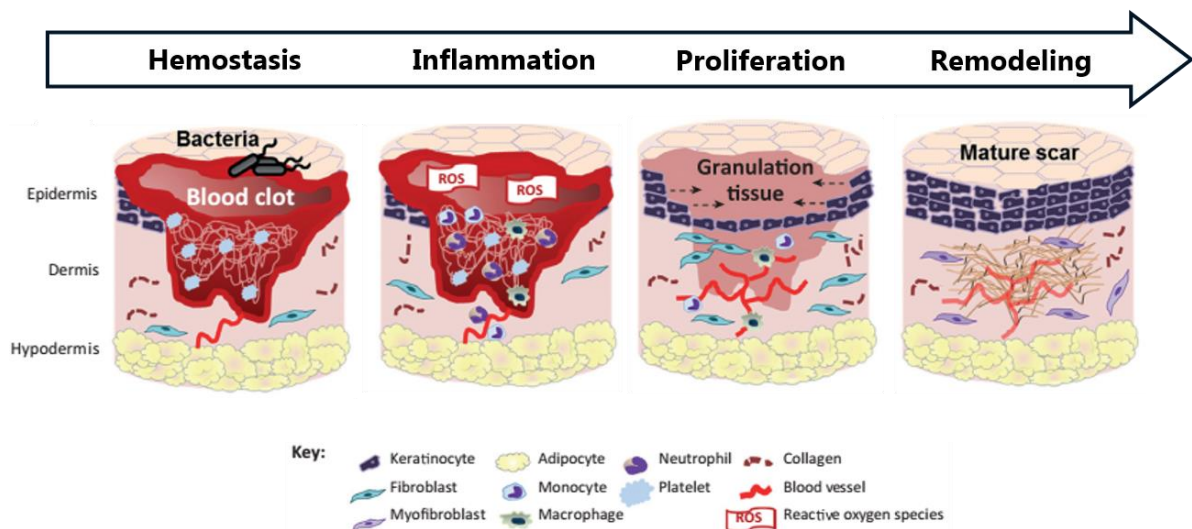


Figure 4.- Wound healing process in acute wounds. Modified from Berthet *et al.* 2017<sup>19</sup>.

**Homeostasis** aims to stop the bleeding through vasoconstriction and the creation of a clot that will act as a physical barrier against invading microorganisms. During the coagulation cascade, signals emitted by damaged blood vessels (like adenosine diphosphate, ADP) lead to platelet aggregation, to their degranulation and, consequently, to the formation of a crosslinked fibrin network with entrapped ECM

proteins (fibronectin, vitronectin and thrombospondin): the clot<sup>20</sup>. This process also induces the release of growth factors and cytokines necessary to the chemotaxis of leukocytes and fibroblasts. The formed clot acts also as a scaffold for these infiltrating cells which are involved in further steps of wound-healing<sup>21,22</sup>.

**Inflammation** normally starts immediately after skin injury, is simultaneous with the homeostasis phase and in normal conditions (acute wounds) can last 48 hours. During this phase, leukocytes (neutrophils, lymphocytes and monocytes) infiltrate and migrate in order to phagocyte cell debris and protect the wound against bacterial colonisation through the production of ROS and proteases. In chronic wounds, the insufficient production of ROS detoxifying enzymes and antioxidant molecules causes high levels of ROS<sup>22</sup>, which prolongs the inflammation phase, hinder an appropriate proliferative phase to take phase, and thus, cause impaired healing.

**Proliferation** is started by the cytokines and growth factors secreted by leukocytes during the inflammation phase and can be fully completed just once the inflammation phase is over. During this phase, fibroblasts, keratinocytes and endothelial cells migrate and proliferate. The aim is to produce new tissues at the wound site. Newly formed capillaries, fibroblasts and macrophages (differentiated monocytes) will transform the fibrin matrix into a granulation tissue. This structure allows fibroblasts to produce structural proteins such as collagen in order to restructure the ECM. Once this is achieved, some fibroblasts are stimulated by macrophages and differentiate into myofibroblasts in order to contract the wound. At the same time, keratinocytes migrate and recover the wound<sup>23</sup>. A process called "Epithelial-Mesenchymal Transition" gives mobility to the keratinocytes so that they can fully re-epithelize the wound area.

**Remodelling** usually starts 2-3 weeks after the initial injury and may last 1 year more. During this phase, the granulation tissue is replaced with a mature scar through the remodelling of collagen fibers by fibroblasts. These cells replace collagen type III by collagen type I, which is more resistant to tensile stress and becomes the predominant protein in the newly formed scar. However, tensile strength is never the same compared to that of healthy skin.

### 1.1.2.2. Chronic wounds

They are wounds where the re-epithelialization process is impaired and thus, they present delayed healing (>12 weeks after initial insult)<sup>17</sup>. Some examples are: diabetic foot ulcers, pressure ulcers (Figure 5-A) and infected burns. Two related main reasons can cause this delay: prolonged inflammation and bacterial colonisation. It is generally acknowledged that the main reason is that the healing process is blocked at the inflammation phase<sup>24</sup>. Excessive inflammation is provoked by the elevation in the levels of pro-inflammatory

cytokines, ROS, and proteases levels which destroy the ECM and the growth factors. In most cases, the existence of a persistent infection continuously stimulates the production of ROS as defensive tools to fight infection, which continues to perpetuate tissue damage. All of this is aggravated by the presence of cells metabolically less active, old and which do not proliferate. The clinical evolution of these chronic wounds can be further complicated by comorbidities of the patient and lead to severe consequences which are translated in permanent handicaps<sup>25,26</sup>.

### **1.1.2.3. Hypertrophic scars and keloids**

Hypertrophic scars and keloids are both classified as hyper proliferative scars, with a raised morphology. However, while hypertrophic scars do not exceed wound boundaries, keloids present a tumor-like fibrous growth and as a result they extend beyond the initial boundaries of the wound (Figure 5-B,C)<sup>27</sup>. Such pathological scarring can have a negative psychological impact. Also, the disorganised collagenous ECM is not good for skin's function as it reduces its flexibility, there is a lack of skin appendages in the newly formed tissue and there is continuous itching and pain.

In order to tackle hyperproliferative scars, most of the research has been performed by comparing the wound-healing process taking place in adult mammals and the analogous scar free wound healing process in other organisms or in mammalian fetuses<sup>28</sup>. However, the precise mechanism by which excessive scarring takes place is still unknown. Retrospective studies have shown that predisposition factors can be diverse: positive family history, age under 30 (possibly linked to decreased inflammatory response and collagen content with age)<sup>29</sup>, presence of hypersensibility or allergy (might be due to increased collagen synthesis and angiogenesis as result of histamine and heparine production by mast cells)<sup>30</sup>, dark phototype (maybe due to increased inflammatory response and innate collagen production capacity of fibroblasts present in dark phenotypes like african or hispanic)<sup>31,32</sup>.

In all cases hyperproliferative tissues present distinctive characteristics in the type of cells present and their activity. The most important is the presence of high proliferative fibroblasts, their continuous activation (differentiation) into myofibroblasts, and the high activity of these last ones resulting in large amounts of ECM being synthesized and the formation of a collagen rich granulation tissue which is not counterbalanced by its degradation.

Important markers of this process and that can be followed while developing and evaluating new therapies to abnormal scarring are:

- Transforming Growth Factor  $\beta$  (TGF-  $\beta$ ): responsible of starting differentiation process of fibroblasts into myofibroblasts<sup>33,34</sup>.

- $\alpha$ -smooth muscle actin ( $\alpha$ -SMA) and keloid collagen (mixture of type I and III): their overexpression is linked to the characteristic increased contract strength of the fibrotic tissue in hypertrophic scars and keloids, respectively<sup>27</sup>.
- IL-22: also implicated in the differentiation process of fibroblasts<sup>34</sup>.

Apart from surgical excision, the most common treatment is intralesional corticosteroid administration (for example: Triamcinolone). However, it is not very efficient alone and it is not comfortable for the patient. In some cases, it is administrated with anti-proliferative drugs (Tracolimus or 5-Fluo uracil), cryotherapy, laser therapy and radiation. Resulting adverse effects such as fat atrophy, pain and high possibility of systemic toxicity show the importance of developing new strategies for the treatment of hypertrophic scars<sup>32,35</sup>.

In this context, attenuating scarring during wound-healing remains a challenge. From the above described, an ideal treatment is the one that would:

- Reduce (but not completely suppress) proliferation of fibroblasts so that their differentiation into myofibroblasts is controlled.
- Control chronic inflammation so that cytokine release will not overactivate fibroblasts and their differentiation.
- Regulate the activity of myofibroblasts
- Increase apoptosis of myofibroblasts in late stages of wound-healing, that is, once all wound is covered by granulation tissue, so the synthesis on new collagen is no more needed.

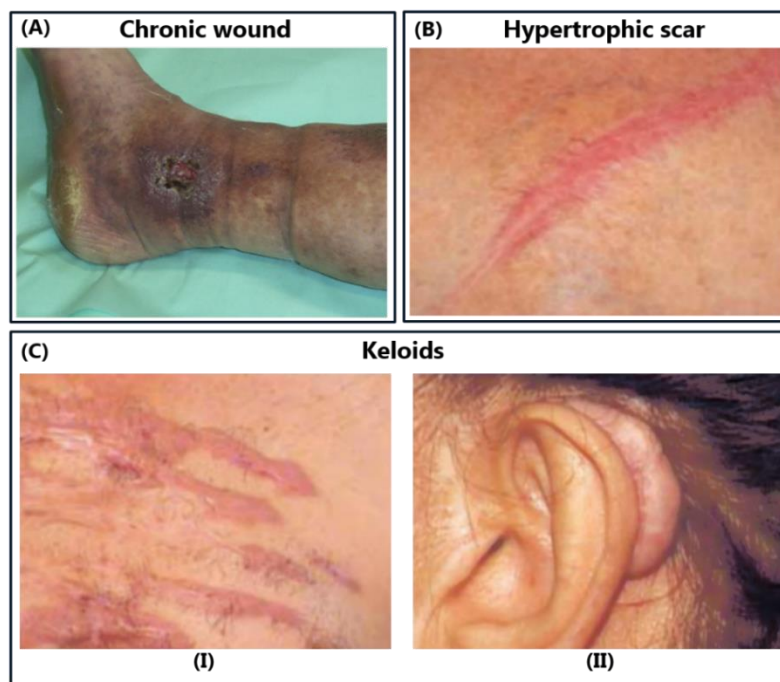


**Figure 5.- Pathological skin conditions examples. (A) Chronic wound:** leg pressure ulcer<sup>36</sup>. **(B) Hypertrophic scar:** typical appearance. **(C) Keloids:** (I) typical appearance, (II) after excision in the ear<sup>32</sup>.

#### 1.1.2.4. Psoriasis

Psoriasis is classified as a common chronic inflammatory disease. Specific starting pathways are still not well known. However, stress, infections, or even alcohol are factors that seem to favour its apparition. In France, around 2% of the population suffers from it, mostly between 20 and 40 years old<sup>37</sup>. Lesions are papulosquamous. That is, presenting red and raised bumps (papules) and flat, thickened areas of skin. In some cases, lesions can be covered with silvery white scales<sup>38</sup>. In most cases, such lesions are small and tend to easily disappear and are known as guttate psoriasis (Figure 6-A). Around 20% of cases are considered as moderate or severe forms of plaque psoriasis (Figure 6-B), with bigger lesions and even with articular pain<sup>39</sup>.

It is an autoimmune disease in which T cells (lymphocytes) provoke the excessive proliferation of keratinocytes. More specifically there is expansion and activation of subpopulations Th-1, Th-17 and T-22, which produce Interferon gamma (IFN- $\gamma$ ), tumour necrosis factor alpha (TNF- $\alpha$ ), as well as interleukins (IL) 17 and 22<sup>40</sup>. In consequence, renewal time of keratinocytes passes from 3 weeks to only 3 days. The excessive accumulation of keratinocytes increases the thickness of the SC giving place to a condition known as hyperkeratosis<sup>38</sup>. Such keratinocyte accumulation can occur with preserved keratinocyte maturation (orthikeratotic hyperkeratosis) or with delayed maturation of keratinocytes seen by retained nuclei (parakeratotic hyperkeratosis)<sup>41</sup>.

As exact mechanisms of the disease remain unknown, to date, there is no treatment to cure psoriasis. Thus, treatments are designed in order to reduce symptoms and to improve quality of life. First-line treatments include hydrophobic ointments containing corticosteroids or vitamin D<sup>10</sup>. When there is more than 30% of the body affected, an oral treatment with retinoids (acitretin), antimetabolites (methotrexate) or antivirals (aciclovir) alone or in combination with exposure to UV is preferred. Efficacy of such is around 50%. If symptoms persist, a third option is the administration of monoclonal antibodies specific to TNF- $\alpha$ . This last option offers an efficacy of 75% in reducing symptoms. However, as any other biotherapy, access remains hindered by its high price<sup>39,42</sup>.

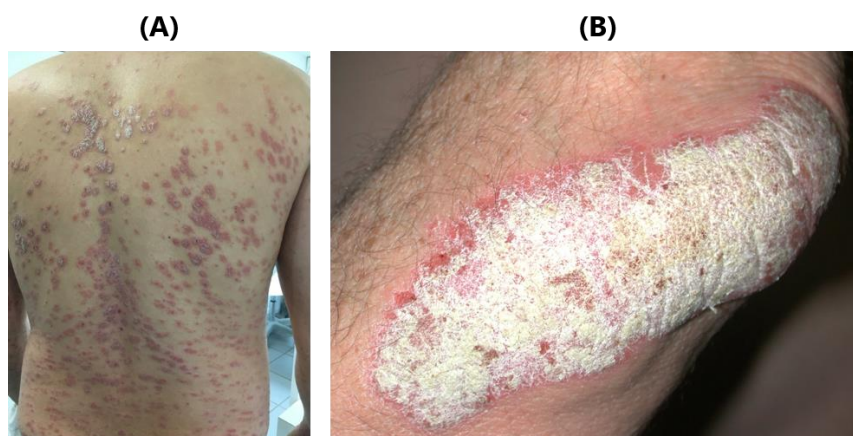


**Figure 6.- Psoriatic lesions. (A) Guttate psoriasis. (B) Plaque psoriasis.**<sup>37</sup>

### 1.1.2.5. Atopic dermatitis

Atopic dermatitis, also known as atopic eczema, is an inflammatory disease in which skin becomes irritated and dry. When condition is acute, lesions are characterized by erythema, papules and serous exudates. In chronic cases, lesions become eroded and present hyperpigmentation<sup>43</sup>.

Its apparition is triggered by exposition to irritants or allergens which provoke an excessive production of IgE. For example, it can take place after exposition to preservatives in cosmetics or daily use products (Figure 7). Most of the time, this condition is associated with other diseases such as asthma, allergic rhinitis or food allergy<sup>44</sup>. As the term "atopic" implies, this condition is associated with a hereditary predisposition. It is believed that the alteration of the skin barrier could be the origin for dryness and increased sensibility to aggressions seen in lesions<sup>45</sup>.

First-line treatments aim to prevent transepidermal water loss (TEWL) by topically applying moisturising formulations without any active ingredient. These can either be ointments or creams. From one side, ointments, due to their high lipid content act as emollients by creating an occlusive barrier that do not allow the passage of water from the skin to the external media. From the other side, creams containing humectant ingredients (propylenglycol for example) will draw water to them helping to hydrate the SC. When symptoms are strong corticosteroids are applied topically<sup>46</sup>.



**Figure 7.- Atopic dermatitis to isothiazolinones lesions. (A)** produced by Methylisothiazolinone. **(B)** produced by Octylisothiazolinone. <sup>43</sup>

### 1.1.3. Skin mechanisms to fight ROS and inflammation

Under physiological conditions, a redox (oxidation-reduction) equilibrium is maintained in the cells. ROS are normally produced as by-products of aerobic respiration. In these cases, endogenous and exogenous antioxidant systems are able to ensure good conditions for aerobic life by regulation of ROS levels in terms of spatial and temporal confinement. However, when ROS levels are increased beyond normal limits in a



determined space and during a certain time, antioxidant systems are no longer able to maintain body homeostasis, leading to oxidative stress. Oxidative stress can be defined as “a disturbance in the pro-oxidant-antioxidant balance in favour of the first one” and also as “a disruption of redox signalling and control” as multiple lines of cellular defences are disturbed<sup>47,48</sup>.

In order to fight this conditions, protection mechanisms can take place at different levels: by preventing ROS formation, intercepting ROS once they are formed, or by repairing the damages caused by ROS<sup>47</sup>.

### 1.1.3.1. Sources of ROS and inflammation

ROS are highly reactive molecules that derive from molecular oxygen. They are formed during cellular metabolism<sup>49</sup>. Main compounds are cited in Table 1:

**Table 1.- ROS free radicals and non-radicals.** Name and chemical formula are presented.

Free Radicals	
Name	Chemical formula
Superoxide radical	$O_2^{\cdot-}$
Hydroxyl radical	$HO^{\cdot}$
Peroxyl	$RO_2^{\cdot}$
Alkoxy	$RO^{\cdot}$
Nitric oxide	$^{\cdot}NO$
Nitrogen dioxide	$^{\cdot}NO_2$
Lipid peroxy radical	$LOO^{\cdot}$
Lipid radical	$L^{\cdot}$
Singlet oxygen	$^1O_2$
Non-radicals	
Name	Chemical formula
Hydrogen peroxide	$H_2O_2$
Peroxynitrite	$ONOO^-$
Lipid hydroperoxide	$LOOH$

When moderate amounts of these compounds are present, they have beneficial effects in fighting pathogens and regeneration processes as they act as signalling molecules<sup>50,51,52</sup>.

**Endogenous sources:** Main ROS endogenous sources are intracellular organelles and enzymes as it is where most metabolic reactions take place.

Mitochondria is one of the main sources as it is in its inner membrane that respiratory chain is localized.

The main function of this organelle is ATP production in order to satisfy energy requirements of the cell. Superoxide radicals are mainly produced at Complex I and Complex III or the respiratory chain. Afterwards,  $O_2^{\cdot-}$  can be converted in  $H_2O_2$ , by different enzymes in the inner mitochondrial membrane, the cytosol or in the matrix<sup>53</sup>. Products of the interaction of  $H_2O_2$  with metals ( $Fe^{2+}$ ) can attack the double bonds in unsaturated fatty acids<sup>54</sup>. This amplification of ROS damages can induce dysfunctions in the cellular membranes of epithelial cells and lead to apoptosis.  $Ca^{2+}$  excess can also initiate an apoptosis process, as it is in the mitochondria that  $Ca^{2+}$  and ADP levels are coordinated to maintain an equilibrium between energy demand and energy supply<sup>55</sup>.

Lysosomes have an important role in providing a pathway for the elimination of iron through protein degradation<sup>56,57</sup>. Iron is stabilised in the interior of these organelles in the ferrous state ( $Fe^{2+}$ ). This reduced state is achieved by the acid interior and the presence of compounds containing thiol groups<sup>58</sup>.  $Fe^{2+}$  can easily react with  $H_2O_2$  which can further form other ROS and affect the integrity of the lipids in the cell membrane. Damages in the lysosome membrane are important in death signalling as they can result in apoptosis or necrosis<sup>59,60</sup>.

NADPH Oxidases (NOX) are a family of enzymes that catalyse the reduction of  $O_2$  into  $O_2^{\cdot-}$ <sup>61</sup>. They are one of the major sources of ROS in skin. They are involved in process such as proliferation, migration, differentiation, apoptosis and inflammation. Importantly, they take part in defence mechanisms, by initiating immune response through the elimination of phagocytosed bacteria and any debris in the interior of macrophages and neutrophils<sup>62</sup>.

**Exogenous sources:** Chemicals coming from the environment or produced by lifestyle factors can enter the body through the skin and generate ROS and initiate cellular damage<sup>63</sup>. For example, trace metals (mercury, copper and iron) or even spores and pollen can directly react with lipids and proteins causing cellular damage, or activate intracellular oxidant pathways that will lead to oxidative stress<sup>64</sup>.

To skin, one of the most important ways of aggression is photo-oxidation caused by photons coming from relatively low-energy parts of the spectra: visible and UV. Such wavelengths can interact with electrons in organic molecules and generate ROS. One of the most common ROS produced is hydrogen removal from an organic molecule in order to form  $R^{\cdot}$ , which can further react with oxygen to produce  $ROO^{\cdot}$ <sup>65</sup>.

### **1.1.3.2. Detoxification mechanisms**

Existing mechanisms to fight oxidative stress and their consequences can be either the prevention of ROS formation, their neutralization once there are formed or the activation of cellular pathways in order to repair the damages.

**Endogenous compounds (enzymes and cytokines):** Enzymes are one of the main antioxidant defences. For example, Superoxide dismutases (SOD) can catalyse the conversion of  $O_2^{\cdot-}$  to  $O_2$  and  $H_2O_2$  in the mitochondrial intermembrane space<sup>66</sup>. Glutathione peroxidase (GPx), converts glutathione (GSH) into oxidized glutathione (GSSH) and reduces  $H_2O_2$  to  $H_2O$  and LOOH to stable alcohols. Regeneration of GSH is performed by glutathione reductase (GSR). This allows the protection of cell membranes from oxidative stress as many isozymes of GPx are found in the cytoplasm, mitochondria and the extracellular compartments<sup>67</sup>. Importantly, catalase, an enzyme mainly found in lysosomes is able to transform  $H_2O_2$  to  $H_2O$  and  $O_2$ <sup>67</sup>.

Face to cell injuries, inflammation occurs as a protective response. However, when this process is uncontrolled pro-inflammatory mechanisms are activated. For example, the recruitment of inflammatory mediators such as NF- $\kappa$ B. NF- $\kappa$ B pathway is activated by pro-inflammatory cytokines such as TNF- $\alpha$  and IL-1<sup>68</sup>. TNF- $\alpha$  at its turn plays an important role in the recruitment of immune cells, and at the same time it can induce ROS producing enzymes<sup>69</sup>. Main producing cells of TNF- $\alpha$  are monocytes and macrophages. IL-1 has been linked to dermal disorders such as dermatitis<sup>69</sup>. Importantly, Nuclear factor erythroid 2-related factor 2 (Nrf2) is a transcription factor that translocate into the nucleus in the presence of an increase in ROS levels<sup>70</sup>. Once in the nucleus, it can bind to the Antioxidant response element (ARE) sequence<sup>71</sup>, up-regulating some antioxidant genes, like those coding GSH<sup>70</sup>.

## **1.2. Topical drug delivery to the skin**

The topical route of administration includes drug application on mucosae (nose or genitourinary tract) and on the skin. In this work, drug delivery is aimed to be on skin. In this line, and in order to be able to formulate and assess a drug delivery system to or through the skin (local or transdermal drug delivery, respectively), knowledge about the principal factors impacting on skin's pharmacokinetics process of liberation from the pharmaceutical form and consequently absorption by skin will be discussed. Then, the most relevant formulation technologies for pharmaceutical and cosmetic fields that allow to tune the action site of a drug applied on skin will be presented.

### **1.2.1. Skin drug-delivery: biopharmaceutical aspects**

In order for a substance to have a local or transdermal action, drug transport has to take place in the skin.

This involves several steps<sup>10,72</sup>:

- 1) Release (totally or partially) from its formulation at its molecular state.
- 2) Dissolution in a complex media (mixture of the vehicle components and components of the application site). For healthy skin, this involves drug partitioning in the SC. (*stratum corneum*)
- 3) Transfer, by diffusion, across the SC.
- 4) Partitioning from the SC to viable epidermis and from this to inner layers.
- 5) If passage to the systemic circulation: uptake by capillary vessels

When describing drug transport across the skin, the terms penetration, permeation and resorption can be used (Figure 8). Penetration will refer as the process by which substances enter into a layer. Permeation refers the migration through a specific skin layer or the whole skin. While resorption applies to the uptake of a drug by the skin capillary blood vessels and transport out of the skin, which leads to a transdermal/systemic action. Dermal absorption will be the sum of the three processes[73][74].

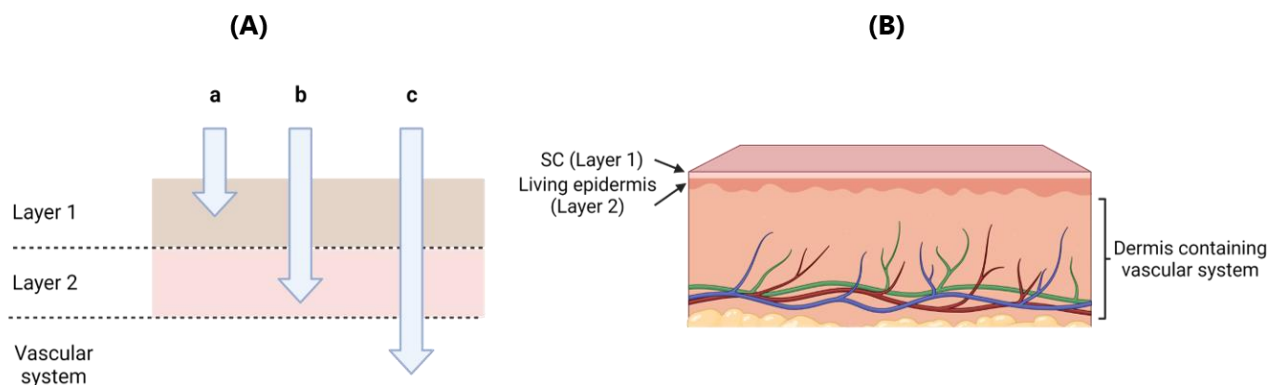


**Figure 8.- Drug transport across skin layers. (A)** General case. a: penetration into layer 1. b: Permeation across layer 1 and penetration into layer 2. c: Resorption, leading to transdermal/systemic drug delivery. **(B)** Example with SC as Layer 1 and Living epidermis as Layer 2. Processes here used to describe the fate of a drug over multiple compartments (skin layers) can also be used to describe the fate of the drug along the skin as a whole layer (penetration into the skin or permeation across the skin).

Created with BioRender.com

When a substance is applied on healthy skin, SC is the main obstacle that it will face during its transport. Two main permeation routes are possible through this layer: a cellular pathway and the passage through the skin appendages, which is very limited. In the cellular pathway (Figure 9), a substance can either go through the transcellular route which implies crossing the intracellular keratinized matrix of corneocytes (hydrophilic path) or through the intercellular spaces between these cells (hydrophobic path)<sup>75,76</sup>.

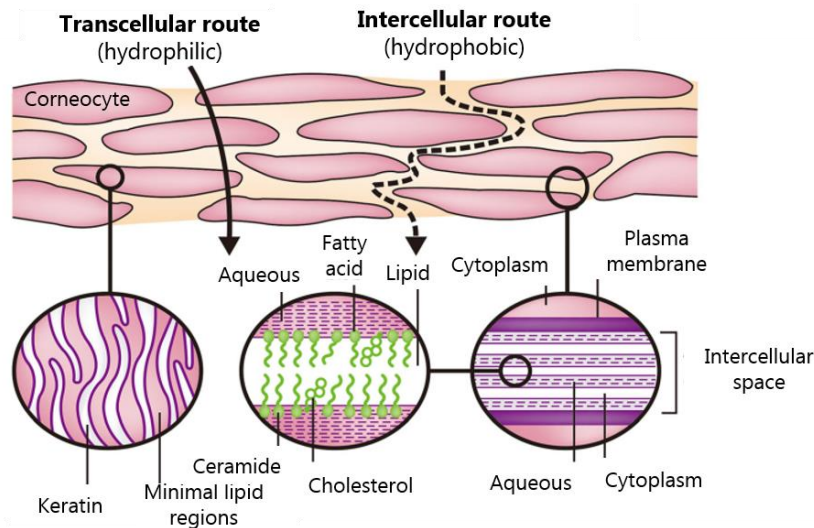


**Figure 9.- Cellular permeation routes across the SC.** Modified from Kim *et al.* 2020<sup>75</sup>.

Due to the lipidic nature of SC and tight junctions present, transfer kinetics will be favoured for small molecules (< 500 Da), with a low melting point and for which the partition coefficient is in favour of a lipophilic application site. However, transfer towards the living epidermis and dermis needs a notorious hydrophilic nature of the permeant molecule. This is why the possibilities of reaching deep layers of the skin are limited for strictly lipophilic molecules and are important for amphiphilic molecules. For hydrophilic substances, the main obstacle for absorption is the SC<sup>76</sup>. Thus, by using absorption promoters, or in cases when the SC is disrupted or even absent (which happens with the presence of a wound or an inflammatory skin disease), dermal absorption and systemic transfer is highly augmented.

To sum-up, three main factors can affect the fate (liberation and absorption) of a substance applied on the skin<sup>77</sup>:

- 1) Physico-chemical properties of the substance (active ingredient)
- 2) Physico-chemical properties of the vehicle (the excipients)
- 3) Physico-chemical properties and state of the skin

Interrelation between the above characteristics are better understood by analysing the diffusion of the substance through the skin, the affinity of the substance for the skin and the permeability of the skin towards the substance:

### **1.2.1.1. Passive diffusion: Fick's 1<sup>st</sup> Law**

Parameters influencing the passive diffusion of substances through the skin can be summed up in Fick's Law, which explains that the flow of a substance crossing the skin (or any semi-permeable membrane) is proportional to the difference in its concentration from one side and the other of the skin or the membrane<sup>75</sup>:

$$J = \frac{dQ}{dt} \times \frac{1}{S} = D \frac{\Delta C}{\delta}$$

J : flow, or speed of transfer ( $\text{g.cm}^{-2}.\text{h}^{-1}$ )

$dQ/dt$  : amount of matter transferred by time unit ( $\text{g.cm}^{-2}.\text{h}^{-1}$ )

S: exposed surface ( $\text{cm}^2$ )

D: diffusion coefficient ( $\text{cm}^2.\text{h}^{-1}$ )

$\Delta C$  : difference in concentration from one side and the other of the skin or membrane ( $\text{g.cm}^{-3}$ )

$\delta$  : length of the diffusion path (cm)

For a local action, formulation parameters and skin's physiology in the application site should allow to have no flow ( $J=0 \text{ g.cm}^{-2}.\text{h}^{-1}$ ), while for a transdermal or systemic action, flow should be maximised ( $J > 0 \text{ g.cm}^{-2}.\text{h}^{-1}$ ).

### 1.2.1.2. The partition coefficient

Drug transfer to the skin is favoured when the affinity of the drug for the skin is high. This affinity can be quantified by the partition coefficient (K) of a substance, which represents the concentration ratio of a drug in two phases at equilibrium. For a transfer to the skin, it would represent the relation of the equilibrium concentrations between the external media ( $C_o$  concentration at the external surface of the skin, non-incorporated) and the skin (concentration  $C_m$  absorbed in the skin):

$$K = C_m/C_o$$

In practice, this coefficient is modelled by the partition coefficient octanol/water of a substance ( $K_{OW}$ ), which represents the tendency of a compound to move between an aqueous phase and a lipid phase:

$$K_{OW} = [\text{drug}]_{\text{octanol}}/[\text{drug}]_{\text{water}}$$

Instead of the K value,  $\log K_{OW}$  is more often used. Values indicate the hydrophobic nature of a compound, with an affinity distinction for the lipidic compartment, the SC of the skin ( $\log K > 3$ ) or a hydrophilic nature of the compound, with an affinity for the protein hydrophilic compartment, the external part of the skin or the dermis ( $\log K < 3$ ). During experimental determinations, other solvents that can be used to replace octanol are: isopropyl myristate and the propylenglycol dipelargonate<sup>77,78</sup>.

### 1.2.1.3. Permeability coefficient

The aptitude of a membrane to let a substance to go through can be expressed by the permeability coefficient (P,  $\text{cm.h}^{-1}$ ):

$$K = \frac{J}{C_o} = D \frac{K}{\delta}$$

All of this if the receiving compartment underneath the skin is not a limiting factor to diffusion. Overall, this parameter brings together, diffusion and partition in order to compare:

- The absorption of different substances by the same membrane (taking into account that the same experimental conditions are met). This can guide for example the choice of a substance for a specific therapeutic aim.
- The resistance of different types of membranes for the passage of a substance. This can compare for example, the penetration a substance in a healthy skin or on a damaged skin. Experimentally, a damaged skin can be modelled by eliminating the SC by stripping, using solvents or detergents to eliminate lipids, occasioning an excessive hydration or by adsorbing exogenous substances<sup>79</sup>.

In summary, drug absorption depends on the excipients building-up the vehicle, but also of the state of the skin at the application site (integrity of the SC, degree of hydration, etc). Once release is achieved, absorption takes place preferentially for low-weight molecules, with a logK between 2-3, that is molecules not very hydrophobic or hydrophilic, and according to Fick's Law passage will be favoured if the difference concentration from one side and the other of the skin is high. This last parameter can be controlled from the formulation by designing a pharmaceutical form that can increase the contact time of the skin with the active substance in order to diffusion to take place<sup>75</sup>.

## **1.2.2. Formulation technologies for skin delivery**

### **1.2.2.1. Common pharmaceutical forms**

The most common used pharmaceutical forms in order to obtain a local or a transdermal delivery of active ingredients are the semi-solid preparations. As established in the EP (European Pharmacopoeia), they should present a homogeneous aspect. These pharmaceutical forms are composed of a single or multiple excipients in which one or several active ingredients are dissolved or dispersed. The nature of the excipients and proportion in which they are present usually directs their use.

**Ointments** are composed of a monophasic excipient in which can be dispersed solids or liquids. The type of the excipient will determine the amount of water that can be absorbed<sup>10</sup>:

- Hydrophobic ointments: can absorb very little amounts of water. Most common excipients are vaseline, paraffin, vegetal oils, synthetic glycerides and silicone oils. The high hydrophobic character of these excipients, confers occlusive properties by forming a physical barrier at the surface of the skin. As a result, water evaporation is hindered and hydration increased<sup>80</sup>.
- Absorbing water ointments: can absorb more important amounts of water due to addition of surfactants to the excipients of hydrophobic ointments.

- Hydrophilic ointments: can absorb important amounts of water as they are often mixtures of polyethylene glycols (macrogols) liquids and solids, which are miscible with water.

The more the hydrophilicity of an ointment, the lower is its capacity to entrap hydrophobic molecules and confer occlusive properties to the skin.

**Creams** are multiphasic formulations composed of a lipophilic phase and an aqueous phase, stabilised by a surfactant<sup>10</sup>. They are emulsions that can be either lipophilic (W/O) or hydrophilic (O/W) in function of their external phase and the HLB value of the surfactant. They can entrap either hydrophilic or hydrophobic molecules, however as their lipid content is less than that for ointments, they do not have very good occlusion properties (skin coverage with impermeable or semipermeable materials), do not hinder water evaporation, but can improve skin hydration by a humectant mechanism<sup>81</sup>.

**Gels** are also multiphasic systems. In these the dispersed phase forms a three-dimensional network, in which a liquid is retained in high proportions. Macromolecules forming that network are known as the jellifying agent. Depending on the nature of the liquid, gels can either be they can be oleogels if the liquid is an oil, or hydrogels if the liquid is water or a mixture of water and a hydrophilic molecule (glycerol, propylenglycol)<sup>10,82</sup>. Jellifying agents can be from different origin. Some examples are described in Table 2:

**Table 2.-Examples of some jellifying agents according to their origin.** <sup>83</sup>

Natural	Semi-synthetic	Synthetic
<ul style="list-style-type: none"> <li>• Alginates, carrageenans (from algae)</li> <li>• Pectin (from fruits)</li> <li>• Hyaluronic acid (from animals/bacteria)</li> </ul>	<ul style="list-style-type: none"> <li>• Carboxymethylcellulose</li> <li>• Hydroxypropylcellulose</li> <li>• Hydroxyethylcellulose</li> </ul>	<ul style="list-style-type: none"> <li>• Acrylic polymers</li> <li>• Polyacrylamides</li> <li>• Poly(vinyl alcohol)</li> </ul>

Due to their capacity to retain high amounts of water, hydrogels can contribute to skin hydration through a humectant mechanism rather than through an occlusive mechanism<sup>80</sup>.

### 1.2.2.2. Physical and chemical enhancement techniques

As the SC is the principal barrier to be crossed by molecules, in a healthy skin, many methods for the enhancement of drug delivery to the skin include its removal or modification. Some physical ways are: elimination of the SC by stripping, the use of microneedles, by applying electric power (iontophoresis,



electroporation), ultrasounds (sonophoresis), or applying magnetic fields (magnetophoresis)<sup>84</sup>. There are also chemicals that can improve drug absorption, like alcohols, propylene glycol, surfactants, glycerides, etc. They can do so by acting at different levels: hydrating the skin, improving the solubility of the drug into the skin, improving the fluidity of the skin by disorganization of the lipids or by destroying the keratinized structures in the corneocytes in the SC<sup>76</sup>. All of the before described procedures would allow the transdermal passage of highly hydrophilic molecules and big molecules (>1000 Da), mainly by altering skin properties<sup>84</sup>.

Alternatively, enhancement in the liberation and absorption of substances applied on skin can be achieved by modifying the physico-chemical characteristics of the substance. This would allow to deliver substances without destroying the barrier function of skin. In order to modify the physico-chemical characteristics of the substance without altering its chemical structure (which may change its therapeutic effect), advanced formulation techniques can be used, such as encapsulation in nanovectors, which will be described in more detail in future parts of this literature review.

### **1.3. Natural compounds to fight ROS and inflammation**

When previously detailed endogenous compounds do not succeed in restoring the antioxidant/pro-oxidant balance, therapy based on exogenous antioxidants administration is sought. Exogenous antioxidants have the ability to neutralise ROS, and will not allow them to act on tissues, so that signalling pathways leading to inflammation are controlled. This can be done by direct hydrogen or electron transfer to ROS, or by being involved in signalling pathways that would lead to increase of antioxidant enzymes that at their turn will fight ROS.

Natural bioactive compounds (NBC) are secondary metabolites synthesized by plants, that is, compounds with a role in adaptability and survival processes. Some examples are phenolic compounds and carotenoids. Their anti-inflammatory and antioxidant properties can contribute to stop inflammation and restore the redox balance necessary to reestablish normal conditions in dermal cells<sup>85</sup>. In this regard, the topical use of NBC such as astaxanthin<sup>86</sup>, gallic acid<sup>87</sup> or curcumin<sup>88</sup>, has been described for the treatment of some skin pathologies.

Dermal topical therapy is a simple and non-invasive route of administration, which allows to locally deliver high amounts of the active ingredient at the site of action, improves compliance and limits some of the side effects related with systemic routes<sup>89</sup>. NBC are usually administered as adjuvant therapy to conventional treatments and their natural origin is usually associated with a low toxicity and high biological activity<sup>90</sup>.

Among other NBC, polyphenols (molecules containing at least two phenolic groups) are interesting as they have demonstrated to activate genes containing the antioxidant response element (ARE), through the activation of transcription factor Nrf2<sup>91,92</sup>. Also, due to their similarities in structure, it has been documented

that polyphenols are able to inhibit major pro-inflammatory enzymes as NOX and eicosanoid-generating enzymes such as cyclooxygenase (COX), lipoxygenase (LOX) and phospholipase A2<sup>93</sup>. In this way, the generation of arachidonic acid-derived inflammation mediators is prevented.

### 1.3.1. Curcumin

Turmeric is the resulting product of drying and grounding the rhizome of *Curcuma longa* L. The polyphenol curcumin, also known as diferuloyl-methane (1,7-bis(4-hydroxy-methoxyphenyl)-1,6-heptadiene-3,5-dione), is the most abundant curcuminoid found in turmeric.

#### 1.3.1.1. Sources

The genus *Curcuma* (family: Zingiberaceae) comprises more than 100 species. Out of them, *Curcuma longa* L. is the commercially most important one. It is a perennial shrub that grows in warm and rainy regions in Asia and South America. It is mostly cultivated and consumed in India<sup>94</sup>.

The process for obtaining curcumin from *Curcuma longa* L. is shown in Figure 10<sup>95,96</sup>.

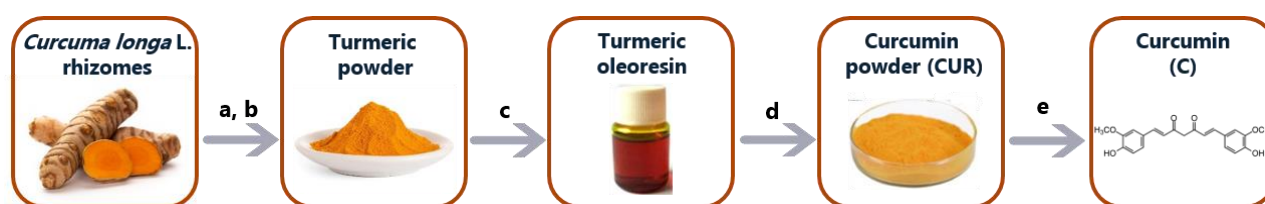


**Figure 10.- Curcumin obtention from *Curcuma longa* L. a:** Drying. **b:** Grounding. **c:** Solvent extraction. **d:** Crystallization. **e:** Column chromatography.

First, rhizomes are dried in either open sun or conventional driers, then they are grounded resulting in a powder (Turmeric powder), which is composed of a variety of compounds: curcuminoids, pigments, aroma compounds, flavour compounds, resins and fats. Among all of them, curcumin content is less than 10 %.

Then, by dissolving Turmeric powder in approved solvents (ethylacetate, acetone, carbon dioxide, dichloromethane, n-butanol, methanol, ethanol or hexane<sup>97</sup>) and then eliminating them by filtration or evaporation, a viscous oil is obtained (Turmeric oleoresin). It contains just 9% of the individual curcuminoid curcumin or diferuloylmethane (designed as "C" in Figure 10). Both, Turmeric powder and Turmeric oleoresin are used as spice and food colorant. They both contain pigments, volatile oils, resins and fats besides curcuminoids.

Curcumin powder, containing no less than 90% or curcuminoids (from which 80% is curcumin<sup>98</sup>) is obtained by crystallization of Turmeric oleoresin and is the most common commercially available product. In food industry it is known as food colorant E100.

Further purification methods, like column chromatography can be employed to separate pure curcumin (C) from the other two major curcuminoids: demethoxycurcumin (DMC) and bisdemethoxycurcumin (BDMC) with a purity  $\geq 98\%$  for C<sup>99</sup>. As individual yields are not very high, pure curcumin is very scarce and expensive, while DMC and BDMC are not commercially available. Even if synthesis of curcumin is possible and is known for very long<sup>100</sup>, extraction and purification continues to be preferred way of obtaining curcumin.

### **1.3.1.2. Uses**

Turmeric, curcuminoids and curcumin is usually described as “nutraceutical” as it has two main uses: as spice and as therapeutic agent.

As spice, Turmeric is mainly used due to its colour and flavour, but also as an additive to improve the shelf life of perishable foods. The curry preparation is the best-known example of this use. However, it can be also found in products like mustard, mayonnaise, salad dressings, oils, sausages, alcoholic and non-alcoholic drinks. In the European Union (EU), curcumin powder is described as colorant E100 while in the United States, turmeric powder and turmeric oleoresin are both labelled as colour additives for use in human food, and either the powder or the oleoresin are named colorant E100<sup>97,101</sup>.

As therapeutic agent, since long time ago, Turmeric has been included in traditional medicine systems, like for example the ancient system of Indian medicine: Ayurveda<sup>102</sup>. Since then, many uses have been described. Some examples are to treat gastrointestinal disorders<sup>103</sup>, arthritis<sup>104,105</sup>, Alzheimer disease<sup>106</sup>, and even cancer<sup>107</sup>.

As curcumin and curcuminoids have proven to have free radicals scavenging properties that can diminish oxidative stress in cells, and thus, be able to lower inflammation, in the context of this work, special attention will be given to curcumin’s antioxidant properties and how these may impact in its potential application on skin regeneration and in skin disorders from an *in vitro* perspective.

### **1.3.1.3. Physico-chemical properties**

Curcuminoids are phenolic compounds (Figure 11), slightly differing in their physico-chemical properties (Table 3). With a log  $K_{O/W}$  of 4.16<sup>99,108</sup>. They are not soluble in water but soluble in organic solvents. With a higher solubility in polar organic solvents (acetone, methanol, ethanol, acetonitrile) than in aliphatic solvents (hexane)<sup>95</sup>.

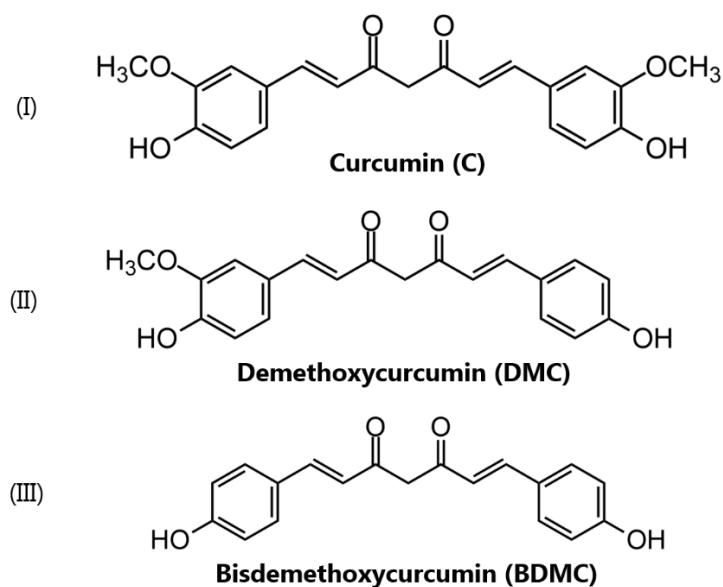


**Figure 11.- Chemical structure of the main curcuminoids. (I)** 1,7-bis(4-hydroxy-3-methoxyphenyl)-1,6-heptadiene-3,5-dione. **(II)** 1-(4-hydroxy-phenyl)-7-(4-hydroxy-3-methoxyphenyl)-1,6-heptadiene-3,5-dione. **(III)** 1,7-bis(4-hydroxyphenyl)-1,6-heptadiene-3,5-dione.

**Table 3.- Physico-chemical characteristics of curcuminoids.**<sup>109</sup>

	<b>C</b>	<b>DMC</b>	<b>BDM</b>
Melting point (°C)	184	172	222
$\lambda_{\max}$ in EtOH (nm)	429	424	419

C: curcumin, DMC: demethoxycurcumin, BDM: bisdemethoxycurcumin

In aqueous media, curcuminoids are present in a keto-enol equilibrium. At alkali pH, curcuminoids undergo deprotonation of the methoxyphenolic group (Figure 12- Site 1) or the diketone moiety (Figure 12- Site 2) and successive hydrolytic degradation in a time-dependent manner giving feruloylmethane, ferulic acid, vanillin and other coloured condensation products. An example of this is given in Figure 12 for curcumin. The degradation rate increases from pH 7.45 to pH 10.2 and decreases at higher pH values<sup>110</sup>. This same behaviour has been observed for pure compounds, combined curcuminoids and turmeric oleoresins. Curcumin (Figure 11-I) is the less resistant to these pH changes while BDMC (Figure 11-III) is the most resistant to alkaline conditions.

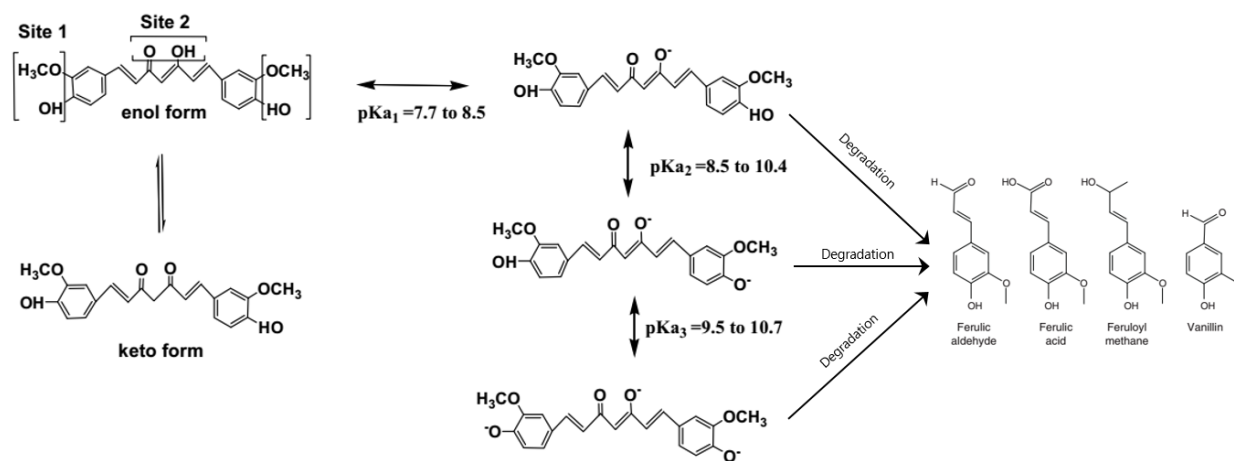


**Figure 12.- Keto-enol equilibrium, deprotonation and degradation of Curcumin in aqueous media.** Modified from <sup>111 110</sup>. Progressive deprotonation of curcumin is signalled by the three calculated values for its acidic dissociation constant ( $pK_{a1}$ ,  $pK_{a2}$  and  $pK_{a3}$ ).

Successively deprotonated forms of curcumin have a red or orange colour (Figure 13-C), however it is difficult to distinguish this coloration from the one presented by its degradation products or even from its reported protonated form (Figure 13-A)<sup>112,113</sup>. The more deprotonated curcumin is, the more it is soluble in water. This implies that the molecule has a good stability in the pH range 1-7 (Figure 13-B), however its solubility in water is very low.

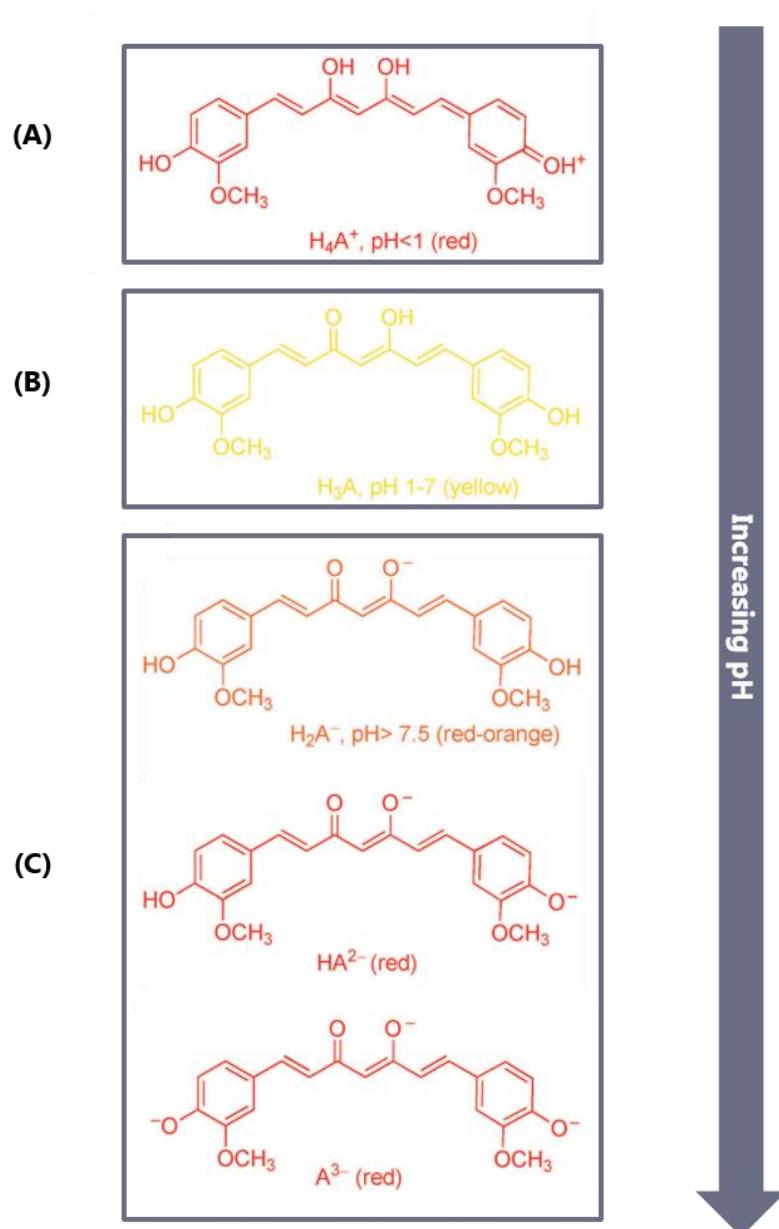


**Figure 13.- pH dependent changes of curcumin in aqueous solutions. (A)** Protonated form when pH < 1. **(B)** Curcumin in its enol form at pH 1-7. **(C)** Deprotonated forms when pH > 7.5. Modified from <sup>112,113</sup>.

Curcuminoid solutions in organic solvents present UV-VIS absorption and fluorescence, which can be used for their identification and quantification. For all curcuminoid solutions, maximal UV-VIS absorption occurs between 300 and 500 nm. Specifically for curcumin, maximal absorption has been reported to be 408 nm in cyclohexane, 420 nm in methanol, 429 nm in ethanol and 430 nm in N,N-dimethyl formamide<sup>114</sup>. Curcumin fluorescence has been reported to occur at an excitation wavelength ( $\lambda_{exc}$ ) of 355 nm and an emission wavelength of 560 nm ( $\lambda_{emm}$ ).

Curcuminoids can also decompose when exposed to the light, giving some of the same products presented in Figure 12 <sup>115</sup>. Photolysis of curcumin has been reported to be dependent on the curcumin state (solid or in solution), the solvent if curcumin is dissolved and the presence of oxygen<sup>116</sup>. Heat can also contribute to

degradation of curcuminoids. Highest effects have been observed for temperatures around 190 °C<sup>117</sup>.

Strategies like encapsulation into cyclodextrins have been used in order to increase apparent water solubility mainly of curcumin. However, the photodecomposition has been showed to increase<sup>118119</sup>. Other strategies to increase curcumin stability under light and alkaline conditions were for example to add acids like gallic, citric and gentisic<sup>95</sup>.

**Antioxidant properties:** Curcumin (C) presents tautomerism when being in solution. The keto and the enol isomers are present in equilibrium as showed in Figure 14.

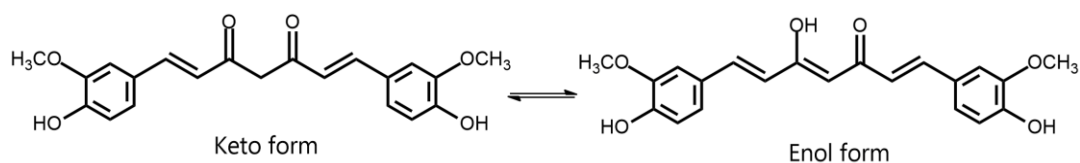


**Figure 14.- Tautomerism keto-enol of curcumin**

The site of action and mechanisms by which curcumin exerts its ability to scavenge free radicals were in debate for very long time. Barzegar<sup>120</sup> performed electron-transfer experiments, voltammetry measurements and quantum chemical computations that indicated that -OH groups in either the phenolic rings or in the  $\beta$ -diketone moiety are important for the antioxidant activity of both isomers (Figure 15) . Also that the enol isomer presents higher antioxidant activity than the keto isomer. However, while the keto isomer mainly reacts by H-atom transfer (HAT), the enol isomer has tendency to predominantly react by electron transfer (ET). This is important, as in conditions where both isomers are present, like inside the cells, both HAT and ET are involved in curcumin's activity of reducing free radicals.

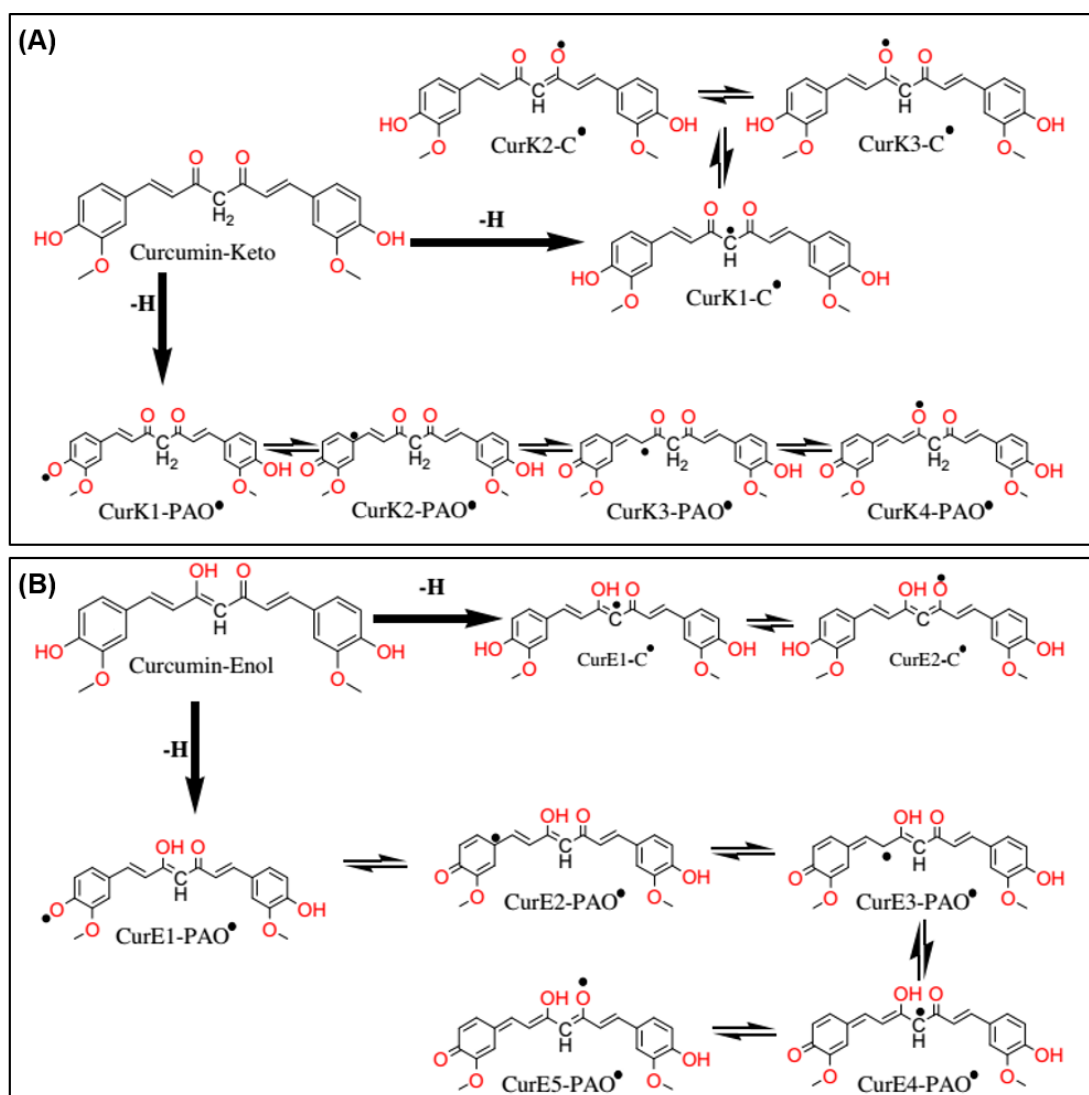


**Figure 15.- Probable sites for free radical reaction with curcumin in its two tautomeric forms. (A)** Keto form. **(B)** Enol form. Phenoxyl radicals (CurK-PAO•, CurE-PAO•) produced by hydrogen abstraction from the phenolic ring OH group (the same phenolic reactions are possible for the other phenolic ring. Carbon-centered radicals of CurK-C• and CurE-C• generated by hydrogen abstraction from CH<sub>2</sub> (keto form) or CH group (enol form), respectively. CurE-PAO• has greater resonance stabilization than does CurK-PAO•. Modified from Barzegar 2014<sup>120</sup>.

This is important, while choosing methodologies for assessing the antioxidant properties of formulations containing curcumin. Whenever possible, preference needs to be given to analysis or tests that would assess similar mechanisms happening in curcumin. In our case, the ABTS assay, inhibition of the radical cation ABTS<sup>•+</sup> is considered to take place by a mixed HAT/ET mechanism<sup>121</sup>. Therefore, ABTS assay was chosen to study the antioxidant activity of the formulations.

### 1.3.1.4. Interaction with cells

Knowing how curcumin interacts with cells is important to understand biological effects that might be seen in experimental settings. However, even if curcumin has been widely used for topical applications, little is



known about the uptake into and intracellular localization of native curcumin (curcumin non-entrapped in any delivery system) in dermal cells. Most of the literature reports the uptake, metabolism and intracellular localization in intestinal and hepatic cell lines, probably due to use of curcumin as spice and consequent interaction with the gastro-intestinal tract. Subcellular curcumin localization is time dependent and cell-line dependent as showed in Table 4. Despite this, main features described for those cell lines, can orient future research in dermal cells such as fibroblasts and keratinocytes. Similar structures and enzymes present in all cell types may give insight of the interactions of curcumin with dermal cells.

**Table 4.- Observed and excluded intracellular localization of native curcumin (non-entrapped curcumin) reported in previous studies.** Adapted from Flory *et al.* 2022<sup>122</sup>.

Cell-line	Curcumin concentration (µM)	Incubation time (h)	Localization		Reference
			Confirmed	Excluded	
WiDr (Human colon carcinoma cell line)	7	6	Lysosomes	Nucleus	Singh <i>et al.</i> 2013 <sup>123</sup>
MCF-7 (Breast cancer cell line)	20	4	Cell membrane, cytoplasm, nucleus, mitochondria	*	Kunwar <i>et al.</i> 2008 <sup>124</sup>
Huh-7 (Human hepatocyte derived carcinoma cell line)	5	3	Endoplasmic reticulum, lysosomes	Nucleus, cell membrane, mitochondria	Sala de Oyanguren <i>et al.</i> 2020 <sup>125</sup>
Huh-7	25	24	Endoplasmic reticulum, lysosomes	Mitochondria	Moustapha <i>et al.</i> 2015 <sup>126</sup>
SF-767 (Human glioblastoma cell line)  HepG2 (Human hepatocyte carcinoma)	20	4 and 24	Nucleus	*	Gosh and Ryan 2014 <sup>127</sup>
SF-767	20	0.5 and 1	Diffuse cytosolic	Nucleus	Gosh and Ryan 2014 <sup>128</sup>
SF-767	20	2 and 4	Nucleus	*	Gosh and Ryan 2014 <sup>128</sup>

(\*) not mentioned

Due to its hydrophobic nature, curcumin will easily associate with cell membranes. Once there, curcumin uptake can take place through a passive mechanism<sup>129,130</sup> or endocytic pathway<sup>122</sup> as it has been reported for Caco-2 cells (colon adenocarcinoma cells).

By association to potassium ion channels, in the cell membrane, curcumin has demonstrated to inhibit

proliferation of human monocyte leukemia cell lines and of effector memory cells, respectively leading to anticancer and anti-inflammatory effects<sup>131</sup>.

Once inside the cell, native curcumin could stay in the cytoplasm or go to the organelles. By density gradient centrifugation and subsequent quantification of curcumin and distribution of marker proteins of organelles, Flory *et al.* 2022<sup>122</sup> have reported that once in contact with Caco-2 cells, only 30 min are required for native and micellar curcumin to be present in mitochondria and lysosomes. After 180 min of incubation, native curcumin was present in mitochondria and peroxisomes, while micellar curcumin only in peroxisomes. Passage through lysosomes of native curcumin is in agreement with endocytosis as pathway for native curcumin incorporation into cells, as already reported<sup>132</sup>.

It is known that inside the cell, curcumin is easily reduced to dihydro-, tetrahydro-, hexahydro- or octahydrocurcumin by reductases<sup>133</sup> found in the cytosol or in organelles. Reduced metabolites could have a pharmacological effect and could be at the origin of an increased antioxidant effect. Curcumin or its reduced derivatives can then be conjugated with glucuronide and sulfate moieties by phase II enzymes (UDP-glucuronosyltransferases and sulfotransferases) in the endoplasmic reticulum (ER)<sup>134</sup>. Hydrosoluble conjugates are taken out from the cell by efflux transporters like P-glycoprotein, which have been identified in dermal cells<sup>135</sup>, especially in epidermal keratinocytes of both human and mouse<sup>136–138</sup>.

It is important to note that curcumin presence in mitochondria is important when fighting oxidative stress, as this organelle is one of the biggest sources of ROS in the cell.

When present in the cytoplasm curcumin binds to Keap1 (Kelch-like ECH-associated protein 1) cysteine groups, contributing to Nrf2 stabilisation and translocation to the nucleus. Here, it binds to antioxidant response elements (ARE) and allows the up-regulation of antioxidant genes encoding antioxidant enzymes, thereby increasing overall cell defences against ROS<sup>70,139</sup>.

Fate of curcumin can be impacted by its formulation, even more if such formulation alters the physico-chemical properties of curcumin. Elucidation of uptake and intracellular trafficking of entrapped curcumin is one of the last parts to complete the biological characterization of a newly formulated delivery system.

### **1.3.1.5. Potential in inflammatory skin disorders**

Most of the therapeutic potential of Turmeric is attributed to its main curcuminoid: curcumin. Even if applications are diverse, most of them rely in the antioxidant properties of curcumin as well as in its ability to inhibit nuclear-factor  $\kappa$ B (NF- $\kappa$ B). In consequence, production of inflammatory cytokines are inhibited and the regulation and proliferation of cells is impacted<sup>140</sup>.

*In vitro* and *in vivo* studies have assessed the effect of curcumin in the context of inflammatory physio-

pathological skin conditions as: acute wounds, chronic wounds, hypertrophic scars, keloids, psoriasis and dermatitis. Results suggest that curcumin would be a good candidate to be used in adjuvant therapy in those cases.

**Potential in wound-healing:** Curcumin formulation for topical application in wound-healing is a research area of great interest<sup>141</sup>. In the last years even nanotechnology has been applied<sup>142</sup>. Most of this research is motivated by the fact that curcumin has shown to inhibit transforming growth factor (TGF)- $\beta$ 1 expression and Wnt/ $\beta$ -catenin signalling *in vitro* and to upregulate VEGF *in vivo*, highlighting its role in the proliferative phase of the wound-healing process<sup>143</sup>. Table 5 shows some examples assessing the curcumin potential to treat cases of acute or abnormal wound healing (chronic wounds, hypertrophic scars and keloids).

**Table 5.- Examples of studies assessing the curcumin potential in cases of acute and abnormal wound-healing.**

Type of acute or abnormal wound-healing aimed	Model (type of study)	CUR formulation	Treatment applied	Effect (results)	Ref.
<b>Keloid and hypertrophic scars</b>	<i>In-vitro</i> (earlobe keloid fibroblasts and burn hypertrophic scar-derived fibroblasts)	CUR dissolved in DMEM 10% FBS	1 – 5 $\mu$ g/mL during 72h on cells seeded at density of 8000 cells/cm <sup>2</sup>	Inhibition of proliferation (by inducing arrest of cell growth but not apoptosis) and contraction of the collagen lattice. Both reversible effects with the removal of CUR from culture media.	Phan <i>et al.</i> 2003 <sup>144</sup>
<b>Keloids</b>	<i>In-vitro</i> (Primary keloid fibroblasts from 7 different cultures: earlobe, chest and shoulder)	CUR dissolved in DMEM 10% FBS	25, 50 and 100 nM for 24h	Bleomycin (100nM) induced synthesis of ECM model: inhibition of expression of total soluble collagen, collagen I, fibronectin production and secretion, as well as expression of TGF- $\beta$ 1/p-SMAD-2 were blocked in dose dependent manner in the 7 fibroblast cultures. CUR up-take was followed and occurred in a dose-dependent manner.	Hsu <i>et al.</i> 2010 <sup>145</sup>
<b>Full-thickness wounds</b>	<i>In-vivo</i> (Wistar rats)	Collagen films loaded with 22 % w/w of	2 x 2 cm fragments for 7 days	When compared with non-treated rats or rats treated with films	Gopinath <i>et al.</i> 2004 <sup>146</sup>

		curcumin		without curcumin : well-formed granulation tissue, increase in hydroxyproline content, decrease in enzyme SOD and % of wound closure.	
<b>Full-thickness wounds</b>	<i>In-vitro</i> (3T3-L1 mouse fibroblasts)  <i>In-vivo</i> (rabbits)	Reduced graphene oxide / Carboxymethyl guar gum composite dressing loaded with curcumin	<i>In-vitro</i> : Cells seeded on surface of the dressing. Observation during 48h  <i>In-vivo</i> 2 x 2 cm fragments for 14 days.	<i>In-vitro</i> (scratch assay): Faster gap closure after 48h.  <i>In-vivo</i> (excision wound model): Smaller wound area after 7 days. More activated fibroblasts and less infiltrated inflammatory cells.	Orsu <i>et al.</i> 2021 <sup>147</sup>
<b>Chronic wounds</b>	<i>In-vitro</i> (L929 mouse fibroblasts)  <i>In-vivo</i> (Sprague-Dawley rats)	Bilayer nanofibrous scaffolds (gelatin nanofibers containing CUR and Lithospermum radix on chitosan scaffold)	400 µg/mL CUR solution electrospun on chitosan scaffold (no information of final CUR concentration in scaffold)	<i>In-vitro</i> : cells attached after 24h of incubation  <i>In-vivo</i> (excision model on STZ induced diabetic rats): Faster recovery (58 ± 7 %) and lower levels of pro-inflammatory markers IL-6 and TNF-α, when compared with treatment with gauze.	Yang <i>et al.</i> 2019 <sup>148</sup>
<b>Chronic wounds</b>	<i>In-vitro</i> (NIH 3T3 mouse fibroblasts, HaCaT keratinocytes)  <i>In-vivo</i> (Sprague-Dawley rats)	CUR co-loaded with EGF in NLCs	<i>In-vitro</i> : CUR-EGF-NLCs at 100 ng/mL CUR) during 24 and 48h* on cells seeded at density of 263 000 cells/cm <sup>2</sup>  <i>In-vivo</i> : carboxymethylcellulose gel (3%, w/v) containing 0.63 g/L of CUR in EGF-CUR-NLCs, each 2 days.	<i>In vitro</i> : EGF-CUR-NLCs increased cell migration when compared with treatment with serum free DMEM.  <i>In vivo</i> (excision model on STZ induced diabetic rats, closure at day 3): EGF-CUR-NLCs: 42.1 ± 10.8 %, Blank-NLCs: 8.4 ± 7.5 %, EGF-CUR mix: 29.0 ± 16.8 %, Free EGF: 17.4 ± 11.7 %, Free CUR: 21.4 ± 11.5 %	Lee <i>et al.</i> 2020 <sup>149</sup>

\*not clearly stated

**Potential in psoriasis and dermatitis:** Psoriasis and dermatitis tend to be extended in more than one area of the body which makes that treatments aiming systemic distribution are preferred. However, oral and intravenous administration have reported to either lack of bioavailability or to promote the appearance of adverse effects, respectively.

Table 6 and Table 7 present examples of studies evaluating the impact of curcumin in psoriasis and dermatitis, respectively. Examples presented are limited to those employing a topical administration, which is the aim of this work.

**Table 6.- Examples of studies assessing the curcumin potential in psoriasis topical treatment.**

Model (type of study)	CUR formulation	Treatment applied	Effect (results)	Ref.
Clinical	Turmeric tonic (no concentration described)	No described	Reduction of erythema, scaling, and induration (thickness of lesions).	Bahraini <i>et al.</i> 2018 <sup>150</sup>
Clinical	Alcohol gel (1% curcumin)	No described	Reduced: phosphorylase kinase (Phk) activity, parakeratosis, expression of keratinocyte transferrin receptor (TRR), and density of CD8+ cells.	Heng <i>et al.</i> 2020 <sup>151</sup>
<i>In-vivo</i> (BALB/c mice)	Hydroxypropyl cellulose alcohol gel (1% curcumin)	50 mg/ cm <sup>2</sup> applied daily.	Decrease of pro-inflammatory cytokines expression and inhibition of keratinocyte proliferation.	Sun <i>et al.</i> 2013 <sup>152</sup>
<i>In-vivo</i> (BALB/c mice)	Carbopol gel containing independently loaded nanoemulsions of imiquimod and curcumin (concentration of each active ingredient in gel: 0.5%)	41.7 mg/cm <sup>2</sup> twice a day.	Reduction of psoriasis-like symptoms: scaling, redness, skin thickening and lymphocyte infiltration (adverse effects of imiquimod application).	Algahtani <i>et al.</i> 2020 <sup>153</sup>
<i>In-vitro</i> (psoriatic human keratinocytes and fibroblasts)	Collagen patch containing 10% w/w curcumin loaded chitosan nanoparticles (loaded at 3%)	Cells seeded at top of patches (~ 16 000 cells/cm <sup>2</sup> )	Inhibition of metabolic activity and/or proliferation after 24h.	Terzopoulou <i>et al.</i> 2020 <sup>154</sup>
<i>In-vivo</i> (BALB/c mice)	HPMC gel containing tacrolimus and curcumin co-loaded in lipospheres gel (curcumin concentration 0.025% w/w)	100 mg/day in 2 cm <sup>2</sup> of the dorsal region for 6 days.	Imiquimod induced psoriatic plaque model: reduction of lymphocyte infiltration and levels of TNF- $\alpha$ , IL-17 and IL-12	Jain <i>et al.</i> 2016 <sup>155</sup>
<i>In-vivo</i> (BALB/c mice)	Carbopol gel containing 0.5 % w/w	62.5 mg of gel, (containing 0.5 mg of	Imiquimod induced psoriatic plaque model: from day 4,	Algahtani <i>et al.</i> 2020 <sup>156</sup>

	curcumin nanoemulsion	curcumin) /day on the dorsal region for 10 days.	reduction in skin thickness, redness, inflammation and scaly lesions. Disappearance of symptoms at day 10.	
<i>In-vivo</i> (BALB/c mice)	Nanohydrogel micellar choline-calix[4]arene amphiphile (CALIX) loaded with curcumin (0.09 mg/mL)	62.5 $\mu$ L of nanohydrogel per day on the dorsal region for 7 days.	Imiquimod induced psoriatic plaque model: diminution of epidermal thickening and mast cells degranulation. Restoration of distribution of tight junctions proteins.	Filippone <i>et al.</i> 2020 <sup>157</sup>
<i>In-vivo</i> (BALB/c mice)	Silk fibroin hydrogel containing 3.5 % w/w curcumin loaded polymeric nanoparticles	4 mg of gel containing 500 $\mu$ g of curcumin in 1 cm <sup>2</sup> of the dorsal, every two days for a total of 5 times.	Imiquimod induced psoriatic plaque model: CUR-NPs-gel greatly inhibited the expression of inflammatory cytokines (TNF- $\alpha$ , NF-kB and IL-6) compared to CUR-NPs	Mao <i>et al.</i> 2017 <sup>158</sup>
<i>In-vitro</i> (keratinocytes: HaCaT cell line) <i>In-vivo</i> (C57/BL6 mice)	Carbopol hydrogel containing curcumin loaded PLGA nanoparticles (cur loading in NPs: 47% w/w, NPs loading in hydrogel: 1% w/v)	<i>In-vitro</i> : ~ 105 000 cells/cm <sup>2</sup> treated with 30 $\mu$ M of CUR or CUR-NPs for 24h. <i>In-vivo</i> : CUR gel or CUR-NPs gel containing 0.25 mg of CUR, applied once a day on the back and right ear for 7 days.	<i>In-vitro</i> : CUR-NLCs caused higher antiproliferation of cells treated than CUR solution. <i>In-vivo</i> (Imiquimod induced psoriatic plaque model): CUR-NPs gel application showed less erythema, desquamation thickening of skin and IL-22 levels than CUR gel.	Sun <i>et al.</i> 2017 <sup>159</sup>

**Table 7.- Examples of studies assessing the curcumin potential in dermatitis topical treatment.**

Model (type of study)	CUR formulation	Treatment applied	Effect	Ref.
<i>In-vivo</i> (Kunming mouse)	Supramolecular gel of $\alpha$ -CD containing CUR loaded MPEG-PCL micelles (1.87 g of CUR/L)	60 $\mu$ g for 6h of left ear.	Croton oil-induced ear edema: supramolecular gel was more effective than dexamethasone ointments in reducing thickness and weight of ears and reducing amount of inflammatory cells in dermis.	Zhou <i>et al.</i> 2019 <sup>160</sup>
<i>In-vivo</i> (BALB/c mice for induced ear edema and White New Zealand rabbits for Draize patch test)  <i>In-vitro</i> (tyrosinase inhibition activity)	Carbopol hydrogel at 0.75 % w/v containing CUR-SLNs (0.07 g of CUR/g of SLN)	Draize test (irritation study): 0.5 g applied on 4 cm <sup>2</sup> of hair free skin rabbits.  (DNCB induced ear edema): 20 $\mu$ L of CUR-SLNs loaded gel.  (Tyrosinase inhibition assay): 0.2 mL of CUR-SLNs loaded gel.	<i>In-vitro</i> (Tyrosinase inhibition assay): higher inhibition than Kojic acid , reference standard, showing potential in skin depigmentation.  <i>In-vivo</i> (skin irritation Draize patch test): no skin irritancy of CUR-SLN gel (DNCB induced ear edema): suppression of ear swelling and reduction in skin water content after 4h from application.	Shrotriya <i>et al.</i> 2018 <sup>161</sup>
<i>In-vitro</i> (BALB/c mice)	CUR dissolved in acetone (25 $\mu$ g/ $\mu$ L)	20 $\mu$ L applied in the ear 30 min before edema induction with TNCB.	TNCB induced ear edema: pre-treatment with CUR inhibited ear swelling, thickness of the dermis, and expression of IL-6, IL-4, IL-13 and INF- $\gamma$	Sakai <i>et al.</i> 2017 <sup>162</sup>
<i>In-vivo</i> (CD-1 mice)	CUR dissolved in acetone (100 nmol/mL)	100 $\mu$ L applied just before exposition to TPA (for group TPA + UVA radiation, UVA 18.72 J/cm <sup>2</sup> were applied 2h after TPA exposition in the dorsal area)	Dermatitis induced by TPA (8 nmol) or TPA + UVA radiation: pre-treatment with CUR inhibited infiltration of inflammatory cells and diminished dermal and epidermal thickness, induced by TPA or TPA + UVA radiation.	Ishizaki <i>et al.</i> 1996 <sup>163</sup>

In order for curcumin to be present at the site of action for treat the previously presented skin conditions, it has to be formulated in a pharmaceutical form that can increase its diffusion towards the skin. Even if that can be done through classical pharmaceutical forms, protection of the active ingredient as well as retention and penetration in skin can be optimised by using drug delivery systems such as lipid nanoparticles as it will be described in section 1.4.

## **1.4. Combining formulation technologies for curcumin delivery to the skin**

### **1.4.1. Lipid nanocarriers**

Lipid based nanocarriers include: nano/microemulsions (NE/ME), liposomes, solid lipid nanoparticles (SLNs), nanostructured lipid carriers (NLCs), lipospheres and Lipidic drug conjugates (LDCs). In most of them the stabilization of the active ingredient into the system is achieved by the presence of a charge in the surface or by surface adsorption of a surfactant or polymer layer, or by both methods combined<sup>164</sup>.

Other systems like micelles and cyclodextrins are not formed by lipids, but they have in common the ability to form a hydrophobic compartment which can entrap lipophilic drugs. In the case of micelles, the compartment is formed by the interaction of the hydrophobic moieties of surfactant molecules when they are dispersed in an aqueous medium<sup>165</sup>. Cyclodextrins are cyclic oligomers of  $\alpha$ -D-glucopyranose, in which the hydrophobic compartment is formed by the carbon atoms and ether groups in the cyclic oligosaccharides<sup>166</sup>.

According to the European Commission, in order to be classified as "nanomaterials", such manufactured formulations need to comprise "particles either in an unbound state or as an aggregate wherein one or more external dimensions is in the size range of 1-100 nm for  $\geq 50$  % of the particles according to the number size distribution"<sup>167,168</sup>. For EMA specifications, the formulations need to be "purposely designed systems for clinical applications, with at least one component at the nanoscale that should not exceed 1000 nm"<sup>169</sup>. FDA adds that a so called "nanomaterial" is "engineered to have at least one external dimension, or an internal or surface structure, in the nanoscale range (approximately 1 nm to 100 nm) or it exhibits properties or phenomena, including physical or chemical properties or biological effects that are attributable to its dimension, even if these dimensions fall outside the nanoscale range, up to 1  $\mu$ m (1000 nm)"<sup>170</sup>.

**Nano/microemulsions (NEs/MEs):** even if both of them are composed of two immiscible liquids and a surfactant, stability is the principal difference between nanoemulsions (NEs) and microemulsions (MEs). In the case of O/W microemulsions, they are thermodynamically stable dispersions of lipidic particles (oil, surfactant, and possibly a co-surfactant) in an aqueous dispersant (O/W). Their formation takes place without an external energy supply, and only takes place when specific amount of their components are mixed. Such amounts are often determined by constructing pseudo-ternary diagrams<sup>171</sup>. In contrast, O/W nanoemulsions are thermodynamically instable systems composed of two immiscible liquids, with one of them being dispersed as droplets (stabilized by a surfactant and a co-surfactant) in the other. Their formation needs an energy input that exceeds the positive free energy associated with increasing the contact area<sup>172</sup>. Using the appropriate components, both NEs and MEs W/O can also be prepared.



**Liposomes:** are formed by self-assembling of lipids, mainly phospholipids, in a bi-layer which delimitates an external and an internal both aqueous compartments. They are interesting systems as they can be loaded with hydrophilic molecules (in the internal aqueous compartment) or with lipophilic molecules (in the bilayer)<sup>173,174</sup>. They have good stability which can be further increased by the inclusion of cholesterol, however they have limited capacity for loading hydrophobic compounds as curcumin. Ethosomes are modifications of liposomes in which the inner aqueous compartment includes ethanol in order to increase in some extent the solubility of lipophilic substances in this compartment<sup>175</sup>.

**Solid Lipid Nanoparticles (SLNs):** share the same composition of NE/ME, so they can exist in either the nanometric or the micrometric range. However, in SLNs the lipidic component is completely crystallized. This highly ordered crystalline structure is normally retained at normal room and body temperatures<sup>176</sup>. Even if these systems are very stable, their main drawback is the risk of drug expulsion during preparation and mostly storage due to polymorphic transitions of the lipidic core ( $\alpha$  or  $\beta'$  towards  $\beta$ )<sup>177</sup>, which reflects in low %EE and %DL, and with that the necessity to administrate high amounts of the vector to reach a pharmacological response.

**Nanostructured lipid carriers (NLCs):** can be considered as second generation of SLNs, in which the lipidic part consists in a mixture of a solid and a liquid lipid (oil). As a result, crystallinity is lowered which increases the amount of a hydrophobic substance that can be entrapped and at the same time, the chances of being expelled during storage<sup>178</sup>. This impacts in the %EE and %DL which are higher when compared to SLNs. Besides, there is more chances to reach a controlled release of the substance as the active ingredient is not just dissolved in the oil, but also entrapped in the solid lipid. Compared to NE and ME, they have shown better penetration on skin<sup>179</sup>. That is why in this work NLCs were used as a vectors for curcumin as they offer the possibility of loading high amounts of it and as a result increase the apparent water solubility of the molecule. Also, there is more chances of obtaining a time-stable and biocompatible formulation which can allow the administration of curcumin in the upper layers of skin as well as in the lower ones. These systems will be more in deep described in the following section.

**Lipospheres:** are composed of a single layer of phospholipids embedded in the surface of an inner solid core, and thus, stabilizing it when dispersed in water<sup>180</sup>.

**Lipid-drug conjugates (LDCs):** are drug molecules that have been modified by the addition of lipids (fatty acids, steroids, glycerides or phospholipids)<sup>181</sup>. The resulting molecule has an increased lipophilicity and can be considered as a pro-drug as a part from being used by itself it can be used in the formulation of the other lipidic systems above described.

From all the lipid delivery systems described above, this work will focus on the study of NLCs as a platform for curcumin entrapment and delivery.

#### **1.4.1.1. Nanostructured Lipid Carriers (NLCs)**

First NLCs formulations, containing Coenzyme Q10, arrived to the market in 2005 with the main characteristic to reach high concentrations of the cargo compared to existing formulations, mainly creams<sup>182</sup>. Since then, NLCs are considered among the above described nanocarriers, as good candidates for the topical/dermal delivery of lipophilic molecules such as curcumin. Even if it escapes from the scope of this work, it is interesting to note that outside the area of topical applications, NLCs have been found to be able to increase the bioavailability of curcuminoids, even if not as much as nanomicelles<sup>183</sup>. Also, their ability to encapsulate higher amounts of drug has been found useful for the delivery of curcumin through the blood-brain barrier (BBB) in comparison to SLNs<sup>184</sup>.

**Types of NLCs:** Even if very similar to SLNs and NE/ME, the mixture of lipids (solid and liquid) present in NLCs is a source of variability in their internal arrangement and the location of the drug, which greatly impacts in the stability of the system and the way it releases the drug. These different internal arrangements make possible the existence of different types of NLCs, as showed in Figure 16:

- **Type I: the imperfect crystal**

In this, "imperfections" are created in the solid lipid matrix, resulting in multiple crystallized states of the solid lipid. This is performed by including sufficient amounts of liquid lipid (oil) into the solid matrix.<sup>185186</sup>. The amount of the oil need to be enough to create imperfections among the solid lipid molecules, but not as high to produce a phase separation.

- **Type II: the amorphous**

The principal characteristic is the use of a lipids that do not recrystallize during the cooling of the system. As there are no transitions in the matrix, drug expulsion is minimized.

- **Type III: the multiple**

In this, oil droplets are located inside the solid lipid matrix as a result of a phase separation due to

surpassing the solubility threshold of the oil in the solid lipid<sup>187</sup>. If even more of liquid lipid is used, destabilization of the carrier by leakage can take place.

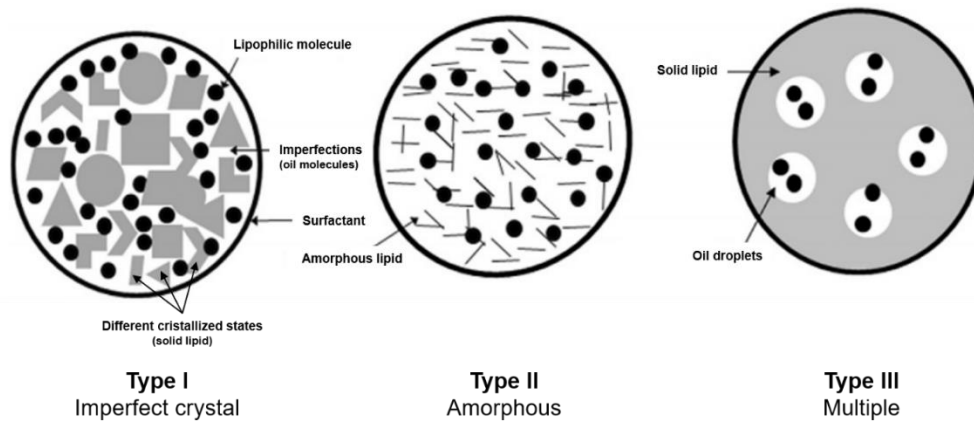


**Figure 16.- Different type of NLCs according to the state of the lipidic matrix.** Modified from Tamjidi *et al.* 2013<sup>186</sup>

**Drug distribution and release:** An active ingredient can be located in different parts of the lipidic core of NLCs during their preparation and storage. Immediately after preparation, this emplacement will mainly depend on the solubility of the active molecule in the solid lipid and in the oil, as well as on the solubility of the oil in the solid lipid which determines the formation of multiple compartments in the NLCs (such as those formed in the inner part of NLCs of type III). During storage and over time, in addition to previous factors, crystallinity and/or amorphous state of the lipidic matrix greatly impact in the expulsion or retention of cargo molecules making them to stay at either the core or the sides of the particles.

As a result, as shown in Figure 17 drug can be homogenously dispersed in the lipid matrix, located in the outer edges (in a shell disposition), in the core, evenly adsorbed forming a monolayer on the surface, or forming clusters (drug patches)<sup>188,189</sup>.

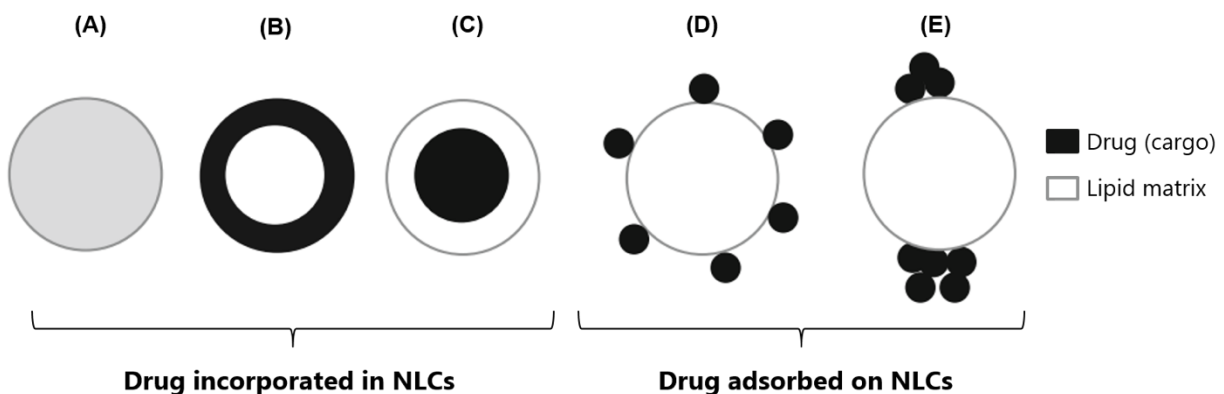


**Figure 17.-Drug distribution on the lipidic matrix of NLCs. (A)** Homogenously incorporated (dispersed). **(B)** Drug enriched outer shell. **(C)** Drug enriched core. **(D)** Drug monolayer adsorbed on the surface. **(E)** Drug clusters on the surface. Modified from Müller *et al.* 2016<sup>189</sup>.

The different placements of the cargo molecules impact in the release profile. For example, a burst release is most likely to take place when molecules are located at the edges (Figure 17-B) or adsorbed on the surface (Figure 17-D, E). On the contrary, a prolonged release takes place in a time dependent manner as result of diffusion of molecules from the core (Figure 17-C), and in some cases, on the degradation of the carrier itself. Such degradation depends on the carrier composition and its biological environment. When drug is homogeneously incorporated in the lipid matrix (Figure 17-A), diffusion and degradation events will allow the sustained release of the drug at a constant rate over time. It is important to note that state of the skin, electrolytes, enzymes and any change in the SC might have an impact in the polymorphic form of the lipid core, its degradation and in consequence in the release of the cargo. Interestingly, the surface adsorption can also be a way of loading the carrier, as it has been done with some proteins<sup>190</sup>. While developing NLCs, imagery techniques accompanied by release studies are a way of getting insight on the internal organization of NLCs.

#### **1.4.1.1.1. Preparation methods**

Methods employed for the preparation of NLCs are based on methods used to preparing emulsions and SLNs. It can be said that in general, all methods are composed of four parts. First, the preparation of two phases: a lipid phase (also known as oil phase) and an aqueous phase. Second, the mixture of them two to form a coarse emulsion. Third, the reduction of the droplet size of by physical means, resulting in a nano-emulsion. And finally, the cooling down of the system which allows the lipid matrix to either crystallise or to fully display its amorphous state, thus, forming NLCs.

It has to be noted that in some specific methods some parts as the mixture of phases and the size reduction might take place simultaneously. However, main differences among reported preparation methods are in the specific procedure through which the emulsion becomes a nanoemulsion (third step). Such procedures can be classified according to the amount of energy they input into the system as "high" or "low" approaches<sup>191,192</sup>.

## High energy approaches

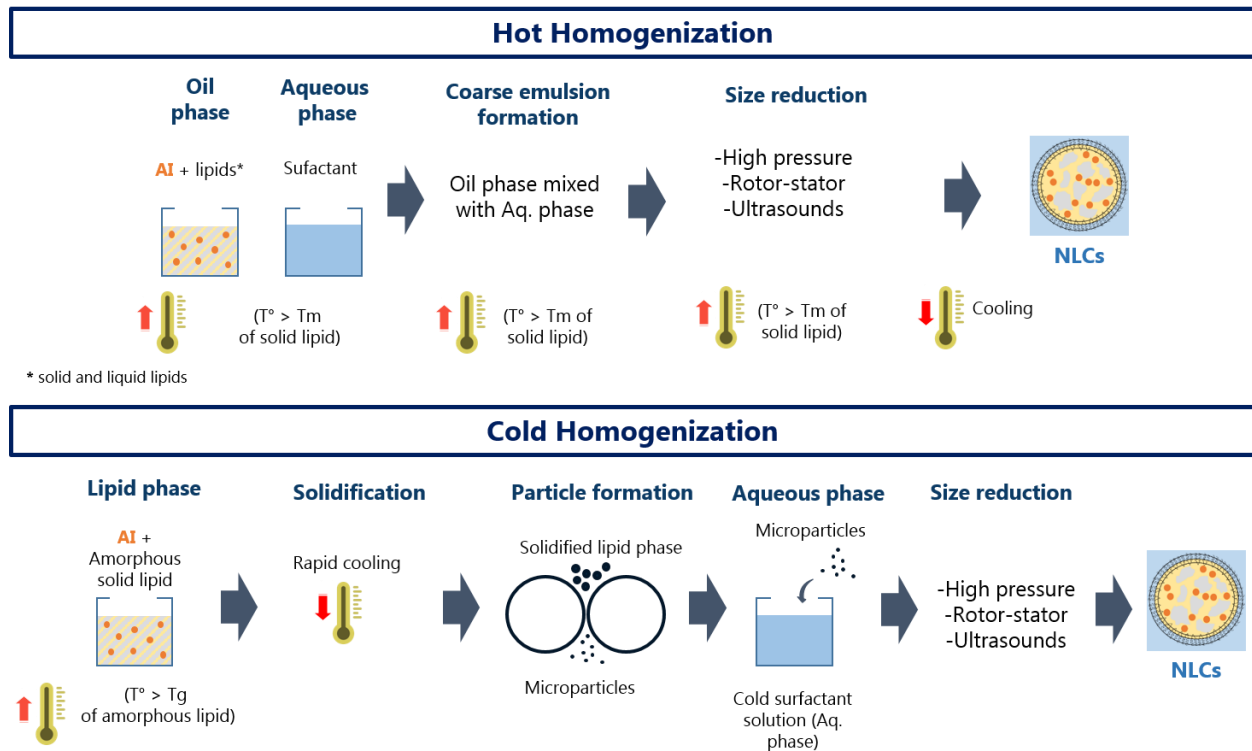


**Figure 18.- High energy approaches for NLCs preparation. Hot Homogenization** which also allows the preparation of NEs and SLNs, if lipids in the oil phase are just liquid or solid, respectively. **Cold Homogenization** which also allows the preparation of SLNs, if the lipid is crystalline. NEs cannot be formed by this method. Further details on each method are described below.

- **Hot-Homogenization**

Procedure is carried-out at temperatures above the melting point ( $T_m$ ) of the solid lipid. Both, lipid matrix and drug are melted and combined with an aqueous surfactant at the same temperature as showed in Figure 18. It has been said that the quality of the coarse emulsion impacts in the quality of the final product. In general, lower particle size can be obtained if higher temperatures are used, as the inner (oil phase) has a lower viscosity<sup>192</sup>. However, if an excess temperature is applied, degradation of the carrier and/or the drug might take place.

Size reduction of coarse emulsion is performed by maintaining the high temperature while letting the coarse emulsion go through a high pressure homogeniser, a rotor stator system or by applying ultrasounds. Each of these devices present apply differently the forces to the coarse emulsion. As final step, the colloidal system is cooled down.

High-pressure homogenization systems: the coarse emulsion is forced to pass through a gap or a channel of a very small diameter ( $<10 \mu\text{m}$ ) by a valve as depicted in Figure 19-A. As a result, the emulsion

undergoes high depressions and pressures (5 to 350 MPa)<sup>192</sup> and droplets are pulverised. Shear can be increased by modifying the surface of channels or using valves with different geometries.

The advantage of this method is that high-pressure homogenizers are used in pharmaceutical industry, particularly for the preparation of parenteral emulsions. That is, a formulation optimized in the lab can be easily scaled-up for industrial purposes<sup>193</sup>.

Rotor-stator system: is the most used homogenizer. It is constituted by a pierced stator or a stator containing gaps and a rotor which spins at very high speeds (Figure 19-B). The coarse emulsion is sucked and forced to pass to a confined zone where it is exposed to high speed gradients where the high shearing, resulting of the small distance between the rotor and the stator ( $\leq 1$  mm), originates its break-up in more little droplets which are finally expelled<sup>192</sup>.

Ultrasounds: sound waves with frequencies comprised between 16 KHz (detectable human limit) and 1MHz, which are emitted by a plane surface vibrating in a sinusoidal way around its equilibrium point with a fixed frequency and an amplitude in the  $\mu\text{m}$  range (Figure 19-C). When exposed to low frequencies ( $\sim 20$  KHz), droplets slightly change their diameter and can be present in the medium for long times. But, when exposed to high frequencies ( $\geq 500$  KHz), the diameter of the droplet can increase several times, until it implodes due to cavitation forces originating smaller droplets with diameters below  $1 \mu\text{m}$ <sup>192</sup>.

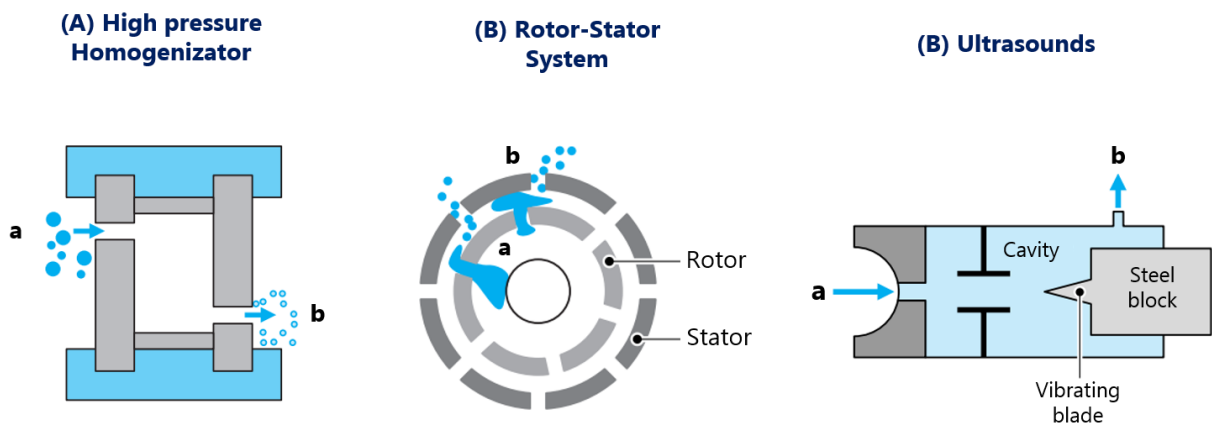


**Figure 19.- Equipment used for size reduction during Hot-Homogenization. (A) High pressure homogenisator:** swirl chamber which can impart pressures from 5 – 80 MPa. For higher pressures (until 350 MPa) swirl jets can be used. **(B) Rotor-stator system:** teathed operating head is depicted. It is used for processing low density mixtures and possess high cutting action.<sup>194</sup> Bladed operating head is also available, but it is used to process highly dense mixtures which are rare while preparing NLCs. **(C) Ultrasounds:** whistle system in which the coarse emulsion is accelerated through a hole and the formed jet hits a blade which starts to vibrate. By changing the speed of the coarse emulsion and the distance between the hole and the blade, the wave frequency (frequency of resonance of the blade) and its intensity can be tuned. Other systems based on piezoelectric or magnetostrictive transducers are available but they present a limited yield when used at high temperatures.<sup>192</sup>. For each equipment: **(a)** Entry of coarse emulsion at high pressures. **(b)** Exit of small sized emulsions at low pressures. Modified from Poux and Canselier 2004<sup>192</sup>.

- **Cold-Homogenization**

This procedure can be applied for NLCs of the amorphous type, so that any liquid lipid is used, but instead an amorphous solid. Briefly, by maintaining relatively high temperatures, the lipid undergoes a phase transition that allows the drug to be incorporated. This mixture is rapidly solidified with dry ice or liquid nitrogen. The speed of this change in temperature will favour a homogenous distribution of the drug into the whole matrix. Next, the lipid phase is grounded to microparticles whose size can be further reduced by dispersion in a cold surfactant solution and subjecting the suspension to a high homogenisation procedure<sup>191,195</sup>.

## Low energy approaches

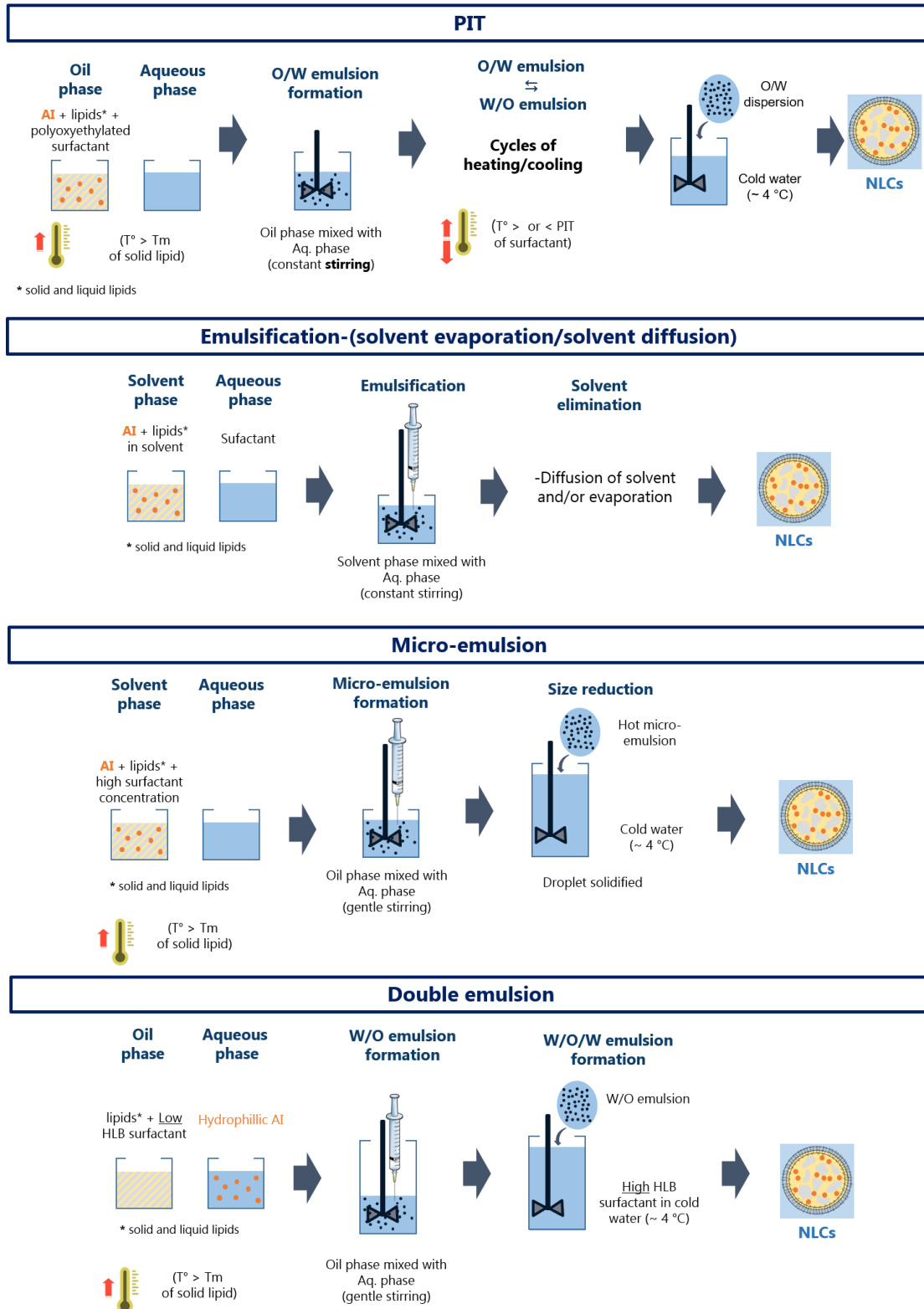


**Figure 20.- Low energy approaches for NLCs preparation.** PIT, which needs the presence of a surfactant with the ability to change its water affinity according to temperature. **Emulsification-(solvent evaporation/solvent diffusion) technique**, which needs the presence of organic solvents or partially water-miscible solvents, depending of lipids used NEs and SLNs can also be prepared by this technique. **Micro-emulsion technique**, which needs important amounts of surfactants. **Double emulsion technique**, for incorporating hydrophilic molecules into NLCs. All techniques can be adapted to the preparation of NEs and SLNs by varying the type of lipids used. Only key components are presented for each method. Further details of each method are described below.



- **Phase inversion temperature (PIT) technique**

This mainly relies in the change of properties of polyoxyethylated surfactants (for example Tweens) at different temperatures. In brief, the HLB value for these surfactants is defined at 25°C, where their hydrophilic parts are hydrated to a certain extent. However, the dehydration of the ethoxy groups occurs at higher temperatures, this implies that the lipophilicity of the surfactant molecules will rise (and the HLB value will decrease). At certain temperature, the affinity of the surfactant molecules for the aqueous and for the lipid phase will be equal. This is called the phase inversion temperature (PIT). At this state the system has a very low surface tension, and if the temperature is further increased the affinity of the surfactant molecules for the lipid phase will become higher enough to stabilize W/O emulsions. If the system is then cooled down, the reverse process takes place. Experimentally, after the lipid and the aqueous phase are both heated, aqueous phase is dispersed in the lipid one by sheering and then usually 3 heating and cooling cycles are applied, and finally the obtained dispersion is diluted with cold water<sup>191</sup>.

- **Emulsification-(solvent evaporation/solvent diffusion) technique**

Either in the emulsification-solvent evaporation technique or in the emulsification solvent diffusion technique, the lipids and the lipophilic active ingredient are first dissolved in either organic solvents like chloroform or ethylacetate (for solvent evaporation technique) or in partially water-miscible solvents like benzyl alcohol, butyl lactate or tetrahydrofuran (for solvent diffusion technique). Then the emulsion is formed by adding the solvent phase to an aqueous surfactant solution under continuous stirring <sup>196-198</sup>. In the case of the emulsification-solvent evaporation, stirring is usually performed overnight in order to let de solvents evaporate under a hood. Vacuum can be used to accelerate the elimination of the solvent. In the case of emulsification-solvent diffusion, the partially water-miscible solvent will diffuse towards the water, leaving behind the lipid components in NLCs form.

Both techniques are interesting while trying to limit the exposition of the drug to high temperatures. However, their main drawback is that they might leave be residues of the solvents in the formulation.

- **Micro-emulsion technique**

Here, the thermodynamic stability of microemulsions is used. For this a high surfactants/lipid ratio is required. Proportions of excipients is essential, so that they fall in the areas of microemulsion formation in pseudo-ternary diagrams. As is previous methods, melted lipids are mixed with a hot surfactant solution with gentle stirring is applied until the microemulsion is formed. Then, the hot microemulsion is dispersed in a high volume of cold water (~ 4 °C) with moderate stirring causing the droplets to solidify. Due to the process, it is more possible that obtained particles have a spherical shape and narrow size distribution. However, obtained suspensions are very diluted (1:25 up to 1:50) respect to the concentrated suspensions obtained by hot emulsion <sup>191</sup>. Very often this will imply the implementation

of further concentration methods (like ultrafiltration or lyophilisation) which need to be fully optimised to reach a batch to batch reproducibility. In addition, the amount of surfactants (and co-surfactants) used can be toxic depending on the application <sup>199</sup>.

- **Double emulsion technique**

This technique is mainly useful for the incorporation of hydrophilic active ingredients, and interesting molecules like peptides into NLCs. First, the melted lipid is mixed with an aqueous solution containing the hydrophilic drug to form a W/O emulsion. For this, it is important that that a surfactant with a low HLB value is used. Then, the primary W/O emulsion is dispersed in an aqueous solution of a hydrophilic emulsifier (with high HLB) in order to form a double W/O/W emulsion. Finally, the double emulsion can be isolated by filtration. Main drawback is that relatively large particles are obtained, but it offers the possibility of modify the surface of NLCs by for example adding PEG molecules<sup>200</sup>.

### 1.4.1.1.2. Components

One of the principal advantages for NLCs development is that they can be formulated using excipients classified as inactive ingredients and GRAS (Generally Recognized As Safe) materials by the FDA<sup>201–203</sup>. In fact, most of them are currently used in pharmaceutical and cosmetic formulations, thus their toxic concentrations as excipients are well known. Some of the most common excipients used for NLCs preparation are listed in Table 8.

During NLCs development, interaction between excipients, interactions of the excipients with the AI and stability during the preparation method are aspects to pay especial attention.

**Table 8.- Most common excipients used in the formulation of NLCs.** <sup>83,204,205</sup>

Excipient	Chemical groups	Examples
<b>Solid lipid</b>	Saturated fatty acids	Stearic acid, Palmitic acid, Decanoic acid, Behenic acid
	Saturated fatty alcohols	Emulcire ® 61
	Fatty acid and fatty alcohol esters	Cetyl palmitate
	Glycerides	Tristearin, Trilaurin, Trimystin, Tripalmitin, Precirol ATO® 5, Compritol ® 888 ATO, Dynasan ® 116, Dynasan ® 118, Softisan ® 154, Imwintor ® 900 P, Geleol ®, Gelot ® 64, Shea butter, Softisan 100, Witepsol W 35, Witepsol H 35.
	Others	Cholesterol
<b>Liquid lipid (oil)</b>	Mineral oils	Paraffin oil
	Fatty alcohols	2-octyl dodecanol
	Unsaturated fatty acids	Oleic acid
	Fatty acid and fatty alcohol esters	Isopropyl myristate
	Glycols	Transcutol ® HP, Lauroglycol ® FCC, Labrasol ®
	Glycerides	Miglyol 812, Labrafil Lipophile ® WL 1349, Labrafac ® PG, Capryol ® 90, Labrafac Lipophile ® WL 1349, Capmul ® MCM EP, Labrafac ® M, Saboderm TCC
	Others	Squalene, Vitamin E
<b>Emulsifiers</b>	Hydrophilic	Poloxamer 188, Poloxamer 407, Poloxamine 908, Tween 20, Tween 40, Tween 80, PVA, Solutol ® HS15, Trehalose, odium deoxycholate, sodium glycocholate, sodium oleate, polyglycerol methyl glucose distearate
	Lipophilic	Myverol ® 18-04K, Span 20, Span 40, Span 60.
	Amphiphilic	Egg lecithin, soya lecithin, phosphatidylcholines (ex. Phospholipon ® 90 G), phosphatidylethanolamines, Gelucire ® 50/13.

### 1.4.1.1.3. NLCs for CUR delivery to the skin

As presented in Table 9, NLCs systems developed for curcumin delivery to the skin have demonstrated to efficiently entrap curcumin while presenting a nanometric size. It is to note that the inclusion in NLCs increased drug deposition in the upper layers of the skin (SC and living epidermis). Also, systems were able to achieve a prolonged drug release which was mainly determined by the excipients composing NLCs. Formulation into multiscale system was performed for six out of nine studies cited below as way is increasing

residence time on the skin and facilitate drug diffusion. Carbomer gels were the most common matrix for the formulation of the multiscale systems, however characterization is mostly limited to the effects on skin penetration of the drug, leaving aspects as physical characterization unattended.

Despite the promising results in treating wounds or psoriasis, only two out of nine systems were evaluated in their antioxidant capacities either by determining their ability to neutralize ROS *in situ* or their potential to promote an antioxidant response after application. However, both types of antioxidant characterization were never performed at the same time for the same NLCs system.

**Table 9.- NLCs systems formulated for CUR entrapment and delivery to the skin**

Reference	CUR source	System and preparation	Multiscale formulation	Results	Antioxidant evaluation
Kang <i>et al.</i> 2018 <sup>206</sup>	CUR from Sigma-Aldrich (St. Louis, MO, USA)	Shea butter + Capmul® MCM EP  Solvent diffusion method (using acetone)	Incorporation in cellulose nanofiber (CNF) film	Size: 534 ± 9 nm. ZP: -24.5 ± 1.7 mV.  Deposition of CUR on skin increased 2-fold by CUR-NLCs/CNF, compared to CUR/CNF  Reduction of pro-inflammatory cytokine levels (TNF-α and IL-6) after 48 h in <i>in vivo</i> IMQ-induced psoriatic mouse model.	Not performed
Rapalli <i>et al.</i> 2020 <sup>207</sup>	CUR from HiMedia (Mumbai, India)	Precirol® ATO 5 + Labrafac M + Tween 80  Hot homogenization (ultrasounds)	Incorporation in Carbopol 974P NF gel (0.75 %, w/v)	Size: 96 ± 1 nm. ZP: -15.2 ± 0.6 mV. PDI: 0.240 ± 0.180. EE%: 70.5 ± 1.7 %  Sustained release until 48 h in PBS/EtOH/Isopropyl alcohol/Tween 80, 78.5%/5%/15%/1.5%, v/v (pH=6.4).  Permeation and skin retention of CUR increased 3.24-fold by CUR-NLCs/gel compared to CUR/gel.  Improved up-take of CUR-NLCs by HaCaT keratinocytes compared with CUR dispersion in PBS/EtOH/Isopropyl alcohol/Tween 80, 78.5%/5%/15%/1.5%, v/v.	Not performed
Espinosa-Olivares <i>et al.</i> 2020 <sup>208</sup>	Turmeric powder (purity :81%) from Sigma-Aldrich (St. Louis, MO,	Labrasol® + Compritol® 888 ATO + Tween 80  Hot homogenization	Not performed	Size: 214 ± 8 nm. ZP: -15.5 ± 0.6 mV. PDI: 0.200 ± 0.020. EE%: 79.70 ± 1.00 %  38% of CUR released during 9h in EtOH/H <sub>2</sub> O 50%/50%, v/v at 37°C.	% ABTS•+ inhibition reduced only after 3 months storage at 25°C (10 %

	USA)	(rotor-stator system)		<i>Ex vivo</i> skin permeation of CUR increased 1.6-fold by CUR-NLCs compared to CUR dispersion in EtOH/H <sub>2</sub> O 50%/50%, v/v. Increased CUR penetration and deposition in skin.	less) or after 9 days without light protection at RT (20% less).
Liakopoulou <i>et al.</i> 2021 <sup>209</sup>	CUR from Acros Organics (New Jersey, USA)	Softisan 100 + Saboderm TCC + Lecithin  Hot homogenization (ultrasounds)	Not performed	Size: 119 ± 3 nm. ZP: -66.2 ± 1.6 mV. PDI: 0.300 ± 0.06.  37% of CUR released during 32h in PBS/EtOH, 50%/50%, v/v (0.1 % ascorbic acid, pH= 5.5) at 32°C.  CUR-NLCs showed increased film forming capacity, CUR protection from photodegradation faster <i>in vitro</i> wound-healing (at lower CUR dose) when compared with equivalent CUR-NEs.	Not performed
Lee <i>et al.</i> 2020 <sup>149</sup>	CUR from Sigma-Aldrich (St. Louis, MO, USA)	EGF + Precirol® ATO5 + Capryol® 90 + Poloxamer 188 + Tween 80.  Double emulsion method	Not performed	Size: 332 ± 29 nm. ZP: -6.64 ± 0.51 mV. EE% : 99.4%  90% released in 24h in PBS at pH 7.4  EGF-CUR-NLCs increased cell migration <i>in vitro</i> of NIH 3T3 fibroblasts and HaCaT keratinocytes, as well as wound closure <i>in vivo</i> .	Increase of activity of antioxidant enzymes (SOD, catalase, GPx) <i>in vivo</i> .
Chen <i>et al.</i> 2016 <sup>210</sup>	CUR from from Zhu'hai Fuxingyuan Food Industry Co. Ltd. (Zhu'hai, China)	Caprylic/capric triglyceride + Solutol® HS15 + Soya lecithin  Solvent evaporation (chloroform/acetone, 50%/50%, v/v)	Incorporation in Poloxamer 407 gel (20 % w/v)	Size: 264 ± 3 nm. PDI: 0.244. ZP: -18.6 mV. EE%: 91.76 ± 0.31%  CUR-NLCs and CUR-NLCs/gel increased respectively, 3 and 2.4 times, the penetration of CUR <i>in vivo</i> , compared to CUR dissolved in propylenglycol.  CUR-NLCs/gel reduced irritation while weakening the SC <i>in vivo</i> .	Not performed
Riaz <i>et al.</i> 2019 <sup>211</sup>	CUR from Sigma-Aldrich (Germany)	Glyceryl monostearate + Phospholipon® 90G + Tween 80 + Isopropyl myristate  Hot homogenization (rotor-stator system) + ultrasounds	Incorporation in Carbopol 934 gel (0.5 % w/v)	Size: 312 ± 2 nm. PDI: 0.305 ± 0.170. ZP: -38.0 ± 0.9 mV. EE%: 88 ± 2 %  80% CUR released in 24 in PBS at pH 7.4 and 5.5  CUR-NLCs compared to CUR in 0.25% v/v EtOH: lower IC <sub>50</sub> against Leishmania promastigotes and amastigote forms  Higher CUR deposition in SC for	Not performed

				CUR-NLCs/gel compared to CUR/gel.	
Kesharwani <i>et al.</i> 2020 <sup>212</sup>	CUR from Arjuna Natural Ltd. (Kerala, India)	Precirol ® ATO 5 + Capmul MCM + Tween 80  Hot homogenization (rotor-stator system) + ultrasounds	Incorporation in Carbopol 980 gel (0.75 % w/v)	Size: 189 ± 3 nm. ZP: -21.5 ± 1.3 mV. PDI: 0.262 ± 0.240. EE%: 86.72 ± 0.90 %  60% of CUR released in 24h in PBS (pH:6.8 at 37°C)  3-fold increase in CUR accumulation in the epidermis of CUR-NLCs/gel compared to CUR/gel	Not performed
Padmini and Gupta 2019 <sup>213</sup>	CUR from Chaitanya Agro Herbals. (Mysore, India)	Caffeine + Stearic acid + Oleic acid + soya lecithin + PVA  Hot homogenization (ultrasounds)	Incorporation in Carbopol 934 gel (0.5 % w/v)	Size: 104 nm. EE%: 62.31 %  75% of CUR released from NLCs in 12h (PBS at pH 7.4)  Caffeine-CUR-NLCs/gels reduced scaling and thickening of epidermis/dermis after 8 days in an IMQ induced psoriatic <i>in vivo</i> model.	Not performed

While aiming a topical administration for curcumin, NLCs are a good strategy as they could not just increase the apparent water solubility, but also offer a better balance between stability and drug entrapment, occlusion properties which contribute to maintain or restore the barrier function of skin, act as a reservoir at the surface of skin and increase the concentration so that by diffusion released curcumin can more easily penetrate into the SC<sup>177,214</sup>. In the cases where the skin is thickened as in psoriasis or keloids, due to their micro/nanometric size, NLCs could offer better chances to reach deep skin layers and let their cargo to be in contact with cells so that it can exert its pharmacological effect. Moreover, in cases where the barrier function of skin has been affected like in acute, chronic wounds or dermatitis, NLCs are mostly biocompatible allowing the delivery of active ingredients, but with low risk of undesirable or toxic effects.

### 1.4.2. Hydrogels

Gels can be defined as a tri-dimensional network of macromolecules (polymers or colloids) holding a liquid phase. Main characteristics of such systems are:

- 1) Their two components form a homogeneous system: a solid phase dispersed in a liquid phase
- 2) Both phases are continuous and occupy the whole volume of the system.
- 3) They behave as viscoelastic materials: intermediate behaviour between an elastic solid (deformation is proportional to the applied shear stress) and that of a liquid (deformation increases in time as long as a shear stress is applied) <sup>215</sup>.

A gel is formed through a sol-gel transition. During this phenomenon, the macromolecules dissolved or dispersed in the liquid aggregate and will form an infinite cluster. Gels can be classified as chemical or physical according to the nature of these interactions. Physico-chemical and mechanic properties are greatly dependant on the nature of the interactions holding-up the cluster:

**Physical gels:** Interactions between macromolecules building-up the gel are low-energy bonds like Van der Waals, ionic interactions and hydrogen bonds, where the energy is no more than  $2 \text{ kcal.mol}^{-1}$ . (Figure 21-A) In these type of gels the sol-gel transition is reversible according to the physico-chemical characteristics of the environment such as the temperature, the pH and the ionic force<sup>216</sup>.

**Chemical gels:** The tri-dimensional network is formed by covalent bonds (chemical bonds) between the macromolecules building-up the gel (Figure 21-B). Chemical reactions like copolymerisation and polycondensation are the origin for these high-energy bonds.

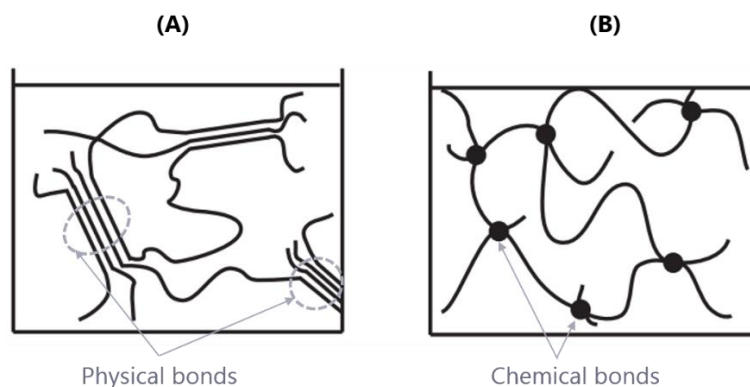


**Figure 21.-** General structures of the network in **(A) a physical gel** and **(B) a chemical gel**. Modified from Papon *et al.* 2006<sup>217</sup>.

According to the type of the liquid phase, gels can be swollen by an organic phase (organogels) or by water (hydrogels). Macromolecules being able to form hydrogels present  $-\text{OH}$ ,  $-\text{CONH}-$ ,  $-\text{CONH}_2-$  and  $-\text{SO}_3\text{H}$ - groups and are interesting for biomedical applications as they can absorb important amounts of water, aqueous solutions or body fluids (thousands of times their dry weight)<sup>218</sup>.

#### 1.4.2.1. Hydrogels as topical therapeutic materials

Hydrogels have been widely used in food industry, art, medicine and cosmetics. The term "hydrogel" appears for the first time in the scientific literature in 1984, and it was used to designate a colloidal system of inorganic salts<sup>219</sup>. In 1960, Wichterle and Lim<sup>220</sup> were pioneers in applying the term "hydrogel" as we know it nowadays: "as water-swollen crosslinked macromolecular network". They used poly(2-hydroxyethyl methacrylate) to develop soft contact lenses<sup>220</sup>.

Since then, the biomedical industry has largely used hydrogels for tissue engineering because of their inherently physico-chemical, mechanical and biological characteristics which greatly depend of the type of polymer (macromolecule) and of the nature of the interactions contributing to form the tri-dimensional structure. In more recent times, hydrogels are being used as scaffolds for controlled drug release. In this way, inherently properties of each gel are combined with the possibility of delivering small molecules, biological macromolecules (proteins, growth factors) and even micro and nanostructures to form systems being able to also exert a therapeutic effect.

Due to its accessibility, variety of pathological conditions and its role in peoples' aesthetics, skin has been one of the most studied organs for the application of hydrogels as tissue engineering materials and/or to drug delivery. Advanced hydrogel formulation has made possible advances in the creation of artificial skin due to the similarities of the ECM and the composition of a hydrogel<sup>221,222</sup>.

In recent times, a new generation of hydrogels: "smart hydrogels" are capable to react to physico-chemical and biological stimuli: presence of ROS, pH, temperature, radiation, magnetic and electric fields<sup>223-225</sup>.

In wound-healing, interest of hydrogels is clear for both acute and chronic wounds. Even if different, hydrogels have adhesion properties, they are easy to remove which allows to prevent any further injury to the treated tissue once therapy is applied. Due to their high water content, hydrogels have the potential to improve wound-healing as it has been shown that healing can be enhanced in a moist environment, especially in acute/superficial wounds. A moist environment can improve reepithelization during wound healing by accelerating collagen secretion and deposition, induction of fibroblasts and keratinocytes migration, stimulation of wound contraction and remodelling, attenuation of scar formation, normalization of pro-inflammatory cytokines and by providing a proper environment for angiogenesis<sup>226</sup>.

In chronic wounds, swelling properties of hydrogels can be exploited to reduce the secretion of fluids. Moreover, some polymers like polyethylene glycol (PEG) can be modified to give them antibacterial properties which can contribute to prevent the formation of biofilms in wounds<sup>227</sup>.

In psoriasis, a wet environment is also important as it has been proved that it can reduce hyperkeratosis, parakeratosis and hyperplasia. Demonstrating the interest of using these highly hydrophilic materials in such conditions.

A particular characteristic of hydrogels is their capacity to adhere to skin which can be used to increase the



residence time of drugs on the skin and to promote penetration to deeper layers. This is interesting for promoting drug penetration through a highly cornified (and thus hydrophilic) SC as the one present in psoriasis cases.

On irritated skin, like in dermatitis, hydrogels can have a cooling and soothing effect while also offering the possibility to deliver molecules to modulate the deregulated anti-inflammatory responses<sup>228</sup>. Moreover, if designed hydrogels contain lipid components similar to those found in skin, less irritation can be expected. This can be achieved for example by formulating composite materials by the inclusion of lipid based micro/nanoparticles.

As it has been mentioned in previous parts of this review, most common treatments for psoriasis, dermatitis and hypertrophic scars involve the systemic or intralesional administration of drugs as corticosteroids which can cause adverse effects. The aim in these cases is to be able to administrate therapies by a topical route in order to reduce the chance of having side effects while diminishing the amount of the required drug to be administrated. Such requirements can be fulfilled by the utilisation of hydrogels which are able to deliver active molecules or particles by different process, like diffusion, deformation, erosion or swelling:

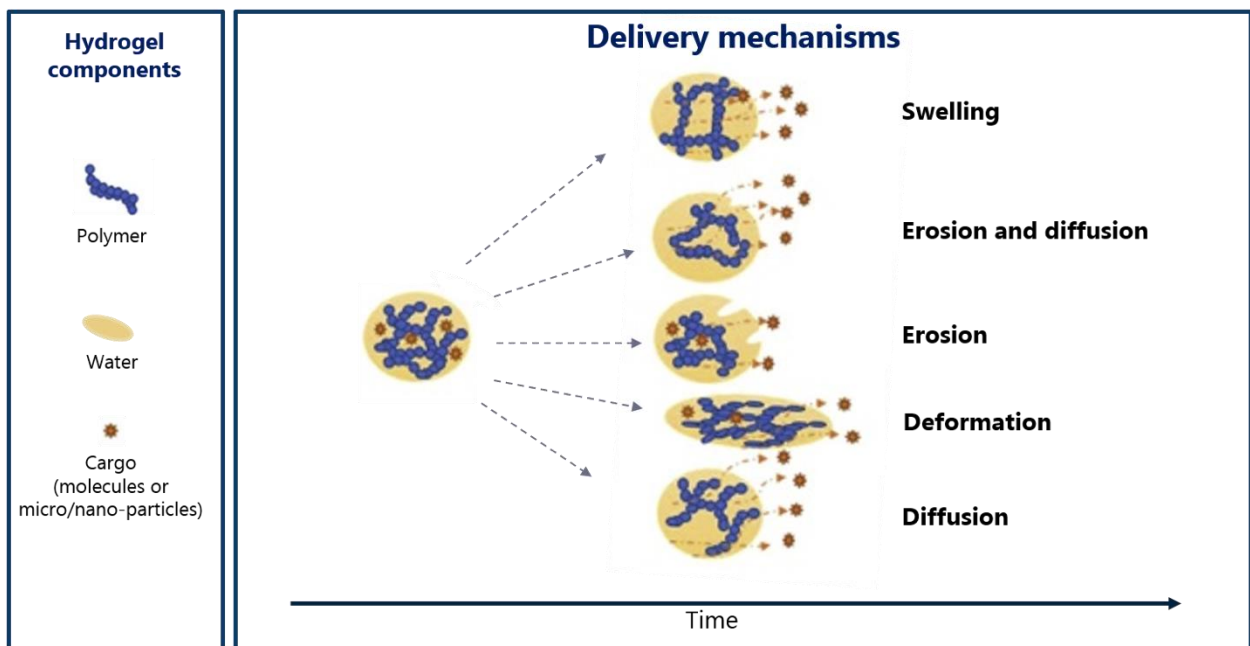


Figure 22.- Delivery mechanisms in hydrogels. Adapted from Esposito *et al.* 2018<sup>229</sup>.

### **1.4.2.2. Hydrogels in pharmaceutical and cosmetic formulations**

Liquids or suspensions of low viscosity are not an optimal pharmaceutical form for a topical administration in which the delivery of a cargo to the skin is aimed for a therapeutic or cosmetic application. The lack of adhesion to the application site of liquids or suspensions, limits the residence time necessary for the transfer of the cargo, hindering its passage to the skin. The more the residence time of a compound on skin's surface, the more the concentration will be at a defined time point. According to Fick's Law this will increase the flux of the drug through the skin.

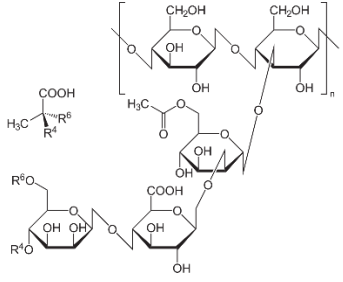
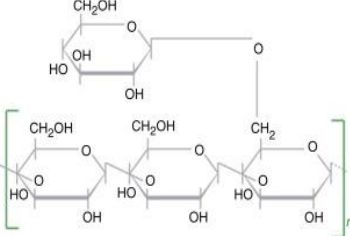
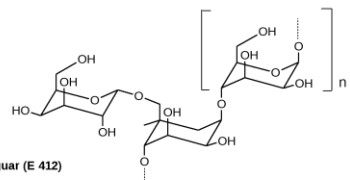
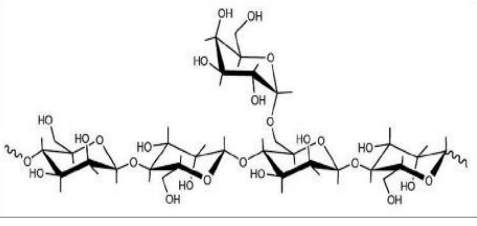
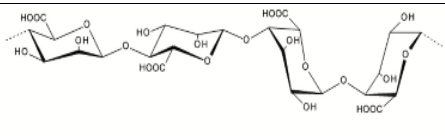
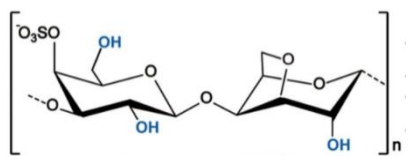
In such scenario, including liquids and suspensions as the media for the formation of the macromolecular networks of hydrogels is an interesting approach to provide a matrix being able to adhere to skin and act as a reservoir for the cargo, facilitating its diffusion to the inner layers. The jellification of liquids or of the continuous phase of suspensions might also facilitate their application as the resulting composite system would present viscoelastic properties that will be mainly translated in the diminution of their viscosity while applying shear forces.

Other advantage of increasing the viscosity of the dispersant, is to increase the stability of suspensions or emulsions during storage. In addition, the translucent aspect that they give to composite formulations is well appreciated by consumers.

It is important to mention that in some cases, macromolecules (polymers) capable of forming the tri-dimensional network of physical hydrogels can be dissolved or dispersed in a continuous aqueous phase in such concentrations that they will not be able to fully interact with others. Even if in such cases there is no formation of the tri-dimensional network, there will be an increase in the density of the formulation. In the formulation science, those polymers used at concentrations below the one needed for the sol-gel transition are called "thickening agents". If concentrations above those required for the sol-gel transition are used they will be referred as "gelling agents" or simply, gels.

Table 10 is a more detailed list than the one in part 1.2.2.1. of this chapter, and presents the main characteristics of some of the most common used thickening/gelling agents found in pharmaceutical and cosmetic formulations and which can be used as part of the composition of fluid gels. They are presented according to their origin: natural, semisynthetic or synthetic.

**Table 10.- Thickening/gelling agents for the formulation of fluid gels in pharmaceutical and cosmetic formulations.**<sup>83,230,231</sup>

<b>Natural</b>				
<b>Common name (<i>INCI</i>)</b>	<b>Chemical structure</b>	<b>% utilisation</b>	<b>Incompatibilities</b>	<b>% of cosmetics having it</b>
Xanthan gum ( <i>Xanthan gum</i> )		0.1-1% (not regulated in EU)	Cations and aluminium salts	17.23 %
Sclerotium gum ( <i>Sclerotium gum</i> )		0.25-2%	Cationic preservatives	0.72%
Carob gum ( <i>Ceratonia siliqua gum</i> )	Motif de base des galactomannanes  n = 1 pour le guar (E 412) n = 2 pour la gomme tara (E 417) n = 3 pour la caroube (E410)	0.1-1%	Cations and aluminium salts	0.23%
Tara Gum ( <i>Caesalpinia spinosa gum</i> )		0.5-2%	Cationic preservatives	0.38%
Alginates ( <i>algin</i> )	 M-block    G-block (1-3)-linked β-D-mannuronate    (1-3)-linked α-L-guluronate	0.2-2%	Divalent ions and metals	0.64%
Carrageenans ( <i>Carrageenan</i> )		0.1-1%	-----	0.6%

Semisynthetic				
Common name (INCI)	Chemical structure	% utilisation	Incompatibilities	% of cosmetics having it
Microcrystalline cellulose ( <i>microcrystalline cellulose</i> )		1-2.5%	-----	1.02%
Hydroxyethylcellulose ( <i>Hydroxyethylcellulose</i> )		0.1-1%	-----	3.72%
Synthetic				
Common name (INCI)	Chemical structure	% utilisation	Incompatibilities	% of cosmetics having it
Acrylic acid derivates (example: <i>carbomer</i> )		0.1-3%	Electrolytes and cationic molecules	9.34%
Associative polymers (example: <i>Polyacrylate crosspolymer-11</i> )		0.1-1.5%	-----	0.03%
Cationic gelifiers (example: <i>Polyquaternium-37</i> )		0.2-5%	Anionic molecules	0.97%

Derivates of acrylic acid can be carbomers, sodium polyacrylates, acrylic acid copolymers, alkyl acid copolymers, alkyl graft acrylic acid copolymers and modified sulfonated acrylic acid copolymers. From all these, carbomers are the more used ones mainly due to the transparent appearance and good sensorial properties they offer to the formulation.

As shown in Table 10, 9.34% of pharmaceutical or cosmetic formulations have carbomers as either a thickening or a gelling agent, compared to sodium polyacrylates (2.23 %), acrylic acid copolymers (0.78 %) and alkyl acid copolymers (0.05%). Data about the presence of alkyl graft acrylic acid copolymers and modified sulfonated acrylic acid copolymers in pharmaceutical products and cosmetics is very scarce<sup>231</sup>.

#### 1.4.2.2.1. Carbomer hydrogels

Carbomers, also known with the brand name of Carbopol® are greatly employed in pharmaceutical products and cosmetics as they endow formulations with a transparent appearance, good suspending ability, as well as good sensorial and adhesion properties. Moreover, they have been reported to have low potential for skin irritation and sensitization<sup>232</sup> and to be biocompatible with dermal cells<sup>233,234</sup>. Even expositions to very high concentrations (> 50% v/v) showed no irritation signals in animal models<sup>232</sup>.

**Chemistry and classification:** Carbomers are polymers of acrylic acid crosslinked with allyl sucrose or allyl ethers of pentaerythritol<sup>83</sup>. Figure 23 shows their general composition.

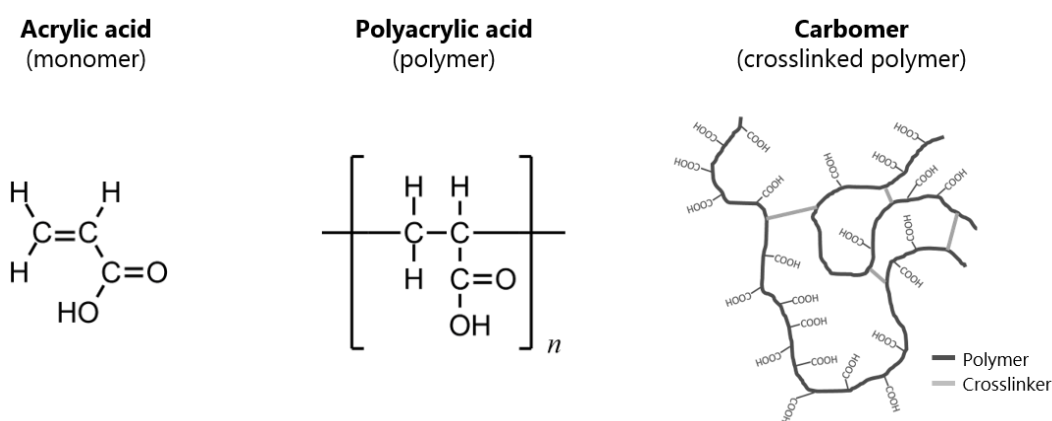


**Figure 23.- General composition of carbomers.**

Differences in the nature of the crosslinker used to hold-together the polymer chains and the formation of copolymers with other chemical identities (alkyl acrylates, polyethylene glycol) characterize the different types of available carbomers as presented in Table 11.

Type A, Type B or Type C polymers refer to increasing degrees of crosslinking of the same polymer. The more the crosslinking degree, the more the viscosity of the resulting gel.

**Table 11.- Carbomer types according to the composition of polymer chains and cross-linker used between them**<sup>235,236</sup>

Carbomer polymer type	Composition	Example
Homopolymers	Polymers of acrylic acid crosslinked with allyl sucrose or allyl pentaerythritol.	Type A: Carbopol® 971G Type B: Carbopol® 974P Type C: Carbopol® 980
Copolymers	Polymers of acrylic acid and C10-C30 alkyl acrylate crosslinked with allyl pentaerythritol.	Type B: Pemulen™ TR-1 Type A: Pemulen™ TR-2
Interpolymers	Carbomer polymers or copolymers containing a block copolymer of polyethylene glycol and a long chain alkyl acid ester.	Type A: Carbopol® Ultrez 10 Type B: Carbopol® ETD 2020.

Initially carbomers were polymerized in benzene. When toxically preferred solvents like ethyl acetate and cyclohexane were introduced, resulting polymers were also preferred as the possibility of applications extended to even oral formulations. Progressive substitution in formulations was based in viscosity of the obtained hydrogels. That is, polymers obtained in benzene were substituted for those polymerized in ethyl acetate and cyclohexane, but which had the same viscosity. Equivalence between polymers of benzene grade and those of ethyl acetate/cyclohexane grade are shown in Table 12.

**Table 12.- Recommended substitutes for benzene grade carbomers based on viscosity criteria.** Modified from The Lubrizol Corporation 2021<sup>235</sup>

Benzene grade polymer	Recommended Non-Benzene polymer
Carbopol® 934	Carbopol® 5984, Carbopol® Ultrez 10
Carbopol® 934P	Carbopol® 974
Carbopol® 940	Carbopol® 980
Carbopol® 941	Carbopol® 71G, Carbopol® 971P, Carbopol® 981
Carbopol® 1342	Pemulen™ TR-1, Carbopol® Ultrez 30

Size estimations of single carbopol macromolecules have shown that they have a size from 0.02 to 0.41  $\mu\text{m}$ .<sup>237</sup> However, when observed in their dry state all carbomers are present as particles of 2-7  $\mu\text{m}$ <sup>83</sup>, as shown in Figure 24. This indicates that commercial carbomers are in fact multimacromolecular agglomerates of many interconnected carbomer molecules (primary particles)<sup>83</sup>. It is hypothesized that this interconnection is based on weak hydrogen bonds<sup>237</sup>. For example, the estimated size of a Carbopol® 974 macromolecule is 100-300 nm, which can be considered as a nano/microgel. Cryo-SEM, images of the same commercial product in its dried state (Figure 24-B) show a large particle of about 5  $\mu\text{m}$ .

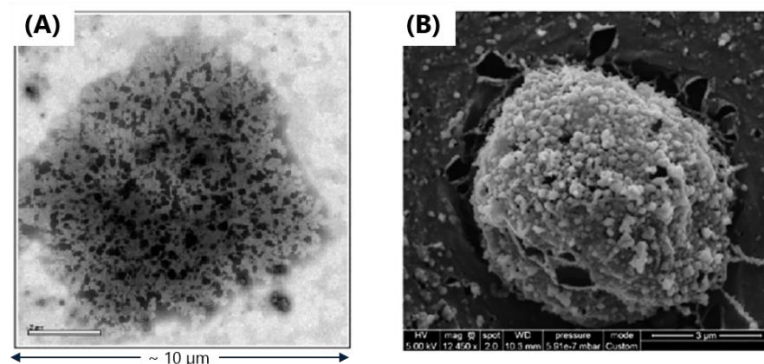


**Figure 24.- Images of Carbopol® 934 and Carbopol® 974 particles in their dry state. (A)** optical microscopy image of Carbopol® 934.<sup>238</sup> **(B)** Cryo-SEM image of Carbopol® 974.<sup>239</sup>.

Due to the presence of  $-\text{COOH}$  groups (52-68 % in dry basis<sup>83</sup>), when carbomer particles are present in an aqueous medium, they will hydrate progressively until completely swell (Figure 25). Structural differences among carbomers: polymer type and crosslinking impact in the viscosity of the obtained aqueous solutions.

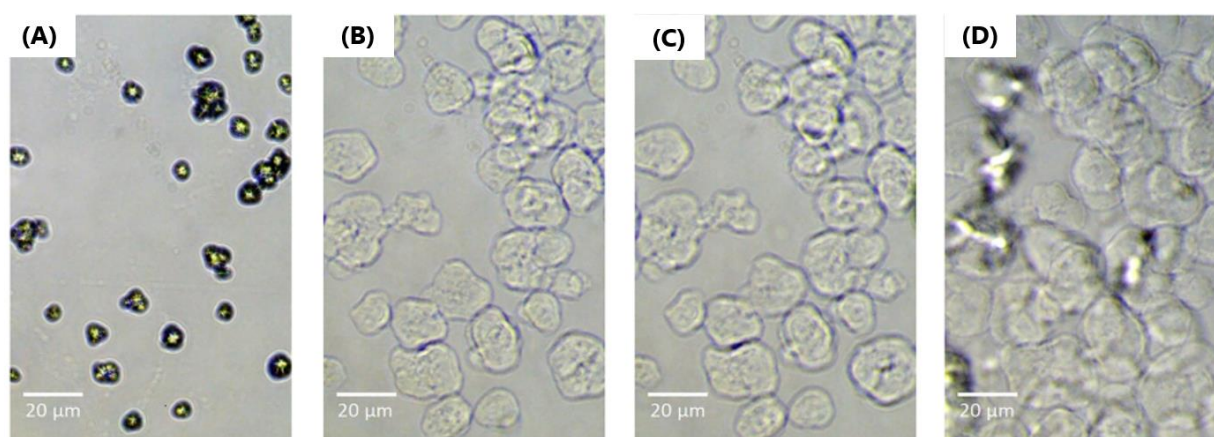


**Figure 25.- Optical microscopy images of the progressive hydration of Carbopol® Ultrez 30 particles in aqueous media. (A)** at time 0 s, diameter: 10 μm. **(B)** After 5 s, diameter: 20 μm. **(C)** After 20s, diameter: 22 μm. **(D)** After 2400 s or 40 min, diameter: 25 μm.<sup>237</sup>

**Gel formation:** The general principle is to provoke the uncoiling of the carbomer polymer chains. This can be done in two ways, either by promoting the electrostatic repulsion between them or by forming hydrogen bonds between them.

- **By neutralization**

In order to form a fully interconnected carbomer-based hydrogel structure, a minimal concentration of 0.5-2 % w/v of a carbomer dispersion is needed, followed by a neutralization step by addition of a base. Carbomer dispersion in water will provoke the ionization of the carboxylic groups. Resulting dispersions have an acidic pH of around 2-3 depending of their concentration<sup>83</sup>. As a result of the presence of

negative charges, polyanion chains will be electrostatically repelled ones from each other's, causing an entangled structure with an increased viscosity (Figure 26-A). By the addition of a base,  $-\text{COO}^-$  groups will be neutralised. There will be an increased concentration of positively charged counter ions interacting with to the  $-\text{COO}^-$  groups along the polymer chains (Figure 26-B). This will increase the ionic strength inside the polymer meshes and a solvent flux towards it product of the increased osmotic pressure<sup>240 237</sup>. This implies that in a fully neutralized carbomer dispersion (pH  $\sim 7$ ), two phenomena contribute to the formation of the fully interconnected, gelled, tri-dimensional and swollen structure of the physical gel: electrostatic repulsion between polyanion chains and ionic strength pressure (Figure 26-C). Commonly used bases for carbomer neutralization are inorganic bases as NaOH and low molecular weight amines like Triethanolamine (TEA).

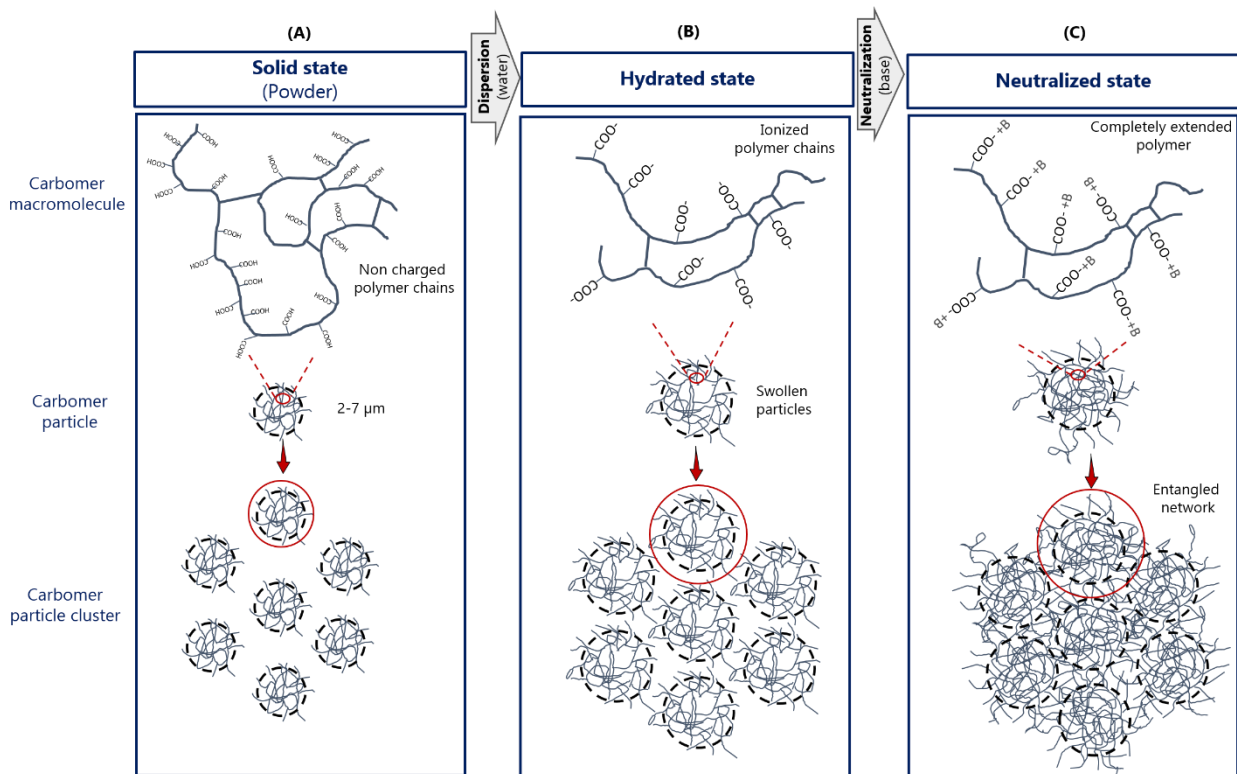


**Figure 26.- Formation of a carbomer gel. (A)** Carbomer in its solid state, carbomer powder is highly hygroscopic. **(B)** Once dispersed in water, particles will hydrate and swell,  $-\text{COOH}$  groups ionize forming  $-\text{COO}^-$ , causing repulsion between the polymer chains. **(C)** Neutralization with a base, increases ionic strength by the presence of counterions, chains will completely extend forming an entangled network between carbomer particles, the tri-dimensional hydrogel network will be fully formed by water flux due to increased osmotic pressure.  $\text{B}^+$  refers to counterions situated along the polyanion carbomer chains. If TEA is used,  $\text{B}^+$ :  $(\text{CH}_2\text{OHCH}_2)_3\text{NH}^+$ . If NaOH is used,  $\text{B}^+$ :  $\text{Na}^+$

- **By hydrogen bond formation**

It has also been reported that gellification of carbomers can be achieved by formation of hydrogen bonds between the  $-\text{COOH}$  groups of carbomers and a hydroxyl donor as: glycerine, propylene glycol (polyols), mannitol, sorbitol (carbohydrate alcohols) and polyethylene oxide. Usually 10-20 % w/v of a hydroxyl donor is recommended for completely uncoil carbomer polymers (Figure 27)<sup>241</sup>.



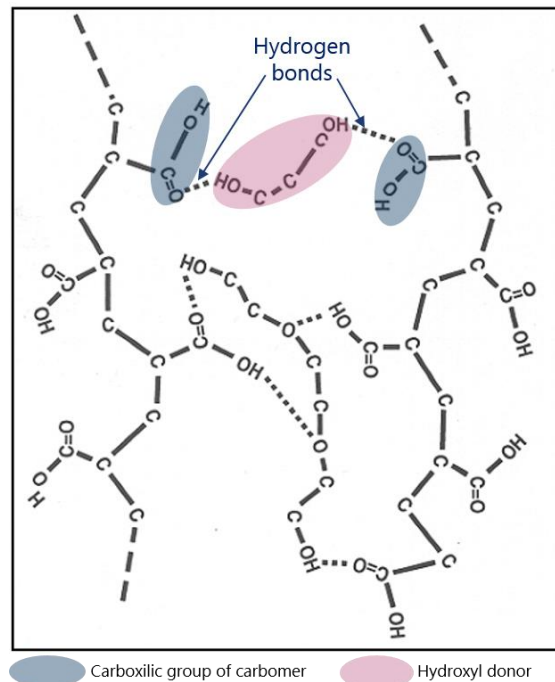


**Figure 27.- Carbomer gel formation by hydrogen bonding.** A hydroxyl group donor needs to be added to the formulation in order to for hydrogen bonds with the ester ( $-C=O$ ) functional group of the carboxylic parts of carbomer molecules.

This way of gel formulation is very useful when it is not possible to increase the pH of the final formulation. However, main disadvantages are the amount of hydroxyl donor added which can be toxic in certain cases and the time required for preparation. Hydrogen bonding is not instantaneous. It can take from 5 min to 3 three hours, and even if it can be speed up by heat, temperatures  $60^{\circ}\text{C}$  should not be used as they might break down the forming hydrogen bonds<sup>241</sup>. During the formulation of a pharmaceutical or cosmetic product the formation of the tri-dimensional network from a carbomer suspension is an important step and needs to be optimised. Special attention needs to be given when drugs or particles are added to the formed gels, as this process should preserve their integrity so that their therapeutic effect will not be affected.

**Gelled consistency and flow behaviour:** Increasing the viscosity of an aqueous media is usually a way to increase the stability of formulations such as emulsions or suspensions. Carbomer gels are specially interesting for this goal as their tri-dimensional arrangement in interconnected particles gives them the ability to act as one of the best suspension systems for formulations.

Different polymers can be used at different concentrations to formulate water-based gels of the same viscosity, as shown in Figure 28 in which different concentrations of guar gum, CMC, Xanthan gum and Carbopol ® 940 were used to formulate gels of 33 000 cP (Brookfield, 20 rpm,  $20^{\circ}\text{C}$ ). As it can be seen, even

if all gels presented have the same viscosity, the carbomer gel has a higher ability to suspend particles. Guar gum and Carboxymethyl cellulose offer minimal resistance to the force of gravity (low yield value), on the contrary Xanthan gum and Carbopol demonstrate more suspending ability, because a greater force needs to be applied in order to provoke flow (high yield value).

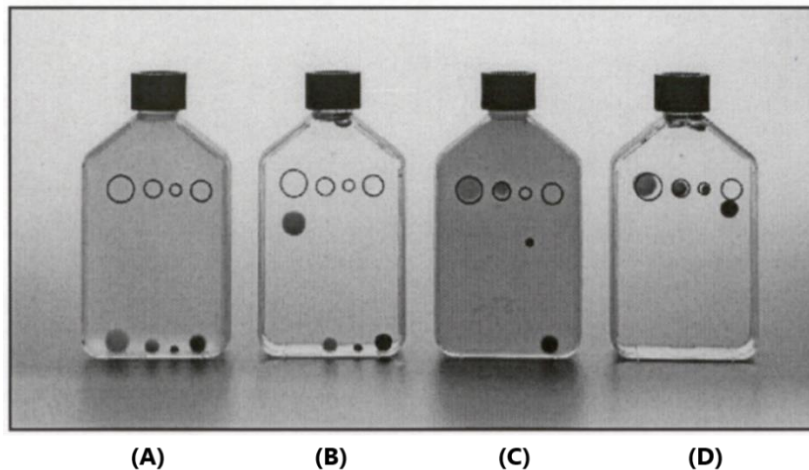


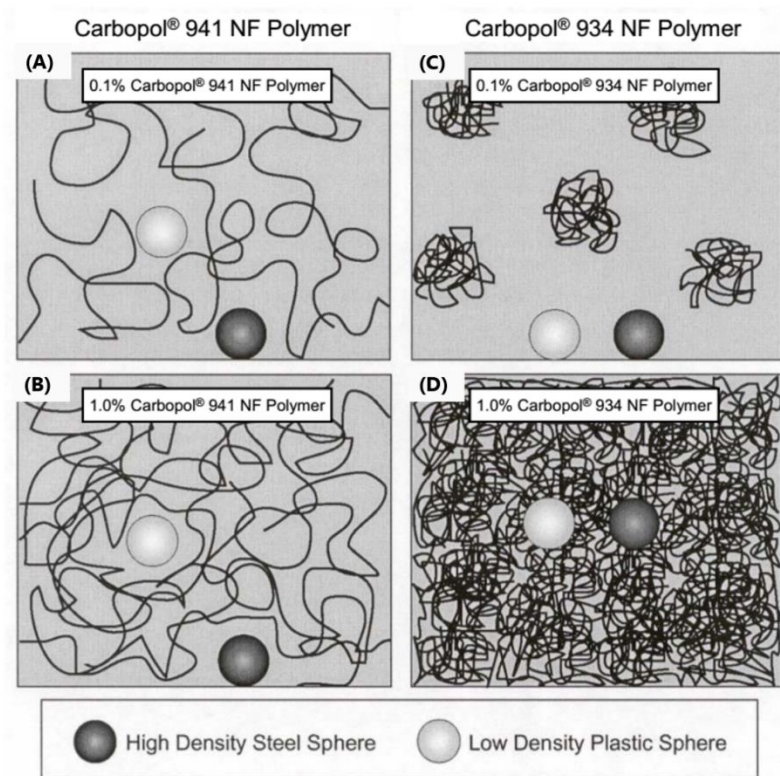
**Figure 28.- Hydrogels with same viscosity and different yield value. (A)** 2.1 % w/v Guar gum. **(B)** 2.3 % w/v Carboxymethyl cellulose. **(C)** 6 % w/v Xanthan gum. **(D)** 0.4 % w/v Carbopol ® 940. Spheres inside hydrogels have different density and size (low-density plastic on the left and high-density steel on the right of each hydrogel), they were kept for 1 month inside the hydrogels. Circles show the initial position of the spheres. Modified from Lubrizol 2008<sup>242</sup>.

In fact, apart from viscosity, for carbomers, two other factors influence their suspension properties: the molecular weight of the polymer(s) and the cross-link density.

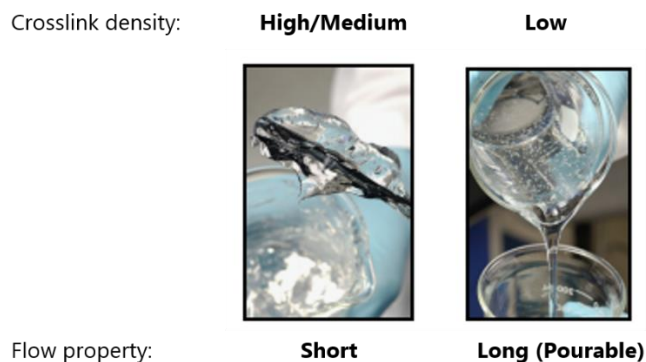
As seen in Figure 29, in lightly cross-linked carbomers like Carbopol® 941, polymer chains are not very constrained, as a result, polymer chains easily extend at low concentrations, causing that spaces between swollen particles are eliminated. However, due to limited crosslinking, the polymer lacks rigidity, so even at higher concentrations, the minimal stress needed to be applied in order to provoke flow (yield value) is low. On the opposite, carbomers like Carbopol® 934 are highly crosslinked polymers. The amount of crosslinks will constrain the mobility of the polymer chains, which will not "open-up" easily even at low concentrations. This will make possible the existence of large spaces between swollen gel particles which will not make possible the correct suspension of particles. However, at higher concentrations, the rigid particles begin to touch, forming a system with a very high yield value. That is, a relatively high stress needs to be applied in order to provoke flow. This is represented in Figure 29-D with the ability of the gel to maintain even high density steel spheres in suspension.

Figure 30 shows the difference in flow of a high/medium crosslinked carbomer gel, and a carbomer with a

low crosslink density. Flow is more easily achieved with carbomer of low crosslink density as its yield value is low and it can be easily surpassed by the effect of the gravity.



**Figure 29.- Effect of crosslinking on the suspending properties of carbomer (Carbopol®) gels. (A-B)** Low crosslinked carbomer (Carbopol® 941) at low (0.1% w/v) and at high concentrations (1% w/v). **(C-D)** Highly crosslinked carbomer (Carbopol® 934) at low (0.1% w/v) and at high concentrations (1% w/v). Modified from Lubrizol 2008<sup>242</sup>.



**Figure 30.-Flow properties of neutralized carbomer polymer dispersions.** Modified from Lubrizol 2008<sup>242</sup>.

This special behaviour of carbomers can be studied by traditional rheometers and viscosimeters and reflects the flow of polymer particles, ones from each other's (macroviscosity) and is different from the flow of the fluid in-between the polymer particles, the interstitial fluid, which defines the microviscosity and is the one to which micro/nano particles, suspensions and emulsions will be immersed while forming composite materials with Carbopol (Figure 31)<sup>242</sup>.

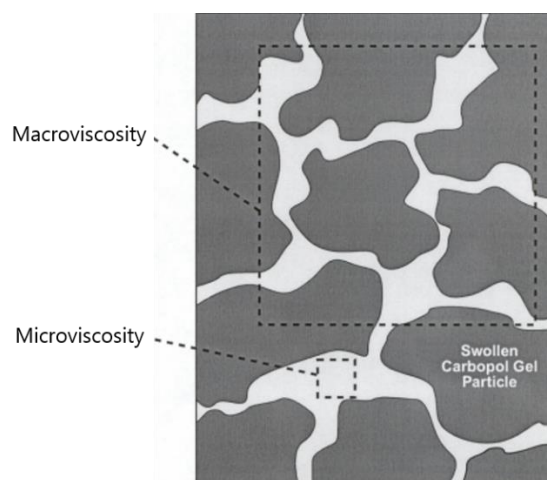


**Figure 31.- Graphical representation of macroviscosities and microviscosities in a carbomer gel.** Modified from Lubrizol 2008<sup>242</sup>.

This interrelation between structure and flow properties are characteristics of great interest specially for formulations which are to be stirred during their preparation or which are conceived to be pumped and easily spread during their utilisation.

Carbopol® 980 being a highly crosslinked carbomer, short flow properties can be expected. So, even after squeezing the dormulation, it will have the ability to easily adhere to skin. In addition, if concentration is adequate, it will offer a system being able to stabilise a suspension system, while giving a transparent appearance to the formulation <sup>235</sup>.

#### **1.4.2.2.2. Carbomer hydrogels containing CUR-NLCs**

Even if CUR-NLCs, as a suspension could be directly applied on skin, the resulting pharmaceutical form lacks of adherence and has poor rheological properties. Thus, not the optimal formulation for being applied on skin. In this context, carbomer gels have been added to CUR-NLCs suspensions in order to facilitate their ease of application. In some formulations like the one proposed by Riaz *et al.*<sup>211</sup> carbopol is dispersed into the NLCs suspension, it is hydrated and then, the neutralizing agent is added.

In other cases, like the formulation proposed by Iriventi and Vishal<sup>213</sup> first carbopol is dispersed in water, neutralized and then NLCs added. Interestingly, Keshewani *et al.*<sup>212</sup> have incorporated CUR-NLCs in its freeze-dried.

During the development of a composite formulation it is important to explore the impact of the formulation procedure on the stability of NLCs. Presented studies lack experiments pointing to the maintenance of NLCs structure during the formulation conditions.



## Chapter 2: Materials and Methods

---



## 1.1. CUR-NLCs/gel components

### 1.1.1. Excipients

#### 1.1.1.1. The solid lipid: Precirol® ATO 5

Glyceryl palmitostearate (reference: 3092, Gattefosse, Nanterre, France) (batch:169604), also known as Glycerol distearate (type I) in the EP (European Pharmacopoeia) or Glyceryl Distearate in INCI (International Nomenclature of Cosmetic Ingredients), was employed as the solid lipid part of NLCs.

It is manufactured without a catalyst, by the direct esterification of Palmitic acid (C16) and Stearic acid (C18) with glycerol<sup>83</sup>. Content of the esterified versions of C16 and C18, are 44.5% and 53.2%, respectively. As described in the certificate of analysis of the product, Precirol ATO 5 contains: 17.4 % of monoglycerides, 50.7% of diglycerides and 30.8% of triglycerides.

As specified by the manufacturer, this fine white powder is composed of particles of around 44 µm, has an average molar weight of 625.018 g/mol, a melting point (capillary method) of 50-60°C, a drop point (Mettler method) of 56.3°C and an iodine number of ≤3 g I<sub>2</sub>/100g.

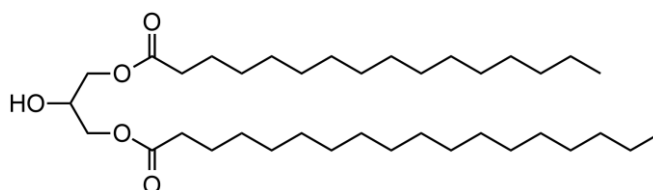


Figure 32.- Chemical structure of the major component in Precirol® ATO 5.

#### 1.1.1.2. The oil: Labrafac® lipophile WL 1349

Glyceryl caprylate-caprate (reference: 3139, Gattefosse, Nanterre, France) (batch:171801), also known as Triglycerides medium-chain in the EP or Caprylic/Capric Tryglyceride in the INCI, was employed as the liquid lipidic part of the NLCs.

Chemically, it is a mixture of triglycerides of saturated fatty acids: C8 (Caprylic acid) and C10 (Capric acid). Esterified versions of those fatty acids are present in 55% and 44.5% respectively. It can be extracted from the hard dried fraction of the endosperm of *Cocos nucifera* L. or from the dried fraction of the endosperm of *Flaeis guineensis* Jacq.<sup>83</sup>

As specified by the manufacturer, this oily liquid has a neutral smell, an average molar weight of 387.537 g/mol, a density (at 20°C) of 0.946 g/mL, a viscosity (at 20°C) of 32 mPa.s and an iodine number ≤1 g I<sub>2</sub>/100g.



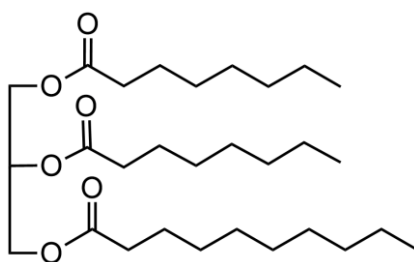


**Figure 33.- Chemical structure of the major component in Labrafac® Lipophile WL 1349.**

### 1.1.1.3. The surfactant: Poloxamer 407

Poloxamers (EP) are a family of non-ionic polyoxyethylene-polyoxypropylene block copolymers. More precisely, Poloxamer 407, (reference: 16758, Sigma-Aldrich, Saint-Quentin-Fallavier, France) (batch: BCBV0465) is composed of 101 units of polyoxyethylene and of 56 units of polyoxypropylene. Due to the fact that the polyoxyethylene segment is hydrophilic while the polyoxypropylene segment is hydrophobic, it has an amphiphilic nature (HLB value ~20) and has been used as emulsifying solubilizing or wetting agent in the formulation of pharmaceutical and cosmetic products. Micellar formulations of these copolymers have also been studied as drug delivery systems. In determined concentration conditions, poloxamer solutions can form thermosensitive gels that can by themselves act as drug delivery systems<sup>243,244</sup>.

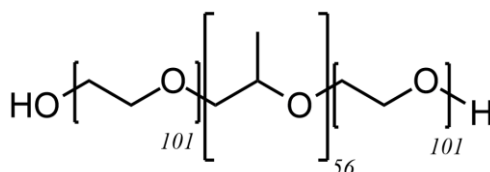


**Figure 34.- Chemical structure of Poloxamer 407<sup>83</sup>.**

### 1.1.1.4. The co-surfactant: Tween® 80

Polysorbate 80 (reference: 59924, Sigma-Aldrich, Saint-Quentin-Fallavier, France), or Polyoxyethylene 20 sorbitan monooleate is a non-ionic surfactant. It has a molecular formula  $C_{64}H_{124}O_{26}$ , a molar weight of 1310 g/mol and a HLB of 15<sup>83</sup>.

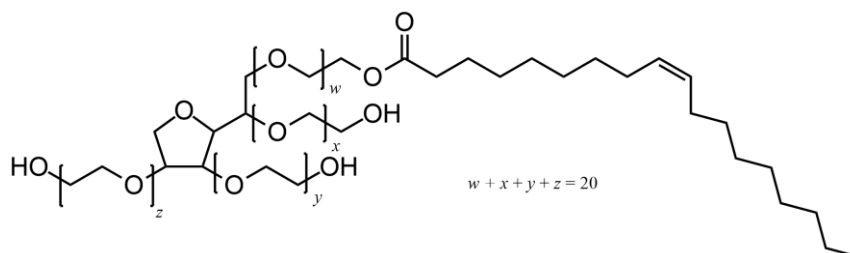


**Figure 35.- Chemical structure of Tween® 80.**

### 1.1.1.5. The hydrogel matrix polymer: Carbopol® 980

Carbopol® 980 (Lubrizol, Rouen, France) was used as the hydrophilic gelling agent of the matrix. Chemically, it is a homopolymer of acrylic acid crosslinked with allyl pentaerythritol. It is also known as Homopolymer type C in the EP and USP. It is a white, hygroscopic and fluffy powder. As reported by the manufacturer it has a maximum of 0.5 ppm of residual benzene, as it is polymerized in a toxicologically-preferred cosolvent (ethyl acetate and cyclohexane). Residual amounts are 0.3 % w/w of ethyl acetate and cyclohexane<sup>245</sup>. Thus, it meets the limits cited in the EP, the USP for carbomers. Recommended use level in formulations is between 0.2 and 1 % w/w<sup>246</sup>.

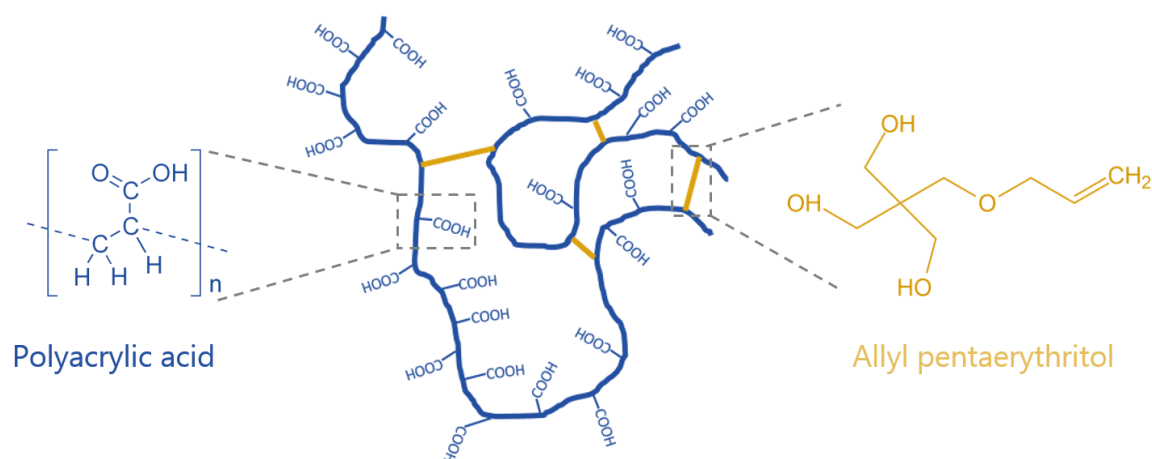


**Figure 36.- Schematic representation of Carbopol® 980 structure.** Two polymer chains with acrylic acid as repeating unit (polyacrylic acid) crosslinked by allyl pentaerythritol. For clarity, crosslinker is represented in its structure before the crosslink reaction.

### 1.1.1.6. The neutralizing agent: TEA

Triethanolamine ( $C_6H_{15}NO_3$ ), or Trolamine in the EP (reference: 90279,  $\geq 99.0\%$ , Sigma-Aldrich, Saint-Quentin-Fallavier, France) is a tertiary amine and weak base. It has a molecular weight of 149.19 g/mol and a melting point around  $20\text{ }^\circ\text{C}$ <sup>83</sup>. It is a clear viscous and very hydroscopic liquid. In aqueous solution it protonates forming triethanolammonium. Due to its method of manufacture, commercial product may also contain traces of diethanolamine and monoethanolamine. It may cause hypersensitivity or be irritant to skin<sup>247,248</sup>.

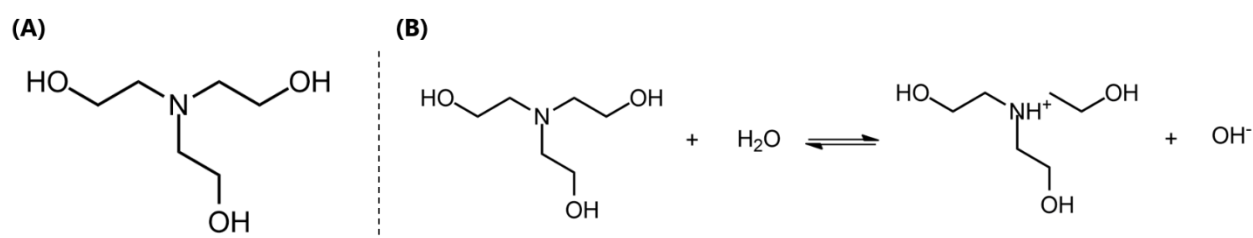


**Figure 37.- Structure and dissociation of TEA. (A)** Chemical structure of TEA. **(B)** TEA protonation in aqueous solution and formation of triethanolammonium.

### 1.1.2. The active ingredient: curcumin

Curcumin (CUR, Curcumin for synthesis, reference: 8.20354.0010, Sigma-Aldrich, Saint-Quentin-Fallavier, France) (batches: S7359554 and S7636054) was chosen as the active ingredient to be incorporated into NLCs. This solid product is composed of the three main curcuminoids in different proportions: 79% of Curcumin (C), 2% of Bisdemethoxycurcumin (BDMC) and 19% of Demethoxycurcumin (DMC). Such proportions were determined by HPLC, following the methodology found in section 1.3.2.2. of this chapter.

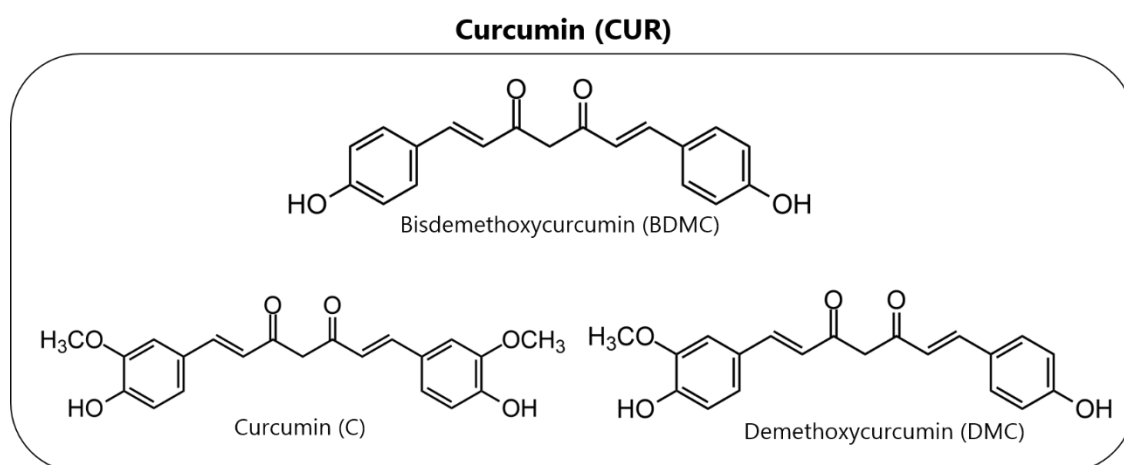


**Figure 38.- Chemical structure of the three curcuminoids present in CUR.**

## 1.2. Formulation procedures

### 1.2.1. CUR-NLCs formulation development

#### 1.2.1.1. General Hot Homogenization Method procedure

Works on NLCs formulation presented in this manuscript had as starting point the method proposed by Rodriguez *et al.* <sup>249</sup>, which was then optimised for CUR entrapment. Briefly, two phases were initially prepared. An oily phase containing a solid lipid (Precirol ® ATO 5), an oil (Sunflower oil or Labrafac ® lipophile WL 1349) and a co-surfactant (Tween 80). And an aqueous phase containing the surfactant (Poloxamer 407), in water. First, both phases were heated separately at a temperature higher than the melting point of the solid lipid (~55 °C). Then, the aqueous phase was added to the oily phase and the mixture went through homogenization for 2 min at 10 000 rpm, followed by a varying time at 20 000 rpm, while maintaining a temperature higher than the melting point of the solid lipid using a Polytron® system (PT3100 homogenizer with a dispersing aggregate of 7 mm of diameter, Kinematica AG, Luzern, Switzerland). Finally, the mixture was cooled down and NLCs were obtained.

Procedure and formulation parameters that were studied and changed are described in red in Figure 39. Methodology followed is explained in parts 1.2.1.2. and 1.2.1.3. of this chapter. Final preparation procedure is given in section 1.2.1.4. of this chapter.

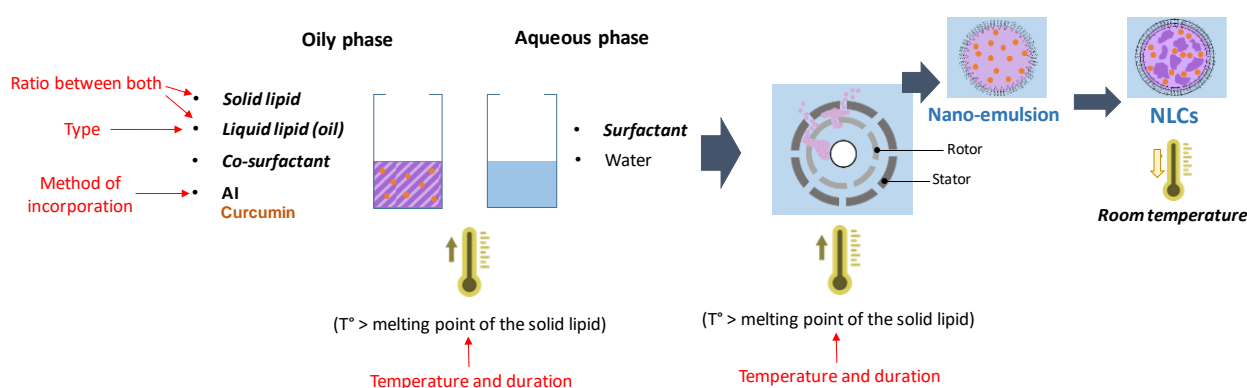


**Figure 39. NLCs general preparation by the Hot Homogenization Method.** In red: formulation and procedure parameters that were studied and modified.

#### 1.2.1.2. Change of method parameters in general procedure

The temperature and the homogenisation time were modified, while maintaining Precirol ® ATO 5 as solid lipid and Sunflower oil at a solid lipid/oil ratio of 82/18 (% w/w). In the whole formulation, Tween ® 80 and Poloxamer® 407 were maintained at 0.4 % w/v and 3 % w/v, respectively. During the homogenization, temperatures tested were 60, 70 and 90 °C and time from 15 min to 180 min. Each preparation was performed twice.

### 1.2.1.3. Change of formulation parameters in general procedure

While maintaining the previously selected method parameters, formulation parameters were changed. The solid lipid / oil ratio was modified from 82/18 (% w/w) to 70/30 (% w/w) and 90/10 (% w/w). With the selected solid lipid / oil ratio, the impact of switching from Sunflower oil to Capryol ® 90 (propylene glycol monocaprylate - Gattefosse, Nanterre, France) and Labrafac ® lipophile WL 1349 oils was investigated. Each preparation was performed twice.

#### 1.2.1.3.1. Differential Scanning Calorimetry (DSC) for oil candidates

DSC is based on the analysis of the changes in the heat capacity (amount of energy needed to raise the temperature of a material by 1 unit) of a material due to temperature. In this technique, a sample of a known mass is heated or cooled. The changes in its heat capacity are registered as changes in the heat flow of the instrument. This allows the detection of transitions, like for example, melting<sup>250</sup>.

Individual samples of Precirol ® ATO 5, Sunflower oil and Labrafac ® lipophile WL 1349, or they mixtures containing 450 mg of Precirol ® ATO 5 and 100 mg of either Sunflower oil or Labrafac ® lipophile WL 1349 were heated at 70 °C for 10 min. Then homogenized at 10 000 rpm for 30 s with a Polytron® system (PT3100 homogenizer with a dispersing aggregate of 7 mm of diameter, Kinematica AG, Luzern, Switzerland). Samples were left to cold down at room temperature and stored until at 4-8°C. The next day, between 5-10 mg were loaded into aluminium pans and hermetically sealed. DSC analysis were performed in a DSC Q100 (TA Instruments, Guyancourt, France) by first equilibrating the sample at 0 °C for 5 min, heating the sample from 0 °C to 250°C at 10°C/min and finally rapidly cooling down to 0°C (36°C/min). This was repeated twice. An empty pan was used as reference for all the experiments. The crystallinity index (CI) was calculated, as in other studies<sup>251,252</sup>, for the mixtures Precirol ® 5 ATO and Sunflower oil or Labrafac ® lipophile WL 1349, based on their enthalpy of fusion and that of Precirol ® 5 ATO alone according to the following equation:

$$CI (\%) = \left( \frac{\Delta H_F \text{ Mixture}}{\Delta H_F \text{ Precirol}} \right) \times 100$$

$\Delta H_F$  Mixture: Enthalpy of fusion of the mixture Precirol ® 5 ATO and Sunflower oil or Labrafac ® lipophile WL 1349

$\Delta H_F$  Precirol: Enthalpy of fusion of Precirol ® 5 ATO

### **1.2.1.3.2. CUR solubility tests in oils**

First, CUR solubility was tested in different oils, the best way to maximize CUR entrapped was investigated. 2 mL of four different oils were mixed with 30 mg of CUR and were kept under magnetic stirring during 14 h, at room temperature and in the dark. Oils used were: Sunflower oil, Labrafac® lipophile WL 1349 and Capryol® 90. Afterwards, samples were centrifuged at 5 000 rpm at 20°C for 2 hours and supernatants were filtered with a 0.45 µm cellulose filter. Finally, they were diluted in DCM/EtOH (60/40 %, v/v) and concentrations obtained by interpolating absorbances at 425 nm with a previously obtained CUR calibration curve in EtOH. Each sample was prepared twice and curcumin quantification was made twice in each sample. Previous tests were performed in order to verify that the filtration step aimed to removed insolubilized curcumin did not remove solubilized curcumin in the oil and that each tested oil formed and homogeneous mixture when mixed with EtOH.

### **1.2.1.3.3. Variation of loading strategy**

The hot homogenization method was performed with the previously established preparation parameters: time (30 min) and temperature (70°C), however curcumin was added in the formulation in four different ways: previously solubilized in the oil (Labrafac), in the co-surfactant (Tween 80), in the mixture oil + surfactant, or in the solid state. Each preparation was performed at least twice. Entrapped curcumin was determined in each preparation by centrifuging samples at 4 000 for 30 min at 20°C and then quantifying loaded-CUR as it is further described in part 1.3.4. of this chapter, using the calibration curve of CUR in in DCM/EtOH (60/40 %, v/v).

### **1.2.1.4. Optimized preparation protocol for CUR-NLCs/gel**

Briefly for CUR-NLCs, two phases were prepared. An oil phase composed of 450 mg of Precirol® ATO 5 (solid lipid), 100 mg of Labrafac® lipophile WL 1349 (oil), 60 mg of Tween 80 (co-surfactant) and 15 mg of CUR (active ingredient). Separately, an aqueous phase was prepared with 450 mg of Poloxamer 407 (surfactant) dissolved in 15 mL of ultrapure water.

Firstly, both phases were heated at 70°C for 10 min. Secondly, the oil phase was homogenized at 10 000 rpm at 70 °C for 2 minutes (Polytron® system, PT3100 homogenizer with a dispersing aggregate of 7 mm of diameter, Kinematica AG, Luzern, Switzerland). During this time the aqueous phase was maintained at 70°C. Then, the aqueous phase was completely added to the oily phase during 1 min while the homogenisation speed was increased until 20 000 rpm. Once all the aqueous phase was added and the speed reached, the homogenization was maintained for 30 min at 70°C. Afterwards, the preparation was cooled down to 20°C for 20 min and stored overnight at 4 – 8°C. One day after preparation, CUR loaded NLCs suspension was centrifuged at 4 000 rpm for 30 min at 20°C. Pellets (corresponding to Excess-CUR) were separated from supernatants (CUR-NLCs, Loaded-CUR).

For Blank-NLCs, curcumin was not added to the oil phase. Then, the same procedure as described above was followed.

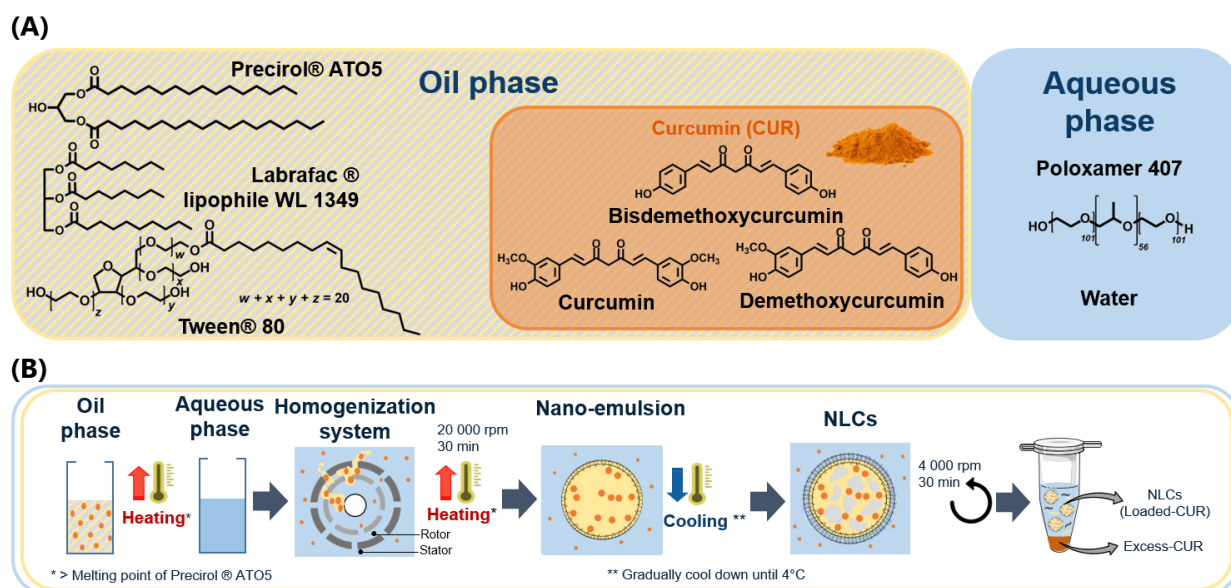


**Figure 40.- Optimized preparation of CUR-NLCs. (A)** Components of NLCs. In yellow and grey striped box, oil phase containing lipids (solid and liquid), co-surfactant and CUR composed of three curcuminoids (orange box). In blue box, aqueous phase containing the surfactant. **(B)** NLCs preparation by Hot Homogenization Method at heating temperature of 70°C and separation of non-loaded CUR (Excess-CUR) by centrifugation. This figure contains modified images from BioRender.com

### 1.2.1.5. Purification by SEC

SEC (Size Exclusion Chromatography) is a separation technique in which molecules are separated according to their size. Bigger molecules are excluded from the pores in the stationary phase of the chromatographic column, and thus elute first. Smaller molecules will be able to go through the pores of the stationary phase and as a result will need more time to elute out of the column<sup>253</sup>.

In order to get rid of any free molecule of excipient, Blank-NLCs and CUR-NLCs samples were passed through a size exclusion chromatography (SEC) column.

Briefly, 1 mL of the sample was deposited in a Bio-Gel P-10 (Fine) polyacrylamide gel column (Bio-Rad, Marnes-la-Coquette, France) with a fractionation range of 1 500 – 20 000 Da. Ultrapure water was used as eluant. Dead volume was 1 mL and subsequent collected fractions were of 500 µL. Fractions number 3, 4 and 5 were pooled and used for cell experiments as these fractions contained the highest concentration of NLCs.

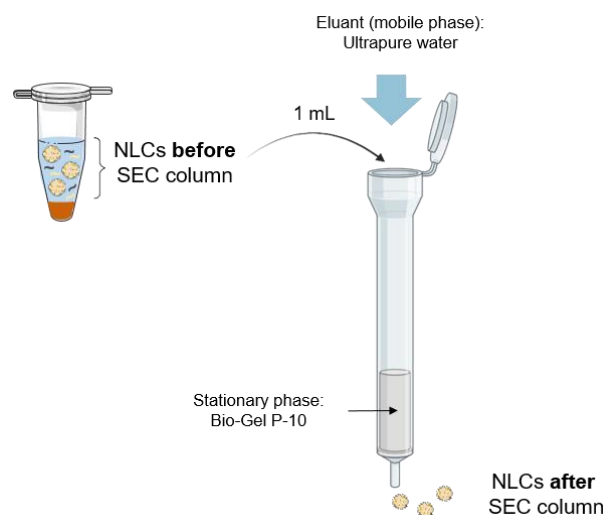


**Figure 41.- Diagram of the purification process of NLCs by SEC.** Created with BioRender.com

## 1.2.2. CUR-NLCs/gel formulation development

### 1.2.2.1. Choice of CUR-NLCs incorporation and neutralization procedure

Carbopol<sup>®</sup> 980 concentration was established to be used at a final concentration of 0.5 % w/v, as it demonstrated to be more easy to handle. Final procedure and the neutralizing agent were chosen based on the stability offered to the NLCs system. Two procedures of neutralization were studied using in each of them NaOH 0.5 M and TEA 20% v/v. For both neutralization procedures, 80 mg of Carbopol<sup>®</sup> 980 NF were dispersed in 11.6 mL of ultrapure water by overnight stirring at room temperature.

**Procedure 1: neutralization after addition of NLCs:** For the neutralization with TEA 20 % v/v, 4 mL of ultrapure water, CUR-NLCs or Blank-NLCs were added to the Carbopol<sup>®</sup> dispersion. Then, 400  $\mu$ L of TEA 20% v/v or 2.2 mL NaOH 0.5 M –previously demonstrated to be required to neutralize 16 mL of Carbopol<sup>®</sup> 980 suspension, (Supporting information on this chapter)- were added to form the unloaded gel (Blank-gel), CUR-NLCs loaded gel (CUR-NLCs-gel) or Blank-NLCs loaded gel (Blank-NLCs-gel), respectively. For the neutralization with NaOH 0.5 M, the volume of added ultrapure water, CUR-NLCs or Blank-NLCs was 2.2 mL. Then, 2.2 mL of NaOH 0.5 M were added and homogenized. In both cases, final pH was checked to be around 6.4.

**Procedure 2: neutralization before the addition of NLCs:** 400  $\mu$ L of TEA 20% v/v or 2.2 mL NaOH 0.5 M were added to the Carbopol dispersion and mixed until obtaining 4 mL of ultrapure water, CUR-NLCs or Blank-NLCs were added to prepare unloaded gel (Blank-gel), CUR-NLCs loaded gel (CUR-NLCs-gel) or Blank-NLCs loaded gel (Blank-NLCs-gel), respectively. For the neutralization with NaOH 0.5 M, volume of added ultrapure water, CUR-NLCs or Blank-NLCs was 2.2 mL. Mixtures were homogenized and final pH was checked to be near 6.4



### 1.2.2.2. Optimized preparation protocol for CUR-NLCs/gel

Carbopol® 980 NF was dispersed at 0.69 %, w/v in ultrapure water by overnight stirring at room temperature. 25 µL of TEA 20 %, v/v in ultrapure water, were added for each mL of the final volume of the gel to be prepared and mixed until obtaining a homogenous mixture. pH was checked to be around 7. Then, Blank-NLCs (to form Blank-NLCs gel) or CUR-NLCs (to form CUR-NLCs gel) were added at 25%, v/v of the final volume of gel aimed. The mixture was stirred and final pH was checked to be around 6.4 - 7. To prepare the unloaded gel, NLCs were replaced by ultrapure water. Final Carbopol® 980 NF concentration in gel was 0.5 % w/v.

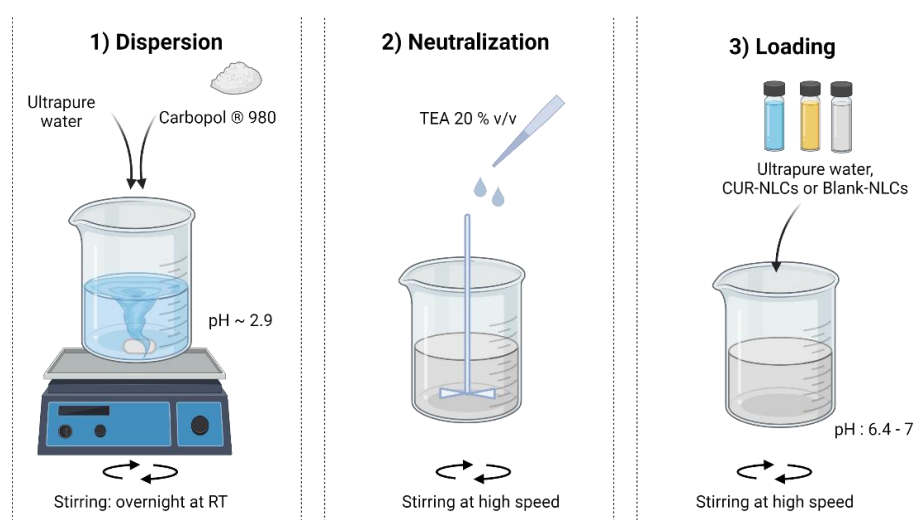


**Figure 42.- Diagram showing the optimized preparation protocol for gel, CUR-NLCs/gel and Blank-NLCs/gel.** Created with BioRender.com

### 1.3. Physico-chemical characterization of CUR-NLCs

#### 1.3.1. Particle size and zeta-potential

Particle size analysis performed by DLS is based on the relationship between Brownian motion and size of nanoparticles. This is done by irradiating the sample with a laser, analysing the intensity fluctuations in the scattered light to calculate the diffusion coefficient ( $Dt$ ) and from this, the hydrodynamic radius ( $R_h$ ) of equivalent spherical particles through the Stokes-Einstein equation. This equation states that  $R_h$  is inversely proportional to  $Dt$ <sup>254,255</sup>. Instead of reporting  $R_h$ , the hydrodynamic diameter ( $D_h$ ) is most commonly reported.

*Stokes-Einstein equation:*

$$Dt = \frac{k_B T}{6\pi\eta R_h}$$

$k_B$ : Boltzmann constant ( $1.38 \times 10^{-23}$  J/K),  $T$ : temperature,  $\eta$ : absolute viscosity,  $R_h$ : hydrodynamic radius

Zeta-potential analysis determines the electrokinetic potential at the slipping plane (Figure 43) of a colloid particle moving under electric field. The slipping plane is the plane between the layer of counter-ions strongly adhered to the particle (Stern layer), and the diffuse layer composed by the dispersant particles.

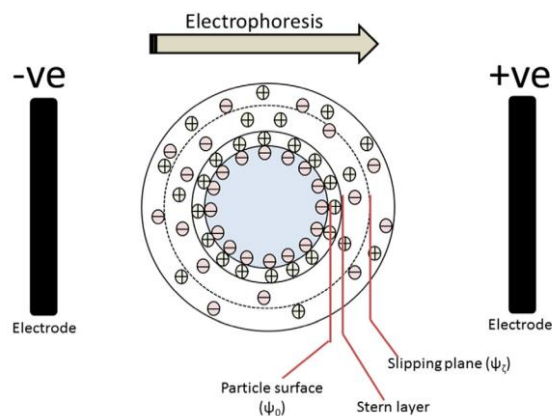


**Figure 43.- Model of the electric double layer (EDL) around a particle during a ZP measurement<sup>255</sup>.**

Experimentally, particle size analysis and ZP measurements were performed using a Zetasizer Nano ZS (Malvern Instruments Instruments Ltd., Worcestershire, UK) equipped with a He-Ne laser ( $\lambda = 633$  nm) at a scattering angle of  $173^\circ$ .

Particle size and polydispersity index (PDI) were determined by Dynamic Light Scattering (DLS). Samples were diluted (1:100) in ultrapure water and placed in polystyrene cuvettes semi-micro (Brand GmbH + Co Kg, Wertheim, Germany). Particle size was described in terms of the Hydrodynamic Diameter ( $D_h$ ). Results were expressed as size distribution by intensity and size distribution by number.

Zeta potential (ZP) was calculated from the electrophoretic mobility obtained from Laser Doppler Micro-electrophoresis. Samples were diluted (1:10) in KCl 1mM and disposed in a folded capillary zeta cuvette (DTS1070). Each measurement was ran at 25°C and in triplicate (n=3).

### **1.3.2. Morphology**

Fresh NLCs samples before and after going through the SEC column were analysed by transmission electron microscopy (TEM), using two different sample preparation: negative stain and cryo technique. In both cases, samples were analysed without previous dilution.

Briefly, during the analysis of a sample by TEM, an electron beam passes through a fixed sample (by negative staining or cryogenesis<sup>256</sup>). As a result, the electrons will either scatter or hit a fluorescent screen at the bottom of the microscope. Resulting formed image will show different shades according to the zones of low or high electronic density of the sample.

#### **1.3.2.1. Negative Staining-Transmission Electron Microscopy (Negative staining-TEM)**

3  $\mu$ L of NLCs samples (~55 mg/mL) were deposited on an air glow-discharged Quantifoil® R2/2 carbon-coated grid (Quantifoil Micro Tools GmbH, Großlobichau, Germany), for 1 minute. The excess of liquid was blotted with a filter paper, and the grid stained with 2 % w/v aqueous uranyl acetate. After allowing drying at room temperature, grids were visualized at 100 kV with a Tecnai 12 Spirit transmission electron microscope (ThermoFisher, New York NY, USA) equipped with a K2 Base 4k x 4k camera (Gatan, Pleasanton CA, USA). Magnification was at 14.700 X at the level of the camera, corresponding to a pixel size at the level of the specimen of 0.34 nm. Images were processed with Digital Micrograph 3.21.1374.0 GMS 3 software and further analysed with Fiji software (ImageJ, HIH, USA).

#### **1.3.2.2. Cryo-Transmission Electron Microscopy (Cryo-TEM)**

3  $\mu$ L of NLCs samples (~55 mg/mL) were deposited on an air glow-discharged Quantifoil® R2/2 carbon-coated grid (Quantifoil Micro Tools GmbH, Großlobichau, Germany), for 1 minute. The excess of liquid was blotted with filter paper, and the grid plunged into liquid-nitrogen-cooled ethane. The grid was rapidly transferred and kept under liquid nitrogen. For observation, the grids were mounted in a 626 Gatan holder using its cryo-transfer device. The observations were made in a Tecnai 200 transmission electron microscope equipped with a field-emission gun (ThermoFisher, New York NY, USA). Images of the samples were recorded with a direct detection camera K2 Summit (Gatan, Pleasanton CA, USA) operated in movie mode. The images were aligned and summed as recommended by the manufacturer. They were recorded at

19.800X magnification (pixel size 0.26nm at the specimen level), using a total dose less than 20 electrons/Å<sup>2</sup>. Images were processed with Digital Micrograph 3.21.1374.0 GMS 3 software and further analysed with Fiji software (ImageJ, HIH, USA).

### 1.3.3. Mass quantification

Mass determination of NLCs suspensions was determined by weight difference before and after freeze-drying. Briefly, a 2 mL micro centrifugation tube is weighted. Then, 300-500 µL of NLCs suspension is added and the tube is weighted again. Samples are stored at -80 °C for at least 1h and then freeze-dried for 24h, and then weighted again. For each batch, at least three determinations are done. Mass concentration was determined as follows:

$$[\text{NLCs}] = \frac{(W_{\text{tube+NLCs}})_{\text{After FD}} - W_{\text{tube}}}{V_{\text{NLCs}}}$$

[NLCs]: NLCs concentration in mg/mL

( $W_{\text{tube + NLCs}}$ )<sub>After FD</sub>: weight of micro centrifugation tube containing NLCs suspension after freeze drying, in mg.

$W_{\text{tube}}$ : weight of empty micro centrifugation tube, in mg.

$V_{\text{NLCs}}$ : volume of NLCs suspension added to the micro centrifugation tube, in mL.

### 1.3.4. Entrapment efficiency

Quantification of loaded-CUR was calculated by two different approaches: direct method and indirect method. In both cases, Encapsulation Efficiency (%EE) and Drug Loading (%DL) were calculated.

%EE refers to the concentration of CUR incorporated into NLCs over the initial CUR concentration (1 mg/mL) at the beginning of the preparation. %DL refers to the amount of CUR incorporated into NLCs per weight of lipids (w/w).

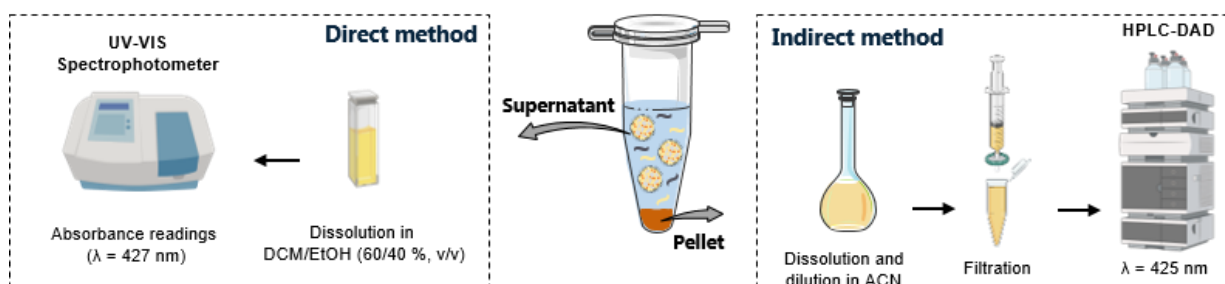


**Figure 44.- Diagram showing the general steps in the quantification of loaded-CUR in CUR-NLCs by the direct method and the indirect method.** This figure contains modified images from BioRender.com

### 1.3.4.1. Direct Method

The amount of loaded-CUR in NLCs was determined using a UVIKON-XS double beam ultraviolet-visible (UV-VIS) spectrophotometer (Secomam-Aqualabo, Champigny sur Marne, France). The supernatant obtained after the centrifugation step described in section 1.2.1.4. was diluted (1:200) in a mixture of Dichloromethane (DCM, purity  $\geq 99.8\%$ , VWR, Fontenay-sous-Bois, France) and Ethanol (EtOH, purity  $\geq 99.8\%$ , VWR, Fontenay-sous-Bois, France): EtOH/DCM (60/40 %, v/v). Then it was transferred to 10 mm quartz cuvettes. Absorbance at  $\lambda=427$  nm was taken from the absorbance spectra of each sample and used to calculate the amount of CUR using a calibration curve in EtOH/DCM (60/40 %, v/v), in the concentration range 1-7  $\mu\text{g}/\text{mL}$ . Concentration derived from the measured absorbance represented all curcuminoids present in the sample.

Complete dissolution and lack of absorption of any component of the nanocarrier was monitored by obtaining the absorbance spectra of Blank-NLCs and setting this as the baseline for all the measurements. CUR determination in each batch was performed in triplicate ( $n=3$ ).

Encapsulation Efficiency (%EE) and Drug Loading (%DL) were calculated using the following equations:

$$\% \text{ EE} = \frac{\text{loaded-CUR}}{\text{total-CUR}} \times 100$$

$$\% \text{ DL} = \frac{\text{loaded-CUR}}{\text{lipids}} \times 100$$

total-CUR: CUR concentration at the beginning of NLCs preparation (1 mg/mL)

loaded-CUR: CUR concentration determined at the end of the preparation.

lipids: total amount of lipids used for the preparation of NLCs, including liquid (Labrafac <sup>®</sup> lipophile WL 1349) and solid (Precirol <sup>®</sup> ATO 5) lipids.

### 1.3.4.2. Indirect Method

Pellets, obtained after the centrifugation step described section 1.2.1.4. (corresponding to excess-CUR) were solubilised in 1.5 mL of Acetonitrile (ACN, Sigma-Aldrich, Milan, Italy), diluted 1:10 in the same solvent and quantified in order to obtain the amount of CUR loaded in NLCs, by difference with the amount of CUR initially used in the preparation of the nano-suspension. Determinations were carried out in a Azura HPLC (Knauer, Berlin, Germany) equipped with an Azura Pump P6.1L and a UV-VIS Azura detector DAD 2.1L, controlled by ClarityChrome software.

Once filtered through a PTFE filter of 0.45  $\mu\text{m}$  (Fisherbrand, Rodano, Italy), 20  $\mu\text{L}$  of the sample were injected into a KnauerEurosphere II C18 column (250 x 4 mm). Samples were injected at 1 mL/min in a gradient mode

using mixtures of water (+ 0.1% TFA) : ACN (+ 0.1% TFA) from 50 : 50 to 0 : 100. Detailed separation program was:

Interval (min)	Separation mode	Mobile phase composition
		H <sub>2</sub> O (0.1% TFA) : ACN (0.1% TFA)
0-3	Isocratic	50 : 50
3-9	Gradient	0 : 100
9-11	Isocratic	0 : 100
11-13	Gradient	50 : 50

CUR was detected at  $\lambda = 425$  nm and its quantification performed using a previously recorded calibration curve in ACN in the concentration range 0.31 – 50  $\mu\text{g/mL}$ . During HPLC analysis, signals corresponding to three individual curcuminoids were integrated together in order to give the amount of CUR: Curcumin (C, 79%), Demethoxycurcumin (DMC, 19%) and Bisdemethoxycurcumin (BDMC, 2%). Retention times (RT) were: 8.04, 7.79 and 7.55 min, respectively. CUR determination in each batch was performed in triplicate (n=3).

Encapsulation Efficiency (%EE) and Drug Loading (%DL) were calculated using the following equations:

$$\% \text{ EE} = \frac{(\text{total-CUR}) - (\text{excess-CUR})}{\text{total-CUR}} \times 100$$

$$\% \text{ DL} = \frac{(\text{total-CUR}) - (\text{excess-CUR})}{\text{lipid}} \times 100$$

total-CUR: CUR concentration at the beginning of NLCs preparation (1 mg/mL)

excess-CUR: amount of CUR not loaded in the NLCs and thus, is present in pellet after centrifugation.

lipids: total amount of lipids used for the preparation of NLCs, including liquid (Labrafac ® lipophile WL 1349) and solid (Precirol ® ATO 5) lipids.

### 1.3.5. Antioxidant activity: ABTS assay

ABTS assay is based on the formation of the radical cation  $\text{ABTS}^{+\cdot}$  (maximal absorption at 734 nm) by oxidation of ABTS (2,2'-Azino-bis(3-ethylbenzothiazoline-6-sulfonic acid) diammonium salt) with  $\text{K}_2\text{S}_2\text{O}_8$  (Potassium Persulfate). Antioxidant molecules can scavenge  $\text{ABTS}^{+\cdot}$  by a mixed electron transfer and hydrogen atom transfer (HAT/ET)<sup>121</sup>, resulting in a decrease of the absorbance at 734 nm due to the formation of uncoloured species as showed in Figure 45-A. Thus, determination of the antioxidant scavenging activity of a sample is determined by mixing it with  $\text{ABTS}^{+\cdot}$  and following the absorbance of the sample at 734 nm as detailed in Figure 45-B.

$\alpha$ -tocopherol (purity  $\geq 75$  % HPLC, Sigma-Aldrich, Saint-Quentin-Fallavier, France) was used as the antioxidant of reference. Procedure was adapted from previously established methodologies<sup>249,257</sup>. Briefly, 7 mM of the radical cation ABTS<sup>•+</sup> was produced by mixing 14 mM ABTS (Sigma-Aldrich, Saint-Quentin-Fallavier, France) solution in ultrapure water with 4.9 mM K<sub>2</sub>S<sub>2</sub>O<sub>8</sub> (purity  $\geq 99$  %, Sigma-Aldrich, Saint-Quentin-Fallavier, France) also in ultrapure water (50/50 %, v/v). Reaction was allowed to take place for 24 h before use, in the dark and at room temperature. Then, the ABTS<sup>•+</sup> solution was diluted (1:70) with ultrapure water in order to reach an absorbance of  $\sim 0.8$  at 734 nm.

Solutions of CUR, CUR-NLCs, Blank-NLCs and  $\alpha$ -tocopherol were prepared in DCM/EtOH (60/40 %, v/v). Afterwards, 300  $\mu$ L of these solutions were added to the diluted ABTS<sup>•+</sup> solution (absorbance  $\sim 0.8$ ) and mixed for 45 min, at room temperature and in the dark. Samples were centrifuged (13 000 rpm, 3 min at 4°C) and the absorbance spectra of the supernatants was immediately obtained between 600 – 800 nm using the UVIKON-XS double beam ultraviolet-visible (UV-VIS) spectrophotometer. Experiments were carried out in triplicate.

Antioxidant activity was defined in terms of the percentage (%) of ABTS<sup>•+</sup> inhibited by each sample. This was calculated using the maximal absorbance of ABTS<sup>•+</sup>, at 734 nm, according to the following equation:

$$\% \text{ inhibition ABTS}^{\bullet+} = \frac{\text{Abs}_{734 \text{ nm}} \text{ ABTS}^{\bullet+} - \text{Abs}_{734 \text{ nm}} \text{ sample}}{\text{Abs}_{734 \text{ nm}} \text{ ABTS}^{\bullet+}} \times 100$$

$\alpha$ -Tocopherol Equivalent Antioxidant Capacity ( $\alpha$ -TEAC) was calculated from the slope ratios of the percentage of inhibition–concentration curves of respectively samples and  $\alpha$ -tocopherol ( $\mu$ M CUR/ $\mu$ M  $\alpha$ -Tocopherol).

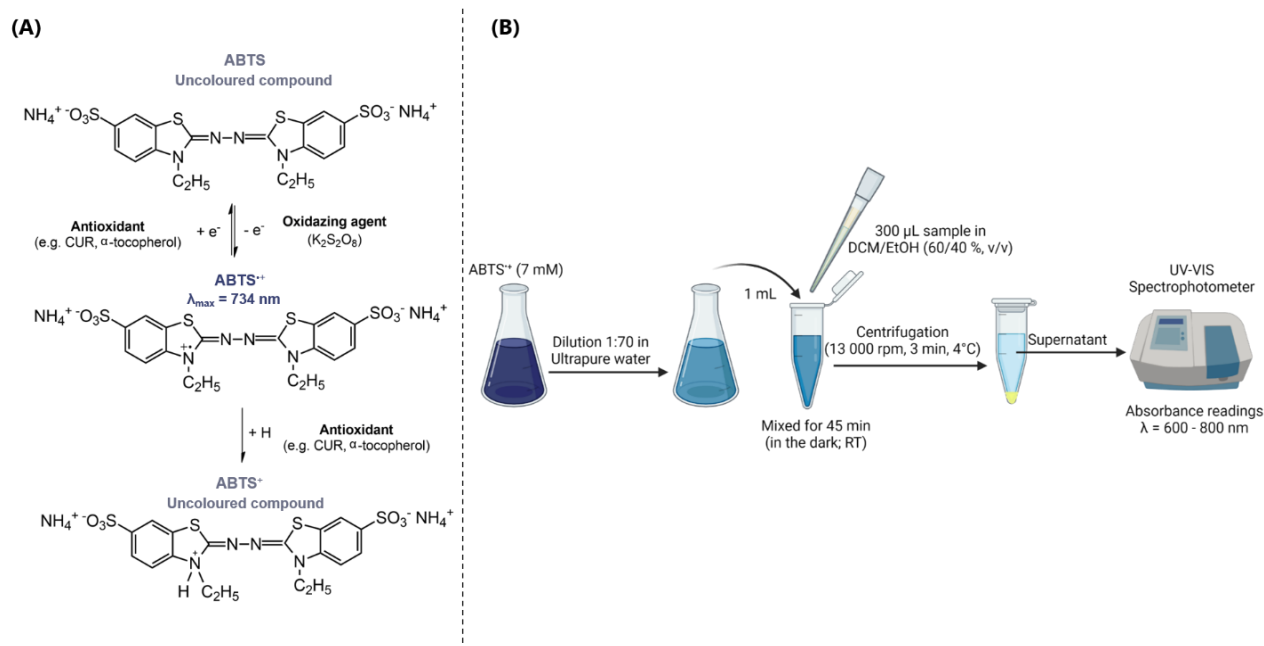


**Figure 45.- ABTS Assay for determination of antioxidant activity. (A)** Formation and scavenging reactions for ABTS<sup>•+</sup><sup>258</sup>. **(B)** Diagram of the experimental method.

### 1.3.6. Stability at different pH

NLCs after going through the SEC column, as described in 1.4., were diluted 1:100 with PBS 10 mM at pH= 5.5, 7.4 or 9. pH at 5.5 was reached by adding HCL 0.01 M, while pH 9 was reached by adding TEA 20% v/v. 1 mL of each sample was immediately taken off and placed in a quartz cuvette of 10 mm and UV-VIS spectra was taken between 300 and 700 nm. Other 1 mL was taken off and placed into a polystyrene cuvettes semi-micro (Brand GmbH + Co KG, Wertheim, Germany) size measurements were immediately performed as described in 1.3.1.

For measurements at 24 h, NLCs were mixed with PBS at the different pH, covered with parafilm and were left at room temperature and hidden from light for 24 h. Then 1 mL were placed in either a polystyrene or a quartz cuvette and absorption spectra or size were analysed as previously described.

### 1.3.7. Freeze-drying

In order to increase shelf-life of formulated NLCs, one of the principal objectives is to get rid of water. During freeze drying, the water in a sample is eliminated by sublimation. First the sample is frozen and then, by lowering the pressure this passes from the solid state to the gas state. A cryoprotectant is a substance that in optimal situations will replace water molecules, as a result, the form of nanoparticles, in this case will be preserved after removal of water molecules<sup>259,260</sup>.

Solutions of maltose, sucrose and dextrose were used as cryoprotectants. First, stock solutions were prepared at 20 % w/v in ultrapure water and filtered through a 0.20  $\mu\text{m}$  syringe filter before utilisation.



For each cryoprotectant, the amount of the stock solutions to be added into a total volume of 1 mL, for final concentrations of 0.5, 1.0 and 1.5 % w/v (maltose and sucrose) and of 0.5, 1.0, 1.5 and 3.0 % w/v (dextrose) were calculated. According to these calculations, mixtures of NLCs and cryoprotectant solutions were prepared. Each sample was kept overnight, under magnetic stirring at 4°C. Then, samples were frozen for 24 hours at -20°C. Freeze-drying was carried at -80°C during 24 hours. Resuspension of freeze-dried samples was performed by vortexing for 5 minutes. DLS measurements were performed as it was described in section 1.3.1., before and after freeze-drying with each cryoprotectant concentration.

### **1.3.8. CUR release in different biological media**

Curcumin release from CUR-NLCs was studied in PBS at pH 7.4, as well as in DMEM 10 % and DBM (without 10% FBS, but supplemented with Keratinocyte Growth Kit, see section 4.1 for detailed components), in static conditions.

Released CUR was indirectly determined by measurement of remaining Loaded-CUR in CUR-NLCs suspension. Briefly, CUR-NLCs samples were diluted until 20 µM of loaded-CUR in the different media. Aliquots (4 mL) were placed in sterile conditions at 37 °C for 0, 24, 48 or 72h incubation times. At the end of each incubation time, samples were centrifuged at 4 000 rpm, 20 °C for 30 min. Released curcumin was obtained as a fine pellet at the bottom of the centrifugation tubes. After centrifugation, supernatants (3 mL, containing CUR-NLCs) were freeze-dried for 24h, then dissolved with 1.3 mL of EtOH/DCM (60/40 %, v/v) for samples in DMEM 10% FBS or in 0.7 mL of EtOH/DCM (60/40 %, v/v) for samples in DBM and in PBS. Afterwards samples were centrifuged at 9 000 rpm, 4°C for 5 min. Absorbance spectra was taken from the supernatants between 350 and 600 nm. Remaining CUR concentration in CUR-NLCs was calculated from their absorbance at  $\lambda = 427$  nm, using the same calibration curve as in section 3.1.2.1.

Samples of Blank-NLCs followed the same procedure and were used to establish the baseline for spectrophotometric measurements.

CUR released was then calculated using the following equation:

$$\text{CUR released (\%)} = 100 - \left( \frac{\text{CUR}_t}{\text{CUR}_0} \right) \times 100$$

CUR<sub>t</sub>: remaining CUR concentration in CUR-NLCs after each incubation time.

CUR<sub>0</sub>: remaining CUR concentration CUR-NLCs before incubation at 37°C (just after dilution in cell media or PBS, t=0).

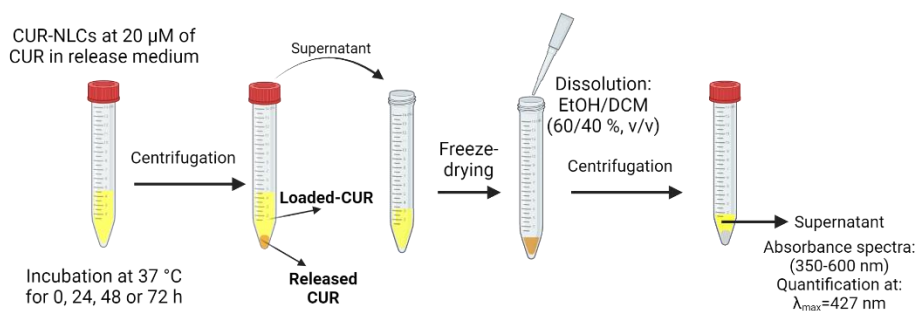


**Figure 46.-** Diagram showing the method for the assessment of CUR release from CUR-NLCs.

### 1.3.9. Permeation and penetration studies on Strat-M® membrane

Vertical diffusion Franz-cell is a setup described for testing *in vitro* the skin absorption of chemicals<sup>261</sup>. It consists of a donor chamber and a receptor chamber between which skin (or a semi-permeable membrane) is positioned. By setting the system under controlled temperature, passive diffusion from the donor chamber towards the receptor chamber takes place. Figure 47-A shows the set-up of the Franz-cell used for the permeation and penetration studies.

Strat-M® membranes have an approximately thickness of 300 µm, and have demonstrated low variability and good correlation with excised skin<sup>262,263</sup>. Their layered structure is increasingly more porous from the top to the down side. Each layer mimics the layers present in the skin. A top lipid coating mostly containing a mixture of ceramides, cholesterol and free fatty acids mimics the composition of the SC. Two layers of polyethersulfone resemble the dermis in the skin, while the polyolefin non-woven fabric support mimics the subcutaneous tissue (Figure 47-B)<sup>263,264</sup>.

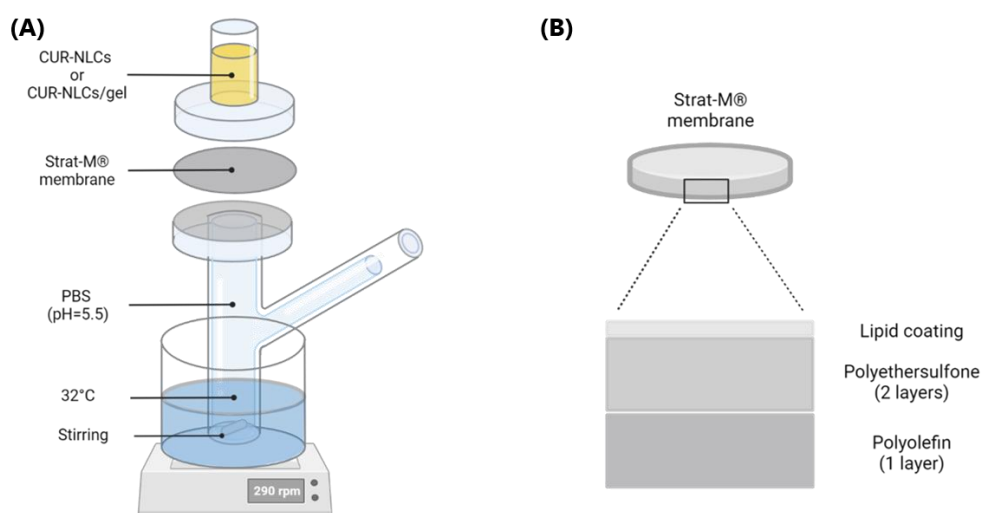


**Figure 47.-** Permeation and penetration studies on Strat-M® membrane. (A) Set-up of the Franz-cell system. (B) Multilayered structure of the Strat-M® membrane. Created with BioRender.com

### **1.3.9.1. Permeation studies on Strat-M<sup>®</sup> membrane**

The ability of the developed nanocarriers to diffuse across Strat-M<sup>®</sup> membranes was assessed by DLS analysis of samples taken from the receptor compartment of the Franz-cell at different time-points after that a fixed volume of CUR-NLCs, with a known CUR concentration, was deposited in the donor compartment and kept in contact with the synthetic membrane. PBS 10 mM at pH 5.5 (regulated with HCl) was used in the donor compartment and the whole system was maintained at 32 °C. Obtained count rates were compared to those obtained from a calibration curve count rate versus CUR-NLCs concentration.

Strat-M<sup>®</sup> membranes (25 mm) were obtained from Merck KGaA (Darmstadt, Germany). Immediately after unpacking, each membrane was clamped between the donor and the receptor compartment of a vertical Franz diffusion cell of 9 mm of diameter. The donor and receptor chambers were filled with 5 and 1 mL of PBS at pH 5.5 (pH regulated with HCl 1 M), respectively, and placed in a water bath at 32°C to mimic the temperature at the surface of skin and under stirring at 290 rpm. After 10 min, PBS was removed in the donor compartment and replaced with 1 mL of CUR-NLCs suspension at  $122 \pm 4 \mu\text{g}$  of CUR in ultrapure water. After 1h, 2h, 4h, 6h and 24h, 1 mL was removed from the receptor chamber and replaced with fresh PBS at pH 5.5 and pre-heated to 32°C. Each aliquot was analysed by DLS and the count rate was registered. All experiments were performed in triplicate (n=3) and count rates were compared to those presented by CUR-NLCs dilutions (0-1.10  $\mu\text{g/L}$  of NLCs, containing 0-20  $\mu\text{M}$  of CUR) in the same PBS.

### **1.3.9.2. Penetration studies on Strat-M<sup>®</sup> membrane**

Penetration studies were performed on the same set-up and conditions used for the permeation test. In addition to the 24 h time-point. Shorter assessment time-points were included: 15 min, 30 min and 1 h, as they could better reflect the real-life applications of a topical formulation. CUR accumulation in Strat-M<sup>®</sup> membranes was assessed for CUR-NLCs and CUR-NLCs/gel after CUR extraction and quantification at each time-point.

Experimental set-up and CUR-NLCs samples preparation ( $122 \pm 4 \mu\text{g}$  of CUR) were performed as described in section 1.3.9.1. After 0.25 h (15 min), 0.5 h (30 min), 1h and 24h of CUR-NLCs contact with Strat-M<sup>®</sup> membranes, membranes were removed and washed 3 times with ultrapure water. Excess of water was removed by blotting and membranes were cut in small pieces and left under magnetic stirring with 2, 3, 5 or 9 mL of ACN/H<sub>2</sub>O (50/50 %v/v) overnight to extract CUR penetrated in membranes. Samples were then centrifuged at 4 000 rpm for 10 min and supernatant was directly analysed using the same HPLC and calibration curve as in section 3.2.2.2.

For determination of the amount of CUR remaining in the donor compartment at the end of each time-

point, 0.5 mL were collected from the donor compartment, freeze-dried and then dissolved in 4 mL of EtOH/DCM (60/40 %, v/v). After centrifugation at 4 000 rpm for 15 min, supernatants were diluted (1:4) in EtOH/DCM (60/40 %, v/v) and absorbance was measured by UV-VIS spectrophotometry at  $\lambda=427$ , using the same calibration curve as in section 1.3.4.1. All experiments were performed in triplicate (n=3).

The amount of drug entrapped ( $D_e$ ) per unit area of Strat-M ® membrane was calculated as follows<sup>265</sup>:

$$D_e = \frac{Q_T}{A}$$

$Q_T$ : amount of CUR extracted from membranes (in  $\mu\text{g}$ )

A: area available for penetration ( $2.54 \text{ cm}^2$ )

The accumulation ( $A_c$ ) was calculated by the relationship<sup>265</sup>:

$$A_c = \frac{D_e}{C_d}$$

$C_d$ : starting CUR concentration in the donor compartment. (in  $\mu\text{g/mL}$  or  $\mu\text{g/g}$ )

## **1.4. Physico-chemical characterization of CUR-NLCs/gel**

### **1.4.1. Swelling properties of the Carbopol ® matrix**

4g of unloaded gel, were put in a 5 mL beaker. Then, 4 mL of either ultrapure water or PBS at 10, 5, 2.5, 1.25 or 0.625 mM were put in the upper part and the whole system was left at room temperature. After 1, 2, 4, 6 or 24 h, the volume remaining was measured with a 5mL micropipette. The % of solvent absorbed (water or PBS at different concentrations) was calculated according to the formula:

$$\% \text{ solvent absorbed by gel} = 100 - \left[ \left( \frac{\text{mL remaining at } t_h}{4 \text{ mL}} \right) \times 100 \right]$$

$t_h$ : time after putting the solvent in the upper part of the gel

### **1.4.2. Rheological characterization**

Rheology studies how materials deform or flow when a force or stress is applied. Thus, it was used to investigate the physical properties of the composite system CUR-NLCs/gel, when forces or stress are applied, similarly at what takes place during a topical application.

All the characterization was performed using a stress controlled rheometer (Discovery HR-1, TA Instruments, New Castle, USA) equipped with a cone-plane geometry (diameter: 40 mm, truncation gap: 27  $\mu\text{m}$  and cone angle: 1.005°). Every analysis was performed at 25 °C (room temperature) and at 32 °C (the temperature on

the surface of the skin). For each condition, experiences were repeated three times (n=3). Results were obtained and processed with Trios V.4.7 software (TA Instruments, New Castle, USA).

**Strain and frequency sweep experiments:** The Linear viscoelastic (LVE) region was determined for each sample. These strain sweep experiments were carried-out at a frequency of 1 Hz and were important to determine the strain range at which rheological experiences could be performed without destroying the structure of each sample. Then, in order to get more insight of the effect of the incorporation of NLCs on the matrix hydrogel, frequency sweep experiments were carried at a fixed strain of 1 %.

**Flow sweep experiments:** In order to study the behaviour of the formulations when applied and rubbed on the surface of the skin, flow curves of the viscosity in function of the shear rate (from  $0.001 \text{ s}^{-1}$  to  $1\,000 \text{ s}^{-1}$ ) were constructed.

**Thixotrophy experiments:** A recovery test was performed in order to mimic the behaviour of the formulations during application. Low shear cycles simulated the formulation at rest, either in the tube or on the skin once it has got out of a tube and before rubbing. High shear cycles simulated the squeezing of a tube in order to get out the formulation, but also the rubbing of the formulation on the skin. Tests were performed by continuously monitoring the viscosity of the sample while applying intercalated low and high shear cycles. Starting with a low shear cycle, a total of five cycles were applied during each single test. The three low shear cycles were performed at  $0.1 \text{ s}^{-1}$  for 150 s and the two high shear cycles at  $100 \text{ s}^{-1}$  for 30 s

### **1.4.3. Penetration studies on Strat-M<sup>®</sup> membrane**

Strat-M<sup>®</sup> membranes (25 mm) were obtained from Merck KGaA (Darmstadt, Germany). Immediately after unpacking, each membrane was clamped between the donor and the receptor compartment of a vertical Franz diffusion cell of 9 mm of diameter. The donor and receptor chambers were filled with 5 and 1 mL of PBS at pH 5.5 (pH regulated with HCl 1 M), respectively, and placed in a water bath at 32°C to mimic the temperature at the surface of skin and under stirring at 290 rpm. After 10 min, PBS was removed in the donor compartment and replaced with 1 g of CUR-NLCs/gel containing  $125 \pm 4 \mu\text{g}$  of CUR. After 0.25 h (15 min), 0.5 h (30 min), 1h and 24h of incubation, membranes were removed, excess of gel was retired with a clean paper and membranes were washed 3 times with ultrapure water. Excess of water was removed by blotting and membranes were cut in small pieces and left under magnetic stirring with 2 or 4 mL of ACN/H<sub>2</sub>O (50/50 %,v/v) overnight to extract CUR penetrated in membranes. Samples were then centrifuged at 4 000 rpm for 10 min and supernatant was directly analysed using the same HPLC and calibration curve as in section 3.2.2.2. For determination of the amount of CUR remaining in the donor compartment at the

end of each time-point, around 500 mg of gel were collected from the donor compartment, freeze-dried and dissolved in 4 mL of DCM/EtOH (40/60 %, v/v). After centrifugation at 4 000 rpm for 15 min, supernatants were diluted (1:4) in EtOH/DCM (60/40 %, v/v) and absorbance was measured by UV-VIS spectrophotometry at  $\lambda=427$ , using the same calibration curve as in section 3.1.2.1. All experiments were performed in triplicate (n=3).

## **1.5. Biological tests for CUR-NLCs**

### **1.5.1. Studied cell lines**

#### **1.5.1.1. BJ-Fibroblasts**

Human foreskin BJ-Fibroblasts primary cell line (ATCC<sup>®</sup> CRL-2522<sup>™</sup>, Manassas, VA, USA) was originally established from skin taken from skin of neonatal normal human foreskin. These adherent cells were cultured in DMEM supplemented with GlutaMAX, already containing phenol red, complemented with FBS (10%), Penicillin/Streptomycin (417 U/mL) and NaHCO<sub>3</sub> (0.625%). Cells were cultured until 90-100 % confluence, passages between 4 and 9 were used.

This cell-line has been greatly used in *in-vitro* essays of wound-healing.<sup>266</sup>

#### **1.5.1.2. HEK<sub>n</sub>**

Human Epidermal Keratinocytes Neonatal, or HEK<sub>n</sub> primary cell line (ATCC<sup>®</sup> PCS-200-010<sup>™</sup>, Manassas, VA, USA) are cells isolated from neonatal foreskin. They have a round morphology, and achieve a maximum of 80% confluence associating themselves in colonies. Culture took place in DBM supplemented with Bovine Pituitary Extract (0.4%), rh TGF- $\alpha$  (0.5 ng/mL), L-Glutamine (6 mM), Hydrocortisone hemisuccinate (100 ng/mL), rh Insulin (5 mg/mL), Epinephrine (1.0 mM), Apo-Transferrin (5 mg/mL), Penicillin (10 U/mL) and Streptomycin (10  $\mu$ g/mL). Such serum-free medium is formulated exclusively to inhibit fibroblast growth and containing a low calcium concentration (60 $\mu$ M) in order to slow differentiation. Phenol red (33  $\mu$ M) was added for cell culture routine procedures. For experiments where curcumin quantification was needed, phenol red was eliminated. Cells were maintained in culture until 80% of confluence, passages between 3 and 7 were used.

These cells have been largely used as models for skin studies such as: wound repair studies, response to UV radiation, psoriasis and eczema.<sup>267,268</sup>

#### **1.5.1.3. Biological reagents**

Dulbecco's Modified Eagle Medium (DMEM), Fetal Bovine Serum (FBS) and Trypan Blue (TB),

Penicillin/Streptomycin and Phosphate-buffered saline (PBS) were obtained from Gibco-Fisher Scientific (Illkirch, France). Dermal Basal Medium (DBM), Keratinocyte Growth Kit (containing: Bovine Pituitary Extract, rh TGF- $\alpha$ , L-Glutamine, Hydrocortisone hemisuccinate, rh Insulin, Epinephrine, and Apo-Transferrin), Phenol red, BJ Fibroblasts (CRL-2522™) primary cell line and HEK293 (PCS-200-010™) primary cell line were purchased from ATCC® (Manassas, VA, USA).

#### 1.5.1.4. Preparation of CUR and NLCs samples for biological tests

CUR samples for biological tests were prepared by adding 30 mg of CUR to 4.5 mL of cell culture media (DMEM 10%FBS or DBM) and stirring for 4 h at room temperature. Then samples were centrifuged at 5 000 rpm for 30 min at 20 °C. Supernatant containing dissolved CUR was separated from the pellet (undissolved CUR). Concentration of dissolved CUR was determined by dilution (1:100) in EtOH/DCM (60:40 %, v/v), centrifuging the mixture for 3 min at 13 000 rpm (Sigma 3K30 centrifuge), reading the absorbance of the supernatant at 427 nm and calculating from it the CUR concentration according to the previously established calibration curve. All materials: vial, magnetic stirrer and spatulas were autoclaved prior to the experiments.

CUR-NLCs and Blank-NLCs preparation for biological tests was performed as previously described in part 1.2.1.4. of this chapter. However, all glass materials were autoclaved, or cleaned with EtOH 70% v/v if autoclaving was not possible. Poloxamer ® 407 solution was passed through a 0.22  $\mu$ m filter (Fisherbrand, Darmstadt, Germany). Then preparation was performed as previously described.

### 1.5.2. Cytotoxicity studies

#### 1.5.2.1. MTT

The MTT (Methylthiazolyldiphenyl-tetrazolium bromide) test was used to study the in-vitro effect of 24 h exposition of CUR, CUR-NLCs and Blank-NLCs on cells. In this test, MTT, a tetrazolium salt is reduced, mainly by mitochondrial dehydrogenases in metabolically active cells, to a purple formazan product whose concentration can be quantified through absorbance measurements<sup>269</sup> (Figure 48).

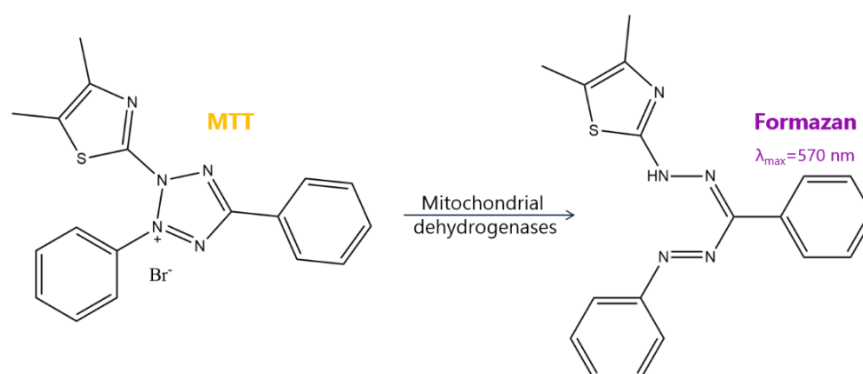


Figure 48.- Transformation of MTT to a formazan product in viable cells.

Cells were seeded in a 96-well plate (Corning®, New York, USA) at a concentration of 50 000 cells/well (156 000 cells/cm<sup>2</sup>) in complete DMEM medium for BJ-Fibroblasts and of 30 000 cells/well (94 000 cells/cm<sup>2</sup>) in supplemented DBM. Plates were incubated for 24h (37 °C and 5 % CO<sub>2</sub>). Medium was taken off and cells were washed with 200 µL of PBS. Immediately, cells were treated with 200 µL of either complete DMEM medium or supplemented DBM containing CUR (1-20 µM), CUR-NLCs (1-20 µM of loaded CUR in 0.05-1.10 mg/mL of NLCs suspension) or Blank-NLCs (0.05-1.10 mg/mL) and incubated for 24 h in the above described conditions. Medium was then removed and cells gently washed with 200 µL of PBS. 200 µL of MTT 0.5 mg/mL in PBS was then added to experimental wells, while 200 µL of PBS were added to cells in wells used to calibrate the baseline absorbance readings at the microplate reader.

Cells were incubated for 2 h 30 min (37 °C and 5 % CO<sub>2</sub>), then MTT or PBS removed and 200 µL of Isopropanol were added to each well. Plates were gently stirred and stored at room temperature and in the dark for 40 min.

Percentage of viable cells was calculated by reading the absorbance of each well at 570 nm with microplate reader (Xenius XM, Safas, Monaco). Metabolic activity (%) of cells treated with the samples (experimental cells) was reported to the metabolic activity of those treated with only DMEM 10% FBS or supplemented DBM (control cells, 100% metabolic activity). Experiments were performed in triplicate. Each experiment was performed in 6 wells and repeated 3 times (n = 3). The following equation was used:

$$\% \text{ metabolic activity} = \frac{\text{Abs}_{570 \text{ nm}} \text{ experimental cells}}{\text{Abs}_{570 \text{ nm}} \text{ control cells}} \times 100$$

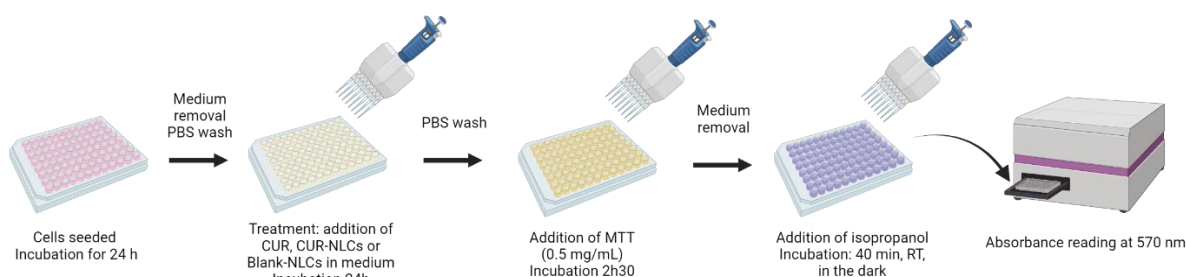


**Figure 49.- Diagram showing the main steps in MTT test.** This figure contains modified images from BioRender.com

### 1.5.2.2. Trypan Blue

The trypan blue test is used to determine the number of viable cells due to their capacity to exclude trypan blue thanks to their intact cell membrane<sup>270</sup>. On the contrary, in dead cells, trypan blue will easily get into the cytoplasm, making possible to distinguish these cells by their blue colour under the microscope.



Cells were seeded at a cell density of 156 000 cells/cm<sup>2</sup> for BJ-Fibroblasts and of 94 000 cells/cm<sup>2</sup> for HEK293 in a 24-well plate (Corning®, New York, USA) and incubated for 24 h at 37°C. Cells were washed with 500 µL of PBS. Then 500 µL of either DMEM 10% FBS or supplemented DMEM containing free CUR (1-20 µM) or CUR-NLCs (1-20 µM of loaded CUR in 0.05-1.10 mg/mL of NLCs suspension) or Blank-NLCs (0.05-1.10 mg/mL) were added to the cells and incubated for 24 h. Subsequently, medium (500 µL) was taken off and stored in 2 mL microcentrifuge tubes. Cells were gently washed with 500 µL of PBS and 200 µL of 0.5 % Trypsin were added. Cells were allowed to detach for 5 min at 37°C and 800 µL of complete DMEM medium of serum-free medium was added. The total 1 mL was collected and gathered with the previously collected 500 µL of either complete DMEM medium or serum-free medium. In order to count dead and live cells, 25 µL of cells suspensions from each eppendorf were mixed with 25 µL 0.04 % v/v TB solution in PBS. Cells were counted in a Malassez chamber using a DMI1 inverted microscope (Leica Microsystems, Wetzlar, Germany). Blue cells were counted as dead. Control cells (treated with culture medium) represented 100% viability. Each experiment was performed in three wells and in triplicate (n=3). Experiments were performed in triplicate.

### 1.5.3. Curcumin uptake preliminary studies

**Impact of CUR-NLCs on HaCaT keratinocytes:** MTT was performed as described in section 1.5.2.1 of this chapter. However, for this cell line 15 000 cells per well (47 000 cells/cm<sup>2</sup>) were seeded.

**UPLC-DAD/MS for determination of intracellular curcumin:** Cells were seeded at 23 500 cells/cm<sup>2</sup> (233 000 cells /well) in a six-well plate. After 24h-treatment with CUR-NLCs in DMEM 10%FBS, CUR concentration in CUR-NLCs of 5 µM, cells were washed three times with PBS and trypsinised. Cell pellet was stored in congelation for 24 h. The next day, cellular debris was separated from the sample and UPLC-DAD/MS determination was ran. First, for separation of curcumin from cellular debris, the freezed pellet was dissolved in 50 µL Tris-HCl 20mM (pH=7.4), well mixed and left in ice for 15 min. 200 µL of ACN 1% formic acid were added, and well mixed again. Cells were passed through the Ostro™ column (Waters, Etten-Leur, Netherlands). Collected sample was directly injected in the UPLC system.

UPLC-DAD/MS was performed on a Waters Acquity H-Class UPLC system (Waters, Milford, MA, USA), including a quaternary solvent manager (QSM), a sample manager with a flow through needle system (FTN), a photodiode array detector (DAS) and a single-quadruple mass detector with electrospray ionization source (ACQUITY QDa). Chromatography was performed on a Phenomenex Kinetex C18 column (100 mm × 2.1 mm i.d., 2.6 µm particle size). Solvent A was 0.1% aqueous Formic acid and solvent B was 0.1% Formic acid in MeOH. The flow rate was 0.5 mL/min and column temperature was set at 35 °C. Elution was performed according the following separation program:

<b>Interval</b> (min)	<b>Separation mode</b>	<b>Mobile phase composition</b> Solvent A : Solvent B
<b>0-0.5</b>	Isocratic	45 : 55
<b>0.5-10</b>	Gradient	20 : 80
<b>10-10.5</b>	Gradient	0 : 100
<b>10.5-12.5</b>	Gradient	100 : 0
<b>12.5-13</b>	Gradient	45 : 55

Mass spectrometric detection was performed in the negative electrospray ionization mode, using nitrogen as the nebulizer gas. Analyses were performed in the Total Ion Current (TIC) mode with a mass range of 50–1000 m/z. The capillary voltage was 0.8 kV, cone voltage 15 V, ion source temperature 120 °C and probe temperature 600 °C. Curcumin quantification was performed by using a standards calibration curve of CUR, following the same separation method.

#### **1.5.4. Migration/proliferation test**

Silicone culture inserts (Ibidi, Martinsried, Germany) were used to evaluate the migration/proliferation of dermal cell-lines. Briefly, cells were seeded at a density of 159 000 cells/cm<sup>2</sup> (35 000 cells per well) for BJ Fibroblasts and of 95 500 cells/cm<sup>2</sup> (21 000 cells per well) for HEK293 in the 2-well culture-inserts which were previously attached in the wells of a 12-well plate. After 24h, inserts were taken off, leaving a cell-free gap. Cells were washed twice with 2 mL of PBS. Then, 2 mL of DMEM 10% FBS or supplemented DBM containing CUR (0-20 µM) or CUR-NLCs (1-20 µM of loaded CUR in 0.05-1.10 g/L of NLCs suspension) or Blank-NLCs (0.05-1.10 g/L) were added to the cells. Phase-contrast images of the gap were taken immediately after adding the treatment using a DMI1 inverted microscope (Leica Microsystems, Wetzlar, Germany). Cells were placed in incubation for 24 h and photos were taken again in the same place. For each photo, areas were measured using the manual area measurement tool in the Fiji software (ImageJ, NIH, USA). For each sample 5 images corresponding to different places along the gap were analysed. Experiments were repeated twice. Pixel size at the specimen level was 0.235 µm. For controls, cell medium (DMEM 10% FBS or supplemented DBM, for BJ Fibroblasts and HEK293, respectively), was used without CUR, Blank-NLCs or CUR-NLCs.

Reduction in the gap area was determined by comparing the areas in the photos at 0h with the ones at 24h with the following equation:

$$\text{Reduction in gap area (\%)} = 100 - \left( \frac{\text{Area at 24 h}}{\text{Area at 0h}} \right) \times 100$$

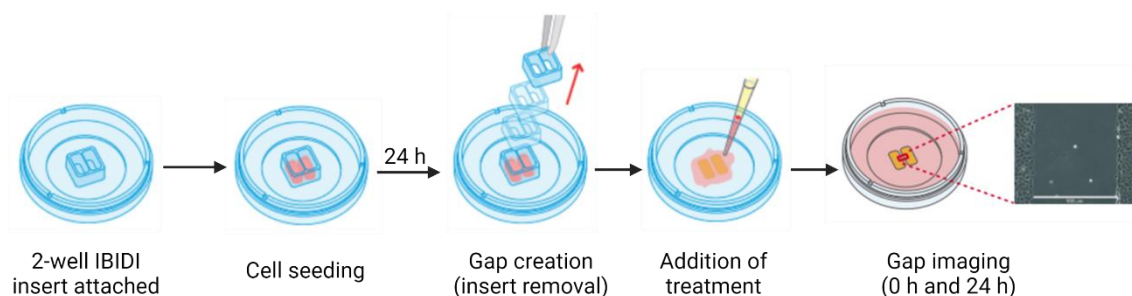


**Figure 50.-Diagram showing the main steps in the migration/proliferation test.** For clarity just 1 well of the 12-well plate is shown. Created with BioRender.com

### 1.5.5. Establishment of an oxidative-stress model

#### 1.5.5.1. Metabolic activity of cells exposed to oxidative-stress inducer: Luperox<sup>®</sup>

Luperox<sup>®</sup> (*tert*-butyl hydroperoxide or t-BOOH, Sigma-Aldrich, Saint-Quentin-Fallavier, France) was used as stressor. Increasing concentrations were tested in order to see which concentrations did not affect the metabolic activity of cells. This was performed by MTT test as described in part 4.4.1. with some modifications. Briefly, after seeding the cells in a 96-well plate, they were kept in incubation for 48h. Medium was taken off and 100  $\mu$ L of freshly prepared Luperox<sup>®</sup> in PBS at 50, 100, 200 or 300  $\mu$ M were put in contact with cells and kept in incubation for 1h. Luperox<sup>®</sup> was removed, cells were washed with 150  $\mu$ L of PBS and MTT test was performed as follows: 200  $\mu$ L of MTT 0.5 mg/mL in PBS were added to experimental wells, then incubated for 2 h 30 min at 37 °C and 5 % CO<sub>2</sub>. MTT was then removed and isopropanol (200  $\mu$ L) was added to each well for 40 min. Absorbance at 570 nm was measured using a microplate reader (Xenius XM, Safas, Monaco). % Metabolic activity was calculated as described in section 4.4.1. Experiments were performed in triplicate. Photos were taken after incubation with MTT using a DMI1 inverted microscope (Leica Microsystems, Wetzlar, Germany). Obtained RGB images were converted to grayscale images using Fiji software (ImageJ, NIH, USA).

#### 1.5.5.2. ROS detection for oxidative stress verification

In order to verify the intracellular production of ROS that has not been neutralized by the cell antioxidant defences, and thus, that induces oxidative stress in cells. 2',7'-dichlorofluorescein diacetate (DCFH-DA) was used. This is a non-fluorescent compound able to cross cell membranes, be deacetylated by intracellular esterases to non-fluorescent DCFH, and finally oxidized by intracellular ROS to dichlorofluorescein (DCF) whose fluorescence can be followed<sup>271,272</sup>.

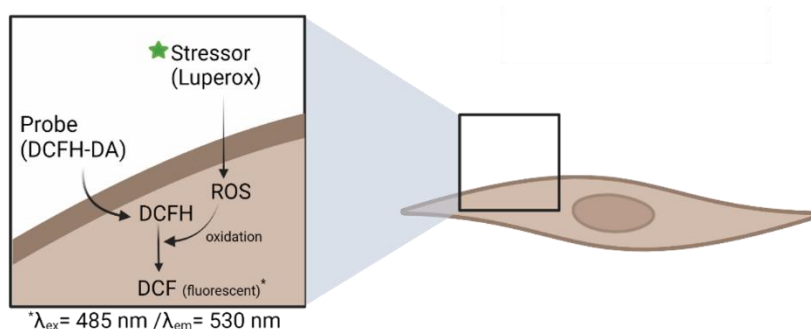


**Figure 51.- Use of fluorogenic probe DCFH-DA for ROS detection in cells.** Created with BioRender.com

For ROS generation and confirmation, BJ-Fibroblasts were seeded at 50 000 cells/well (156 000 cells/cm<sup>2</sup>) in a 96-well plate, in DMEM 10% FBS medium for 48h. Medium was removed and cells were incubated with 100  $\mu\text{L}$  of fluorogenic probe DCFH-DA (2',7'-dichlorofluorescein diacetate, Sigma-Aldrich, Saint-Quentin-Fallavier, France) 20  $\mu\text{M}$  for 1 h. Next, cells were washed with PBS and 100  $\mu\text{L}$  of Luperox at 50, 100 and 200  $\mu\text{M}$  were added. Fluorescence (at  $\lambda_{excitation} = 485 \text{ nm}$  /  $\lambda_{emission} = 530 \text{ nm}$ ) was recorded during 180 min by using a Synergy HTX Multi-Mode Reader (BioTek® Instruments, Vermont, USA) set at 37 °C. Samples without probe, either with or without stressor were used as blanks.

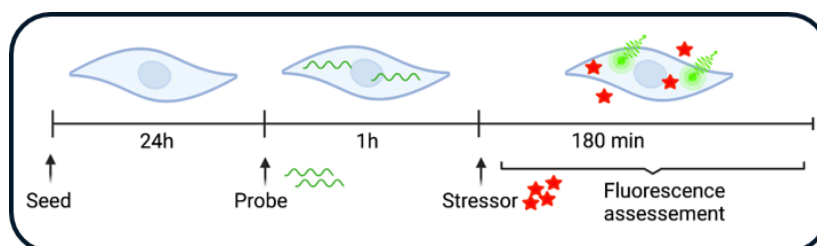


**Figure 52.- In vitro model for ROS generation and confirmation.** Created with BioRender.com

### 1.5.6. Effect of NLCs on BJ-Fibroblasts under oxidative stress

The influence of NLCs on cell viability was also studied under stress conditions for BJ Fibroblasts. They were seeded in a 96-well plate at a concentration of 50 000 cells/well (156 000 cells/cm<sup>2</sup>) in DMEM 10% FBS medium. Plates were incubated for 24h, at 37 °C and 5 % CO<sub>2</sub>. Medium was taken off and cells were washed with 200  $\mu\text{L}$  of PBS. After 24h incubation with CUR-NLCs (10  $\mu\text{M}$  and 20  $\mu\text{M}$ ), Blank-NLCs (0.54 g/L and 1.10 g/L) or Trolox at 10  $\mu\text{M}$  in DMEM 10% FBS, medium was removed and cells were washed with 200  $\mu\text{L}$  of PBS. Then, cells were treated with Luperox® at 100  $\mu\text{M}$  for 1h. Afterwards, Luperox® was removed and MTT test was performed as in no stress conditions: 200  $\mu\text{L}$  of MTT 0.5 g/L in PBS were added to experimental wells, then incubated for 2 h 30 min (37 °C and 5 % CO<sub>2</sub>). After incubation photos were taken using a DMI1 inverted microscope (Leica Microsystems, Wetzlar, Germany). Obtained RGB images were converted to grayscale images using Fiji software (ImageJ, NIH, USA). MTT was then removed and 200  $\mu\text{L}$  of Isopropanol were added to each well. Plates were gently stirred and stored at room temperature and in the dark for 40

min. Percentage of viable cells were calculated as in no stress conditions through absorbance readings at 570 nm as described in section 4.4.1. with a microplate reader (Xenius XM, Safas, Monaco).

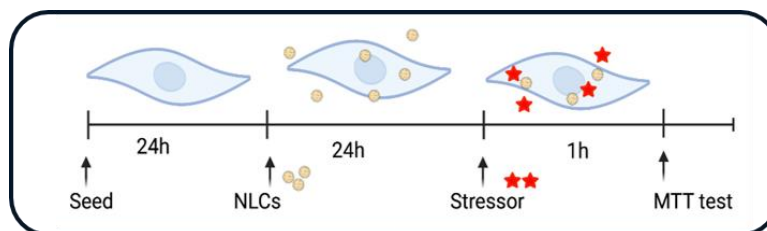


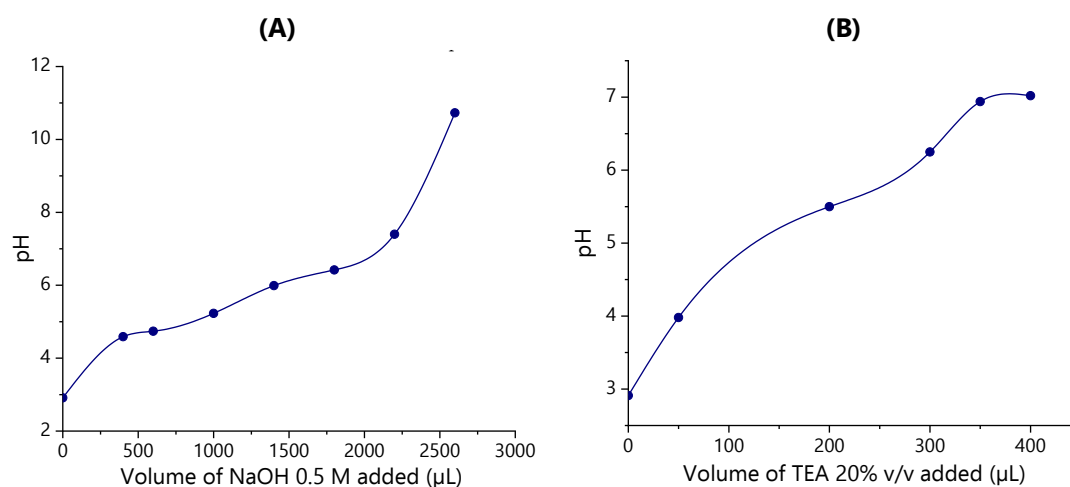
**Figure 53.- *In vitro* model for the evaluation of the effect of NLCs on BJ-Fibroblasts metabolic activity after undergoing oxidative stress.** Created with BioRender.com

### 1.6. Supporting information

#### pH variation of 16 mL of Carbopol® 980 0.5 % (w/v) in function of the volume of neutralizing agent added

pH changes were followed for NaOH 0.5 M (A) and for TEA 20 % (v/v) (B).

As the maximal viscosity of Carbopol ® 980 gel is achieved at neutral pH, two neutralizing agents were evaluated in their capacity to neutralize the same volume of a 0.5% w/v Carbopol ® 980 dispersion. As it can be seen, either 2.2 mL of NaOH 0.5M or 400 µL of TEA 20% v/v should be used for achieving a neutral 0.5% w/v Carbopol ® 980 dispersion. That is, by using TEA 20% v/v, 1.8 mL more of NLCs could be included for the formulation of the gel compared to the formulation of the same gel but neutralized with NaOH 0.5M.



## **Chapter 3: Development of CUR-NLCs**

---



## **1.1. Introduction**

From existing NLCs preparation techniques, the Hot Homogenization method is of great interest mainly as it avoids the use of organic solvents. However, it implies the exposition of the formulation components to high temperatures and high shearing. Thus, parameters of the technique, as well as the formulation could determine the physico-chemical properties of the loaded-NLCs.

In this chapter, the development of the CUR-NLCs formulation is presented. First, the preparation of CUR-NLCs is optimized in order to obtain a reproducible and stable NLCs formulation capable of entrapping as much as CUR as possible. This is performed by varying the method parameters of the Hot Homogenization technique and of the formulation. Then, the optimized formulation is characterized at a physico-chemical and at a biological level. Special interest is given to the stability of the formulation, the preservation of CUR antioxidant activity, and their cytotoxic toward dermal cells: fibroblasts and keratinocytes.

## **1.2. Results and discussion**

### **1.2.1. Optimization of CUR-NLCs preparation**

The optimization of CUR-NLCs preparation comprised preformulation studies aiming to choose:

- 1) Hot Homogenization method parameters that were suitable for obtaining a repeatable NLCs production.
- 2) The best components for NLCs preparation and conditions for curcumin loading.

As a starting point, the method and formulation developed by Rodriguez-Ruiz *et al.*<sup>249</sup> aiming the preservation of the antioxidant activity of astaxanthin through its entrapment into NLCs. From this, different method and formulation parameters were tested in order to adequate the formulation to curcumin entrapment.

#### **1.2.1.1. Impact of changing method parameters**

The two key parameters during the Hot Homogenization method are: 1) the temperature used, as it serves to melt the solid lipid component (Precirol ATO ® 5) so that it can mix well with the other formulation components. 2) the duration of the homogenization step as this is when droplets are exposed to the shear forces which can determine the final size of the nano-emulsion preceding the formation of the NLCs. Even if the study of these two parameters was prioritized in this part of the work, other parameters that could have been changed in the method, but that were maintained constant here, are: the speed of homogenization, the type of probe and the cooling speed after the homogenization step.

As seen in Figure 53, no clear tendency for NLCs size distribution and the duration of the homogenisation process at each temperature tested (60, 70 and 90°C) was evidenced. At all three temperatures, two populations were found by DLS analysis.



The disadvantage of performing the procedure at 60°C was judged to be the initial time that was needed to melt the solid lipid, and thus, to add before the homogenization step: minimum 30 min. At 70°C, comparable size distributions were obtained, however, only 10 min were required to melt the solid lipid previous to the homogenization step. For preparations performed at 90°C, a rancid smell was identified the day following their preparation. This along with their final lower pH (Table 13) made to suspect that lipid degradation took place. The decrease in pH is also present when performing the preparation at 70°C for 60 min (pH=4.6) compared with the pH when the preparation occurs at 70°C for 30 min (pH=6.5).

Lipid degradation in the presence of heat, due to too high temperatures or prolonged times of exposition, is a very well-known phenomenon. Some changes taking place just by heat action could be hydrolysis of ester bonds, carbon-carbon bonds cleavage and aromatization<sup>273</sup>. It is also to note that as experiments were not performed in an inert atmosphere, oxidation reactions could also be taking place when both, an acidic pH and a characteristic rancid smell were found. That is why using the lowest temperature possible was kept in mind during the set-up of the NLCs preparation methodology.

A homogenization at 70°C for 30 min was chosen as it was judged the one with the best balance between time initially needed to melt the solid lipid, size distribution, and no degradation of the lipidic components in NLCs. This chosen temperature is in accordance with temperatures employed by other researchers in the development of NLCs by the hot homogenization method aiming to curcumin entrapment.: 65-80 °C.<sup>208,209,211-213,274</sup>. It is to note that when a rotor-stator system is employed, speeds go from 15 000 rpm to 26 000 rpm.<sup>208,211,212</sup>. In our case, speed starts at 10 000 rpm and reaches at 20 000 rpm for most part of the process. Generally, the more the speed is, the shortest is the preparation method (10-15 min). However, in the cited works, an ultrasonication step is added at the end for nearly the same amount of time. In our case, the addition of an ultrasonication step was also tried, however no substantial change in the size distribution occurred. As result, differently from the previously cited works, we performed the preparation for 30 min, but eliminated the ultrasonication step, thus avoiding the possibility of further increase in temperature occurring at the zone of contact of the ultrasound probe and the formulation, which could have been source of degradation of NLCs components.

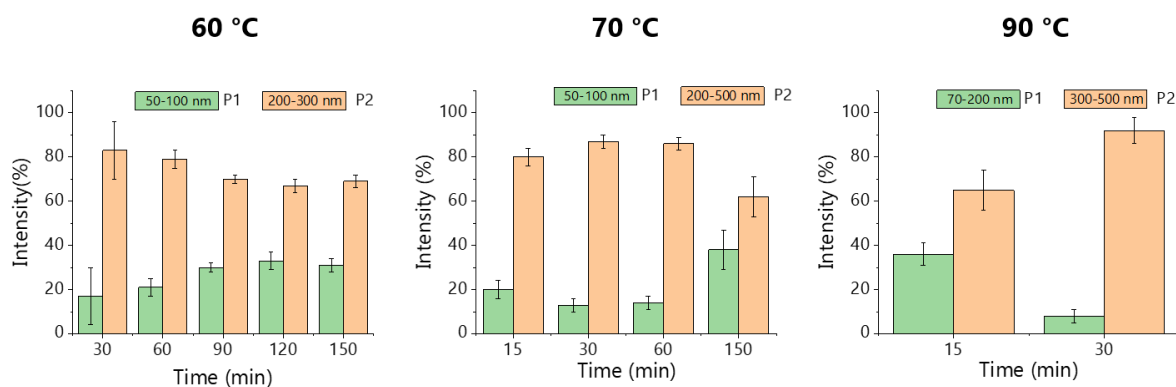


**Figure 54.- Size distribution (expressed in % intensity) of NLCs prepared by the Hot Homogenization Method at different temperatures and times of homogenization.** P1: Population 1, with the lower Dh and distribution. P2: Population 2, with the higher Dh and distribution.

**Table 13.-Size distribution parameters and pH of NLCs prepared by the Hot Homogenization Method at different temperatures and times of homogenization.** P1: Population 1, with the lower Dh and distribution. P2: Population 2, with the higher Dh and distribution.

Temperature	Homogenization (min)	Z-average (nm)	PDI	Dh (nm)		pH
				P1	P2	
60 °C	30	228 ± 12	0.376 ± 0.006	88 ±	39 ± 8	6.8
	60	175 ± 6	0.382 ± 0.018	66 ±	8 ± 23	6.5
	90	146 ± 2	0.383 ± 0.007	64 ±	2 ± 15	6.1
	120	137 ± 6	0.411 ± 0.008	64 ±	8 ± 31	6.2
	150	117 ± 1	0.333 ± 0.046	56 ±	3 ± 4	6.6
70 °C	15	369 ± 24	0.599 ± 0.003	102 ±	20 ± 21	6.7
	30	249 ± 16	0.409 ± 0.034	76 ±	23 ± 20	6.5
	60	183 ± 9	0.337 ± 0.049	57 ±	1 ± 19	4.6
	150	121 ± 4	0.344 ± 0.030	67 ±	9 ± 35	4.2
	180	Not possible to be measured by DLS				3.5
90 °C	15	331 ± 31	0.389 ± 0.008	213 ±	3 ± 7	5.9
	30	282 ± 7	0.254 ± 0.030	73 ±	7 ± 26	5.9

### 1.2.1.2. Impact of changing formulation parameters

Keeping the previously chosen parameters of the method, the optimization of the NLCs formulation aimed to replace the liquid lipid originally used: sunflower oil. As the works of Rodriguez-Ruiz *et al.*<sup>249</sup> were aimed to develop an oral drug delivery form, in this part, special interest was given to choose a more appropriate liquid lipid (oil) for the topical dermal route, without insaturations that could be source of decomposition at high temperatures for sunflower oil (90% composed of insaturated fatty acids).

Precirol® ATO 5, Poloxamer 407 and Tween 80 were maintained from the departing formulation.

Importantly, Precirol was kept because of its fusion point around 55°C. This allows to minimize curcumin exposure to heat while forming a homogeneous lipid melt at the beginning of the preparation process as discussed in previous section 1.2.1.1. Poloxamer 407 and Tween® 80 are wide used surfactants in pharmaceutical and cosmetic formulations. Tween® 80 is especially interesting as lipid nanocarriers containing it present lower cytotoxicity than those containing Tween 20 or Spans.

From Figure 54-A, formulations composed of a ratio solid lipid/oil of 82/18 (%w/w) were the ones presenting the best balance between size distribution of NLCs and the possibility to include more solubilised active ingredient in the NLCs, if assuming that most of the active ingredient is entrapped in its solubilized form. From Figure 54-B, Labrafac ® WL 1349 seemed a good candidate to replace Sunflower oil as even if NLCs sizes were slightly increased (Table 14), there was no further increase in number of NLCs populations (Figure 54-B, Table 14). It is to note that all tested oils did not produce a phase separation while mixed with Precirol ® 5 ATO.

From Table 15, it can be seen that the lower the viscosity, the higher the PDI (Polydispersity Index), and bigger the size of the NLCs. One hypothesis could be that the viscosity of the oil limited the mobility of the surfactant and co-surfactants to the water/oil interface, however, this would have result in the formation of bigger NLCs at lower viscosities<sup>275</sup>. This, as surfactants molecules would not be able to quickly arrive to the interface before the solidification of the lipid matrix during cooling-down. Montenegro *et al.*<sup>251</sup> also formulated NLCs by keeping constant the total amount of surfactant and co-surfactant in the formulation. Just by exchanging the amount of the oil (initially lower) and the amount of the solid lipid (initially higher) they passed from around 90% of 27 nm NLCs to a 100%. Both, our findings and scientific literature highlight the outstanding importance of the lipid matrix to the control of the size of NLCs.

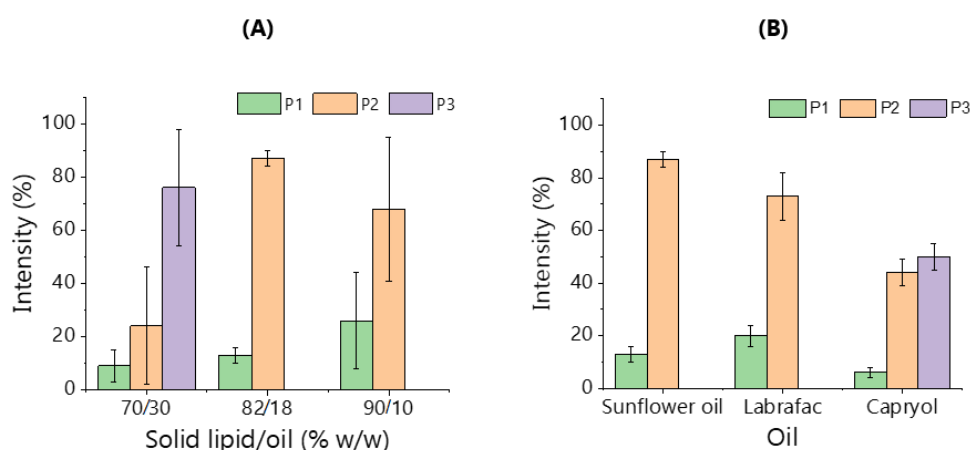


**Figure 55.- Size distribution (expressed in % intensity) of NLCs prepared by the Hot Homogenization Method at different temperatures and times of homogenization. (A)** by varying the solid lipid/oil ratio (% w/w) between Sunflower oil and Precirol ATO ® 5 (Size distribution parameters can be found in Table 14). **(B)** by maintaining the solid lipid/oil ratio at 82/18 % w/w and replacing the Sunflower oil by Labrafac (Labrafac Lipophile ® WL 1349) or Capryol (Capryol ® 90). P1: Population 1, with the lower Dh and distribution. P2: Population 2, with the intermediate Dh and distribution. P3: Population 3, with the higher Dh and distribution.

**Table 14.- Size distribution parameters of NLCs prepared by the Hot Homogenization Method by varying the solid lipid/oil ratio (% w/w).** The solid lipid used was Precirol ATO ® 5 and oil was Sunflower oil.

Precirol : Sunflower oil (% w /w)	Z-average (nm)	PDI	Dh (nm)		
			P1	P2	P3
70 /30	243 ± 2	0.458 ± 0.035	46 ± 32	136 ± 108	422 ± 89
82 /18	249 ± 16	0.409 ± 0.034	76 ± 23	311 ± 20	No present
90 / 10	218 ± 4	0.299 ± 0.019	370 ± 284	214 ± 46	No present

**Table 15.- Size distribution parameters of NLCs prepared by the Hot Homogenization Method, using 3 different oils.** Oils tested were Sunflower oil, Labrafac (Labrafac Lipophile ® WL 1349) and Capryol (Capryol ® 90).

Oil			Z-average (nm)	PDI	Dh (nm)		
Type	$\eta$ at 20 °C (mPa.S)	HLB			P1	P2	P3
Sunflower oil	70	7	218 ± 4	0.299 ± 0.019	70 ± 28	214 ± 46	No present
Labrafac	25-33	1	214 ± 1	0.391 ± 0.002	94 ± 13	357 ± 42	No present
Capryol	20	5	217 ± 2	0.476 ± 0.012	58 ± 2	186 ± 15	808 ± 168

Figure 55 and Table 14 show that when mixed at a solid/lipid ratio of 82/18% w/w, crystallinity of Precirol is greatly lowered by Sunflower oil (CI=86%) than by Labrafac.(CI=80%). The lower the crystallinity of the lipidic matrix, means that more imperfect it is. This can be translated in less expulsion of the active ingredient during storage<sup>186</sup>. The higher ability of Sunflower oil to disrupt the ordered crystalline structure of Precirol when compared to Labrafac can be due to the fact that it is constituted of a more heterogeneous mixture of lipids and other components like vitamins, whereas Labrafac presents a more homogeneous composition. It is to note that both oils present an amorphous behaviour as no phase transitions were detected (Figure 55-A).

Other approach that could be used to diminish the crystallinity of the lipidic matrix is to use components that will no present polymorphic transition during storage. For example, Corzo *et al.*<sup>276</sup> have employed polyglycerol esters of fatty acids to entrap dexamethasone.

Importantly, surfactants as Tween 80 and Poloxamer 407 can further disrupt the crystallinity of lipids while forming NLCs<sup>277</sup>. In this way, it could be interesting to perform a similar DSC analysis as the one presented here, but in the final NLCs formulation, in order to get more insight of the crystallization phenomena taking place when curcumin is entrapped in NLCs. Even more, X-Ray diffraction analysis<sup>193</sup> can be used to more deeply assess the transitions of lipids, and see how they are impacted while varying the formulation on incorporating an active ingredient.

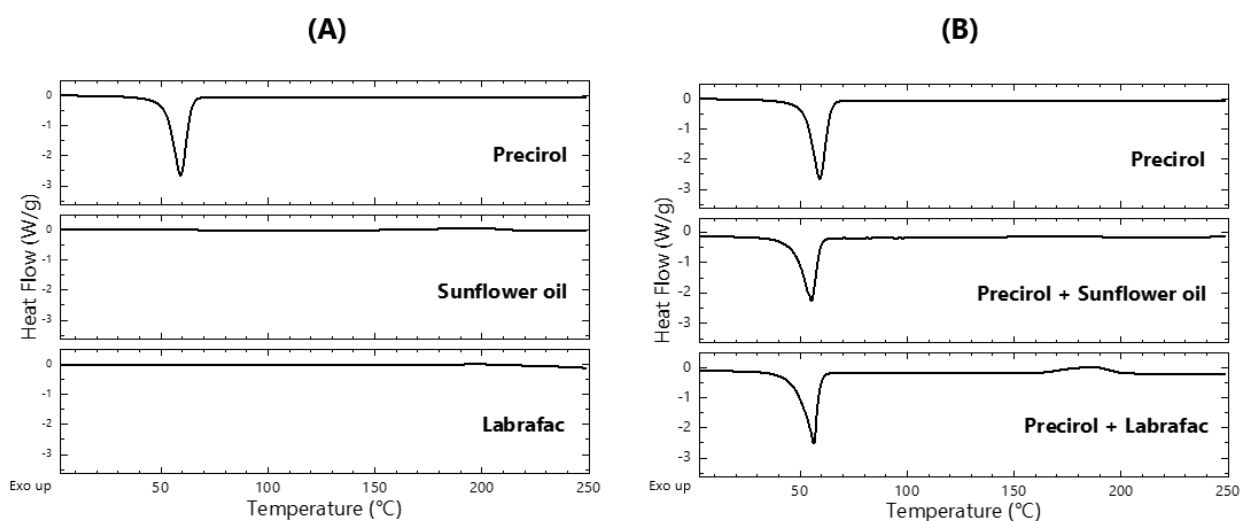


**Figure 56.-Thermograms of lipids used for NLCs preparation. (A)** Thermogram of solid lipid (Precirol) and oils (Sunflower oil and Labrafac). **(B)** Thermogram of solid lipid and its mixtures with respective oils at a solid lipid:oil ratio 82:18 % w:w.

**Table 16.- Thermal properties of precirol and its mixtures with Sunflower oil and Labrafac at solid lipid:oil ratio 82:18 % w:w.** CI: Crystallinity index.

Sample	Melting Point (°C)	Onset (°C)	Endset (°C)	Enthalphy of fusion (J/g)	CI (%)
Precirol	59.1	37.0	68.4	139.8	100
Precirol + Sunflower oil	55.2	36.6	65.7	111.3	80
Precirol + Labrafac	56.4	35.9	63.6	119.8	86

Even if reduction of crystallinity and polymorphic transitions are important aspects while developing NLCs, other aspects such as drug solubility in order to maximise drug incorporation in the nanocarrier need to be taken into account. Thus, the final choice of Labrafac as the liquid lipid took also in to account the ability of the oils to solubilise curcumin, as it will be presented in the following section 1.2.1.3.

### 1.2.1.3. Impact of the loading technique

In order to fully stablish NLCs formulation and preparation methodology, a study of the best conditions for curcumin loading needed to be performed.

It is generally accepted that the active ingredient entrapped in NLCs is mainly located in the oil component of the lipid matrix, as the solubility of a lipophilic drug in liquid lipids (oils) is higher than in solid lipids<sup>191</sup>. In line with this approach, CUR solubility was tested in Labrafac, Capryol and Oleic acid.

Labrafac was chosen as previous researches have shown that curcumin solubility is higher in medium chain triglycerides<sup>278,279</sup>. These are triglycerides containing fatty acids of 8 carbons (caprylic acid) and 10 carbons (capric acid), which is the exact composition of Labrafac, and could be translated into an increased curcumin

incorporation in the NLCs matrix. The absence of double bonds in it limits the possibility of degradation when exposed at high temperatures. Capryol was interesting to test as even if contains caprylic and capric acids, they are not in a triglyceride form, but esterified with propylene glycol. Oleic acid was included as it is present in 28% in sunflower oil.

As it is shown in Figure 56-B, CUR presented higher solubility in Labrafac, which is in accord with its rational choice. Compared to Sunflower oil, CUR solubility is increased in nearly 4 times. This is why, despite the higher decrease in crystallinity while using Sunflower oil (Figure 55, Table 16), Labrafac was finally chosen as the oil for the formulation. Even though this change implied an increase in NLCs size, the size range remained the same (Table 15).

From Table 17, adding CUR in the solid form to the formulation considerably increased the CUR content in NLCs. This seems to indicate that CUR in CUR-NLCs is not found just solubilised in the oil, but also in the solid lipid matrix and in contact with the stabilizing agents.

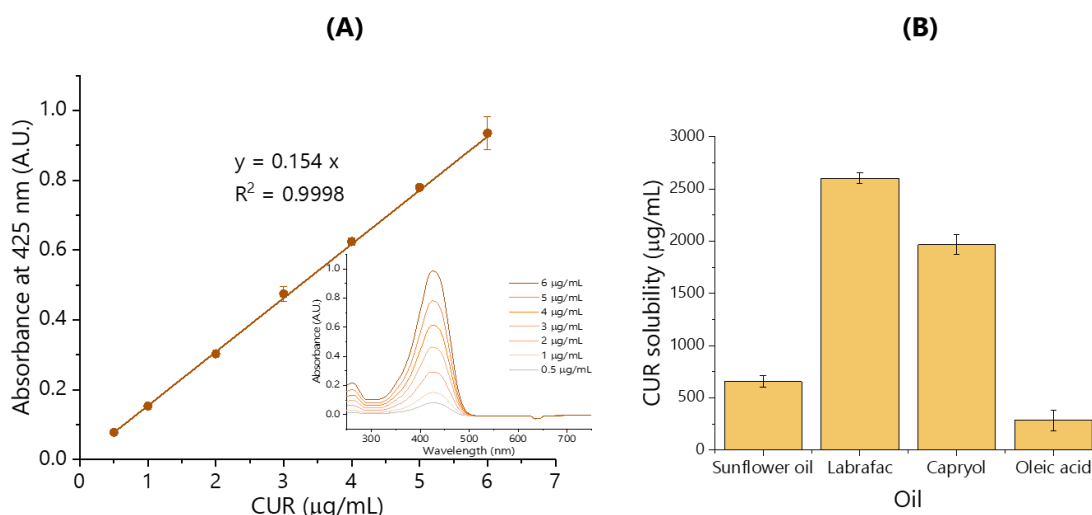


**Figure 57.- Determination of CUR solubility in four different oils. (A)** Calibration curve for CUR in EtOH,(n=3) and respective absorption spectra of standards. **(B)** Calculated curcumin solubility, using previously established calibration curve. (n=2)

**Table 17.-Amount of CUR entrapped in NLCs by employing different techniques**

Loading strategy		Curcumin content in NLCs suspension (µg CUR/ mL)
CUR previously solubilised	in Labrafac	15*
	in Tween 80	88 ± 12
	in Labrafac + Tween 80	131 ± 22
Added in solid form		840 ± 40

\*Preparation was performed once (n=2)

The established way of loading the NLCs implies that an excess of curcumin would be found at the end of the preparation. In order to get rid of this curcumin excess, a centrifugation step needs to be added to the procedure. Because of CUR low water solubility, Excess-CUR (entrapped CUR) will precipitate during centrifugation and can be separated from CUR-loaded NLCs which will be found in the supernatant at the end of the process.

It has to be kept in mind that the loading method can have an impact in for example the release of the active ingredient, as it was studied by Xue *et al.*<sup>280</sup> for SLN. It was stated that adding the active ingredient in the solid form could lead to accumulation in the outer parts of the nanocarrier and lead to a burst release.

### **1.2.2. CUR-NLCs physico-chemical characterization**

While non entrapped curcumin (excess-CUR) can be removed by centrifugation, any other unstructured material, lipids or surfactants in excess may remain together with NLCs. In order to get rid of them, so that there will be no risk of toxicity when in contact with cells, NLCs formulation is passed through a SEC column. Characterization of NLCs elution will be reviewed in section 1.2.2.3. of this chapter and in most parts, the study of the samples before and after passing through the SEC column will be presented.

As curcumin entrapment is defined after the centrifugation step (and before SEC), drug loading and entrapment efficiency results will be referred as obtained before passing through the SEC column.

#### **1.2.2.1. Drug loading and Entrapment efficiency**

As previously explained, during the established preparation method for CUR-NLCs, total-CUR introduced in the preparation is distributed between the NLCs (loaded-CUR) and the pellets (excess-CUR). NLCs remain in the supernatant. This implies that for the direct quantification method, lipids need to be fully solubilized, so that their absorbance will not interfere with that of curcumin. This is why the supernatant is diluted with a binary solvent composed of DCM/EtOH (60/40 %, v/v). This binary solvent was chosen for its high solubility power for lipids as reported in a previous study<sup>249</sup> and used for all spectrophotometric measurements where loaded-CUR was quantified.

As depicted in Figure 57, for the direct method, the standard CUR and Loaded-CUR show the same absorption spectra with a  $\lambda_{\max}$  = 427 nm, indicating that NLCs constituents are fully solubilized and they do not interfere with curcumin spectra. CUR calibration curve gives an extinction coefficient of  $\epsilon_{427\text{nm}} = 0.144$   $\mu\text{g/mL}$ .

As also showed in Figure 57, but for the indirect quantification method, the pellet is dissolved in ACN for

HPLC analysis. The obtained standard CUR and excess-CUR chromatograms present the same peaks corresponding to the three components of CUR: Bisdemethoxycurcumin with a retention time ( $R_t$ ) of 7.55 min, Demethoxycurcumin ( $R_t = 7.79$  min) and Curcumin ( $R_t=8.04$  min). The percentages of these three components of CUR were determined from relative area peaks: Curcumin (79%), Demethoxycurcumin (19%) and Bisdemethoxycurcumin (2%). These results confirm the purity given by the supplier and were used to calculate a mean molecular weight for CUR:  $MW=361.4$  g/mol.

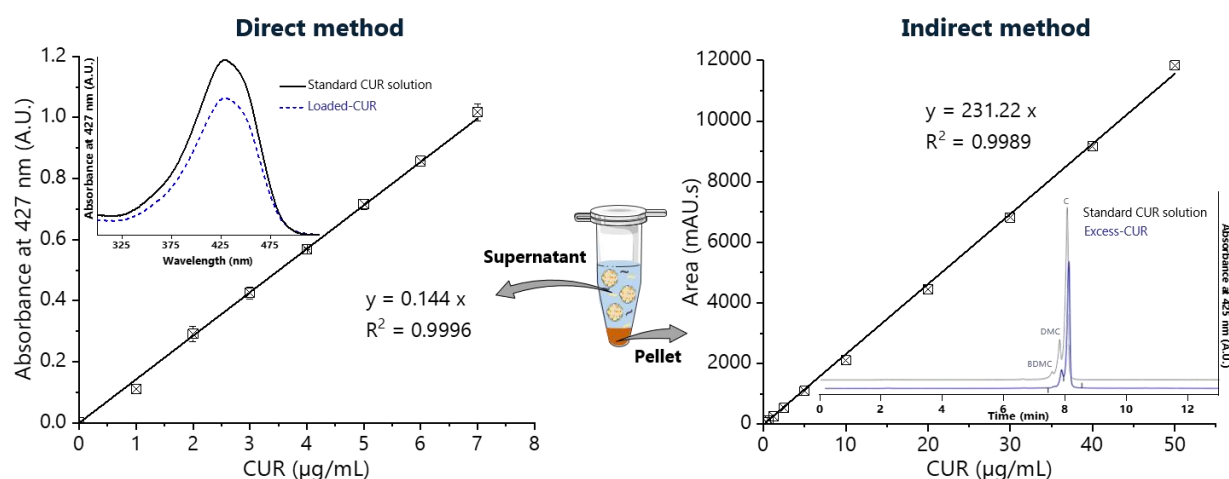


**Figure 58.- Obtained calibration curves for curcumin determination by Direct Method and Indirect Method.** Direct Method was performed using a UV-VIS spectrophotometer, while Indirect Method was performed using a HPLC-DAD. For Indirect Method, obtained chromatogram for CUR shows individual peaks for the three individual curcuminoids. C: curcumin,  $R_t=8.04$  min. DMC: demethoxycurcumin,  $R_t=7.79$  min. BDMC: bisdemethoxycurcumin,  $R_t=7.55$  min.

CUR content was directly determined with a UV-VIS spectrophotometer and indirectly by HPLC in samples before going through the SEC step. Similar results were obtained with both techniques (Table 18). This confirms the accuracy of the UV-VIS spectrophotometry method, face to the HPLC and allowed us to use confidently the direct method in further biological and antioxidant assays for the determination of CUR entrapment in our nanosystem.

After preparation of CUR-NLCs, nearly 85% of CUR was entrapped, showing that most of the CUR initially added at the beginning of the preparation is preserved in the nanocarrier at the end of the procedure. This %EE remains in the reported range for curcumin loaded NLCs<sup>210,281,282</sup>, and is higher than curcumin loaded SLN (Solid Lipid Nanoparticles)<sup>283,284</sup>. Moreover, the total amount of curcumin loaded, around 0.85 mg/mL ( $2 \times 10^{-3}$  M), represents a very important increase in the apparent water solubility of curcumin, which is estimated at  $3 \times 10^{-8}$  M<sup>119</sup>.

%DL of nearly 2.3 % demonstrates the lipid nature of CUR-NLCs. This highlights the importance of taking



unloaded (Blank-NLCs) as a control group for antioxidant and biological experiments in order to get a truthful understanding of the effects of the loaded drug. as small %DL are reached in lipid nanoparticles, it is of major importance that the excipients used in the formulation do not represent a toxicological risk. This justifies the initial choice of components which are not only approved for cosmetic or pharmaceutical use, but that are in quantities lower to the maximal amounts established for dermal products.

**Table 18.- Curcumin loading into NLCs before passing through SEC column**

	Direct method	Indirect method
CUR loaded (mg/mL)	0.85 ± 0.04	0.83 ± 0.03
% EE	84.56 ± 4.48	83.40 ± 3.63
% DL	2.33 ± 0.10	2.23 ± 0.12

While analysing the variation of curcumin loaded into NLCs over 45 days (Figure 58), no statistically significant change was evidenced. This gives two important informations about CUR-NLCs. First, crystallisation of the lipidic matrix during storage, if it takes place, seems to not expel curcumin for the tested time period. Second, CUR-NLCs can be stored for at least 45 days, at 4-8°C and protected from light, in order to perform experiments.

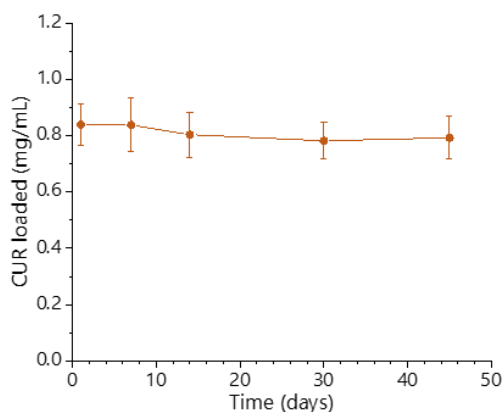


**Figure 59.- Variation of the amount of curcumin loaded into CUR-NLCs over 45 days after preparation.** Samples were stored at 4-8°C between measurements and protected from light (n=3).

During drug delivery development, a part from the amount of active ingredient that can be loaded in a nanocarrier, knowledge about size, size distribution, ZP, morphology, and ability to preserve interesting properties of the active ingredient (like antioxidant activity) of new nanoparticle formulations, are important features to be studied. They are useful to identify a specific type of nanoparticle, and give insights on for example the stability of the system, behaviour during processing (purification steps and freeze-drying) as well as their impact while interacting with biological systems.

### 1.2.2.2. Particle size and zeta-potential

From a regulatory point of view, size and size distribution characterization are paramount in order to be inline with guidelines defining nanomaterials. Special guidelines specify that for being classified as a nanomaterial, at least 50% of the distribution of nanoparticles need to have a size between 1-100 nm.

Tools for determining the size and size distribution of nanoparticles can be either direct or indirect. While in a direct method, the researched dimension is directly measured by the instrument, in an indirect method, the magnitude of the dimension is calculated from another measured characteristic by the instrument. Main advantage for indirect methods is their easiness to handle, which makes them appropriate when a lot of measurements are required. That is why in this work, initial characterization and follow-up of stability were performed using an indirect technique: DLS.

Established formulation and method resulted in suspensions of homogeneous aspect (Figure 59-A). Nevertheless, particle size analysis, expressed in % of intensity (Figure 59-B) or number (Figure 59-C), evidenced two populations of NLCs: a small size NLCs population (P1, 70-85 nm) and a large size NLCs population (P2, 280-360 nm). Distribution of these two populations was ~ 80 % (P2) and ~ 20% (P1) expressed in % of intensity. However, when NLCs size was expressed in % of number, the small size NLCs population, P1 represented the principal peak (98.5%, versus 1.5% for P2). In all cases PDI was between 0.34-0.45, describing the bi-dispersed nature of the formulations. Blank- and CUR-NLCs present similar size and distribution profiles.

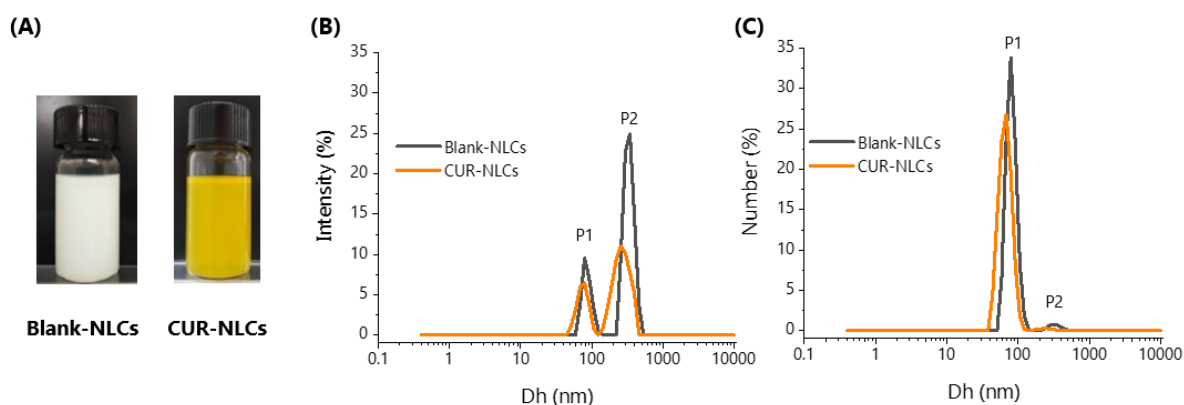


**Figure 60.- Aspect and particle size of Blank-NLCs and CUR-NLCs at day 1 after preparation. (A)** Pictures of Blank-NLCs and CUR-NLCs. **(B)** Dh and distribution in % intensity. **(C)** Dh and distribution in % number.

As showed in Figure 60-A, repeated measurements at 7, 14, 30 and 45 days after preparation show that these parameters do not significantly change over time. Nonetheless, a bigger dispersion in the PDI is observed at day 45. ZP was  $-9.69 \pm 1.02$  mV for Blank-NLCs and  $-10.08 \pm 1.78$  mV for CUR-NLCs one day after preparation. Repeated measurements until day 45 do not show a significant change over time (Figure 60-C).

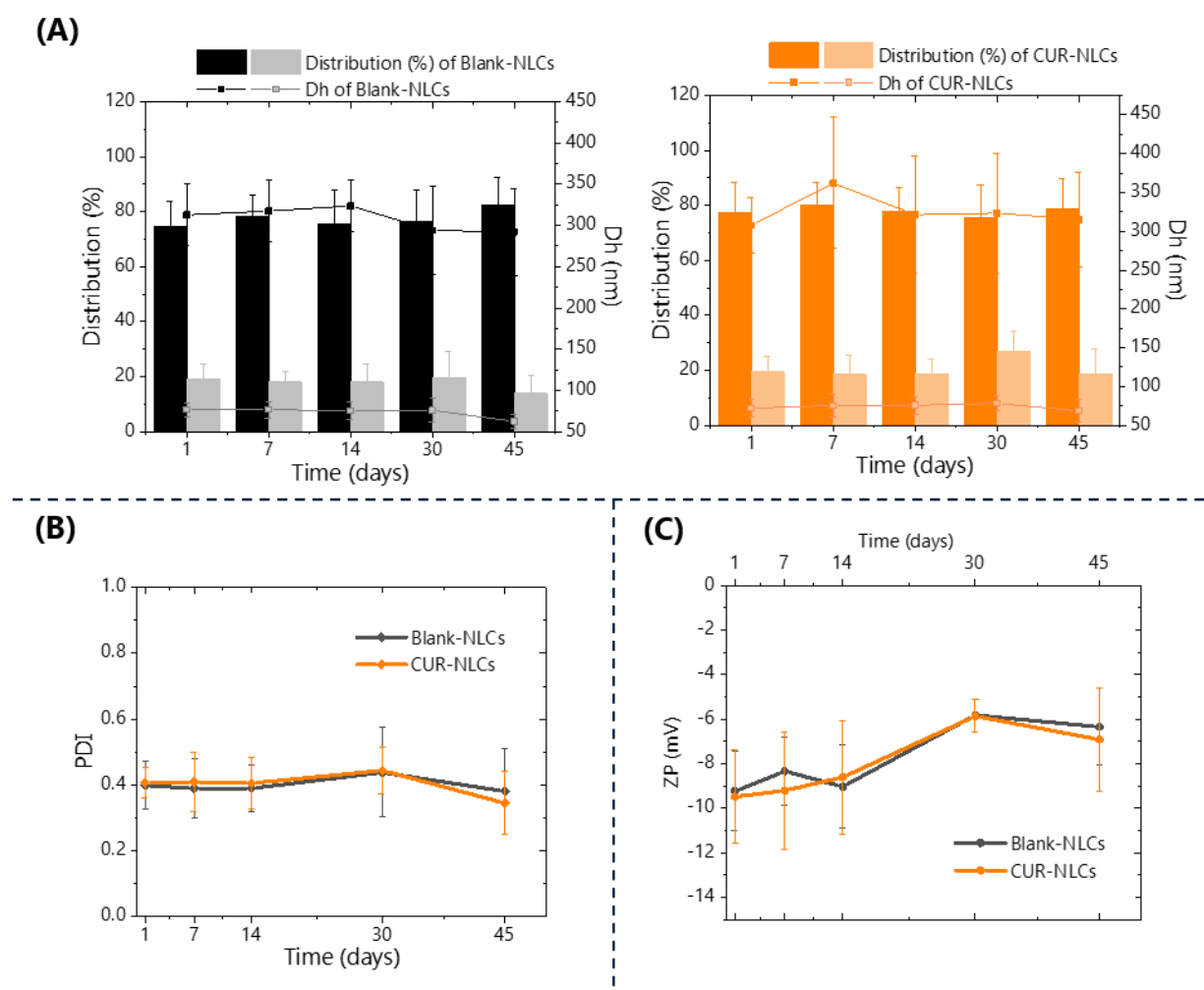


**Figure 61.-Particle size and zeta potential of Blank-NLCs and CUR-NLCs over 45 days after preparation. (A)** Variation in the Dh and the distribution in % intensity. Bar graphs indicate the distribution in % intensity of NLCs while line and dot graphs indicate the size of each NLCs population in terms of their Dh. **(B)** Variation in the PDI. **(C)** Variation in the ZP. (n=3).

Sizes of Blank-NLCs and CUR-NLCs fall around the range reported for other formulations for CUR-NLCs: 90-534 nm.<sup>206-209,211-213,285</sup> It is interesting to note that, both populations found for Blank-NLCs and CUR-NLCs are smaller than 500 nm, therefore both could be potentially internalized by cells<sup>286</sup>. After internalization, nanoparticles of different sizes might have different fates. Hence, the possibility of a multi-target therapy for curcumin could be considered. As formulated NLCs are made-up of biodegradable components, their potential cytotoxicity is low, which in accordance with further biological characterization performed. Values for PDI obtained are similar to those found for other lipid nanoparticles formulations<sup>287</sup>. ZP of around -10 mV evidences that stability of formulation is less likely to be due to electrostatic forces. Instead a phenomena of steric repulsion could be taking place. Such phenomenon is common in particles formulated with non-ionic surfactants as Poloxamer 407 and Tween 80<sup>288</sup>. In this cases, surfactants molecules present in the surface of nanoparticles could hinder the coalescence between them. This stability

mechanism is supported by the homogeneous appearance of NLCs during the observation time after preparation.

### **1.2.2.3. NLCs purification by permeation through SEC column: impact on particle size and zeta potential**

Size exclusion chromatography (SEC) allows the separation of molecules due to their size. Separation ability mainly depends on porosity of the stationary phase. BioGel P-10 is composed of porous polyacrylamide beads as stationary phase, when packed it presents a fractionation range of 1 500 – 20 000 Da<sup>253</sup>. Every molecule with a molecular weight (MW) above the exclusion limit (20 000 Da) will be excluded from passing through the pores of the beads and will get out of the column first. Based on calculations for Dh of globular proteins<sup>289</sup>, formulated NLCs would present an estimated molecular weight of around 222 567 kDa for P1 (of ~80 nm) and around 11 739 219 kDa for P2 (of ~300 nm), -calculs in supporting data in this chapter-. This implies that they will get out of the column first. Oppositely, every molecule with a molecular weight lower than the permeation limit (1 500 Da), will completely penetrate the pores of the stationary phase and will elute out of the column at the same time. NLCs components that are below this limit are: Tween 80 (MW = 1 310 g/mol), Precirol (MW = 625 g/mol) and Labrafac (MW=388 g/mol). Also, any molecule between the permeation limit and the exclusion limit will variably penetrate into the pores. Penetration will depend on their size. From the components used for NLCs preparation, only Poloxamer 407 (MW=14 600 g/mol) has a molar mass in this range.

According to this, if any component used for NLCs preparation is in its molecular form, that is, not being part of NLCs, it can be separated from them by going through the BioGel P-10 SEC column. Detection of all components could be performed analysing the eluted fractions with the appropriate detector. For NLCs components at their molecular state, a refractive index detector or a mass spectrometer would have been the more appropriate ones as any of the molecules present absorbance or fluorescence. Due to the unavailability of these detectors, during this work detection and identification of individual components was not performed. Another possibility for detecting these compounds could be to derivatize some of them.

Alternatively, DLS was used. For each eluted fraction, the Dh and the derived count rate were registered. On one hand the Dh will give an idea of how big are the particles in solution are. On the other hand, the count rate reflects the intensity sensed by the detector and can give a clue of the amount of particles present in the sample. As depicted in Figure 61-A, for Blank-NLCs and CUR-NLCs, the derived count rate increases as the elution volume increases, reaching a maximum at fraction IV in both cases, after when it decreases again. Fractions I, II, VI, VII, VIII and IX present low count rates compared to fractions III, IV and V. As derived count rate is the amount of photons per unit of time (kilo counts per second) arriving to the DLS detector,

and this depends on the size and concentration of the particles in suspension. This behaviour indicates that fractions III-IV are the ones presenting the higher amount of NLCs. As showed in Figure 61-B, the size distribution remains unchanged from the one of the NLCs suspension before going through the SEC column. Thus, by pooling together fractions III, IV and V, the maximal amount of NLCs will be recovered. These NLCs are more likely to be separated from components alone in their molecular form (Tween 80, Precirol, Labrafac and Poloxamer 407 that are able to penetrate into the stationary phase and in consequence, they will flow-out later. The higher amount of NLCs in fractions III-IV is qualitatively seen in Figure 61-C, as this fractions present more turbidity. For fractions VI or higher, their more transparent aspect is in accord with the lower derived count rates depicted in Figure 61-A.

The fact that both NLCs populations (P1 and P2) flow out of the column together is in accordance with their calculated molecular weight which is higher that the exclusion limit of the column. If order to separate both NLCs populations, a SEC column with a fractionation range comprising the calculated molecular weight of both populations would be needed (around 200 000 kDa – 12 000 000 kDa).

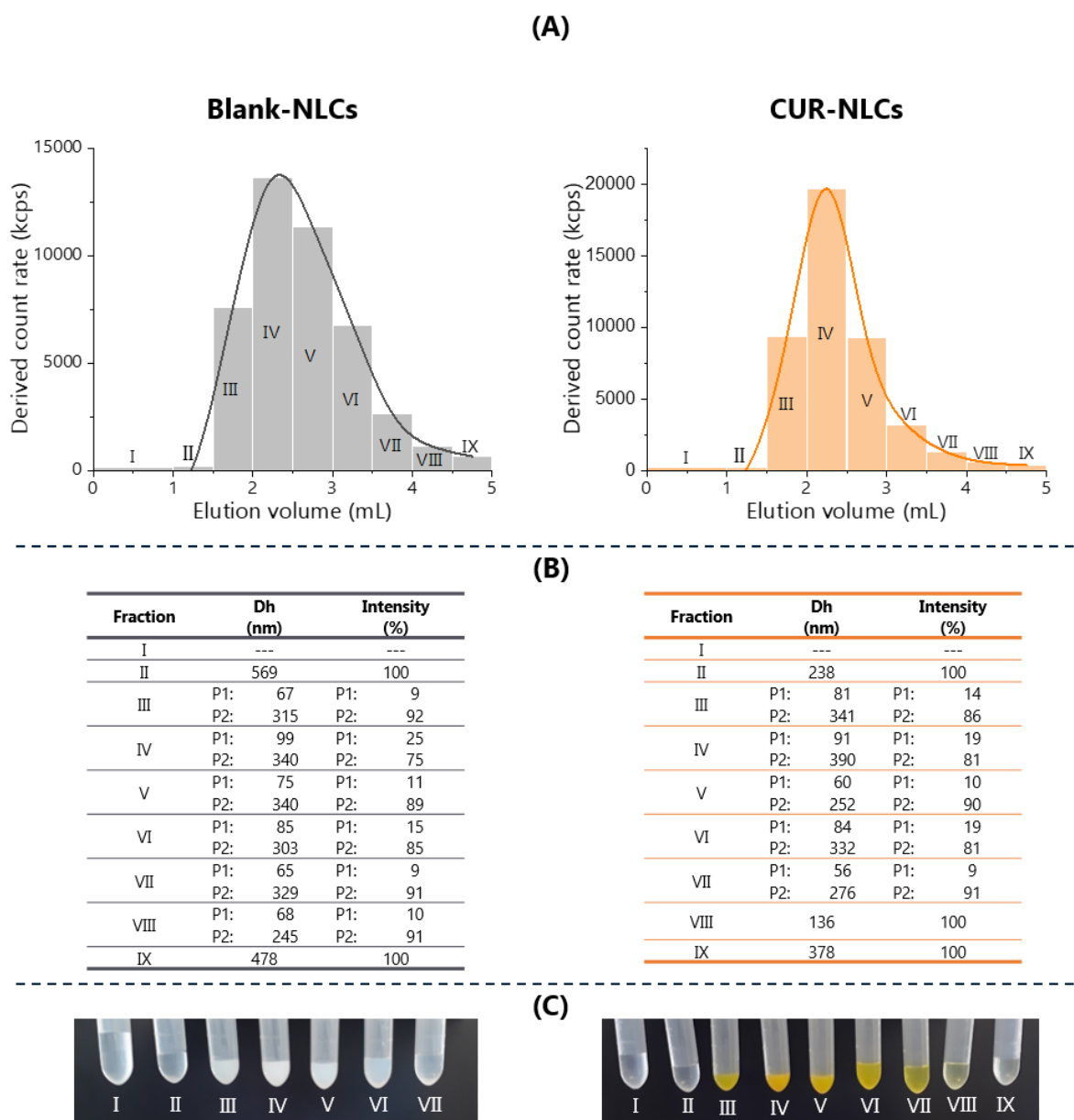


**Figure 62.- NLCs separation using SEC column (Bio-Gel P10).** (A) Example of the chromatogram obtained when eluting Blank-NLCs or CUR-NLCs. Derived count rate was obtained from the mean count rate and the % Transmission at which were taken the DLS measurements. For explanation of calculus see Supporting information, on this chapter. (B) Size distribution for the different fractions obtained when eluting Blank-NLCs or CUR-NLCs. (C) Aspect of eluted fractions. Fractions I-VII for Blank-NLCs and fractions I-IX for CUR-NLCs are presented. For CUR-NLCs, volume for fractions III-V is half (250  $\mu$ L) of the original eluted volume (500  $\mu$ L) as for this particular sample half of the volume was used to perform other experiments.

Even if detection of single molecules, 'unstructured' NLCs components, was not performed due to lack of the appropriate detectors, arguments previously presented allow to confirm that it is possible to separate NLCs from any other component that might be left after the preparation and the centrifugation step. This is important as it allows us to perform biological characterisation more confidently. By putting cells in contact with the NLCs after going through the SEC column, we can be sure that the observed behaviour is caused by NLCs and not by individual molecules of the excipients. This is important specially as single

surfactant molecules, like Tween 80 can interact with cell membranes.

It is to note that other researchers skip this purification step. In other cases, they are able to separate NLCs as a precipitate by ultracentrifugation. Experience with our system shows that designed NLCs did not precipitate by ultracentrifugation.

Blank- and CUR-NLCs suspensions after going through the SEC column present a similar appearance as suspensions before going through it (Figure 62-A). However, similarities between Blank- and CUR-NLCs distribution profiles is more evident for samples after the SEC column Figure 62-B, C.

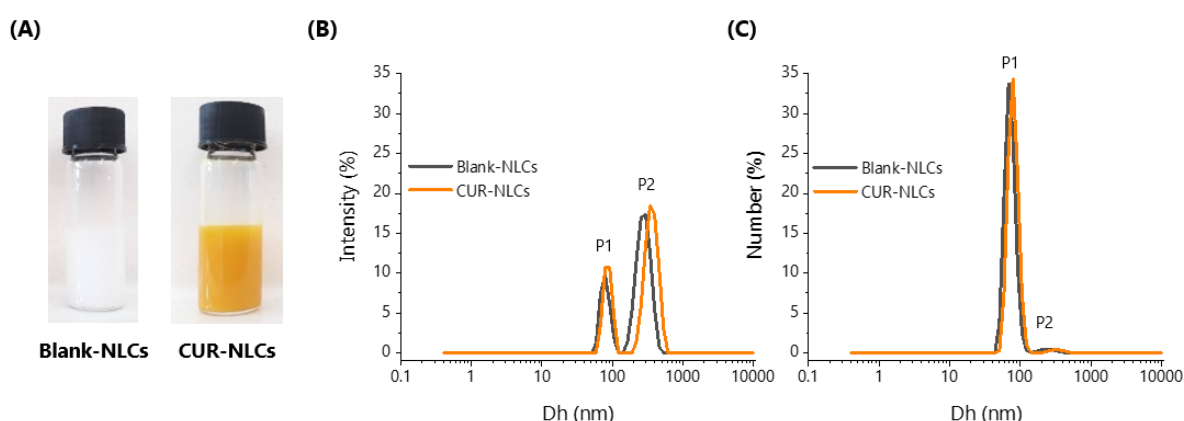


**Figure 63.- Aspect and particle size of pooled fractions 3-5 of Blank-NLCs and CUR-NLCs after permeation through SEC column. (A)** Pictures of Blank-NLCs and CUR-NLCs. **(B)** Dh and distribution in % intensity. **(C)** Dh and distribution in % number.

Table 19 shows that sizes and PDI for samples after the SEC column are similar to those of NLCs suspensions after preparation. Measures at day 7 show that sizes remain unchanged:  $73 \pm 23$  nm ( $14 \pm 9$  %)  $329 \pm 30$  nm ( $87 \pm 9$  %) for Blank-NLCs and  $79 \pm 18$  nm ( $15 \pm 7$  %)  $348 \pm 30$  nm ( $83 \pm 7$  %) for CUR-NLCs. Respect to ZP measurements, a slight difference is evidenced before and after the SEC column ( $\sim -9$  mV and  $\sim -16$  mV, respectively).

Difference in ZP before and after the SEC column may be due to difference in the nature of amount of molecules present in the continuous phase of liquid suspensions in samples before and after going through the SEC column. Different free molecules in suspension can alter the conformation of the layer of counter ions around each particle (stern layer) as well as the composition of the electrophoretically mobile particles at the slipping plane in the diffusion layer<sup>255</sup>. As ZP reflects the potential difference between the stern layer and the slipping plane, difference in their composition could be translated in differences in ZP detected when an electric field is applied. We can hypothesize that in samples before going through the SEC column, such free molecules present are Labrafac, Precirol, Poloxamer or Tween 80 molecules not being part of NLCs.

**Table 19.- Sizes, PDI and Zeta Potential of CUR- and Blank-NLCs before and after permeation through SEC column.** (n=3) Size is expressed as Dh.

	Before SEC column				After SEC column			
	Blank-NLCs		CUR-NLCs		Blank-NLCs		CUR-NLCs	
	P1	P2	P1	P2	P1	P2	P1	P2
<b>Size (nm)</b>	77 ± 8	313 ± 37	72 ± 11	308 ± 36	79 ± 6	280 ± 11	85 ± 6	362 ± 26
<b>PDI</b>	0.40 ± 0.07		0.41 ± 0.05		0.34 ± 0.04		0.44 ± 0.02	
<b>ZP (mV)</b>	-9.23 ± 1.77		-9.48 ± 2.10		-15.85 ± 0.64		-17.25 ± 1.20	

#### 1.2.2.4. Morphology

In the past sections DLS has been greatly used to characterise prepared NLCs due to its easiness in operation. However, its main disadvantage is that as nanoparticles are not directly seen, information about their morphology is inaccessible. DLS technique will give the Dh of a sphere that diffuses at the same speed than that of the studied nanosystem. In consequence, some lack of accuracy in the dimensions found can be expected, as it has been demonstrated that depending of their morphology nanosystems diffuse differently. Because the Dt of anisometric particles is bigger than that of a sphere with the same volume, the Dh derived of DLS measurements result slightly high than the real ones<sup>290</sup>.

By employing a direct technique like Transmission Electron Microscopy (TEM), NLCs would be directly seen, their dimensions confirmed and their morphology identified.

As shown in Figures 63-64, particle size results obtained by DLS were confirmed by Cryo-TEM and negative stain-TEM analyses for samples before and after going through the SEC column (Figure 63 and Figure 64, respectively). Either through negative stain-TEM and Cryo-TEM, the main 2 size NLCs populations observed in all samples (P1, ~ 60 nm) and (P2, ~ 270 nm) were slightly smaller than size NLCs analysed by DLS technique. Moreover, the polydispersity of the NLCs was verified. In this regard, measurements of most representative NLCs sizes, can be seen in both images.

It can be observed that by employing the column, quality of the samples increased in terms of purity. For Cryo-TEM images fewer big chunks were seen while selecting the area for image acquisition (data not shown). For negative stain-TEM images, by comparing images before and after SEC column for the same sample, more particles can be seen. As before and after the SEC column the same sample concentration (g/L) was analysed for both Blank-NLCs and CUR-NLCs, the fact that more particles are present for the same mass concentration in samples 'after column' could mean that some of the mass weighted for samples 'before SEC column' was in fact 'non-structured materials' that is, excipients (Precirol, Labrafac, Tween 80 and Poloxamer) that did not elute out of the SEC column at the same time that NLCs.



A circular shape was observed for both populations by negative stain-TEM. Cryo-TEM technique showed that small sized NLCs can be distinguished by two preferential conformations, a circular shape conformation when observed on the top view and a rod shape when NLCs are observed on the side view (yellow arrows in Figure 63 and Figure 64). Only circular shape conformation was observed for large size NLCs (red arrows in Figure 63 and Figure 64). Both observations point to a main circular platelet shape of NLCs. Even if existing NLCs formulations for curcumin entrapment lack a morphological characterization, other studies have also reported these observations in SLNs as well as in NLCS and thus, confirm the platelet shape described in our results.<sup>290-293</sup>

Interestingly, for Cryo-TEM images some particles present a darker edge, in both the top and the side view (red and yellow arrows). This could indicate the presence of a more solid lipid state in this area. Jores *et al.*<sup>290</sup> tested this hypothesis by comparing such structures to those seen while formulating unloaded NLCs and nanoemulsions (no solid lipid in the formulation). For nanoemulsions, droplets of the same size and similar contrast were identified. However, for NLCs, darker regions were seen. Researchers hypothesised that difference in contrast was due to separation of the solid lipid from the oil. They called these structures "nanospoons" as it seemed that the oil was sticking as a droplet, while the lipid was present as a platelet. It is to be note that in our formulation, lack of contrast of what could be the oil might be explained by the low density of Labrafac (0.946 g/mL), which is very similar to water (medium in which samples were preserved).

In negative stain-TEM images, a small compartment seems to be present in some particles, either inside or at the surface. However, these results need to be interpreted carefully as during negative stain pre-treatment for TEM, samples need go through a drying step so that uranyl acetate (the stain) becomes solid. Even if more easily to perform than Cryo-TEM, this step can originate some artefacts resulting from the cracking of the dried stain layer. This could be the case for some white spots (like cracks) showed by green arrows. Due to this, it is difficult to tell, just from negative stain-TEM images that there could be compartments in the particles.

It can be noted that for both, negative stain-TEM as well as for cryo-TEM, some particles are not completely circular on the top view. This can be explained by lipid modifications taking place during storage. Bunjes and Unruh<sup>294</sup> and Salminen *et al.*<sup>295</sup> reported that size occurred due to changes in the shape of lipid nanoparticles, and that these were correlated to polymorphic transitions of the lipid content to a more stable form elucidated by XDR ( $\alpha \rightarrow \beta' \rightarrow \beta$ )<sup>296</sup>. Over time, such lipid modifications may explain the tendency of lipid particles to merge, as particles would deform resulting in increasing contact area with other adjacent particles (coagulation). If adjacent particles fusion, then coalescence, an irreversible phenomenon takes

place<sup>297</sup>.

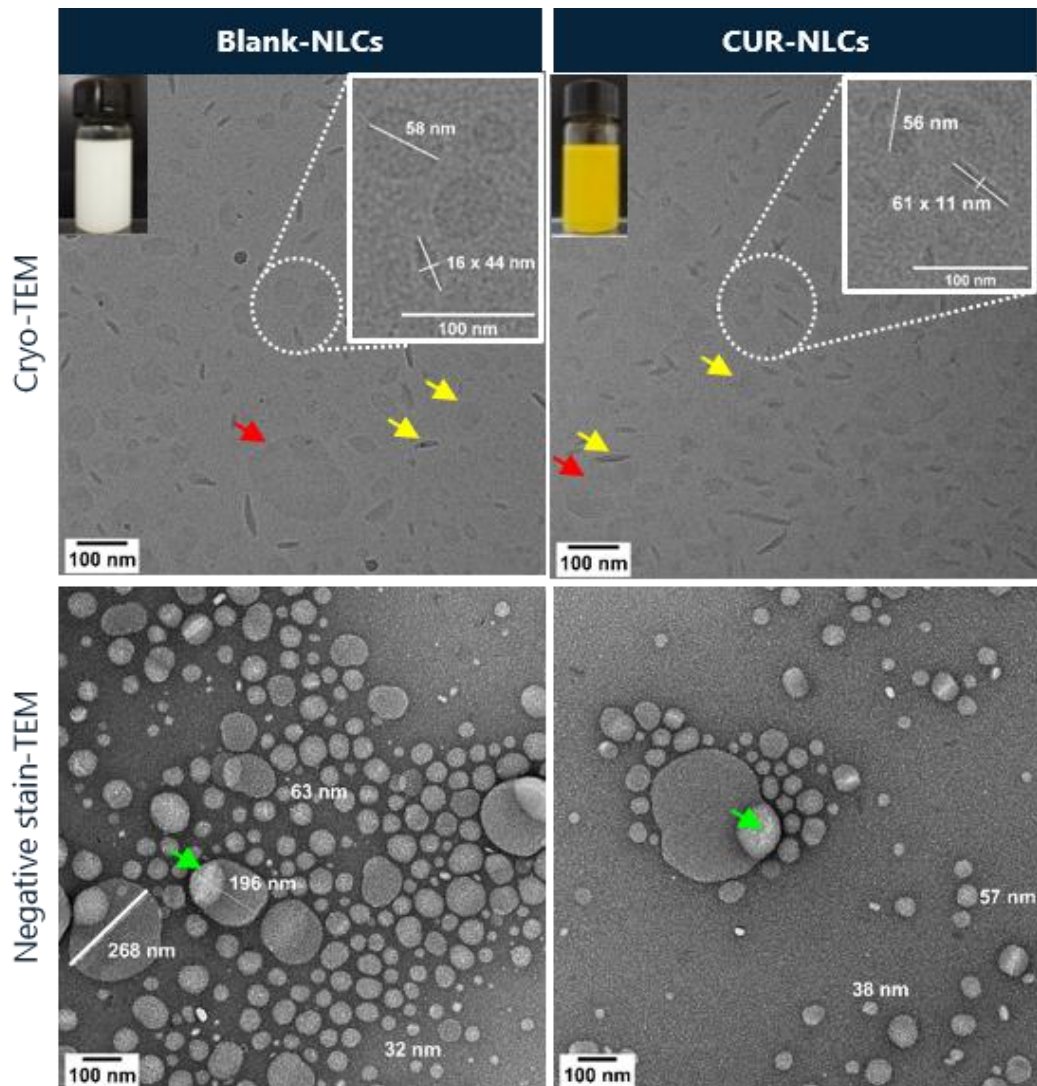


**Figure 64.- Morphological characterization of Blank-NLCs and CUR-NLCs suspensions before passing through the SEC column.** For Cryo-TEM images, yellow arrows show the circular platelet shape (top view) or rod shape (side view) of small size NLCs population while red arrow shows the top view of large size NLCs population. For Negative stain-TEM images, green arrows show possible artefacts due to negative staining pre-treatment.

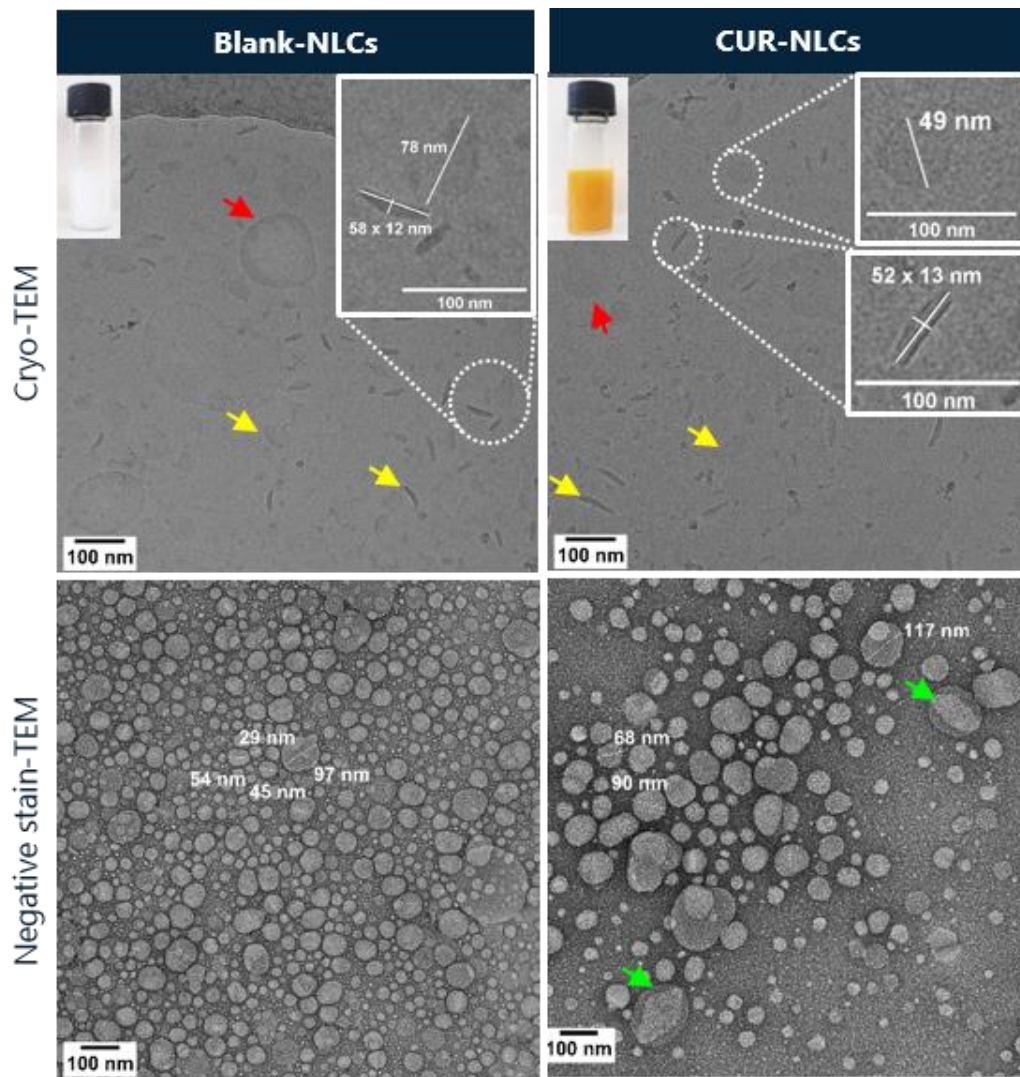


**Figure 65.- Morphological characterization of Blank-NLCs and CUR-NLCs suspensions after passing through the SEC column.** For Cryo-TEM images, yellow arrows show the circular platelet shape (top view) or rod shape (side view) of small size NLCs population while red arrow shows the top view of large NLCs population. For Negative stain-TEM images, green arrows show possible artefacts due to negative staining pre-treatment.

### 1.2.2.5. Antioxidant activity

During CUR-NLCs preparation, the main risk for curcumin stability are the high temperatures at which it is exposed during the Hot Homogenization Method. Chen *et al.*<sup>117</sup> have observed that higher degradation effects for curcumin occur at 190°C. This temperature is not reached during NLCs preparation, however, it is important to assess if antioxidant properties of curcumin are impacted in any extend.

It is known that curcumin can exert its antioxidant properties either by electron transfer (ET) or hydrogen atom transfer (HAT)<sup>120</sup>. During the ABTS assay, inhibition of the radical cation ABTS<sup>•+</sup> is considered to take place by a mixed HAT/ET mechanism<sup>121</sup>. Therefore, ABTS assay was chosen to study the antioxidant activity of the formulations.

Figure 65-A shows the inhibition curves for Blank-NLCs and CUR-NLCs, performed within 7 days after preparation. It can be seen that unloaded nanocarrier does not have any antioxidant activity, as the % of

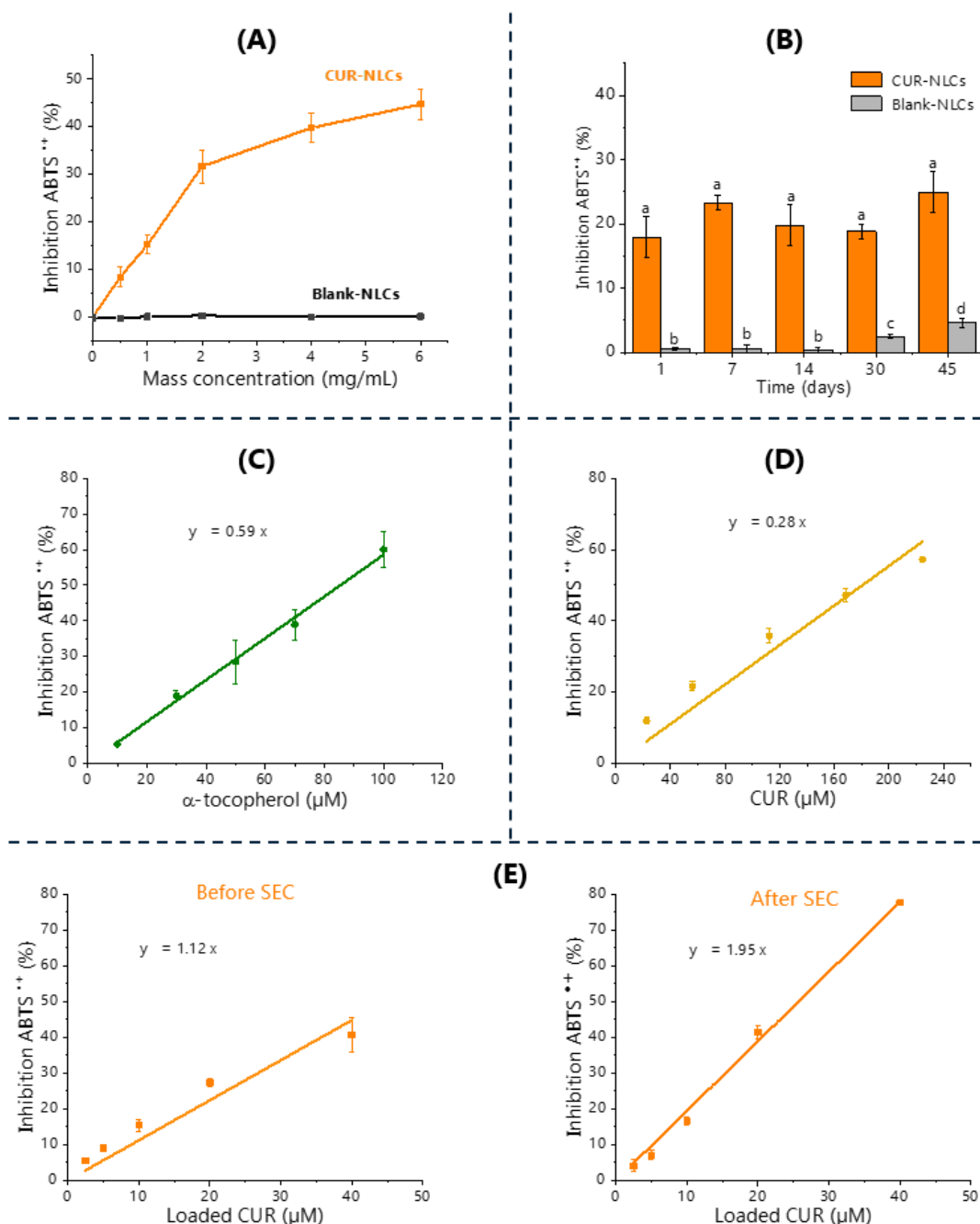
ABTS<sup>•+</sup> inhibition remains nearly 0 for all tested mass concentrations. For CUR-NLCs, antioxidant activity is directly proportional to the mass concentration until 2 mg/mL (containing 54  $\mu$ M of CUR). Between 2 and 6 mg/mL (161  $\mu$ M of total CUR), increments in NLCs concentration result in little increase in the antioxidant activity, until reaching a maximum inhibition plateau of 45 % of ABTS<sup>•+</sup> inhibition at around 6 mg/mL.

Figure 65-B shows the variation in the antioxidant activity of Blank-NLCs and CUR-NLCs at 1.1 mg/mL (containing 20  $\mu$ M of CUR for CUR-NLCs) over a 45 days after preparation. This is the point at the middle of the linear part of the ABTS<sup>•+</sup> in Figure 65-A. Nearly 0% of antioxidant activity was detected for the unloaded nanocarrier until day 14, however it reached nearly 5% at day 45, becoming significantly different from previous days. For CUR-NLCs, even if there was fluctuation between the values, these were not significantly different from each other.

Inhibition curves for CUR (Figure 65-D), and CUR-NLCs before SEC and after SEC column (Figure 65-E) were obtained by plotting of the % ABTS<sup>•+</sup> inhibition vs the concentration of CUR entrapped in NLCs.  $\alpha$ -tocopherol (Figure 65-C) was used as an antioxidant standard. A background activity was observed for Blank-NLC, which was subtracted from activity of CUR-NLC in order to take into account only the antioxidant activity of CUR.

The % inhibition of ABTS<sup>•+</sup> was proportional to the CUR concentration in NLCs up to 50  $\mu$ M (Figure 65-E). For higher CUR concentrations in NLCs before the SEC column a saturation activity was observed with an inhibition plateau at around 45 % of ABTS<sup>•+</sup> inhibition (Figure 65-A). This saturation effect was not observed at the same range concentrations for the other antioxidant formulations (CUR, CUR-NLCs after SEC column and  $\alpha$ -tocopherol).

Figure 65-D shows the antioxidant activity of CUR with a slope of 0.28. Higher slopes of CUR-NLC (before and after SEC column) were found (1.12 and 1.95, respectively, Figure 65-E) when compared to the CUR. Table 20 shows the  $\alpha$ -TEAC scores, calculated as  $\alpha$ -Tocopherol equivalents ( $\mu$ M CUR /  $\mu$ M  $\alpha$ -Tocopherol).



**Figure 66.- Inhibition of ABTS<sup>•+</sup> in NLCs formulations and no entrapped antioxidant compounds. (A)** CUR-NLCs and Blank-NLCs at day 1 after preparation (before SEC column). **(B)** CUR-NLCs and Blank-NLCs at 1.1 mg/mL (containing 20 μM of CUR for CUR-NLCs) at days 1-45 after preparation (before SEC column). One-way analysis of variance (ANOVA) was performed for % ABTS<sup>•+</sup> inhibition, with a p-value = 0.01 (\*\*p<0.01). Means with the same letter are not significantly different from each other. **(C)** α-tocopherol, antioxidant standard. **(D)** CUR. **(E)** Comparison of loaded CUR in CUR-NLCs before and after the SEC column. (n=3).

**Table 20.- Antioxidant activity measured by lipophilic ABTS assay.**

	α- TEAC <sup>1</sup>
CUR	0.47
CUR-NLCs before SEC	1.90
CUR-NLCs after SEC	3.31

<sup>1</sup>α-TEAC is expressed as μM CUR/μM α-Tocopherol. (n=3)

For analysis performed within 7 days after preparation, unloaded NLCs did not have any antioxidant activity. This is mainly due to the fact that excipients used in the formulation of NLCs did not have reducing groups in their structure. Neither Labrafac or Precirol are composed of unsaturated lipids which could form epoxides, producing radicals that might attack and degrade CUR. This implies that whole inhibition of ABTS<sup>•+</sup> is to be attributed to entrapped CUR. Nevertheless, for days 30 and 45 between 2-5% of inhibition is observed. Even if no double bounds are found in the lipids composing NLCs, diacylglycerols and triacylglycerols in Labrabac and Precirol, respectively might be transforming in components being able to inhibit ABTS<sup>•+</sup>. One explanation could be the formation of hydroperoxides during long-term storage, as it was studied by Kato *et al.* in canola oil<sup>298</sup>.

It is interesting to note that antioxidant activity of curcumin entrapped in NLCs is higher than that of free curcumin. This enhancement of the antioxidant activity of curcumin when loaded in lipidic nanoparticles has also been reported by other authors<sup>143,287,299</sup>. Interestingly, Karimi *et al.*<sup>287</sup> also used saturated lipids to formulate Turmeric-NLCs. They found that antioxidant activity assessed by DPPH assay, also a HAT/ET based assay, was higher in Turmeric-NLCs than in Turmeric extract. They explained that such enhanced antioxidant activity could be due to the OH groups present in the oil (Miglyol, also a capric/caprylic trygliceride but from a different brand). However, they did not assess the antioxidant activity of the unloaded NLC. According to our results, where little or no antioxidant activity was measured for unloaded NLCs, it is less likely that OH groups present in the caprilic/capric tryglicerides are completely responsible of the superior antioxidant activity of loaded hydrophobic compounds. It is more likely that surfactants are playing a role. As CUR-NLCs are destroyed with EtOH/DCM (60/40 %, v/v) and CUR released before the assay, surfactants which are originally part of NLCs structure are now present in the samples taken in contact with the ABTS<sup>•+</sup> aqueous solution. Due to their amphiphilic nature, surfactants could favor the solubility of curcumin in aqueous media and as a result, its contact with ABTS<sup>•+</sup>. This can lead to the electron or hydrogen atom transfer which is the basis of the reaction. This surfactant mediated curcumin contact with ABTS<sup>•+</sup> does not happen for free curcumin as these samples contain just curcumin dissolved in a less polar solvent than water: EtOH/DCM (60/40 %, v/v), but any surfactant molecule is present.

The fact that higher inhibition was seen for CUR-NLCs after SEC column reinforce the hypothesis that 'unstructured' components are removed from the formulation. In samples before SEC column, excess of Precirol or Labrafac would hinder the interaction of ABTS with CUR, while in samples after SEC column the steric hindrance is resolved by eliminating such molecules in excess.

$\alpha$ -tocopherol, a molecule that is part of vitamin E, was chosen as a control. Like curcumin,  $\alpha$ -tocopherol is a hydrophobic natural antioxidant.  $\alpha$ -TEAC values in Table 20 show that ability to scavenge ABTS<sup>•+</sup> is about

twice times higher for  $\alpha$ -tocopherol than for curcumin, but about the half than that of CUR-NLC. Results for pure compounds are in accordance to those obtained by AK *et al.*<sup>300</sup> who tested the scavenging of various compounds, including CUR and  $\alpha$ -tocopherol by different methods. Even if CUR showed a lower scavenging effect of ABTS<sup>•+</sup>, CUR ability to scavenge reactive oxygen species such as hydrogen peroxide and superoxide anion radical was higher than that of  $\alpha$ -tocopherol. These findings showed that despite similar physico-chemical properties between CUR and  $\alpha$ -tocopherol, different antioxidant mechanisms are involved. As during skin physiological process, an excess of reactive oxygen species (ROS) may be at the origin of inflammation and hinder the regeneration of the skin barrier, curcumin could be a promising therapy. In this scope, *in-vitro* assessment of the effect of our formulations in protecting cells from oxidative stress would be of interest, as it will be shown in further parts of this work.

It is to note that NLCs formulations designed for curcumin delivery to the skin lack assessment of antioxidant activity of the loaded molecule. This is an important parameter as it will determine the ability of the formulation to fight ROS by neutralizing them *in situ* or by increasing cell defence mechanisms in cells like increase in expression or activity of antioxidant enzymes. In other studies, where CUR-NLCs were designed for achieving an oral delivery, evaluation of antioxidant properties of the formulation is usually performed. For example, for evaluating the antioxidant activity of NLCs entrapping Turmeric extract Karimi *et al.*<sup>287</sup> performed the DPPH assay, while Park *et al.* performed both, the DPPH and ABTS assays<sup>301</sup>. In both cases, the aim was to enhance CUR bioaccessibility through the gastrointestinal tract.

Overall, evaluation of the antioxidant activity demonstrated that curcumin retained its antioxidant properties after being exposed to 70°C during its incorporation into NLCs. This implies that the established formulation process is safe for curcumin and will allow to obtain NLCs bearing antioxidant properties. A feature that could be further exploited in topical drug delivery. This is a major advantage of formulating lipidic nanocarriers over other nanoparticulate systems for the drug delivery of claimed thermos-sensible molecules. For example Montanari *et al.*<sup>302</sup> reported that about 30% of curcumin antioxidant activity, determined by ABTS<sup>•+</sup> test, was lost during its encapsulation in nanohydrogels.

#### **1.2.2.6. Behaviour at different pH**

Figure 66 shows the variation in pH over a 45-day period for Blank-NLCs and CUR-NLCs. Initial pH of around 6.4 slightly drops reaching a minimum of around 5.2 for Blank-NLCs and of around 6 for CUR-NLCs. The little acidification of NLCs suspensions may result from the presence of fatty acids released during the oxidation of acylglycerides.<sup>298</sup>

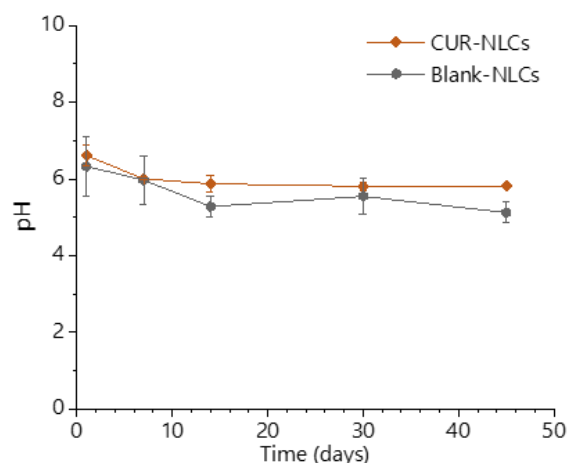


**Figure 67.- pH variation for Blank-NLCs and CUR-NLCs suspensions over 45 days after preparation. (n=3).**

As pH of healthy skin is around 5.5, but it tends to become alkaline in inflammatory cases or when the skin function is disrupted, it is interesting to know how the formulated delivery system will behave in conditions simulating those pH changes.

Here, the influence of pH in the stability of CUR loaded NLCs was assessed by DLS, UV-VIS spectrophotometry and macroscopic observations of CUR-NLCs samples after their dilution in PBS 10 mM at pH=7.4, PBS 10 mM at pH=5.5 (regulated with HCl), or PBS 10 mM at pH=9.0 (regulated with TEA).

Figure 67-A shows the variation in the size and distribution (% intensity) for CUR-NLCs, before and after 24 h of exposition to the different pH. For all pH, both NLCs populations did not showed significant change in Dh or % of distribution. Thus, CUR-NLCs structure seem to not be affected during the 24 h exposition to the different pH.

Figure 67-B shows that UV-VIS absorption spectra of curcumin can be distinguished at all tested pH, with a maximal absorbance at 423 nm. This maximal absorbance is diminished after 24 h for all the pH, but the reduction is higher at pH 9. As NLCs are more likely to be stable in the same conditions, and that curcumin interaction with alkaline environments can be evidenced by colour changes resulting in the deprotonation of OH residues (Figure 67-C)<sup>112,113</sup>, it seems that colour changes are due to curcumin that has been released from NLCs, and thus, that was able to interact with it. As it will be seen in following parts of this work, about 15% of CUR is released from NLCs during 24 h in PBS at pH 7.4. Even if release experiments were not performed at a pH different from 7.4, the greater decrease for the CUR peak at pH=9.0 might indicate that CUR release is higher at this pH, as more CUR is able to interact with the alkaline media. One point that remains to be evaluated is if at those conditions curcumin is just protonated or fully hydrolysed, in which case its bioactivity would be compromised.



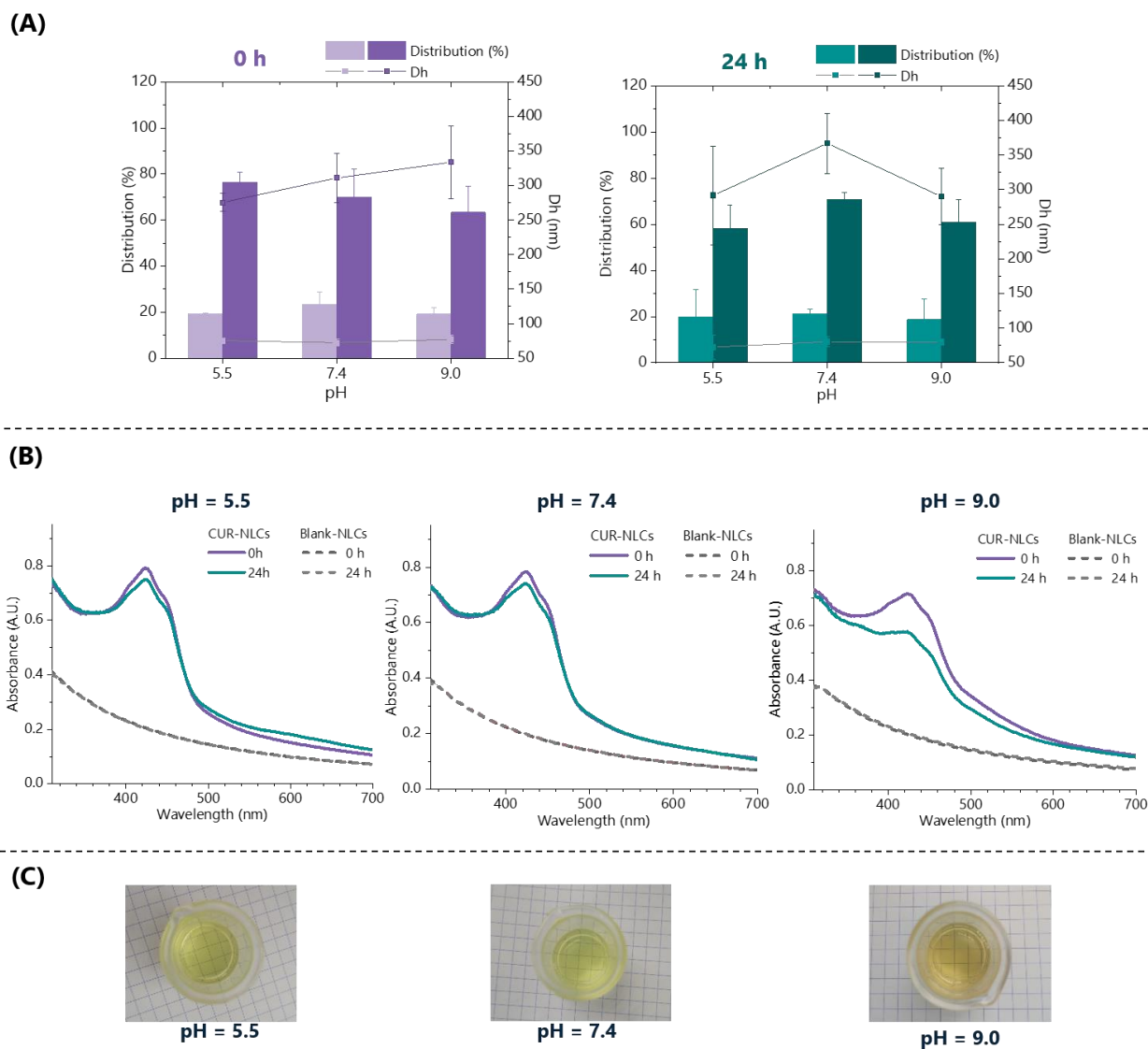


**Figure 68.- Blank-NLCs and CUR-NLCs stability at different pH. (A)** Size distribution (% intensity) for CUR-NLCs at the beginning and after incubation at different pH. (n=2). **(B)** UV-VIS spectra for Blank-NLCs and CUR-NLCs at the beginning and after incubation at different pH. (n=2). **(C)** Pictures of CUR-NLCs suspensions when diluted 1:100 at different pH.

It has been shown that curcumin stability in aqueous media is pH dependent. Under acid conditions, curcumin solubility is reduced and crystallization can take place due to the predominance of the keto tautomer<sup>303</sup>. However, in alkaline or even neutral conditions, successive deprotonation of the molecule can finally lead to degradation through hydrolysis into vanillin, ferulic acid and feruloylmethane<sup>304</sup>. Successive deprotonation takes place at the three estimated pKa of curcumin (7.5-8.5, 12.5 and 13.6) and is evidenced by a colour change towards red<sup>111</sup>. From Figure 67-C, change of colour was just seen at pH=9, confirming that at pH 5.5 and 7.4 it is less probable that curcumin is in contact with the alkaline media, as any sign of deprotonation or even degradation is perceived.

Complementary to our results, some studies show that acidic pH could be a factor influencing in the size of NLCs. For example, Chen *et al.*<sup>305</sup> also used Precirol and Tween 80 to formulate lovastatin loaded NLCs. They observed an increment in size at pH of 1. Authors attributed this change to the breakdown of the lipid formulation during aggregation process. Compritol® 888 (glyceril behenate) and Tween 80 were used by Tamjidi *et al.*<sup>306</sup> to formulate astaxanthin loaded NLCs. During 15 days, they observed that NLCs size was increased in suspensions with pH < 5, while remaining unchanged for pH = 6-8. However, differently from our study, in these two articles the behaviour of the formulation at pH higher than 8 was not assessed.

It has been suggested that due to their free OH groups, partial glycerides such as Precirol and Compritol can be in some extent placed at the water/oil interface forming rigid surfactants films<sup>178</sup>. Being in such contact with the external media, hydrolysis of the ester bond could conduct to the destabilization of the nanosystem. In both previously cited works, it seems that an acidic hydrolysis is taking place as changes in size were seen after the addition of HCl. In our case, as TEA is in aqueous solution, an alkaline hydrolysis would be able to take place at pH=9<sup>307,308</sup>. If this happens, the extent of this degradation is not detectable by DLS, but may play a role in the release of curcumin from NLCs and thus, the stronger decrease in the absorbance at 24 h. During this reaction, nucleophilic groups of TEA might attack the carbonyl group in the ester bond starting a reaction that originates a carboxylate salt and an alcohol. As a consequence, the cargo (curcumin) could be exposed to the environment in higher amounts, explaining a higher decrease in the absorption peak at 426 nm, as it has been demonstrated by our observations. These findings, and those reported in literature show that both acidic and alkaline environments can lead to the destabilization of lipid nanoparticles and thus, that depending on the pH, curcumin could be release by a combination of diffusion and of erosion of the NLCs.

It is to highlight that any further process involving the established formulations should expose as least as possible the NLCs to both an acidic or an alkaline environment.

#### **1.2.2.7. Impact of freeze-drying on NLCs size distribution**

Table 21 shows the size distribution for Blank-NLCs and CUR-NLCs, before and after freeze-drying in either the absence of any cryoprotectant, or the presence of maltose (0.5-1.5 % w/v), sucrose (0.5-1.5 % w/v) or dextrose (0.5-3 % w/v) as cryoprotectant. It can be seen that in all cases, the size of both NLCs populations is increased compared to the sizes before freeze-drying. Presumably in consequence of the fusion of NLCs. In some cases, like for Blank-NLCs freeze-dried with 0.5 % w/v of maltose or sucrose 1.5 % w/v, only one population is population was detected. For each of the tested cryoprotectants, the more concentration is, the lower the sizes are.

The lower change in sizes was obtained for dextrose at 3 % w/v as cryoprotectant. It could be interesting to test this cryoprotectant with a faster cooling cycle in order to diminish the size of water crystals formed, and thus, damages on the nano-system during the freezing step that could lead to agglomeration and be the origin of the increase in size.

**Table 21.- Size distribution (% intensity) of Blank-NLCs and CUR-NLCs before and after freeze-drying and using different cryoprotectants.** P1: NLCs of lower Dh and lower % distribution. P2: NLCs of higher Dh and higher % distribution. n=3, for data before freeze-drying. n=2, for data after freeze-drying.

Before Freeze-drying									
Blank-NLCs				CUR-NLCs					
P1		P2		P1		P2			
67	± 9	nm		267	± 45	nm			
29	± 9	%		71	± 9	%			
73	± 17	nm		282	± 60	nm			
32	± 10	%		68	± 10	%			
After Freeze-drying									
Cryoprotectant  (% w/v)		Blank-NLCs			CUR-NLCs				
		P1		P2		P1		P2	
		Dh, Intensity %		Dh, Intensity %		Dh, Intensity %		Dh, Intensity %	
None	0	251	nm	851	nm	238	nm	1403	nm
		47	%	53	%	22	%	78	%
Maltose	0.5	1366	nm	No detected		251	nm	1403	nm
		100	%			30	%	70	%
	1	221	nm	861	nm	163	nm	571	nm
		34	%	67	%	15	%	85	%
Sucrose	0.5	205	nm	534	nm	226	nm	934	nm
		28	%	72	%	29	%	71	%
	1	280	nm	1048	nm	280	nm	1048	nm
		37	%	63	%	37	%	63	%
Dextrose	1	213	nm	640	nm	213	nm	0	nm
		18	%	82	%	18	%	82	%
	1.5	298	nm	No detected		298	nm	No detected	
		100	%			100	%		
Dextrose	0.5	254	nm	1006	nm	254	nm	1006	nm
		29	%	71	%	29	%	71	%
	1	187	nm	579	nm	187	nm	579	nm
			16	%	84	%	16	%	84
Dextrose	1.5	136	nm	501	nm	136	nm	501	nm
		8	%	92	%	8	%	92	%
Dextrose	3	109	nm	450	nm	109	nm	450	nm
		7	%	93	%	7	%	93	%

Other studies aiming the freeze-drying of lipid nanoparticles, SLNs and NLCs in particular, show that concentrations of cryoprotectant needed to preserve the size are very high: 10-15 % w/v. For example, Rodrigues Santiago *et al.*<sup>309</sup> used 10 % w/v of maltose to cryoprotect amphotericin C-loaded NLCs. However even at that concentrations, results are debatable as an increase of 60 nm was reported for NLCs originally of 122 nm. Blasi *et al.*<sup>310</sup> as well as Schwartz and Mehnert<sup>311</sup> used threalose in concentrations of 10 % w/v and 15 % w/v, respectively to cryoprotect SLNs. Despite of the high concentration of cryoprotectants used changes of around 30 nm and of 200 nm were detected for each of them.

The principal disadvantage of using such high concentrations of cryoprotectants is that eventually they would have to be retired of the reconstituted suspension. Otherwise, they can be present in toxic concentrations that would hinder the direct biological evaluation of the system.

This is why in this work, the freeze-drying of NLCs was omitted, in order to be sure to work in the best conditions, mainly for cell culture experiments. The principal disadvantage of this is that NLCs production had to be often, no sample was stocked for more than 45 days.

#### **1.2.2.8. CUR release in different biological media**

Figure 68 shows the release profile of CUR in the medium for cell culture of fibroblasts (DMEM 10% FBS), the medium for cell culture of keratinocytes (DBM, a serum-free medium) and in PBS. While being in DMEM 10% FBS nearly 40% is released in 24h, reaching to a total of about 75% in 72h. This is much more compared to the 10-15 % of curcumin released in 24h, or even 35% in 72h when CUR-NLCs are placed in PBS or DBM at 37°C in static conditions.

There does not seem to be a burst release. We can thus, interfere that most of the drug is homogeneously dispersed in the nanocarrier and that there is not drug adsorbed on the surface of at the edges of NLCs<sup>189</sup>. Moreover, the form of the curves indicates a monophasic release. In consequence, it seems that the main mechanism for CUR release from the nanocarrier is through diffusion, which is in line with the observations of the stability at different pH already analysed. However, for a deeper investigation of the release mechanisms it would be necessary to add time-points, especially in the first hours of the experiment.

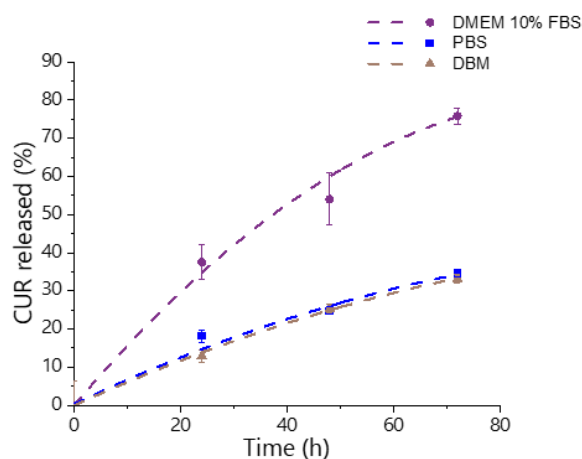


**Figure 69.- CUR release from CUR-NLCs in different biological media.**

About the biological potential of CUR-NLCs, the fact that CUR is released faster in fibroblast culture medium than in the keratinocytes one, could give a hint of why fibroblasts seem to be more sensitive to CUR-NLCs than keratinocytes after 24h contact, as analysed in the following section (1.5.2.). Other NLCs systems encapsulating curcumin show a release of 10-15% of the cargo in PBS during 24h<sup>312</sup>. However, there is a lack of information about the release profiles in relevant biological media such as culture medium as was studied in this work. For a topical application, a time frame of 24h could seem excessive as most topical products are applied more than once during the day. However, experiments in this work were conceived also to get insight of the whole biological potential of the developed formulation. For example, a possible extended release effect thanks to the nanocarriers, or even hints to time dependent interactions of the nanosystem with cells as for example different ways of internalization. This last one is an important aspect as even in cases in which release is not so big, chances that the active ingredients (curcumin in our case) arrive to dermal cells can also depend on the interaction of these cells with the nanoparticle formulation. For example, no released curcumin could display its antioxidant effect if incorporated (internalized) by the cells.

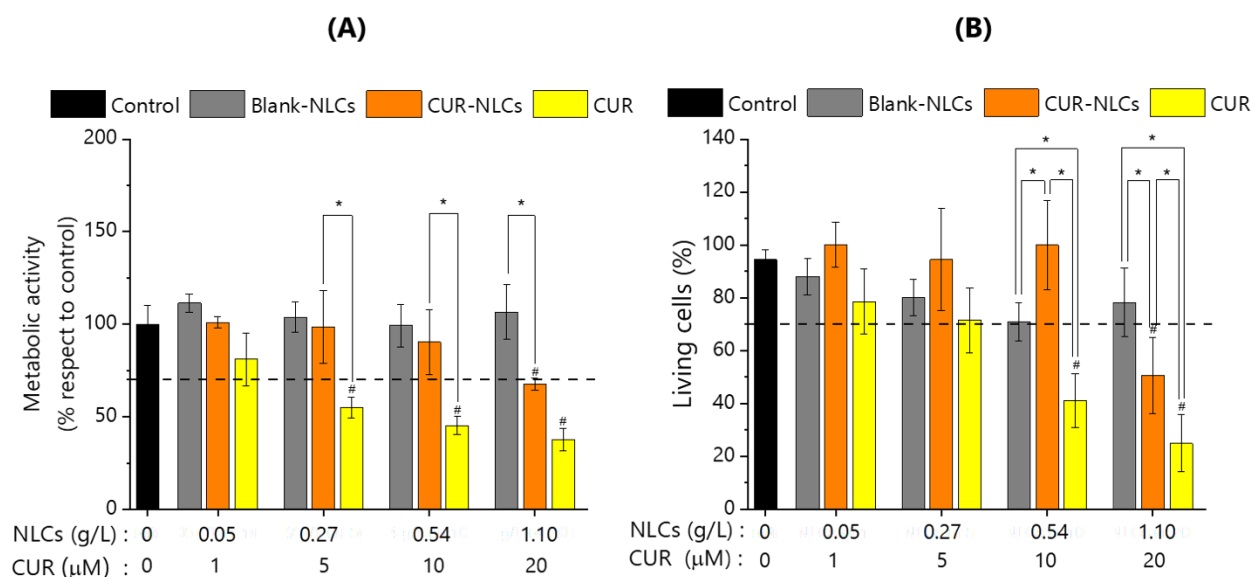
### 1.2.3. CUR-NLCs biological characterization

#### 1.2.3.1. Cytotoxicity studies

The impact of CUR, CUR-NLCs and Blank-NLCs in BJ-Fibroblasts and HEK293T was studied by analysing the metabolic activity, membrane integrity and morphology after 24h of exposition.

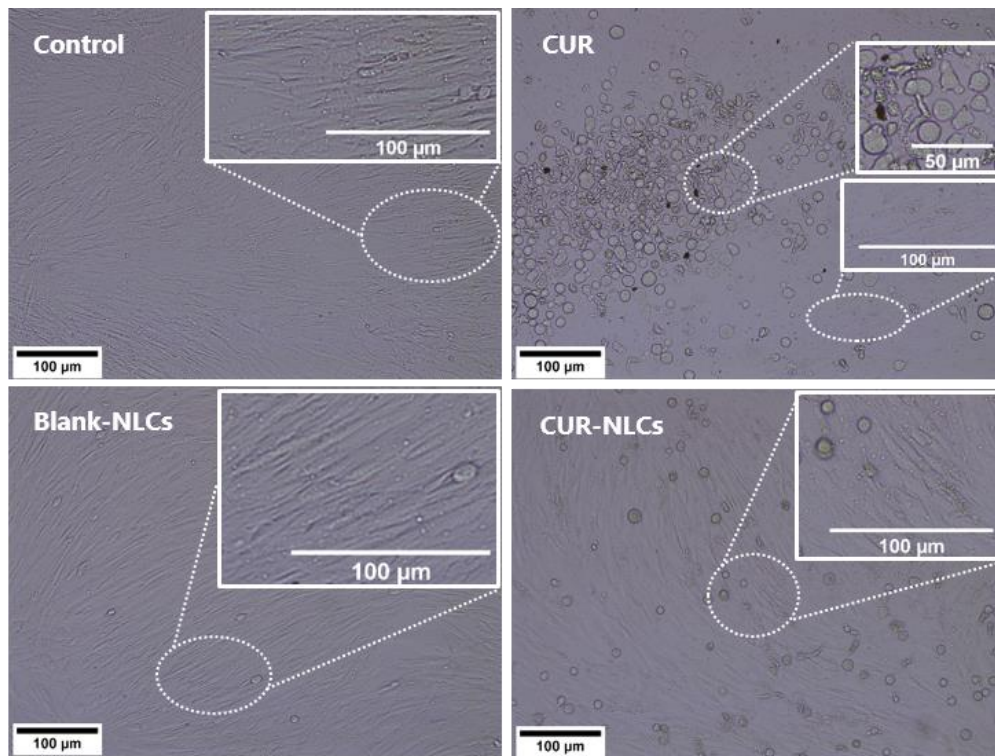
In the case of BJ-Fibroblasts, after 24h treatment with CUR ( $\geq 5 \mu\text{M}$  of CUR), cells showed a loss of metabolic activity and an important diminution of the number of living cells (Figure 69-A, B) compared to the control cells ( $p < 0,05$ ). Treatment of BJ-Fibroblasts with CUR-NLCs or Blank-NLCs did not induce cellular behaviour changes compared with the control group up to 0.54 g/L of NLCs (containing  $10 \mu\text{M}$  of CUR for CUR-NLCs).

On the contrary, cells cultured with 20  $\mu\text{M}$  CUR-NLCs showed a diminution in their metabolic activity and in the number of living cells with intact membrane ( $p < 0.05$ ).



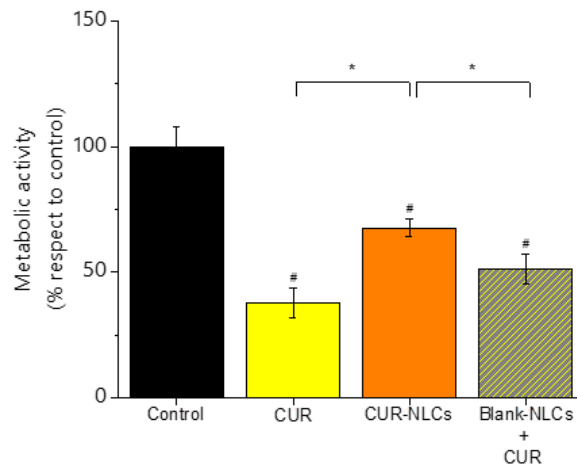
**Figure 70.- Cell viability assays on BJ-Fibroblasts in basal conditions after 24h treatment with CUR, CUR-NLCs or Blank-NLCs. (A) MTT assay. (B) TB assay.** Hashes denote statistically significant differences between an experimental group and the control group, while asterisks denote statistically significant differences between two experimental groups. One-way analysis of variance (ANOVA) followed by Tukey's multiple comparison HSD post hoc test were carried out and statistically significant differences were identified when p-values were lower than 0.05 (\* $p < 0.05$  or # $p < 0.05$ ). (n=3).

Phase contrast images of cells monolayers after 24h exposition to CUR, CUR-NLCs or Blank-NLCs (Figure 70) confirm these observations. While only elongated cells can be distinguished in control conditions and after exposition to Blank-NLCs at 1.1 g/L, only a fewer elongated cells are seen after exposition to CUR 20  $\mu\text{M}$ . Morphology of most of the cells exposed to CUR has changed from elongated to a round one. Despite of this change, cells continue to be adhered to the plate. However, accordingly to MTT and TB results, their metabolic and cellular integrity is compromised. For CUR-NLCs, also elongated cells are present at the same time than round cells. However, there are fewer cells with altered morphology. This is in line with release results in which only  $37.5 \pm 4.6\%$  of CUR is released from CUR-NLCs in 24 h. Thus, the alteration of cells is not at the extend of that observed for CUR.



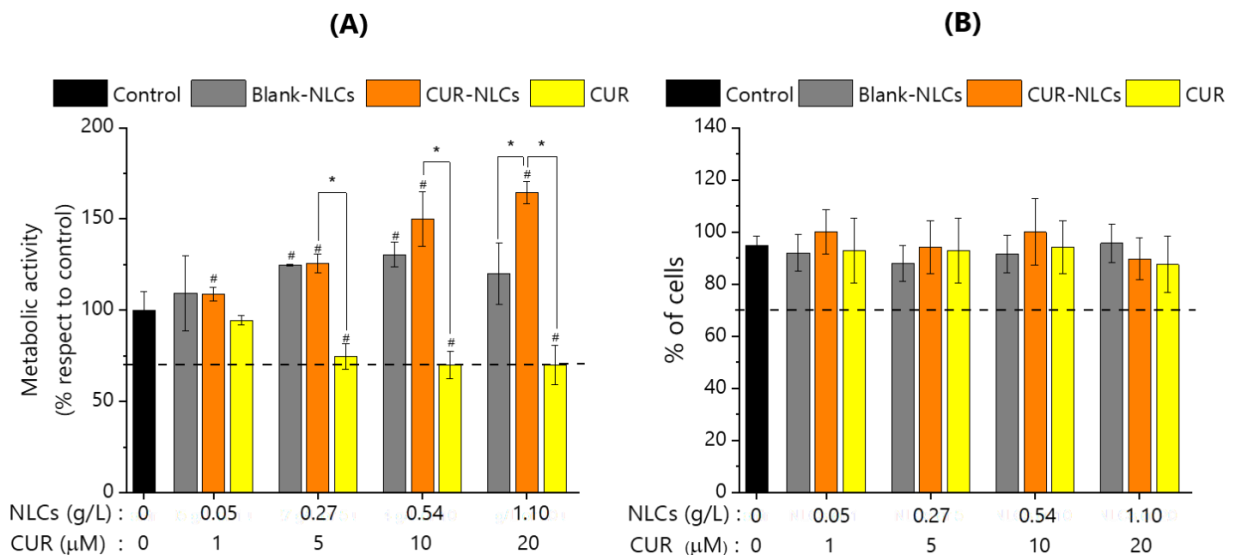
**Figure 71.- Phase contrast images of BJ-Fibroblasts after 24h treatment with DMEM 10%FBS, Control; CUR at 20 µM; Blank-NLCs at 1.1 g/L or CUR-NLCs at 1.10 g/L containing 20 µM of Loaded CUR.**

Figure 71 shows the metabolic activity of BJ-Fibroblasts after 24h treatment with the highest concentrations of CUR-NLCs and Blank-NLCs as in Figure 69, but here another experimental group was added. In this experimental group, cells were exposed to Blank-NLCs at 1.10 g/L dispersed in media culture containing 20 µM of CUR, as a way to mimic the environment that cells will encounter if all CUR was released. Results show that there is a statistical significant difference between CUR-NLCs and CUR and between CUR-NLCs and Blank-NLCs with non-entrapped curcumin. However, the difference is not significant between CUR and Blank-NLCs with non-entrapped curcumin. These result support the observation that not all CUR is released from CUR-NLCs in 24h and that in consequence curcumin toxicity towards cells is diminished by its entrapment into NLCs.



**Figure 72.-MTT assay on BJ-Fibroblasts after 24h treatment with CUR (20  $\mu$ M), CUR-NLCs (20  $\mu$ M of CUR entrapped in 1.10 g/L CUR-NLCs) or Blank-NLCs + CUR (1.10 g/L Blank-NLCs added to 20  $\mu$ M of CUR non entrapped).** Hashs denote statistically significant differences between an experimental group and the control group, while asterisks denote statistically significant differences between two experimental groups. One-way analysis of variance (ANOVA) followed by Tukey's multiple comparison HSD post hoc test were carried out and statistically significant differences were identified when p-values were lower than 0.05 (\*p<0.05 or #p<0.05). (n=3).

For HEK<sub>n</sub>, treatment with CUR ( $\geq 5 \mu$ M of CUR) induced a loss of metabolic activity visible after 24 h (Figure 72-A) (p<0.05). However, the TB test showed a number of living cells (Figure 72-B) comparable to the control cells. Surprisingly, the treatment of HEK<sub>n</sub> keratinocytes with CUR-NLCs or Blank-NLCs induced the increase of the cellular metabolism compared with the control group. For the TB test, the membrane integrity showed no difference in the % of living cells, when compared to the control.



**Figure 73.- Cell viability assays on HEK<sub>n</sub> in basal conditions after 24h treatment with CUR, CUR-NLCs or Blank-NLCs. (A) MTT assay. (B) TB assay.** Hashs denote statistically significant differences between an experimental group and the control group, while asterisks denote statistically significant differences between two experimental groups. One-way analysis of variance (ANOVA) followed by Tukey's multiple comparison HSD post hoc test were carried out and statistically significant differences were identified when p-values were lower than 0.05 (\*p<0.05 or #p<0.05). (n=3).



Phase contrast images of keratinocytes (Figure 73) confirm their lower sensibility to higher concentrations of either CUR or CUR-NLCs. Characteristic morphology can be distinguished for all samples. Interestingly, when NLCs are present either loaded or unloaded, darker spots appear in the interior of the cells.

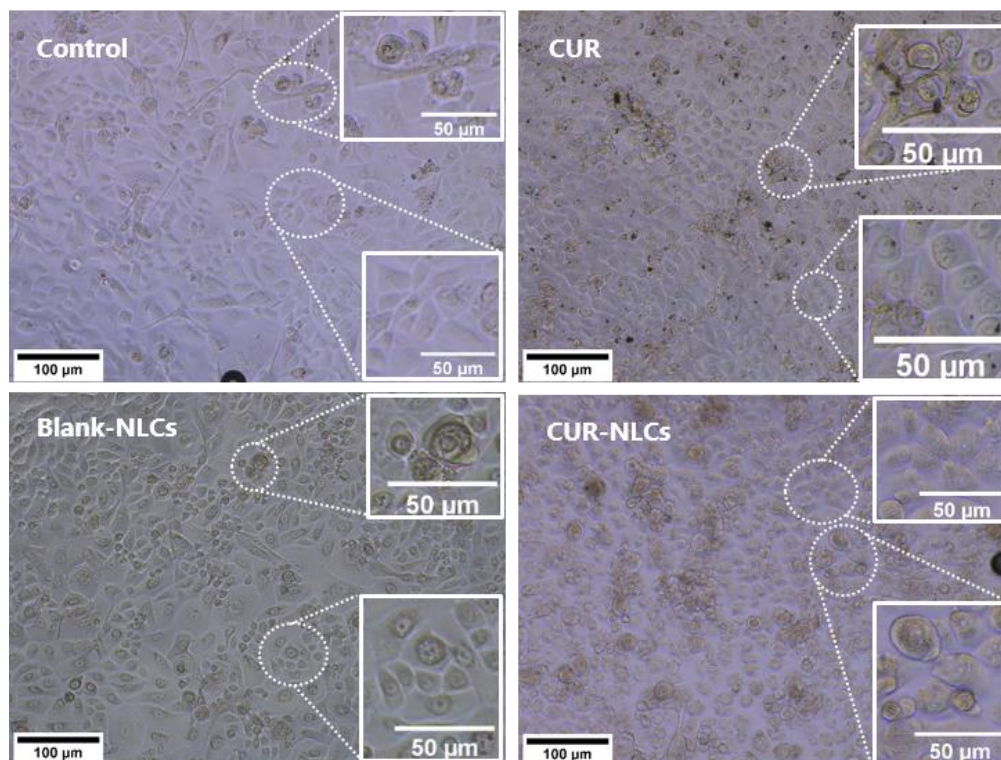


**Figure 74.- Phase contrast images of HEK1 after 24h treatment with DMEM 10%FBS, Control; CUR at 20 $\mu$ M; Blank-NLCs at 1.1 g/L or CUR-NLCs at 1.10 g/L containing 20 $\mu$ M of Loaded CUR.**

Taking into account the ISO 10993-1:2018 norm criteria regarding the evaluation of medical devices<sup>313</sup>, it can be generalized that CUR-NLCs and Blank-NLCs have no toxic effect at the concentrations  $\leq 10 \mu\text{M}$  of CUR (0.54 g/L of NLCs) for fibroblasts and of  $\leq 20 \mu\text{M}$  of CUR (1.10 g/L of NLCs) for keratinocytes. On the contrary, the CUR tested concentrations might be classified as cytotoxic as the cell viability is  $\leq 70\%$  compared to the control when CUR concentration  $\geq 5 \mu\text{M}$ . This means that the cytotoxic effect of curcumin entrapped in NLCs has proven to be less than that of free curcumin.

The observed lower cytotoxic effect of curcumin when loaded in nanocarriers has also been described by Kloesch *et al.*<sup>314</sup>, who studied the cytotoxicity of unloaded curcumin and curcumin loaded liposomes towards synovial fibroblasts. Toxicity could be due to the induction of apoptotic pathways which exceed the induction of antioxidant cytoprotective mechanisms induced by curcumin<sup>315</sup>. Regarding our results, the observed fibroblast cytotoxic effect at 1.10 g/L of nanocarrier loaded with 20  $\mu\text{M}$  of CUR could be the effect of the  $\sim 38\%$  of initial CUR that is present as free curcumin in the medium after 24 h incubation at 37°C.

The fact that there seems to be a difference in the metabolic effects between fibroblasts and keratinocytes when exposed to curcumin has also been described by Lundvig *et al.*<sup>316</sup>. In their investigation they attribute the observed effect to a higher induction of cytoprotective enzymes in keratinocytes than in fibroblasts when both of them are exposed to the same curcumin concentrations. Our results seem to indicate that this effect is somehow increased when curcumin is loaded in NLCs, probably because their incorporation by cells varies from one cell type to the other. The above described differences between fibroblasts and keratinocytes response to the developed formulation could be also explained because much less curcumin is released in 24h when CUR-NLCs are incubated at 37°C (around 15% of initial curcumin) in keratinocytes cell medium. In the light of these results, one thing that remains interesting to investigate is if non released curcumin (curcumin contained in NLCs) is also responsible of the observed effect. In order to answer this question, take-up experiments would be important to be performed at the same time points: 24, 48 and 72h.

For both cell lines, Blank-NLCs do not seem to negatively affect the metabolic activity of the membrane integrity at all tested concentrations. This is in line with the review of Doktorovova *et al.*<sup>317</sup> who mention that most of lipid nanoparticles of around 90 nm of size induce reduction to 50% of viability at concentrations between 2-5 g/L, and that in most of the cases a concentration of 1 g/L is safe.

Regarding the impact on dermal cells of the formulation, it has to be kept in mind that for the composite system (CUR-NLCs loaded in the carbopol hydrogel matrix) impact on dermal cells would be modified as the carbopol gel can potentially modulate the release of curcumin or of CUR-NLCs towards the cells. This is the reason why cytotoxicity of the whole NLCs loaded gel and the release from the gel has also been addressed, but for which technical limitations, principally the disintegration of the carbopol gel in the cell culture media have been encountered.

### **1.2.3.2. Curcumin uptake: preliminary studies**

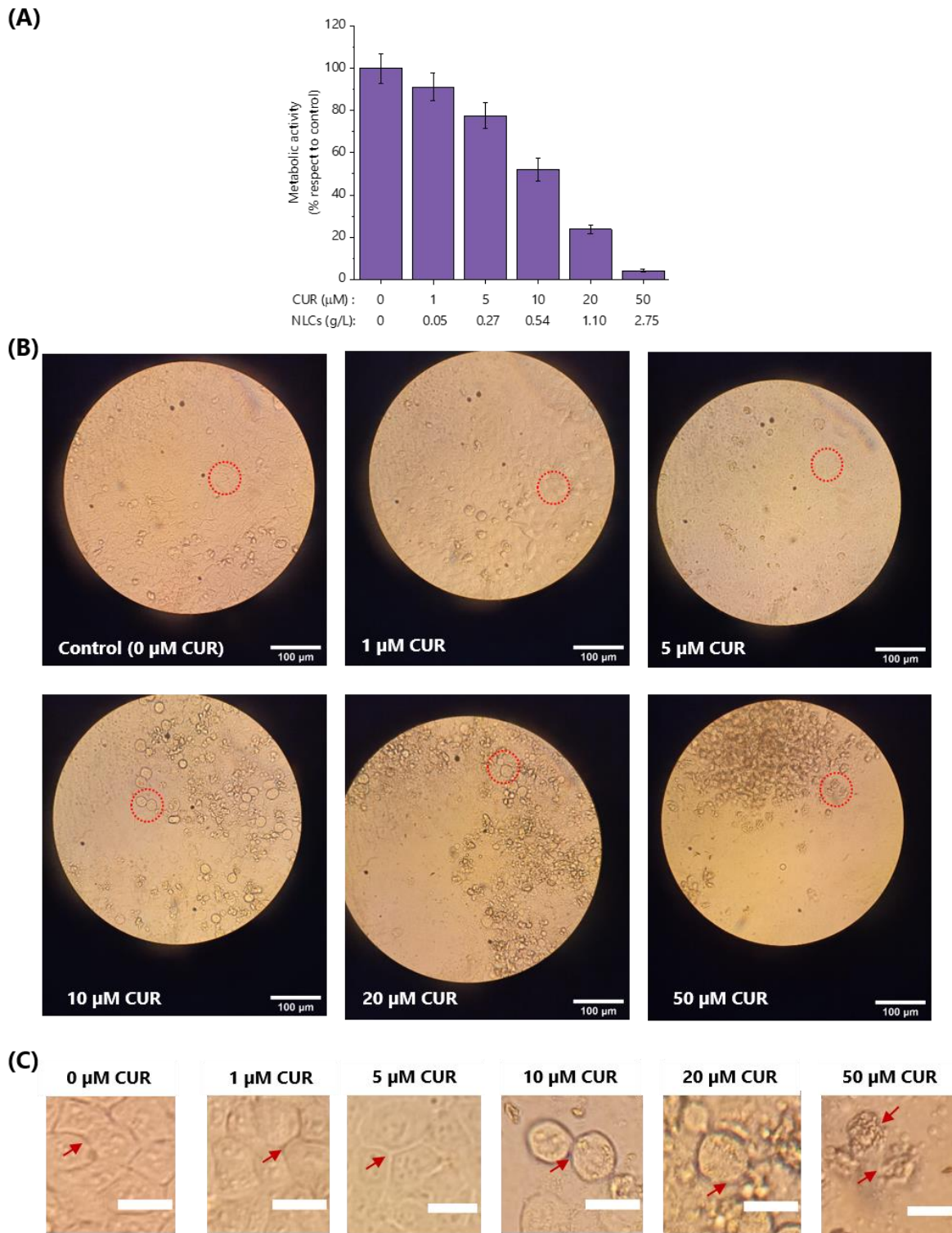
This part of the works was performed at the Department of Biochemical Sciences of Sapienza University of Rome. For testing the uptake for the first time in our system, we analysed the behaviour of HaCaT keratinocytes, an immortalized cell-line in which curcumin has demonstrated to inhibit proliferation and decrease apoptosis at concentrations  $< 5 \mu\text{M}$ <sup>318</sup>. As these cells were used for the first time in this thesis, first, viability had to be assessed. Then, it was possible to explore the possibility of quantifying the amount of curcumin (C) that cells were able to incorporate after being in contact with the higher non-toxic CUR-NLCs concentration for 24 h.

Figure 74 shows the impact of a 24h treatment on HaCaT keratinocytes. Figure 74-A shows the impact in

the metabolic activity of cells. As previously seen with other cell-lines, the higher the concentration, the lower is the metabolic activity. For HaCaT keratinocytes, concentrations below or equal to 5  $\mu\text{M}$  of CUR (in CUR-NLCs, corresponding to 0.27 g/L of NLCs) can be classified as non-cytotoxic (viability > 70%). Thus, it was determined that maximum concentration that could be administered to HaCaT cells in order to further investigate uptake was 5  $\mu\text{M}$  of CUR in CUR-NLCs. Due to time, Blank-NLCs at the same mass concentrations were not assessed.

Interestingly, the cytotoxicity profile is different from that observed for HEK293, also a keratinocyte cell line, but a primary one. In addition to the differences in metabolic activity between both cell-lines, it is important to take into account, as demonstrated in this work, that CUR release is higher in DMEM 10% FBS (HaCaT medium) than in supplemented DBM (HEK293 medium). In 24 h,  $37.5 \pm 4.6$  % of Loaded-CUR were released from CUR-NLCs in DMEM 10% FBS, while only  $13.0 \pm 1.6$  % were released in supplemented DBM.

Figure 74-B shows that there is a change in morphology of cells when they were exposed to concentrations higher than 5  $\mu\text{M}$  CUR in CUR-NLCs, mainly at the cellular membrane and union sites with other cells (Figure 74-C). These changes at the membrane level were difficult to perceive in most photos taken for BJ-Fibroblasts and HEK293. However, the round morphology here presented for HaCaT keratinocytes exposed to 50  $\mu\text{M}$  is similar to that presented in BJ-Fibroblasts when exposed to 20  $\mu\text{M}$  CUR, and to a less extent to 20  $\mu\text{M}$  CUR in CUR-NLCs. Even if not further studied here, these membrane-bound fragments could evidence the formation of apoptotic bodies<sup>319</sup>. Importantly to point-out, data presented here do not allow us to further know if such effect is due to CUR entrapped in CUR-NLCs or CUR that has already been released from them.



**Figure 75.- Impact of CUR-NLCs on HaCaT keratinocytes. (A)** MTT test after 24h incubation. **(B)** Images of the monolayer. Scale bar: 100 µm. **(C)** Zoom on the monolayers. Red arrows indicate membrane of cells intact or not. Scale bar: 25 µm.

Figure 75 shows the typical chromatogram and mass spectrum for curcumin (C) standards and the respective calibration curves for curcumin (C) detection by DAD/MS after its separation by UPLC. As in this method, final detection is performed according structure, only curcumin concentration was determined,

and not CUR concentration which would have implied mass determination of the other two curcuminoids: dimethoxycurcumin (DMC) and bisdemethoxycurcumin (BDMC). These results demonstrate that it was possible to quantify curcumin (C) it between 1  $\mu$ M and 100  $\mu$ M.

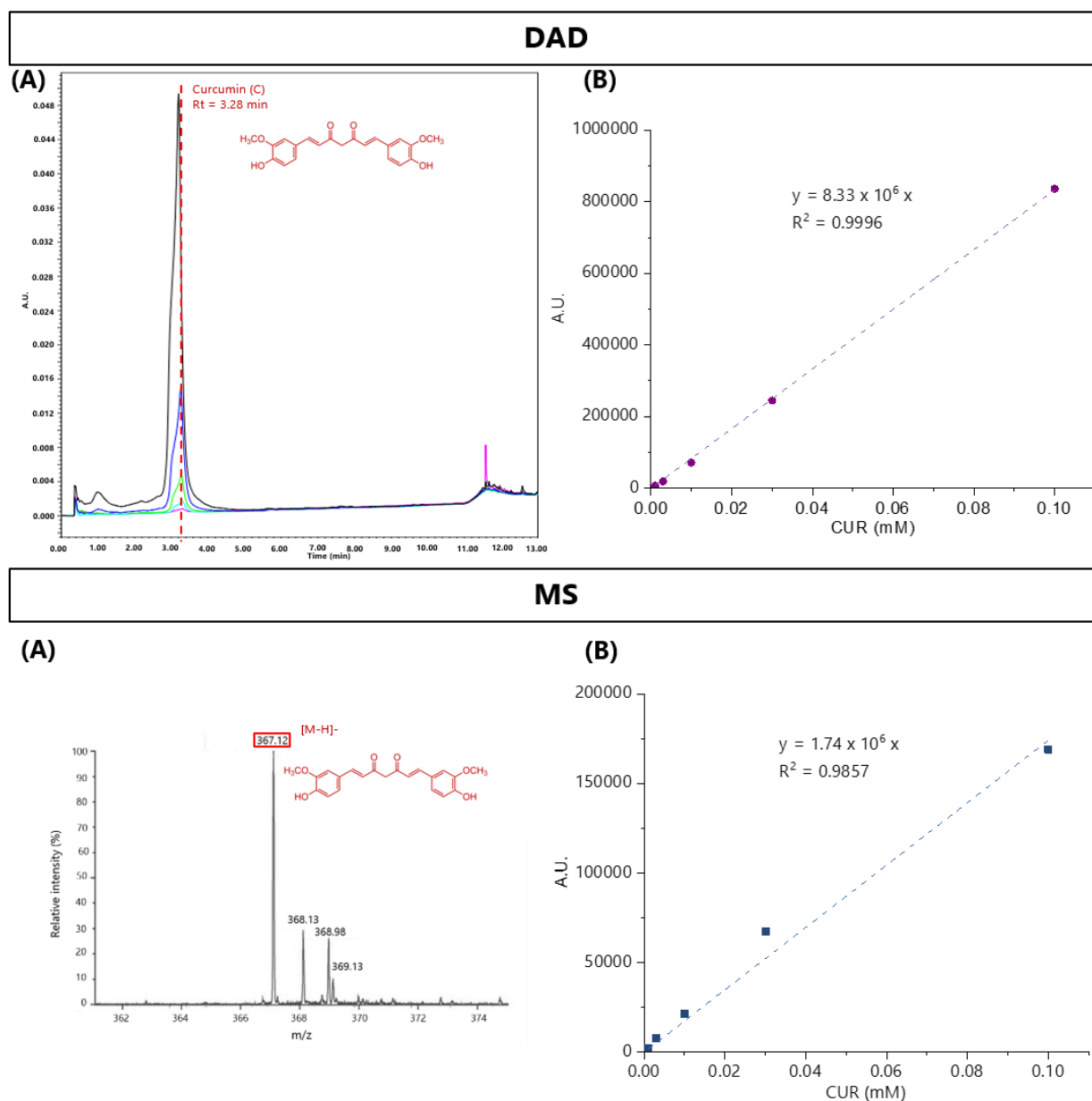


**Figure 76.- Curcumin (C) determination by UPLC-DAD/MS.** Determination by **DAD**: **(A)** Chromatograms for standard solutions.  $R_t$  of curcumin (C) is signalled at 3.28 min. It was at this  $R_t$  that MS analysis was then performed. **(B)** Calibration curve for curcumin (C) at  $\lambda = 423$  nm. Determination by **MS**: **(A)** Example of mass spectrum of curcumin in negative ionization mode (C). Peak at  $m/z = 367.12$ , molecular ion, was used to construct the calibration curve. **(B)** Calibration curve for curcumin (C) at  $m/z = 367.12$ .

Figure 76 shows that that any peak was detected in the chromatogram sample at 3.28 min. Moreover, MS analysis did not show any peak for the molecular ion previously identified in C mass spectra, meaning that intracellular curcumin concentration after a 24h treatment was less than 1  $\mu$ M for HaCaT cells.

During the incubation time, curcumin in CUR-NLCs could be either released or remain entrapped, and thus, could be incorporated differently into cells. The fact that almost no intracellular curcumin was detected could mean that it never got into the cells, or, that it got metabolised by them during the 24h of incubation. A possible metabolization of curcumin seems to be supported by experiments realized by Kunwar *et al.*<sup>124</sup> who demonstrated that unentrapped curcumin uptake depends on the cell type and can occur as early as 0.5 h – 2 h. Also, Rapalli *et al.*<sup>274</sup> showed that even after 6h, it was possible to semi quantify higher fluorescence in HaCaT cells treated with CUR-NLCs than in those treated with CUR suspension. However, in the cited study, cells were treated with 25 $\mu$ M of CUR in CUR-NLCs, which is 5 times more concentrated than the concentration used in this thesis and that confusingly is already qualified as a cytotoxic concentration by the authors. In order to further test our proposed hypothesis, it could be interesting to assess curcumin uptake at shorter intervals, for example: 1 h, 2 h, 4 h, 6 h either by the method here described or by fluorescence means.

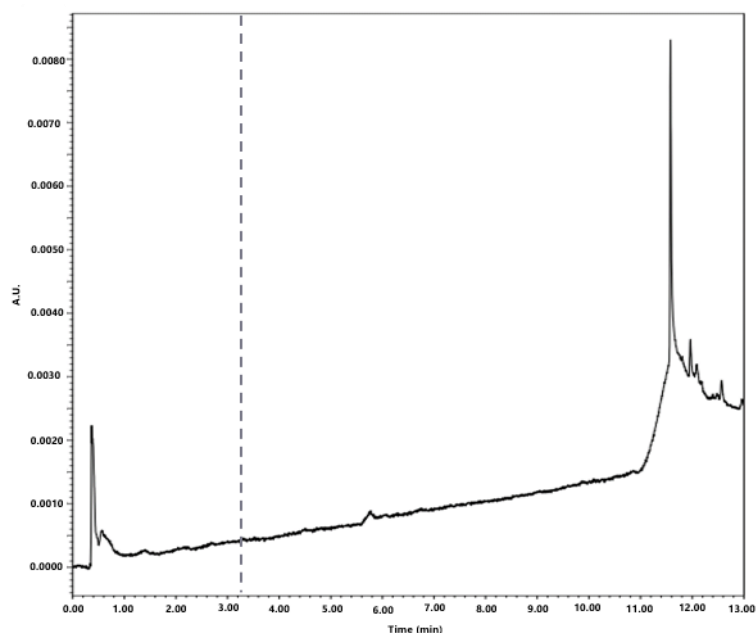


**Figure 77.- Chromatogram for the sample.** No signal was identified at 3.27 min.

### 1.3. Supporting information

• **Calculation of the derived count rate from the mean count rate and attenuator index in DLS measurements**

(Adapted from Malvern Panalytical 2015: <https://www.materials-talks.com/blog/2015/06/11/derived-count-rate-what-is-it/>)

The count rate showed during a DLS measurement refers to the scattering intensity of the sample under specific conditions (specific instrument and specific optical settings). It is expressed as the average number of photons per second arriving at the detector (kcps, kilo counts per second), it is usually called the mean count rate.

In order to adequate the amount of light for the photon detector, typically 200-500 kcps, if there is too much light, part of it can be blocked by an attenuator. Malvern instruments are equipped with attenuators 0-11, as showed below. As it can be seen, each attenuator allows the transmission of a fixed amount of the original light scattered by the sample (% Transmission).

Attenuator Index	% Transmission	Attenuator Index	% Transmission
0	0	6	0.3
1	0.0003	7	1
2	0.003	8	3
3	0.01	9	10
4	0.03	10	30
5	0.1	11	100

In order to calculate the real amount of light scattered by a sample, one needs to calculate the derived count rate, which expresses the count rate one would obtain at 100% laser power with no attenuation. This can be done by employing the following formula:

$$\text{Derived count rate} = \frac{\text{Mean count rate}}{\% \text{ Transmission}}$$

For example, a sample with a mean count rate of 100 kcps, and for which the zetasizer used an attenuator of 0.3% (attenuator index 6), the derived count rate would be:  $100 \text{ kcps} / 0.3\% = 100 \text{ kcps} / 0.003 = 33\,333 \text{ kcps}$ .

• **Calcul of the molecular weight from the hydrodynamic diameter.**

Calculs were performed as proposed by Erickson 2009<sup>289</sup>, who used the partial specific volume -also described as the reciprocal of the density- of globular proteins (0.73 cm<sup>3</sup>/g), to formulate the following equation:

$$R_{\min} = 0.066 M^{1/3}$$

$R_{\min}$ : minimal radius of the sphere that could contain a protein the given mass of the protein. (nm)

M: given mass of the protein. (Daltons)



## 1.4. Conclusions

Optimization of CUR-NLCs preparation by the Hot-Homogenization method allowed to fix the temperature of preparation at 70°C, 30 min as the duration of homogenization, to establish Labrafac® lipophile WL 1349 as the oil and to set incorporation of CUR in its solid form in order to maximize drug entrapment. This led to a formulation showing 85% of E.E, %, 2.3% of DL and CUR content of 0.85 mg per mL of suspension.

CUR-NLCs present a platelet-like shape, a ZP ~ -9 mV and a bi-dispersed size distribution. In terms of % intensity, a small size population of 70-85 nm (~ 20%) and a bigger population of 208-360 nm (~ 80%). When expressed in % number, the small size population represents 98.5% of the total number of NLCs. These dimensions are similar to those of Blank-NLCs, are maintained for at least 45 days, and remain unchanged in pH between 5.5 and 9. CUR-NLCs preservation in its freeze-dried form would require concentrations of cryoprotectant higher than 3% w/v.

CUR-NLCs permeation through the SEC column preserves the size distribution, diminishes the ZP and increases the antioxidant activity. Thus, it seems to be successful at removing molecules of excipients that might be in excess in the formulation.

Loaded-CUR maintains its antioxidant activity and is released from CUR-NLCs in a time dependent manner. Amount released varies according to the biological media and is increased in the presence of FBS.

Cytotoxicity of CUR-NLCs depend on the cell line. No cytotoxic effects are perceived for BJ-Fibroblasts up to 10 µM, for HEK293 up to 20 µM and for HaCaT until 5 µM of CUR entrapped in CUR-NLCs (equivalent to 0.54, 1.10 and 0.27 mg/mL, in mass concentration of loaded NLCs, respectively). Preliminary results show that after 24h of treatment of HaCaT cells with 5 µM of CUR in CUR-NLCs, no intracellular CUR could be detected and quantified.

## **Chapter 4: Potential of CUR-NLCs and CUR-NLCs/gel delivery systems for topical applications**

---



## **1.1. Introduction**

During the development of CUR-NLCs, the formulation and method of preparation were optimized. Then, physico-chemical characteristics and non-cytotoxic concentrations of resulting CUR-NLCs were determined. Once knowing these key characteristics of the CUR-NLCs system, in this chapter, its potential to be used as a drug delivery system in the topical dermal route is explored.

In one hand, the potential is studied at a cellular level by assessing the impact of CUR-NLCs on migration/proliferation of dermal cells (keratinocytes and fibroblasts). In order to mimic the oxidative stress conditions being at the origin of some physio-pathological inflammatory skin conditions (wounds, psoriasis, dermatitis, keloids and hypertrophic scars), a model capable of inducing oxidative stress and detecting ROS presence is completely developed for fibroblasts.

In the other hand, the potential to be used in the topical dermal route is explored by incorporating CUR-NLCs in a Carbopol® hydrogel matrix. The rheological properties of the composite system are characterized. Also, its ability to deliver drug to the skin by means of Franz-cells diffusion experiments is assessed in order to get insight of the multiscale properties of the system.

## **1.2. Results and discussion**

### **1.2.1. Effects of CUR-NLCs on dermal cells**

#### **1.2.1.1. Impact of CUR-NLCs on the migration/proliferation of healthy cells**

During skin conditions like dermatitis, psoriasis and wound healing, migration and proliferation of cells are natural events taking place in order to restore skin physiological conditions. In order to assess both of the processes simultaneously, the ability of fibroblasts and keratinocytes to fill a gap created by physical exclusion was assessed.

It is important to highlight the fact that in order to study both capacities at the same time, cells were cultured in their normal conditions. Contribution of proliferation to filling the gap was not inhibited by serum starvation or exposition to anti-proliferative drugs (Mitomycin C for example). Even if individual study of both processes does not mimic real-life conditions, it would have been interesting for better understand the impact of the formulation on cells. However, it has been demonstrated that serum starvation could elicit complex effects in cells metabolism<sup>320</sup>, whereas the utilisation of proliferation inhibitors may alter the capacity of the cells to migrate<sup>321</sup>.

Figure 77 shows the % in gap reduction for BJ-Fibroblasts and HEK293T after a 24 h treatment with different concentrations of CUR, Blank-NLCs or CUR-NLCs. Tests were initially performed only at non-cytotoxic concentrations after 24 h exposition (upto 10  $\mu$ M of CUR in CUR-NLCs for BJ-Fibroblasts and upto 20  $\mu$ M of CUR in CUR-NLCs for HEK293T), but then in order to get a full-picture of the proliferation/migration

inhibition, cytotoxic concentrations were included.

It is interesting to note that for fibroblasts, a 24 h incubation without curcumin or NLCs does not allow the completely closure of the gap. There is only  $53 \pm 7$  % of gap reduction (Figure 77-A). However, for keratinocytes this time frame is enough for reaching complete closure, 100% of gap reduction (Figure 77-B).

As it can be seen from Figure 77, the higher the concentration of NLCs or CUR, the less is the reduction in the gap area for both cell lines. It can be seen that curcumin loaded NLCs has the strongest effect in reducing the migration/proliferation of cells, while CUR, the lowest one.

Taking as example the experimental point  $5 \mu\text{M}$  CUR and  $0.27 \text{ g/L}$  NLCs for fibroblasts, similar results as the control were found. After 24 h of cell treatment with CUR or Blank-NLCs ( $52 \pm 5\%$  and  $50 \pm 9\%$  of gap reduction, respectively), whereas with CUR-NLCs, a slight-moderate diminution in the cell motility and/or proliferation was observed compared to the control ( $35 \pm 3\%$  of gap reduction). Neither of treatments (CUR, Blank-NLCs or CUR-NLCs) seems to affect the morphology of BJ-Fibroblasts when compared to the control (Figure 78-A).

On their side, HEKn showed an important proliferation and/or cell migration capacity with a complete reduction of the gap ( $100 \pm 3\%$  of gap reduction) at control conditions (Figure 79-A). Taking also as example the experimental point  $5 \mu\text{M}$  CUR and  $0.27 \text{ g/L}$  NLCs, the same behaviour was observed on cells treated for 24 h with CUR or Blank-NLCs ( $90 \pm 8\%$  and  $96 \pm 6\%$  of gap reduction, respectively). When CUR-NLCs were added to the medium and put in contact to the HEKn cells, a slight-moderate diminution of cell migration/proliferation capacity was observed ( $80 \pm 4\%$  of gap reduction).

For both cell-lines, a diminution of 20% of cell proliferation/migration seems to take place in presence of CUR-NLCs. However, for HEKn, cell morphology is altered by the presence of CUR, Blank-NLCs and CUR-NLCs, showing in all cases a rounder shape compared with the control. It should be noticed that at these NLCs concentrations ( $0.27 \text{ g/L}$ , corresponding to  $5 \mu\text{M}$  of CUR) neither Blank-NLCs nor CUR-NLC presents cell toxicity. In the MTT assay even an increase in the metabolic activity is observed. Under these conditions, keratinocytes are not in an optimal environment, however there are alive, metabolically active and can remain attached to the plate.

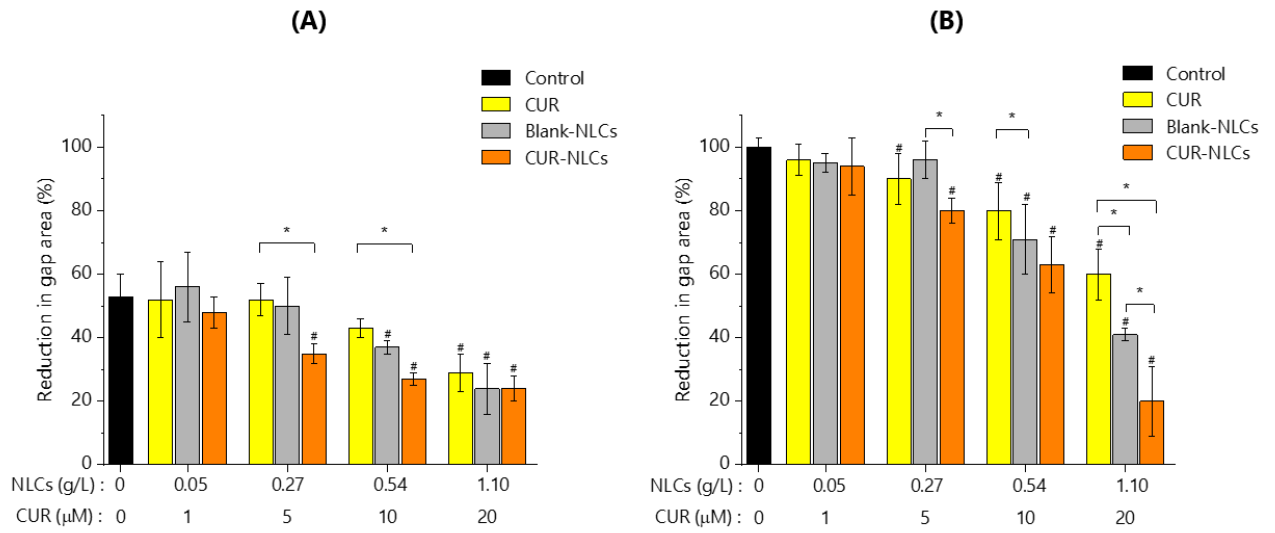


**Figure 78.-Reduction in the gap area during the migration/proliferation assay. (A) On BJ-Fibroblasts. (B) On HEK293T. One-way analysis of variance (ANOVA) followed by Tukey's multiple comparison HSD post hoc test were carried out and statistically significant differences were identified when p-values were lower than 0.05 (\*p<0.05 or #p<0.05).**

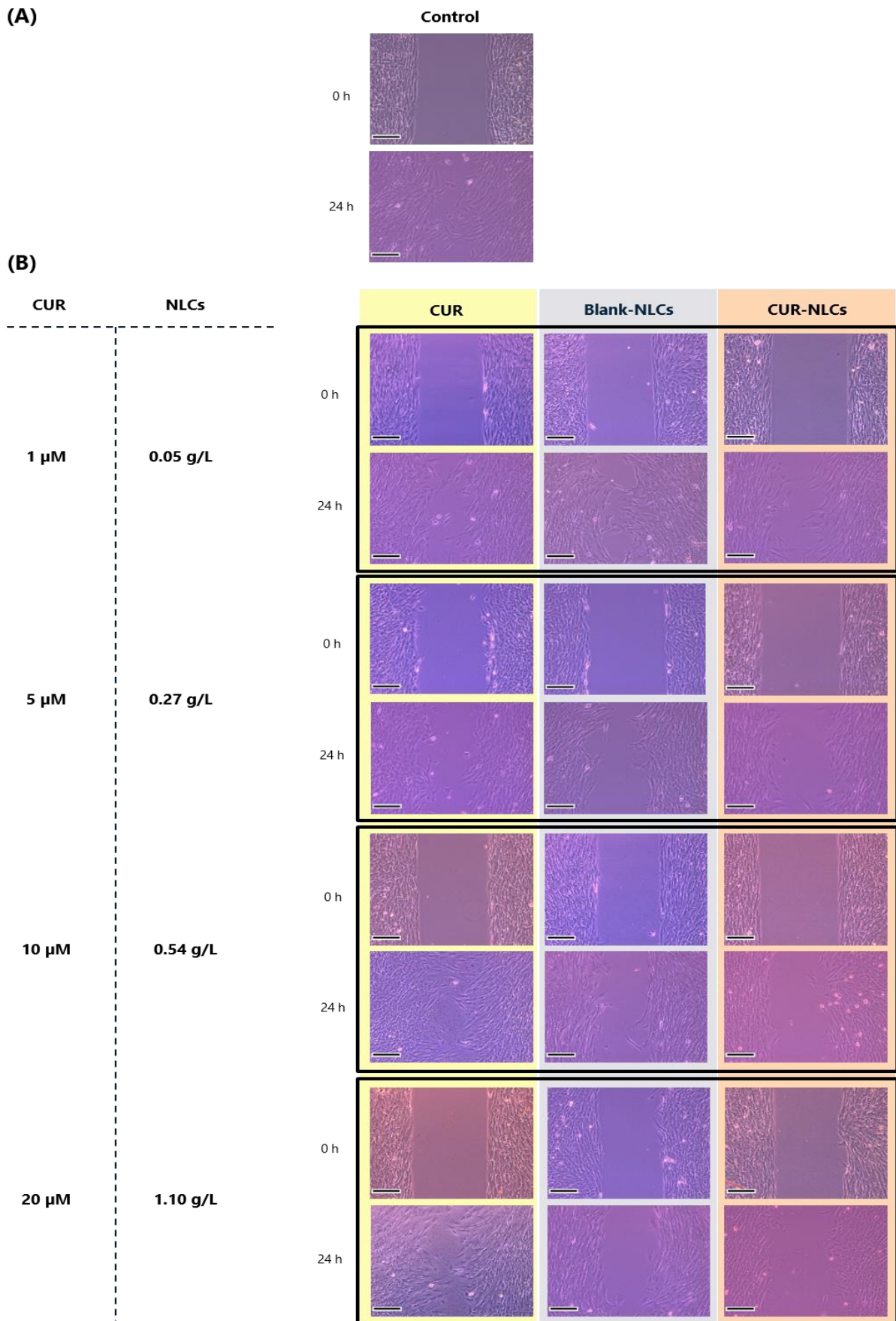


**Figure 79.-Phase-contrast images of the gap during the migration/proliferation assay on BJ-Fibroblasts. (A)** Before (0 h) and after (24 h) treatment of control cells with DMEM 10% FBS. **(B)** Before (0 h) and after (24 h) treatment of control cells with DMEM 10% FBS containing CUR, Blank-NLCs or CUR-NLCs at different concentrations.

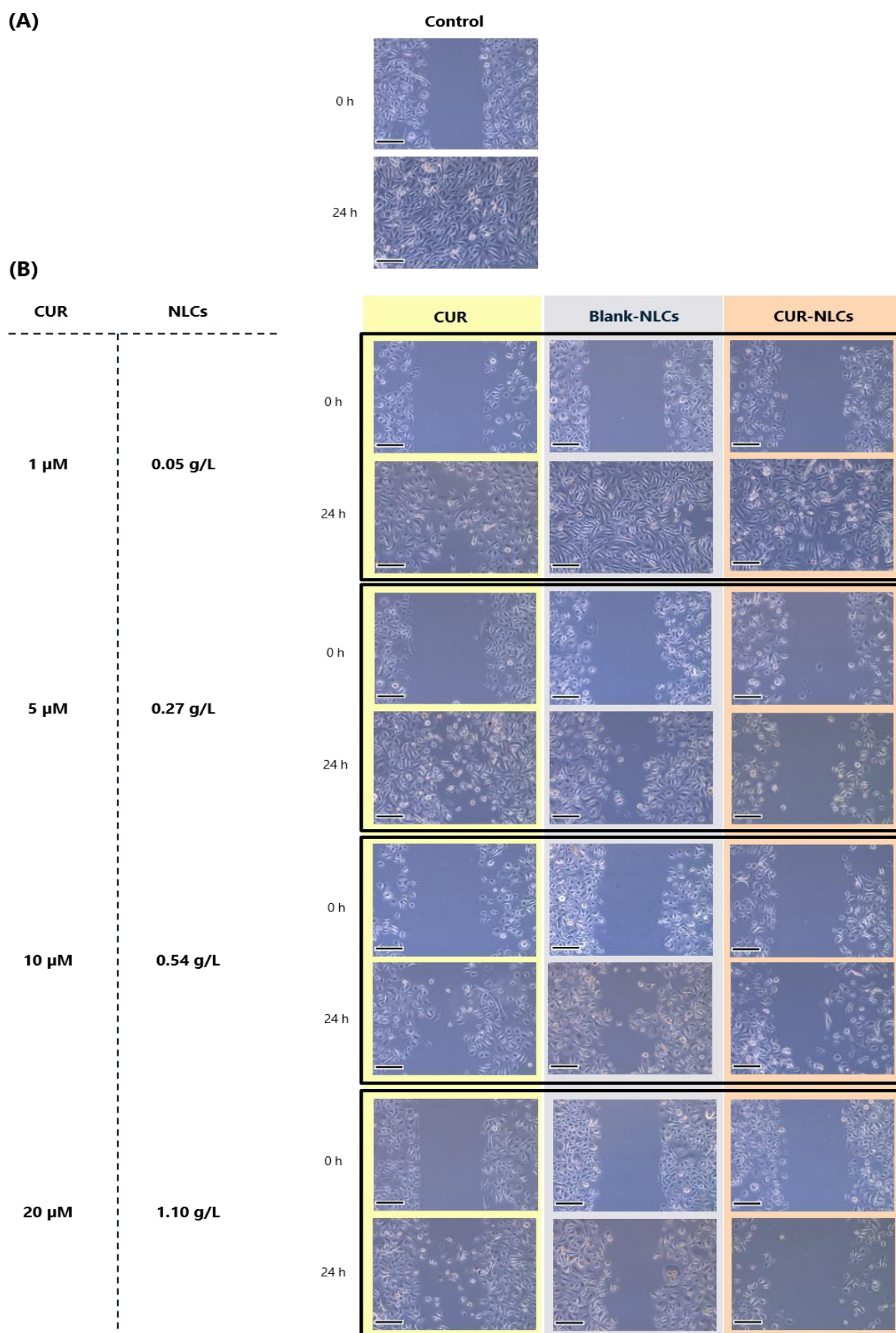


**Figure 80.- Phase-contrast images of the gap during the migration/proliferation assay on HEKn. (A)** Before (0h) and after (24h) treatment of control cells with DBM. **(B)** Before (0h) and after (24h) treatment of control cells with DBM containing CUR, Blank-NLCs or CUR-NLCs at different concentrations.



Overall, results point to an inhibition of the migration and/or proliferation by the developed formulations and in both studied cell lines.

Even if the creation of a gap by physical cell exclusion does not allow extracellular matrix (ECM) deposition as it happens while scratching the cells out of a monolayer with a micropipette tip, this does not hinder the ability of cells to migrate. This was demonstrated by Block *et al.*<sup>322</sup> who found the same migration rates for epithelial monolayers in which the gap was created either by “scratching” or by using agarose strips. They explain that even if scrapped monolayers presented higher levels of intracellular Ca<sup>2+</sup> release in the leading cells which was able to initiate the healing response, this was unable to sustain the healing for many hours<sup>323</sup>. This confirms that the observed effects are not an artifact of the employed model, but that they reflect the effect of the formulations in a 24 h time-frame.

Even if some research aiming to find treatments for acute wounds have found that curcumin *in vitro* can lead to faster gap closure, mechanisms still remain unclear<sup>147,149</sup>. In line with these, early phases of this work aimed to develop a formulation that would increase wound-closure rate. Even though previously presented results were not the ones initially expected, they remain interesting as some curcumin has been reported to be effective face to hyperproliferative wound-healing conditions such as keloids and hypertrophic scars<sup>324,325</sup> by inhibition of cell proliferation but not apoptosis<sup>144</sup> or decrease in expression of collagen and fibronectin<sup>145</sup>. In psoriatic cases, the ability of curcumin to modulate, without suppressing, migration and proliferation is an important feature that may act at the main problem: deregulated migration and maturation of keratinocytes. Researches in this field have demonstrated the ability of curcumin to modulate metabolic activity and proliferation during 24 h *in vitro*<sup>154,159</sup>, as well as to reduce inflammation markers and psoriatic-like symptoms like redness, inflammation, skin thickness and scaly lesions *in vivo*<sup>152,153,155–158</sup>.

Our findings are in agreement to those found by De Campos *et al.*<sup>318</sup> while studying cell migration and cell-cell adhesion. Briefly, by analyzing different cell lines including immortalized fibroblasts and keratinocytes, they found that low curcumin concentrations (<5 µM) were able to inhibit proliferation while decreasing apoptosis, whereas high concentrations (> 50 µM) increased apoptosis and cell death. Reduction of speed of migration was reduced in a concentration dependent manner. Reasons for this were impairment in directionality which lead to ‘non-productive’ migration and alteration of cohesion between cells through the reduction of the cell-cell adhesion marker E-cadherin, a type of adhesion present during two-dimensional collective sheet migration<sup>326</sup> of fibroblasts and keratinocytes.

Importance of the presented results is that they allow to better direct the application of the developed

system as an adjuvant therapy in the context of wounds and extend their possible applicability to other skin condition contexts, psoriasis in particular. It has been reported that curcumin entrapped in nanocarriers has been able to inhibit intracellular oxidative stress in keratinocyte cells and modulate their migration<sup>327</sup>. That is why following steps of the research were oriented to assess the effect of the developed formulation in oxidatively stressed cells.

It is to note that from our results, unloaded (Blank) NLCs also influence on the migration/proliferation of cells. However, it remains to investigate if the mechanisms differ from those of curcumin presented by other researchers.

### **1.2.1.2. Development of a model of oxidatively stressed cells**

During inflammatory skin conditions, as those present during dermatitis, psoriasis or abnormal wound-healing, dermal cells, mainly fibroblasts and keratinocytes, undergo oxidative stress.

In order to mimic those conditions, ROS production needs to be induced and detected. These are the two points addressed in this section. As in the future, interest will be to assess the ability of treated cells to initiate an antioxidant cell response, it is important that during ROS production metabolic activity is not affected.

While induction of ROS production and assessment of its impact in the metabolic activity of cells was performed for both fibroblasts and keratinocytes, due to time limitations and easiness of handling, ROS detection was fully developed only for BJ-Fibroblasts.

*Tert*-butyl hydroperoxide (t-BOOH, brand name: Luperox®), was used to induce ROS formation in cells. It was preferred face to hydrogen peroxide (H<sub>2</sub>O<sub>2</sub>), due to its higher stability, its ability to decompose to other alkoxy and peroxy radicals and ROS (including H<sub>2</sub>O<sub>2</sub>) and its proved capacity to enhance the response of antioxidant enzymes<sup>328</sup>, thus yielding an excellent model of oxidative stress in cell culture.

As it can be seen from Table 22, keratinocytes are more sensitive than fibroblasts to chemically induced oxidative stress. For keratinocytes, the maximum concentration of Luperox that can be used in order to generate ROS without interfering with cells metabolic activity is 100 µM, while for fibroblasts its 200 µM. At these two concentrations cell morphology is maintained (Figure 80).

Retaining metabolic ability of cells while inducing oxidative stress is important as the model will be used to evaluate the impact of formulations in their ability to develop cellular antioxidant responses that will help them to face and endure the oxidative stress. Figure 80 evidences that the higher the Luperox®

concentration, the lower the amount of intracellular formazan crystals (darker zones) for both cell lines. For keratinocytes, the reduction in the amount of cells attached to the plate, better exemplifies the ability of Luperox® to damage cells and produce their detachment from the plate. Information about Luperox® impact on dermal cells is scarce, however it has been reported that a 3 h treatment with 200 µM of Luperox® evoked an increase of LDH activity in cell medium indicating cell death in HepG2 human hepatocarcinoma cell line<sup>329</sup>. This results are inline with our results and confirm the limit of exposition to Luperox® for 1h and at 100 uM for keratinocytes and 200 uM for fibroblasts.

**Table 22.- Metabolic activity of BJ-Fibroblasts and HEKn after 1h exposition to stressor (Luperox).** (n=2).

Luperox (uM)	% Metabolic activity			
	Fibroblasts (BJ)		Keratinocytes (HEKn)	
50	93	± 3	78	<sup>a</sup>
100	87	± 8	74	± 14
200	84	± 8	59	± 15
300	62	<sup>a</sup>	64	<sup>a</sup>

<sup>a</sup> Test was performed once

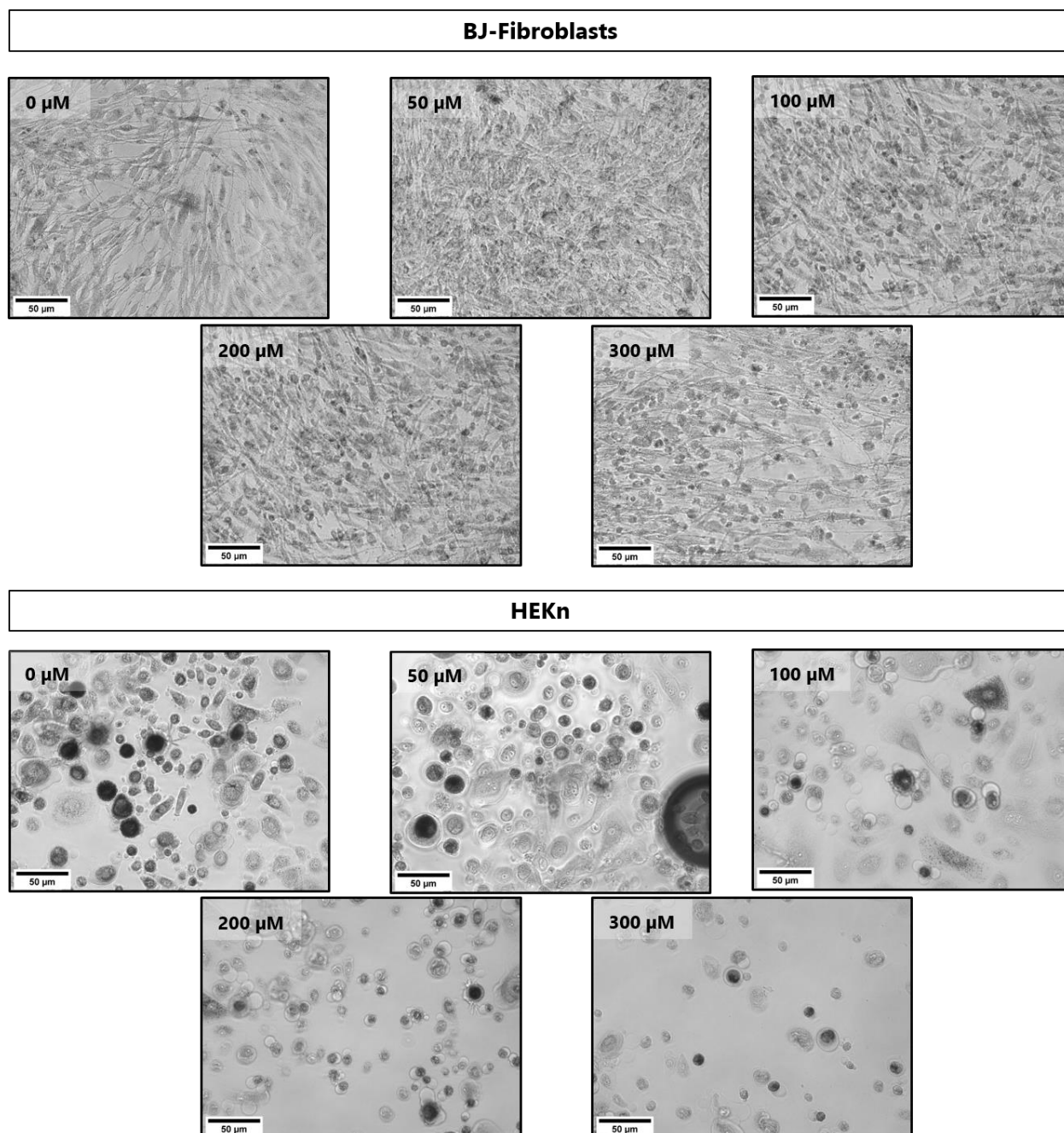


**Figure 81.- Phase contrast images of BJ Fibroblasts and HEK293 after treatment with different Luperox concentrations and subsequently incubation with MTT.** Cells were treated for 1h with Luperox and subsequently incubated with MTT for 2h30.

By using the fluorogenic probe DCFH-DA, ROS production and confirmation was performed. Figure 81 depicts the intracellular kinetics of ROS production in cells harbouring a fixed concentration of the fluorogenic probe and then treated with Luperox® for 3 h. Fluorescence was recorded when fibroblasts were exposed to different concentrations of the stressor (Luperox®). The higher the fluorescence intensity, the higher the amount of ROS that cells were not able to neutralize.

Overall, the higher the Luperox® concentration, the higher the maximum fluorescence reached. It is to note

that by using 200  $\mu\text{M}$ , just a little increase in fluorescence is obtained compared to the use of 100  $\mu\text{M}$ , maybe because of the depletion of the fluorescent probe. As no significant increase in fluorescence was obtained, a working concentration of 100  $\mu\text{M}$  would be preferred over 200  $\mu\text{M}$  while working with 20  $\mu\text{M}$  of the probe (DCFH-DA).

When Luperox® is present, maximal fluorescence seems to become constant after 1 h of incubation at 37°C. Cells not exposed to Luperox® (0  $\mu\text{M}$  Luperox®) but incubated with the fluorescent probe show that experimental conditions in the reader plate for 3 h (37°C but no controlled atmosphere) by themselves tend to stress cells.

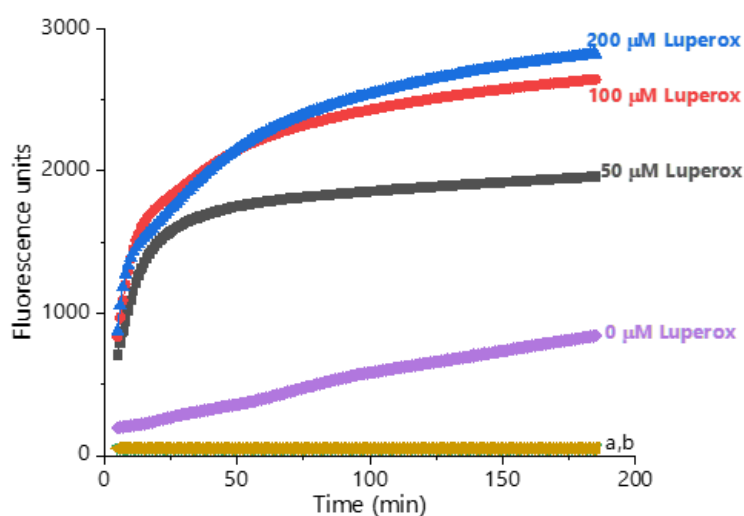


**Figure 82.-Evaluation of oxidative stress induced by different concentrations of Luperox on BJ-Fibroblasts.** Graphs present the fluorescence of cells incubated with probe (DCFH-DA, 20  $\mu\text{M}$ ) and different concentrations of Luperox. a: cells exposed to the probe but not the stressor. b: cells not exposed to neither the probe nor the stressor. Each curve shows the average results from 12 wells of a 96-well plate.

Results allow to fix the concentration of 100  $\mu\text{M}$  of Luperox® as the one to produce a fluorescence that is significantly different from the one of cells also containing the fluorescent probe, but without Luperox®, that is, which are stressed because of the experimental conditions of the test. This model can be used to evaluate the antioxidant cellular response induced by cell treatment with CUR, Blank-NLCs and CUR-NLCs when applied before the induction of the stress.

It has to be pointed out that in real-life use, oxidative stress will occur more often before the application of the formulation. Only a preventive use of the formulation, for example applied on a daily basis would mimic the experimental conditions here tested. Testing of response by first inducing the stress and then applying the formulation was difficult to carry-on as Luperox® damages in the cells seem to take place faster than

the time required for our formulations to act and generate an antioxidant response. By applying other stressors like for example Antimycin A or cumene peroxide (CumOOH), which tend to induce only peroxide radicals and lipid peroxy radicals, respectively, a less generalized cellular damage compared to Luperox® could be obtained<sup>330,331</sup>.

Overall, the developed cell-model allows to produce and verify the oxidative stress in fibroblasts. By maintaining a metabolic activity no different to the control cells, cell capacity to induce the production of antioxidant enzymes can be suspected. Also, the production of ROS can be quantified by fluorescence measurements. A complementary part for the model would have been to assess the antioxidant defence systems initiated in cells. This would include on one hand the assessment of non-enzymatic defence, for example glutathione (GSH) concentrations, and on the other hand the assessment of enzymatic defence, for example glutathione reductase (GSR), glutathione peroxidase (GPx) and catalase.

Eventhough, these results allow to affirm that 100 µM Luperox ® produces intracellular ROS production in BJ-Fibroblasts, inducing oxidative stress without affecting cellular metabolic activity (as showed in previous section).

The combination here tested of DCFH-DA (20 µM, exposition for 1 h) and Luperox ® (100 µM, exposition for 1 h) could be used for assessing the impact of CUR-NLCs in the ability of BJ-Fibroblasts to fight oxidative stress, however, first it would be needed to verify that developed nanocarriers do not affect the cellular viability of cells even if they are undergoing oxidative stress. This will be addressed in the following section.

### ***1.2.1.3. Impact of CUR-NLCs on the viability of oxidatively stressed cells***

This part of the study of the biological potential of the developed NLCs formulation is intended to gain insight in whether CUR-NLCs (at their maximal non cytotoxic concentration: 10 µM of CUR, in 0.54 g/L of CUR-NLCs) could be used to treat cells without affecting their metabolic activity, even during oxidative stress conditions. This is important, as it will lay the groundwork for, in the future, investigate if the already proven conserved antioxidant properties of CUR incorporated in NLCs will allow to enhance the antioxidant cytoprotective mechanisms of cells.

Results on Figure 82 show the metabolic activity of fibroblasts pre-treated with Blank-NLCs or CUR-NLCs compared to that of cells without pre-treatment with neither the antioxidants or NLCs. No statistical significant difference was observed for Blank-NLCs at 0.54 g/L or CUR-NLCs at 0.54 g/L (containing 10 µM of CUR, respectively). The metabolic activity of pre-treated cells was confirmed by the images of cells after incubation with MTT (Figure 82-B), where cell morphology was conserved and in which, darker zones denote the formation of formazan crystals (signalled ramifications), demonstrating that cells were metabolically

active as their mitochondrial dehydrogenases were able to transform MTT to formazan. Interesting to note, density of ramifications was higher for cells pre-treated with Trolox, but this is not translated into a significant higher metabolic activity of cells pre-treated with CUR-NLCs.

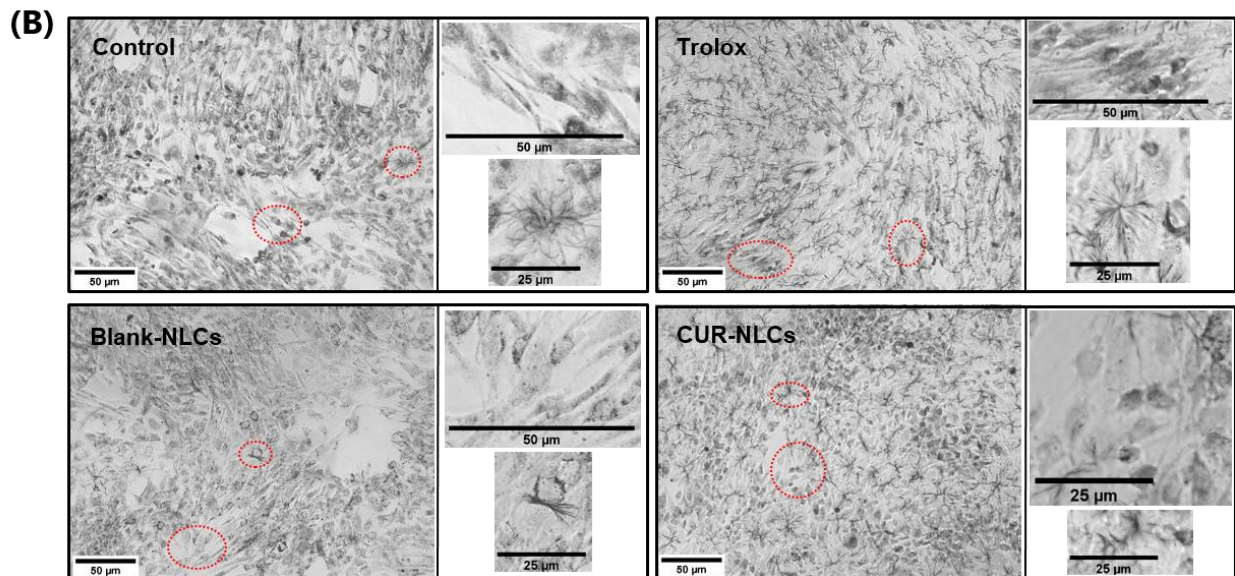
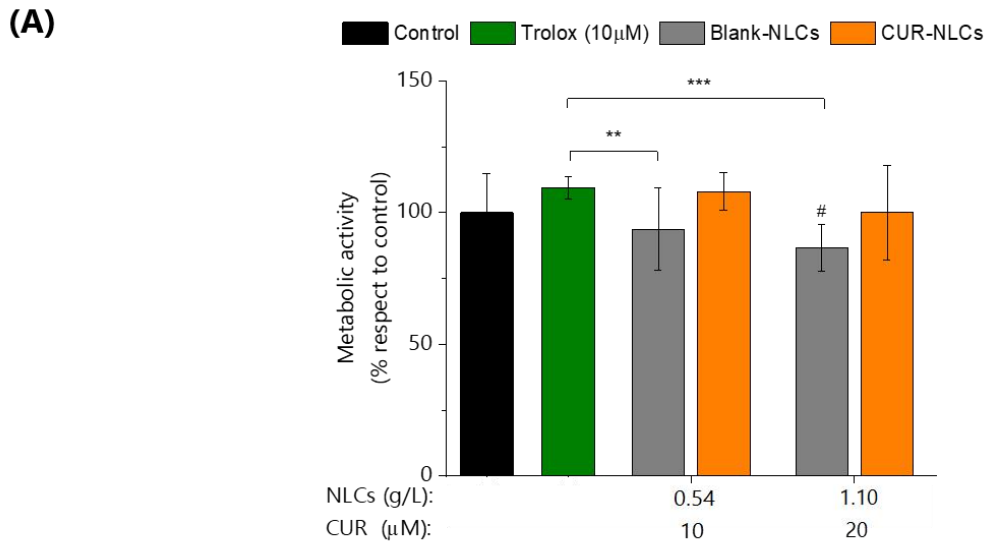


**Figure 83.-Effect of NLCs on BJ-Fibroblasts under oxidative stress. (A)** Impact of Blank-NLCs and CUR-NLCs on the metabolic activity of BJ Fibroblasts undergoing oxidative stress; Trolox 10 µM was used as an antioxidant standard. Hash denote statistically significant difference between an experimental group and the control group, while asterisks denote statistically significant differences between two experimental groups. Kruskal-Wallis analysis of variance (ANOVA) followed by Mann-Whitney test were carried out and statistically significant differences were identified when p-values were lower than 0.05 (\* $p < 0.05$  or # $p < 0.05$ ) than 0.01 (\*\* $p < 0.01$  or ### $p < 0.01$ ) or 0.001 (\*\*\*) $p < 0.001$  or ### $p < 0.001$ ). (n=3). **(B)** Phase contrast images of BJ Fibroblasts after treatment with DMEM 10% FBS, control, or 1.10 g/L of CUR-NLCs containing 20 µM of CUR for 24h; exposition to 100 µM of stressor for 1h and subsequently incubation with MTT for 2h30. Images in the down part correspond to the magnifications of the indicated zones in the upper images: extended morphology of fibroblasts as well as the formation of formazan crystals can be distinguished, evidencing metabolically active cells.

These results allow to affirm that even in oxidative stress conditions, the viability of BJ-Fibroblasts is not affected by the pre-treatment with CUR-NLCs at 10 µM of CUR in CUR-NLCs. Thus, further cellular

antioxidant response could be assessed using this model.

### **1.2.2. Incorporation of CUR-NLCs into a carbopol hydrogel matrix**

In order to facilitate the application of NLCs on the skin and increase its residence time, CUR-NLCs were included in a hydrogel matrix. Carbopol® 980 (Carbomer) was chosen as it is approved for topical use by the European Pharmacopeia<sup>332</sup>. In solution and in presence of a neutralizing agent, the carboxylic groups present along the polymer chains get ionized<sup>333</sup>. Negative charges all over the polymer are repelled from each other, causing the extension of the polymer and an increase in its viscosity. Two neutralizing agents were studied to reach this point. Both of them were chosen from the compounds recommended for increasing the pH of carbopol dispersions<sup>334,335</sup>. Being NaOH more economically affordable than TEA. For these two neutralizing agents, any advantage in the formulation of composite systems containing lipidic nanoparticles has not yet been described.

#### **1.2.2.1. Impact of neutralizing agent in the formulation of CUR-NLCs/gel**

According to preliminary tests on Carbopol® 980 dispersions in water at 0.5, 1 and 2 % w/v, the 0.5 % w/v (Supporting information on this chapter), the 0.5 % w/v concentration was chosen due to its easiness of stirring (before and after) neutralization, and due to the possibility to include higher volumes of NLCs. On this dispersion, the impact of a strong base: NaOH 0.5 M, and that of a weak base: TEA 20% v/v, was studied. Implications of incorporating the NLCs before or after the neutralization step were also analysed.

On one hand, adding NLCs before the neutralization step either with NaOH or TEA produced a change of color of the formulation (Figure 83). Even if this color change was less intense when using TEA, a destruction of NLCs could be suspected as curcumin was able to interact with the alkaline environment and change of colour could be attributed to its deprotonation or degradation. On the other hand, adding NLCs after the neutralization step did not produce a change of colour when using both bases. However, when NaOH was used, the obtained gel had a creamy texture compared to the translucent aspect for the gel formulated with TEA, as showed in Figure 83. In brief, if TEA is used before the addition of NLCs, a gel with no creamy aspect is obtained. Thus, no destruction of the nanocarrier giving rise to lipids dispersed in the gel and responsible of the creamy aspect can be suspected.



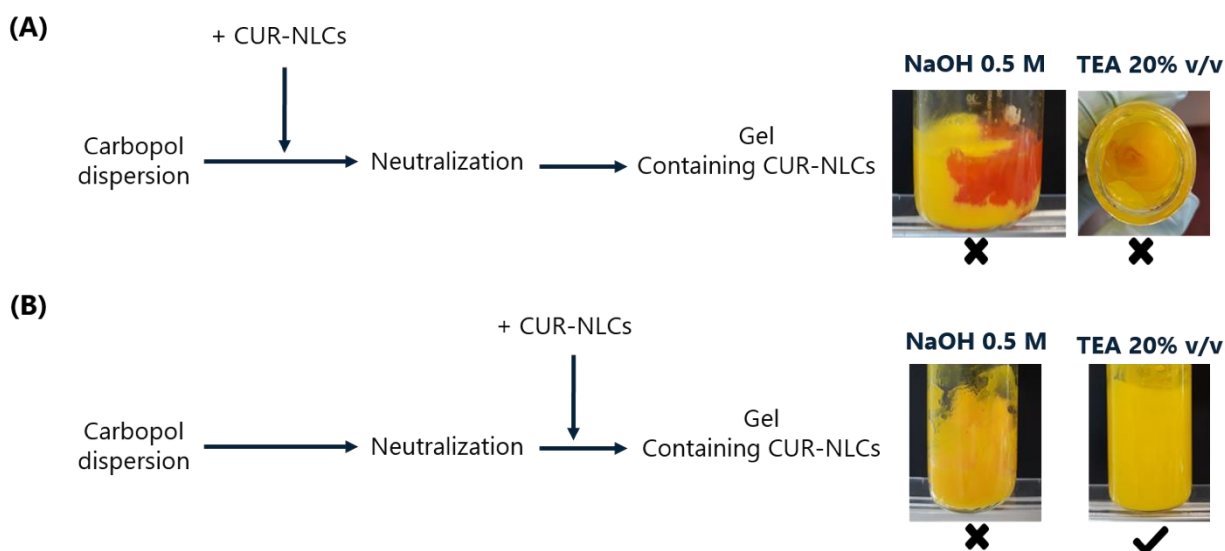


**Figure 84.- Impact of the addition step of CUR-NLCs and employed neutralizing agent into the final appearance of CUR-NLCs/gel. (A)** Neutralization after the addition of CUR-NLCs with NaOH 0.5 M or TEA 20 % v/v. **(B)** Neutralization before the addition of CUR-NLCs with NaOH 0.5 M or TEA 20 % v/v.

The incorporation of lipid nanoparticles in a gel matrix in order to increase their ease of application on the skin has also been reported by other authors. Some of them have included the nanoparticle system before the neutralization step<sup>336–339</sup> while others after it<sup>340,341</sup>. In all cases, any justification for their choice has been given. For example, Kang *et al.*<sup>338,341</sup> also included NLCs in a Carbopol® gel matrix. In a first study they included celastrol and indomethacin loaded-NLCs in the dispersion media for Carbopol® 940, the mixture was then neutralized<sup>338</sup>. However, any comment on the evolution of the appearance of the formulation was given, nor even a study of the stability of the formulation at the pH values to which they are exposed during the preparation of the gel. In a second study, the same authors included voriconazole loaded-NLCs in a Carbopol® 980 gel matrix and neutralized the formulation before the addition on NLCs<sup>341</sup>. Even if the final formulation is not compared to the unloaded gel, the transparency of the gel is commented.

As it has been discussed in Chapter 3 (section 1.2.2.6.), there is a risk of destroying the NLCs if they are exposed to alkaline or acidic environments. Therefore, we aimed to formulate the gel matrix at a neutral pH. In order to reach this endpoint, percentages of NaOH and TEA in the whole formulation are: 0.5 % w/v and 0.275 % v/v, respectively. These amounts do not exceed the percentages allowed in topical formulations: 10% for NaOH<sup>342,343</sup> and 5% for TEA<sup>344</sup>.

In one side, adding the NLCs before neutralization implies their exposition to an initial acid environment (due to the ionization of the carboxylic groups of Carbopol®), and a latter highly alkaline microenvironment at the moment of the addition of the NaOH 0.5 M (pH = 13) or TEA 20% v/v (pH=10.8) during the neutralization step. As no colour or change in texture was seen when NLCs came in contact with the

Carbopol® dispersion, curcumin seems to remain stable, and so it is suspected that nanocarriers structure is not affected by acidic environments. However, the fact that there is a change of colour during the addition of both neutralizing agents confirms the previously discussed results on the stability of NLCs at different pH, in which deconstruction of the nanocarrier is suspected at pH 9, as curcumin reacts with the alkaline media.

On the other side, when NLCs are incorporated once the Carbopol® gel has reached a neutral pH, any colour change is perceived. Only a change in texture when NaOH is used instead of TEA. This change in the texture of the final product might indicate that NaOH hydrolysed the lipids as it has been previously described. Difference in aspect with TEA neutralized gels may be due to the fact that NaOH is a strong base and TEA a weak one. This may imply that NaOH has a stronger nucleophilic nature compared to TEA.

In the light of these results, NLCs integration into the hydrogel matrix should take place when formulation has reached a neutral pH. At this point, it is suspected that ionized TEA molecules are immobilized by ionic interactions with the carboxyl groups of carbopol. This might prevent TEA molecules to react with oils and fats in the formulations. Thereby saponification (alkaline hydrolysis) cannot take place preserving the structure of the NLCs system. The resulting formulations have a transparent aspect, as shown in Figure 84.

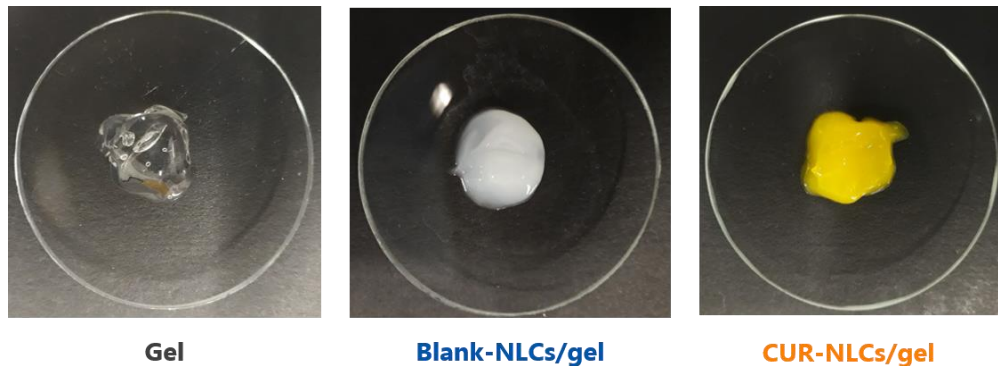


**Figure 85.- Aspect of Gel, Blank-NLCs/gel and CUR-NLCs/gel.** Final Carbopol ® 980 NF concentration in all formulations is 0.5 % w/v. For Blank-NLCs/gel and CUR-NLCs/gel, final concentration of Blank-NLCs or CUR-NLCs suspension is 25 % v/v.

#### **1.2.2.2. Swelling properties of Carbopol® 980 hydrogel**

In order to gain insight of whether the loaded gel could release the NLCs, first an adequate release medium had to be found. From the ones described in the literature, ultrapure water and PBS were chosen as they differ in their content of ions and thus, can differently impact on the network formed within a Carbopol® gel. Moreover, PBS at 10 mM at pH 7.4 is usually used to mimic physiological conditions.

Changes in Carbopol® 980 NF 0.5 % w/v unloaded gel were followed at different time intervals by measuring the volume of either water or PBS that remained in contact with it.

Figure 85 shows that in a 24 h time-frame, water is completely absorbed by the gel (Figure 85-A), while PBS destroys the gel in a concentration dependent manner (Figure 85-B). This implies that the use of water will not allow to have samples where NLCs or curcumin are accessible to quantification, while the use of PBS will entrain the destruction of the gel and as a result, the release of the Carbopol® microparticles which at they turn will interfere with the identification of NLCs in the media by techniques such as DLS. However, the capacity of the gel to disintegrate in an ion-rich media remains interesting for a topical application.

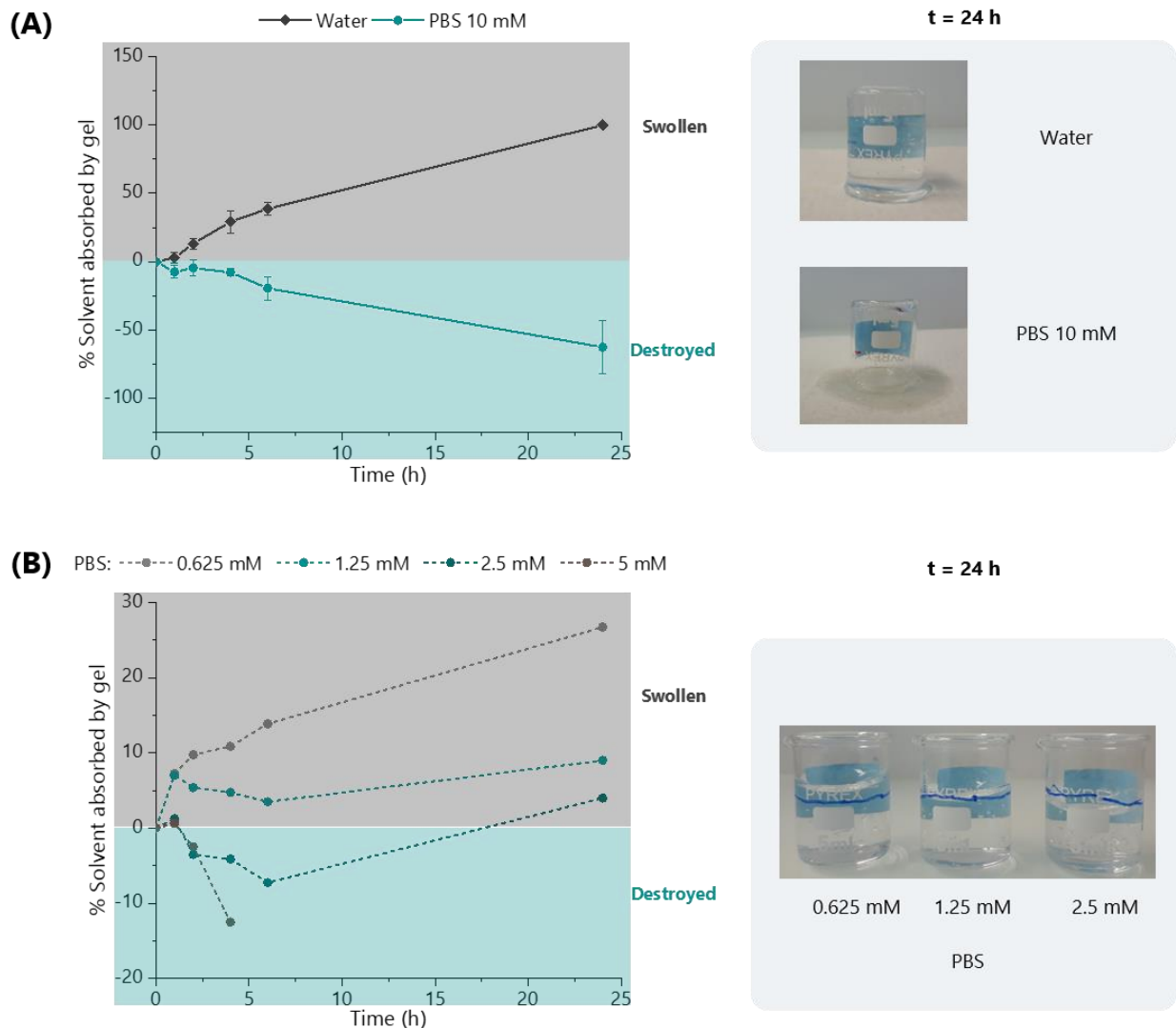


**Figure 86.-Swelling and deconstruction behaviour of Carbopol® 980 NF 0.5 % w/v unloaded gel in water and in PBS. (A)** % of solvent absorbed or expelled from the gel when ultrapure water or PBS 10 mM (pH=7.4) where put in contact for different periods of time with the gel and pictures depicting the final state of the gel at 24h. **(B)** % of solvent absorbed or expelled from the gel when PBS at concentrations 0.625 – 5 mM (pH=7.4) was put in contact for different periods of time with the gel and pictures depicting the final state of the gel at 24 h.

When in contact with water, the gel absorbs all the liquid and swells until its maximal expandability. This implies that the polymeric chains become far one from each other and that the repulsive interactions

between the negative charges of the acidic groups are minimized. However, in presence of PBS, it seems that the ionic strength is higher for the external environment and this causes the diffusion of the solvent from the inner part of the gel. In consequence, the solvent flux that allows to have a highly entangled network after the neutralization is reversed, individual carbomer particles shrink and separate from each other.

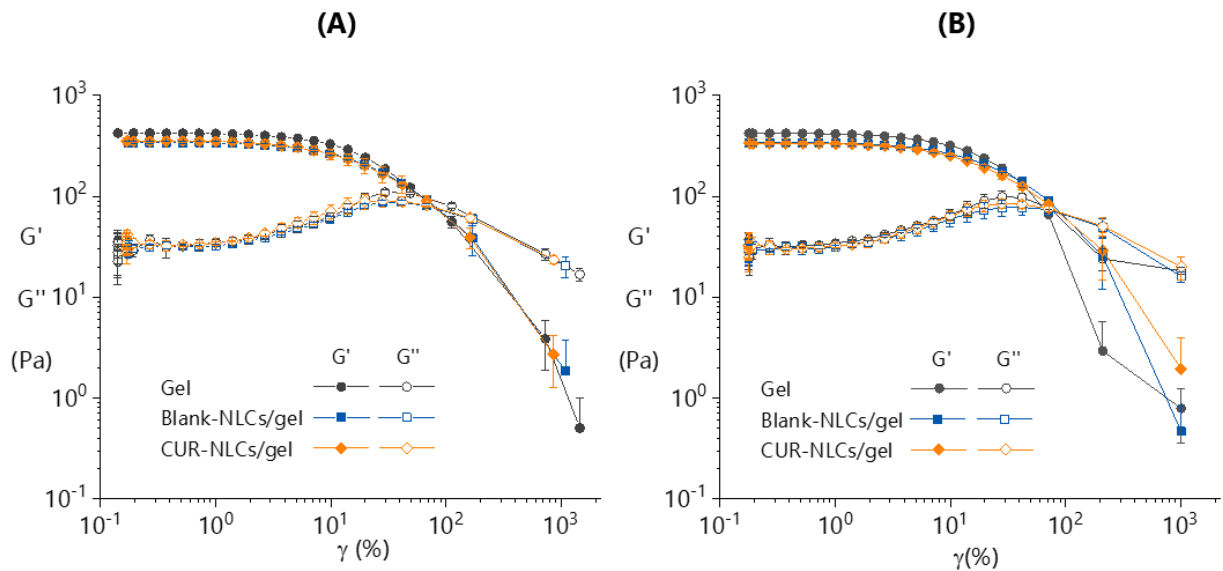
The ability of the gel matrix to disintegrate in contact of salts could mean that the developed composite system (CUR-NLCs/gel) may be able to deliver CUR-NLCs by an erosion/diffusion mechanism. Briefly, once the composite system is applied on the surface of skin or on the surface of acute wounds, its disintegration will lead to the release of CUR-NLCs.

### **1.2.2.3. Rheological characterization of CUR-NLCs/gel**

CUR-NLCs were incorporated in a Carbopol® 980 gel matrix in order to form a multiscale composite platform for curcumin delivery to the skin. In consequence, the rheological characterization was designed in order to know the impact that the inclusion of the NLCs in the hydrogel matrix might have, as this will define the ease of application of the formulation and its retention at the site of application. Therefore, tests were carried-on at the temperature at which the formulation is more likely to be stocked (room temperature, 25°C) and the temperature that it would encounter during application (temperature of the surface of the skin, 32°C).

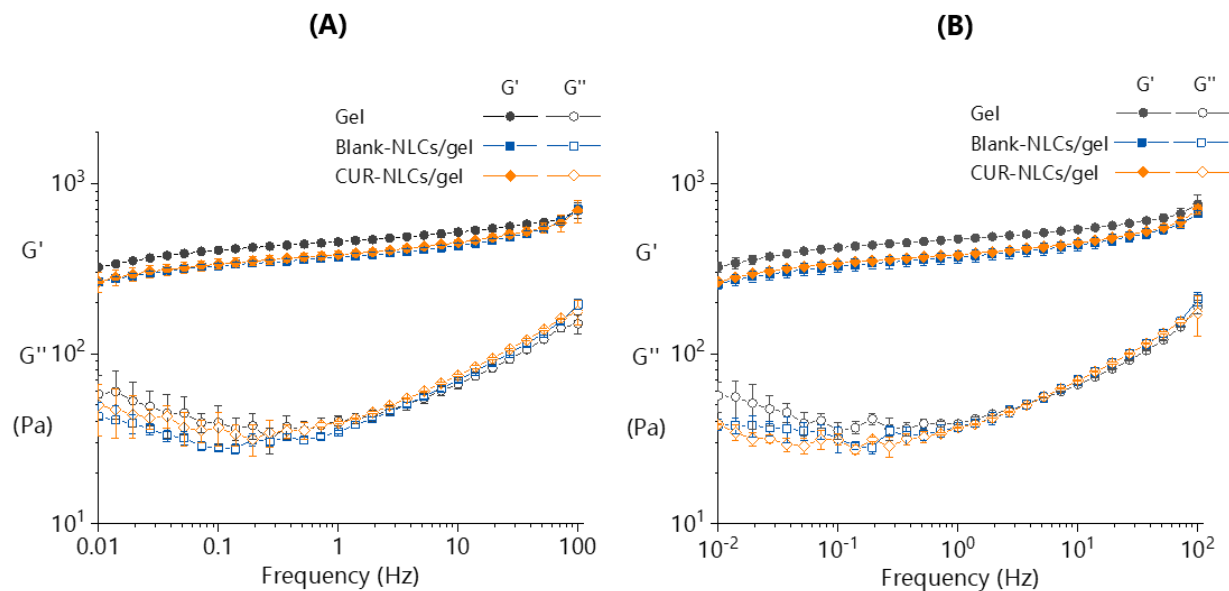
For all performed tests, there was no difference between the behaviour of the different samples when a deformation strain was applied (Figures 86-88).

As shown in Figure 86, there was no statistically significant difference in the flow point of the gel alone or the gel containing NLCs (CUR or Blank). In all cases three regions can be distinguished in the graphs. At the beginning of the test, while  $G' > G''$  and their magnitudes remain constant, a consistent structure characteristic of the tridimensional network of a gel is evidenced. Thus, the addition of NLCs did not hinder the formation of the superstructure of the gel during the preparation. Then, while still  $G' > G''$ , but  $G''$  increases and  $G'$  decreases (roughly before  $\gamma = 2\%$ ), the gel superstructure starts to break until the cross-over ( $G' = G''$ ). After this point, the viscous behavior prevails over the elastic behaviour and there is no more a tridimensional structure. The formulation becomes fluid.



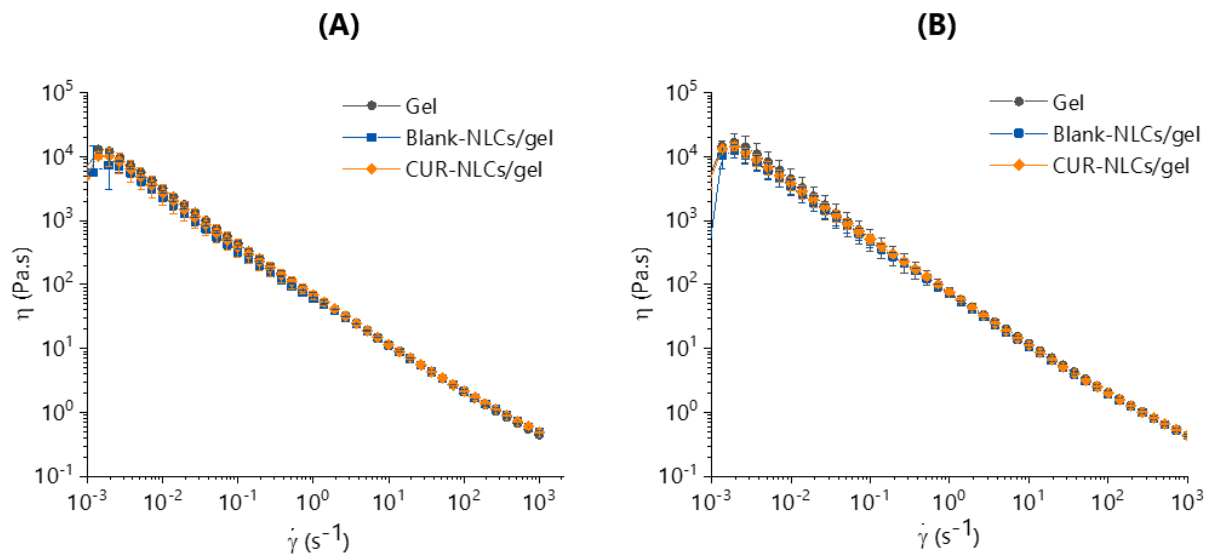
**Figure 87.- Strain ( $\gamma$ ) sweep for Carbopol® 980 NF 0.5% w/v unloaded and loaded gels. (A) at 25°C, room temperature. (B) at 32°C, temperature of the surface of the skin. Storage modulus ( $G'$ ) and Loss modulus ( $G''$ ) are presented in function of applied strain. (n=3).**

Figure 87 shows that  $G' > G''$  for all samples in the non-destructive deformation range ( $\gamma=1\%$ ). This reveals that gel alone and gel containing NLCs behave as a viscoelastic solid material. That is, deformation is proportional to applied stress.



**Figure 88 .- Frequency sweep for Carbopol® 980 NF 0.5% w/v unloaded and loaded gels. (A) at 25°C, room temperature. (B) at 32°C, temperature of the surface of the skin. Storage modulus ( $G'$ ) and Loss modulus ( $G''$ ) are presented in function of the frequency of oscillation. (n=3).**

The negligible impact of NLCs on the structure of the gel is confirmed when assessing the flow behaviour of the formulations. Figure 88 evidences that the inclusion of NLCs in the formulation did not change the shear-thinning behaviour of the gels. Even if for every sample, viscosity decreases with an increasing shear rate, gels rapidly recover their structure after undergoing a high shear period of time as depicted in Figure 89. In the context of a topical application, this can be translated into an easy squeezing from a tube, a successively good staying in the skin, and finally a good spreading during application.



**Figure 89.- Flow curves for Carbopol® 980 NF 0.5% w/v unloaded and loaded gels. (A)** at 25°C, room temperature. **(B)** at 32°C, temperature of the surface of the skin. (n=3).

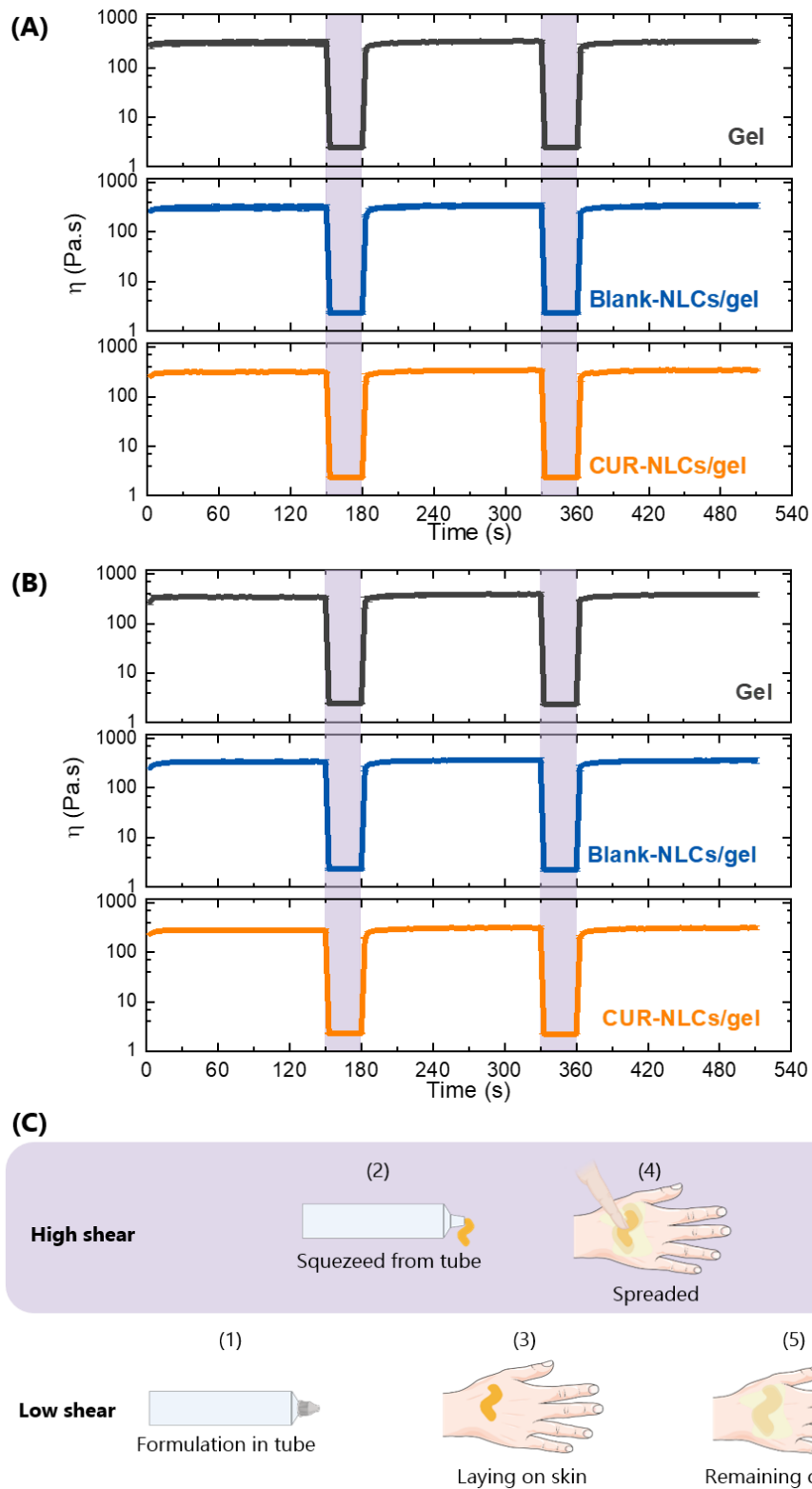


**Figure 90.- Evaluation of time dependent flow behavior (Recovery Test) for Carbopol® 980 NF 0.5% w/v unloaded and loaded gels. (A)** at 25°C, room temperature. **(B)** at 32°C, temperature of the surface of the skin. Variation in viscosity ( $\eta$ ) along time. Shaded zones indicate time intervals where a shear rate of  $100 \text{ s}^{-1}$  was applied (high shear cycles) while non shaded zones indicate time intervals where a shear rate of  $0.1 \text{ s}^{-1}$  was applied (low shear cycles). ( $n=3$ ). **(C)** Events during storage and application to which the CUR-NLCs/gel formulation could be exposed. Events in the shaded area indicate exposition of the formulation to high shear forces, while events in non-shaded area indicate exposition of the formulation to low shear forces.

All the rheological results here presented might be explained by the nature of the interactions between NLCs and the microstructure of the Carbopol® gel. It could be hypothesized that the formulated NLCs of around 300 nm and 80 nm are free to move together with the Carbopol® microparticles, which could reach diameters of 200 µm after swelling and neutralization<sup>345</sup>. In consequence, the measured viscosity is that of the surrounding media. By tracking fluorescent particles trajectories, Oppong *et al.*<sup>346</sup> suggested that when this happens two regions coexist. A region formed by the highly cross-linked cores of the microgels, and a more viscous region containing the polymer chains. If particles are found in the first region, they are going to be trapped and will have limited movement. Taken to the experiences performed in this study, under flow conditions it is probable that they would interfere with the behaviour of Carbopol® microgels. However, if they are found in the viscous region, the low density of entanglement of the polymer chains can form mesh sizes that will allow the particles to freely move. Thus, under flow conditions, the movement of the Carbopol® microgels are not hindered by the particles. Kowalczyk *et al.*<sup>347</sup> showed that an increment in the Carbopol® polymer concentration from 0.1% to 0.75 % was translated in a restriction in the movement of polystyrene particles of 510 nm of diameter. This due to the increased entanglement density at the viscous zones which are responsible of diminishing the mesh size to below 500 nm. This might imply that the formulated NLCs could interfere with the flow behaviour of the gel if higher Carbopol® concentrations are used.



### 1.2.2.4. Permeation and penetration studies of CUR-NLCs and CUR-NLCs/gel

In order to get more knowledge of the interaction of CUR-NLCs and CUR-NLCs/gel with skin, in this part of the work, a first approach mimicking healthy skin conditions was developed. For this, permeation and penetration studies were performed on vertical Franz diffusion cells using synthetic Strat-M<sup>®</sup> membranes between the donor and the receptor compartment. Due to their multi-layer composition, this membranes have demonstrated to be good at mimicking intact skin barrier properties<sup>262,348</sup>.

#### 1.2.2.4.1. Permeation of CUR-NLCs

Figure 90-A shows that count rate in the receptor compartment do not significantly change over the 24 h of contact of CUR-NLCs with the Strat-M<sup>®</sup> membrane in the Franz-cell. Average count rate was about 80-90 kcps. As seen for the calibration curve, this does not differ from the count rate corresponding to PBS (0 g/L NLCs or 0 μM CUR). Thus, no NLC permeation across the membrane was able to be detected by DLS. CUR quantification was also tried on the same samples, however CUR detection was not possible either by HPLC or spectrophotometry. It could be hypothesized that CUR (in NLCs or released from it) was not able to go across the membrane.

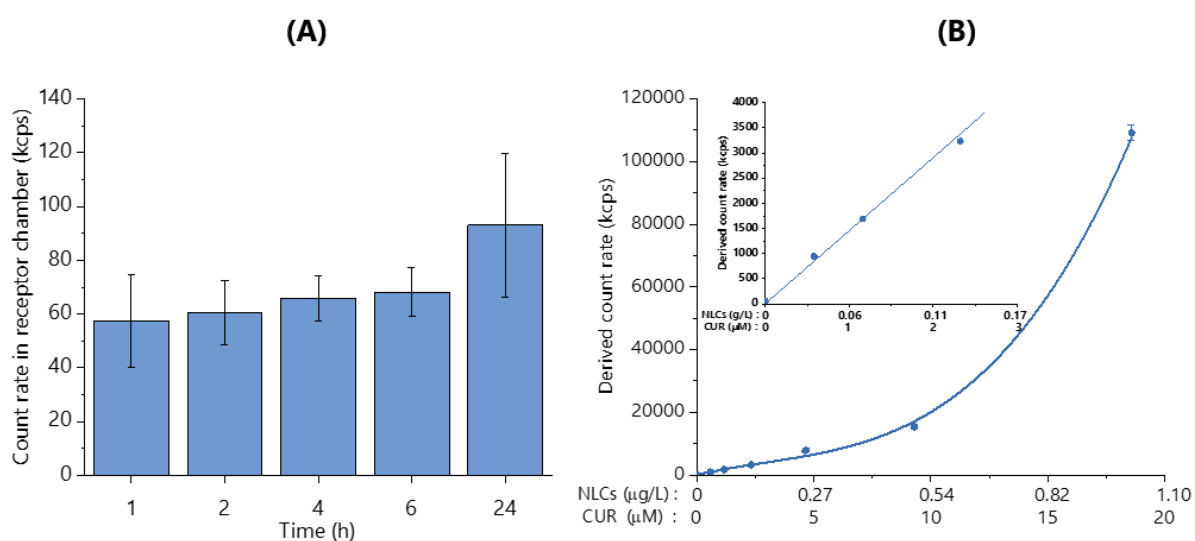


**Figure 91.- CUR-NLCs permeation through Strat-M<sup>®</sup> membrane. (A)** Variation in the count rate in samples from the receptor chamber of Franz-cell. **(B)** Calibration curve of the count rate versus NLCs and CUR concentration. (n=3)

#### 1.2.2.4.2. Penetration studies on CUR-NLCs and CUR-NLCs/gel

Figure 91-A shows the penetration profiles for CUR-NLCs and CUR-NLCs/gel. For each formulation, the initial CUR concentration in the donor compartment of the Franz cell was  $122 \pm 4$  μg/mL and  $125 \pm 4$  μg/g, respectively. CUR accumulation in Strat-M<sup>®</sup> membranes was time-dependent for both CUR-NLCs and CUR-

NLCs/gel, but higher for CUR-NLCs at all time-points. CUR penetrated expressed in % from the initial amount in the donor compartment was  $1.97 \pm 0.76 \%$  and  $0.78 \pm 0.06 \%$  for CUR-NLCs and CUR-NLCs/gel after 15 min, while  $22.06 \pm 1.59 \%$  and  $5.07 \pm 0.53 \%$  for CUR-NLCs and CUR-NLCs/gel at 24 h. Figure 91-B shows that the decrease in the amount of CUR in the donor compartment corresponds to the amount of CUR penetrated in the membrane, evidencing that CUR was not able to cross the membranes.

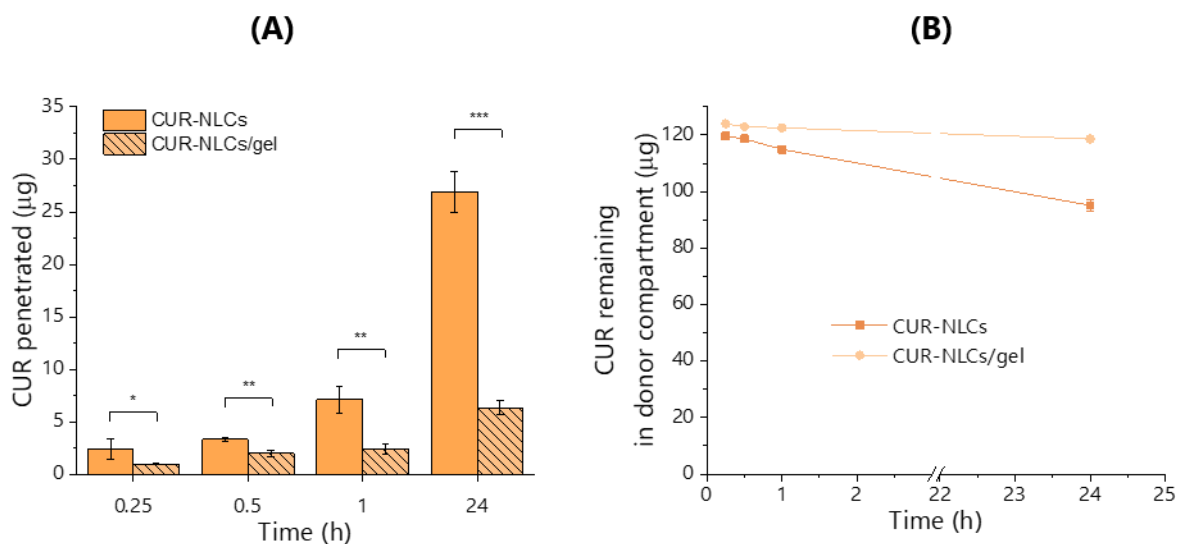


**Figure 92.- CUR penetration studies into Strat-M® membrane. (A)** Penetration profiles of CUR into Strat-M® membrane from CUR-NLCs suspension and CUR-NLCs incorporated into the gel. **(B)** Amount of CUR remaining in the donor compartment at the end of each time-point. Asterisks denote statistically significant differences. Two sample Student-t test was carried out and statistically significant differences were identified when p-values were lower than 0.05 (\* $p < 0.05$ ), 0.01 (\*\* $p < 0.01$ ) or 0.001 ( $p < 0.001$ ). (n=3)

**Table 23.- Amount entrapped of CUR per unit area ( $D_e$ ) and accumulation ( $A_c$ ) on Strat-M® membranes.**

Time (h)	$D_e$ ( $\mu\text{g}/\text{cm}^2$ )		$A_c$ (cm)	
	CUR-NLCs	CUR-NLCs/gel	CUR-NLCs	CUR-NLCs/gel
0.25	$0.94 \pm 0.36$	$0.97 \pm 0.07$	$0.0077 \pm 0.0030$	$0.0031 \pm 0.0002$
0.5	$1.31 \pm 0.05$	$2.01 \pm 0.30$	$0.0107 \pm 0.0004$	$0.0063 \pm 0.0011$
1	$2.79 \pm 0.49$	$2.41 \pm 0.44$	$0.0229 \pm 0.0040$	$0.0076 \pm 0.0014$
24	$10.58 \pm 0.76$	$6.33 \pm 0.66$	$0.0867 \pm 0.0062$	$0.0199 \pm 0.0021$

Due to its partition coefficient around 3, and a molecular weight lower than 500 Da, curcumin transfer to SC and the diffusion through it could be expected following the 1<sup>st</sup> Fick Law. However, even if a concentration gradient is established between both sides of the skin (or of the synthetic membrane in our case), curcumin ability to fully cross all the layers underneath the SC is hindered by its lipophilic nature.

During this work, testing of non-entrapped curcumin was not performed as this would have implied to use organic solvent or propylenglicol which would have altered the permeability of the membranes, as it will be further discussed.

However, while entrapped into NLCs, curcumin diffusion will mainly depend on the compatibility of the nanocarrier with each layer to be crossed (as CUR release from NLCs in the same conditions is minimal). In healthy skin (and Strat-M® membranes), the SC (or lipid coating for membranes) is the first barrier for NLCs to cross in order to permeate across the full thickness of the skin. The fact that no NLCs permeation was detected (thus, no risk of transdermal or systemic action in a real context) could be explained by their strong lipidic nature, and thus strong affinity with the lipophilic layers in the skin.

Our results are inline with the results of Rapalli *et al.*<sup>274</sup> who did not detect curcumin permeation after 24 h contact of CUR-NLCs with goat ear skin. By retiring layer by layer of skin (tape-stripping technique), they demonstrated that curcumin was preferentially accumulated in the SC than in the viable epidermis and dermis. Differently to us, they used PBS at pH=6.4 with 1.5% Tween® 80 in the receptor media. Such concentration of Tween® 80 should not induce any destructurement of the skin barrier<sup>349</sup>, but might induce micelle formation as it is higher to the cmc (critical micelle concentration) of Tween® 80 ( $1.4 \times 10^{-3} \%$ )<sup>350</sup>. As in our study, we aimed to analyse the samples by DLS, thus addition of Tween® 80 was omitted.

Some other studies have concluded that NLCs could enhance curcumin permeation through animal skin samples with reported flux between 0.092 and 2.45  $\mu\text{g}/\text{cm}^2/\text{h}$ . However, composition of the receptor media containing at least 20 % v/v of EtOH<sup>208,210–212</sup> can let think of the possibility of disruption of the skin barrier function (by lipid disordering or lipid extraction)<sup>351,352</sup>. In any of these studies, identification of NLCs in the receptor compartment was performed. Thus, curcumin detected could also be result of the NLCs dissolution by EtOH and subsequent passage to the receptor chamber through the disordered /disintegrated lipid barrier of the skin.

As it has been already reported, it is the high lipophilicity of NLCs that make them to preferentially accumulate in the upper layers of skin<sup>177,182</sup>.

Investigations in other systems demonstrated the importance of the compatibility of the nanocarrier in order to reach different layers. For example, chitosan nanoparticles tested in the Strat-M® membranes, were able to reach a flux of  $0.54 \pm 0.03 \mu\text{g}$  of CUR/ $\text{cm}^2/\text{h}$ <sup>353</sup>. Authors explain that permeation is due to the capacity of chitosan to retain water and disrupt the structure of SC and its hydrophilicity which allows its diffusion through the inner layers of the epidermis and dermis. Also, curcumin-loaded organogels

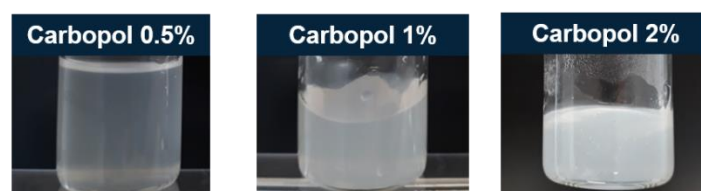
composed of Pluronic® F-127, Pluronic® L-81 and oleic acid yielded a curcumin flux across Strat-M® membrane of  $0.102 \pm 0.006 \mu\text{g}/\text{cm}^2/\text{h}$ . Probably due to low viscosity, higher deformability of these systems and possibility for the excipients to act as absorption enhancers once the nanosystem is destabilised<sup>354</sup>.

In both, CUR-NLCs and CUR-NLCs/gel, the increase of curcumin concentration could be explained by the ability of both formulations to increase the contact time with the skin, important to have an effective transfer of NLCs. Lower curcumin accumulation for CUR-NLCs/gel points out to a decrease of NLCs mobility due to the increase of the viscosity of the dispersant phase. This seems to allow fewer CUR-NLCs to be deposit at each time-point and with it a decrease in their transfer to the skin (or the membrane). Our results confirm the multiscale character of the developed system for curcumin delivery.

However, it has to be taken in mind that the described penetration is more likely to be altered in no healthy skin and in the case of inflamed or scarred skin.

### 1.3. Supporting information

• Aspect of Carbopol® 980 dispersions at 0.5, 1 and 2 % w/v, before neutralization



- 
- More difficult to incorporate NLCs once gel has been neutralized
  - Less volume of NLCs that could be incorporated

### 1.4. Conclusions

CUR-NLCs, as well as Blank-NLCs and CUR reduce the migration/proliferation of BJ-Fibroblasts and HEK293T. Higher inhibitory effect is seen for CUR-NLCs which would open the perspective of its use for as an adjuvant therapy for psoriasis, keloids and hypertrophic scars.

It is possible to induce and evidence ROS production in BJ-Fibroblasts by 1h exposition to 100 µM of Luperox® without affecting their metabolic activity.

Metabolic activity of BJ-Fibroblasts pre-treated with CUR-NLCs is not affected even after undergoing oxidative stress. This opens the door to applications as adjuvant therapy in context of inflammatory skin conditions such as psoriasis, dermatitis and even in the first stages of healing in acute wounds.

CUR-NLCs are loaded in a Carbopol® gel matrix, following a preparation method that would minimize the degradation of both, the nanocarrier or the cargo. CUR-NLCs inclusion into the composite system does not affect the rheological behaviour of Carbopol®. Moreover, the formulated CUR-NLCs/gel is compatible with a topical application, as it easily recovers its viscosity after short periods of deformation.

The ability of the composite system CUR-NLCs/gel to release CUR to the skin is proven by the ability of Carbopol® hydrogel to disintegrate in the presence of salts at the pH at which NLCs maintain their size distributions (pH = 5.5, 7.4 and 9) and the ability of CUR-NLCs and CUR-NLCs/gel to differently induce the penetration of CUR in Strat-M® membranes. The system is able to deliver CUR to Strat-M® without risk of a transdermal passage of neither the active ingredient or NLCs.

**Chapter 5: Conclusions and perspectives**

---



With a physical and immune barrier function, skin is one of the first lines of defence of the body. It is thus, an organ subjected to numerous situations in which oxidative stress and inflammation play a central role, for example: wounds (acute and chronic), abnormal wound-healing with scarring, psoriasis and dermatitis. Even if there are established treatments for these states, the utilisation of an adjuvant therapy in order to diminish the symptoms and re-establish normal appearance of skin will greatly benefit not only the physiological, but also the psychological and social aspects of patients' life.

Exogenous compounds, and especially those of natural origin, also described as natural bioactive compounds (NBC), have demonstrated interesting antioxidant properties. They are able to directly regulate ROS, but also to modulate cellular metabolic pathways in order to induce antioxidant and anti-inflammatory responses in dermal cells. Curcumin, the main polyphenol in *Curcuma longa*, is one of these compounds. Even if its benefits in several skin conditions have been proved, its use is hindered mainly by its lack of solubility in aqueous systems. In consequence, there is a need to develop adapted formulations capable of allowing a controlled delivery of curcumin to the skin. Even if classical forms for curcumin formulation have been proposed, there is still a challenge to meet at the same time the key characteristics: high entrapments, ease of application, adherence to the skin, moisturizing effect, controlled release as well as well-known behaviour at the cellular level.

By using innovative drug delivery systems associated in composite formulations, multiple key characteristics can be met at the same time.

Nanostructured Lipid Carriers (NLCs) are considered the second generation of lipid nanoparticles. They are mainly composed by the mixture of a solid lipid and a liquid lipid and present several advantages face to first generation Solid Lipid Nanoparticles (SLNs), such as higher stability, higher entrapment of hydrophobic drugs and better controlled release. The lipophilic nature of NLCs makes them excellent candidates for curcumin entrapment. However, when applied as a topical formulation, they do not possess optimal adherence properties which are important in order to facilitate a topical application and to establish curcumin transfer to the skin.

Hydrogels are pharmaceutical forms with good moisturizing effects due to the high amounts of water they contain. Because of their viscoelastic properties, they can be easily applied on skin. Moreover, they offer the possibility of control the release of their cargo (molecules or particles).

Combining NLCs and hydrogels appears as an interesting approach for curcumin delivery to the skin.

In this thesis, works aimed to **develop a composite platform (CUR-NLCs/gel) for the delivery of curcumin to the skin** and to **explore the potential that the proposed formulation may have for a topical application**.



The first part of the works presented here aimed to **achieve a reproducible CUR-NLCs production by the Hot Homogenization method and to characterise their physico-chemical properties as well as their cytotoxicity towards dermal cells (fibroblasts and keratinocytes).**

By changing the method and formulation parameters, stable CUR-NLCs formulation was obtained. They are composed mostly of nanoparticles of 70-85 nm, with a disk-like morphology. This formulation was capable of entrapping high amounts of curcumin (0.85 mg/mL of NLCs suspension), and thus, significantly increase its apparent water solubility, while preserving its antioxidant properties and controlling its release in different biological media (37.5 % of CUR released in DMEM 10%FBS, while 18.2% in PBS at pH 7.4, during 24 h). These release experiments could be also performed at different pH, in an effort to mimic pathological conditions like wounds in which an alkaline environment is present.

Permeation through a SEC column seems to be able to remove excipient molecules that are not in the form of NLCs allowing to assess the effect of only CUR-NLCs on cells behaviour.

Cytotoxic evaluation according to the norm ISO 10993-5 showed that cytotoxic profiles differ according to the cell-line and that curcumin release might play a major role on the observed effects. Maximal non-toxic concentrations for primary cell-lines, after a 24 h-exposition, were of 10  $\mu$ M of entrapped curcumin in 0.54 mg/mL of NLCs for BJ-Fibroblast and of 20  $\mu$ M of entrapped curcumin in 1.10 mg/mL of NLCs for HEK293. Unloaded NLCs (Blank-NLCs) did not display any toxicity for concentrations lower than 1.10 mg/mL for both cell-lines.

In order to complete the characterization of the interaction of CUR-NLCs with cells, three main points remain to be addressed:

1. The role of NLCs in the uptake of curcumin by dermal cells: Do curcumin get inside the cells while entrapped in NLCs or once released from NLCs?
2. NLCs uptake by cells: Do NLCs get inside the cells? If so, which are the mechanisms involved?
3. The intracellular fate of NLCs and of curcumin once inside the cell: Do they remain in the cytoplasm or are they directed to an organelle (like the mitochondria)? Does fate of NLCs is the same as that of curcumin?

A first quantitative approach to get insight in whether curcumin could be found inside the cells once it was administered entrapped in NLCs, was performed through UPLC-DAD/MS. However, no intracellular curcumin was detected after 24 h of HaCaT (immortalized keratinocytes cell-line) treatment with CUR-NLCs. Taking into account that during 24 h, curcumin can be incorporated by cells, metabolized and also expelled,

future works would need to assess the intracellular delivery of curcumin after shorter periods, for example: 30 min, 1 h, 2 h, 4 h and 6 h. Exposition to shorter times may imply the possibility of administrating higher CUR-NLCs concentrations to cells.

In order to solve possible problems linked with limits of quantification, but being able to answer to the question of curcumin being incorporated by cells or not through its entrapment in NLCs, qualitative or semi-quantitative methodologies could also be used. The more adapted ones seem to be those based in fluorescence like fluorescence microscopy, confocal microscopy and FACS (Fluorescence Activated Cell Sorting).

These techniques can also be used to follow the uptake and the intracellular fate of the nanocarrier. For this, one of its components (surfactants or lipids) would need to be transformed in a fluorescent compound. By specifically marking organelles (with for example MitoTracker™-Invitrogen, for mitochondria), and analysing co-localization of fluorescence signals, the intracellular destination of NLCs could be explored. Alternatively, coloration of NLCs once they are incorporated by cells can be tried. Unpublished experiments in our research group with SLNs, demonstrated that Oil-Red-O dye could be used to stain the neutral triglycerides and lipid components of the nanocarrier once they have been incorporated by cells.

The second part of the work aimed **to explore the potential of the developed CUR-NLCs following an application in a skin context**. In one hand these studies were performed at the cellular level by the assessment of CUR-NLCs impact on the migration/proliferation of healthy cells and the evaluation of the impact of CUR-NLCs on the metabolic activity of oxidatively stressed cells (for which a model for induction of oxidative stress and ROS detection was developed). In the other hand, assessment of the potential of CUR-NLCs for a topical application was performed by formulating a composite system: CUR-NLCs/gel and the study of its physical characteristics in similar conditions, as those when applied in skin.

It was found that CUR-NLCs decreases the migration/proliferation of dermal cells (BJ-Fibroblasts and HEK293). However, while being applied as a pre-treatment, they do not affect the metabolic activity of oxidatively stressed cells. The model using Luperox® as stressor and DCFH-DA as a fluorogenic probe could be used for evaluating the impact of CUR-NLCs on the antioxidant response in dermal cells. For this, besides the quantification of fluorescence reduction (indicative of ROS presence), assessment of the change in the activity and expression of antioxidant enzymes, as well as evaluation of DNA damage can help to fully describe the induced oxidative stress taking place inside the cells.

Nevertheless, presented findings confirm the potential of the developed system in the treatment of dermal oxidative stress as well as inflammatory skin conditions such as psoriasis, dermatitis and even different

stages of wound-healing. Nevertheless, experiments using pathological cells lines or even *in vivo* will be useful to better direct the potential adjuvant therapeutic applications of the developed system.

Complementary, as curcumin has been described to present antibacterial effect, it would be interesting to assess if the formulated CUR-NLCs have an effect on pathogenic bacteria such as *S. aureus*.

With curcumin as a natural active compound incorporated in a composite system NLCs/gel, a formulation with rheological properties compatibles with a topical application was obtained. The ability of this system to deliver curcumin to synthetic Strat-M ® membranes mimicking healthy skin was demonstrated. It has been shown that CUR-NLCs are able to penetrate and accumulate in the membrane without permeating across it and that the inclusion in the gel matrix further contributes to have a controlled transfer of CUR to the membrane.

In this line, future works should address the penetration/permeation profiles of the developed systems (CUR-NLCs and CUR-NLCs/gel) on healthy and non-healthy skin, as barriers for NLCs and/or CUR transfer can be affected.

One important aspect that remains interesting to be investigated is the release of CUR from CUR-NLCs when they are found in the gel. Even if release experiments show that release in PBS at pH 7.4 is minimal, such experiments would allow to know if curcumin penetrated in the membranes (or skin) is the one entrapped in NLCs or the one that has been released from it.

Concerning the hydrogel matrix, current works in the research team aim to incorporate phages (viruses infecting bacteria) in order to obtain a composite system with a dual effect: an antioxidant effect given by CUR-NLCs and an antibacterial effect given by the phages. This would open the possibility of applying the formulated system to prevent biofilm formation such as in the case of chronic wounds.

## References

---

1. Zhang XJ, Wang AP, Shi TY, et al. The psychosocial adaptation of patients with skin disease: A scoping review. *BMC Public Health*. 2019;19(1):1-15. doi:10.1186/s12889-019-7775-0
2. Seth D, Cheldize K, Brown D, Freeman EE. Global Burden of Skin Disease: Inequities and Innovations. *Curr Dermatol Rep*. 2017;6(3):204-210. doi:10.1007/s13671-017-0192-7
3. Flohr C, Hay R. Putting the burden of skin diseases on the global map. *Br J Dermatol*. 2021;184(2):189-190. doi:10.1111/bjd.19704
4. Hollestein LM, Nijsten T. An insight into the global burden of skin diseases. *J Invest Dermatol*. 2014;134(6):1499-1501. doi:10.1038/jid.2013.513
5. Rawlani S, Rawlani S. *Textbook of General Anatomy*. Second. New Delhi: P (LTD); 2013.
6. Sandby-Møller J, Poulsen T, Wulf HC. Epidermal Thickness at Different Body Sites: Relationship to Age, Gender, Pigmentation, Blood Content, Skin Type and Smoking Habits. *Acta Derm Venereol*. 2003;83(6):410-413. doi:10.1080/00015550310015419
7. Rice G, Rompolas P. Advances in resolving the heterogeneity and dynamics of keratinocyte differentiation. *Curr Opin Cell Biol*. 2020;67:92-98. doi:10.1016/j.ceb.2020.09.004
8. Eckhart L, Lippens S, Tschachler E, Declercq W. Cell death by cornification. *Biochim Biophys Acta - Mol Cell Res*. 2013;1833(12):3471-3480. doi:10.1016/j.bbamcr.2013.06.010
9. Dréno B. Anatomy and physiology of skin and cutaneous annexes. *Ann Dermatol Venereol*. 2009;136(SUPPL. 10):S247-S251. doi:10.1016/S0151-9638(09)72527-X
10. Brunton L, Chabner B, Knollman B. *Goodman & Gilman's The Pharmacological Bases of Therapeutics*. Twelfth. New York: Mc Graw Hill; 2011.
11. Zimoch J, Zielinska D, Michalak-Micka K, et al. Bioengineering a prevascularized human tri-layered skin substitute containing a hypodermis. *Acta Biomater*. 2021;134:215-227. doi:10.1016/j.actbio.2021.07.033
12. Schmidt BA, Horsley V. Intradermal adipocytes mediate fibroblast recruitment during skin wound healing. *Dev*. 2013;140(7):1517-1527. doi:10.1242/dev.087593
13. Schaubert Jürgen, Richard G. Antimicrobial peptides and the skin immune defense system. *J Allergy Clin Immunol*. 2008;122(2):261-266. doi:10.1016/j.jaci.2008.03.027.Antimicrobial
14. Karlsbad A, Kopp S. Intramuscular and skin surface temperatures of the resting human superficial masseter muscle. *Acta Odontol Scand*. 1991;49(4):225-231. doi:10.3109/00016359109005912
15. Bhanu B, Pavlidis I. Emissivity of Human Facial Skin. In: *Computer Vision Beyond the Visible Spectrum*. California; 2004:181-183.
16. Guyton A, Hall J. *Textbook of Medical Physiology*. Eleventh. Philadelphia: Elsevier Saunders; 2006.
17. Singh S, Young A, McNaught CE. The physiology of wound healing. *Surg (United Kingdom)*.

- 2017;35(9):473-477. doi:10.1016/j.mpsur.2017.06.004
18. Korting HC, Schöllmann C, White RJ. Management of minor acute cutaneous wounds: Importance of wound healing in a moist environment. *J Eur Acad Dermatology Venereol.* 2011. doi:10.1111/j.1468-3083.2010.03775.x
  19. Berthet M, Gauthier Y, Lacroix C, Verrier B, Monge C. Nanoparticle-Based Dressing: The Future of Wound Treatment? *Trends Biotechnol.* 2017;35(8):770-784. doi:10.1016/j.tibtech.2017.05.005
  20. Ben R, Pereira F, Bá Rtoló PJ. COMPREHENSIVE INVITED REVIEWS Traditional Therapies for Skin Wound Healing. *208 j Adv WOUND CARE.* 5(5). doi:10.1089/wound.2013.0506
  21. Rodrigues M, Kosaric N, Bonham CA, Gurtner GC. Wound Healing: A Cellular Perspective. *Physiol Rev.* 2019;99:665-706. doi:10.1152/physrev.00067.2017.-Wound
  22. Auf Dem Keller U, Kü Min A, Braun S, Werner S. Reactive Oxygen Species and Their Detoxification in Healing Skin Wounds. *J Investig Dermatology Symp Proc.* 2006;11:106-111. doi:10.1038/sj.jidsymp.5650001
  23. Rittié L. Cellular mechanisms of skin repair in humans and other mammals. *J Cell Commun Signal.* 2016;10(2):103-120. doi:10.1007/s12079-016-0330-1
  24. Frykberg RG, Banks J. Challenges in the Treatment of Chronic Wounds. *Adv Wound Care.* 2015;4(9):560-582. doi:10.1089/wound.2015.0635
  25. Chin JS, Madden L, Chew SY, Becker DL. Drug therapies and delivery mechanisms to treat perturbed skin wound healing. *Adv Drug Deliv Rev.* 2019;149-150:2-18. doi:10.1016/j.addr.2019.03.006
  26. Beyene RT, Derryberry SL, Barbul A. The Effect of Comorbidities on Wound Healing. *Surg Clin North Am.* 2020. doi:10.1016/j.suc.2020.05.002
  27. Gauglitz GG, Korting HC, Pavicic T, Ruzicka T, Jeschke MG. Hypertrophic scarring and keloids: Pathomechanisms and current and emerging treatment strategies. *Mol Med.* 2011;17(1-2):113-125. doi:10.2119/molmed.2009.00153
  28. Erickson JR, Echeverri K. Learning from regeneration research organisms: The circuitous road to scar free wound healing. *Dev Biol.* 2018;433(2):144-154. doi:10.1016/j.ydbio.2017.09.025
  29. Mahdavian Delavary B, Van Der Veer WM, Ferreira JA, Niessen FB. Formation of hypertrophic scars: Evolution and susceptibility. *J Plast Surg Hand Surg.* 2012;46(2):95-101. doi:10.3109/2000656X.2012.669184
  30. Smith C, Smith J, Finn M. The possible role of mast cells (allergy) in the production of keloid and hypertrophic scarring. *J Burn Care Rehabil.* 1987;8(2):126-131.
  31. Taylor SC. Skin of color: Biology, structure, function, and implications for dermatologic disease. *J Am Acad Dermatol.* 2002;46(2 III):41-62. doi:10.1067/mjd.2002.120790
  32. Alster T, Tanzi E. Hypertrophic Scars and Keloids-Etiology and Management. *Am J Clin Dermatol.* 2003;4(4):235-243. doi:10.2165/00128071-200304040-00003

33. Profyris C, Tziotzios C, Do Vale I. Cutaneous scarring: Pathophysiology, molecular mechanisms, and scar reduction therapeutics: Part I. the molecular basis of scar formation. *J Am Acad Dermatol.* 2012;66(1):1-10. doi:10.1016/j.jaad.2011.05.055
34. da Cunha Colombo Tiveron LR, da Silva IR, da Silva MV, Peixoto AB, Rodrigues DBR, Rodrigues V. High in situ mRNA levels of IL-22, TFG- $\beta$ , and ARG-1 in keloid scars. *Immunobiology.* 2018;223(12):812-817. doi:10.1016/j.imbio.2018.08.010
35. Ekaterina K, Ho D, Jagdeo J. Successful Treatment of Keloid With Fractionated Carbon Dioxide (CO<sub>2</sub>) Laser and Laser-Assisted Drug Delivery of Triamcinolone Acetonide Ointment in an African-American Man. *J Drugs Dermatology.* 2017;16(9):925-927.
36. Gohel MS, Poskitt KR. Chronic ulceration of the leg. *Surgery.* 2013;31(5):224-228. doi:10.1016/j.mpsur.2013.02.004
37. Viguier M, Beylot-Barry M, Ly S. Société Française de Dermatologie: Le Psoriasis. <https://dermato-info.fr/fr/les-maladies-de-la-peau/le-psoriasis>. Published 2019. Accessed October 30, 2020.
38. Plaza JA, Prieto VG. Inflammatory Skin Conditions. In: *Modern Surgical Pathology*. Vol 2. Second. Amsterdam: Elsevier Inc.; 2009:1843-1889. doi:10.1016/B978-1-4160-3966-2.00048-5
39. Inserm. Psoriasis - vers un traitement curateur. <https://www.inserm.fr/dossier/psoriasis/>. Published 2017. Accessed October 30, 2021.
40. Davidovici BB, Sattar N, Jörg PC, et al. Psoriasis and systemic inflammatory diseases: Potential mechanistic links between skin disease and co-morbid conditions. *J Invest Dermatol.* 2010;130(7):1785-1796. doi:10.1038/jid.2010.103
41. Farci F, Mahabal G. *Hyperkeratosis*. Florida: StatPearls Publishing LLC.; 2021.
42. France-Psoriasis A. Qu'est-ce que le psoriasis? <https://francepsoriasis.org/la-maladie/comprendre/psoriasis/quest-ce-que-le-psoriasis/>. Published 2016. Accessed October 30, 2021.
43. Kurihara F, Soria A. Eczémas de contact aux isothiazolinones (Contact allergy to isothiazolinones). *Ann Dermatologie Vénérologie - FMC.* 2021;1(3):193-197. doi:10.1016/j.fander.2020.08.004
44. Raveendran R. Tips and Tricks for Controlling Eczema. *Immunol Allergy Clin North Am.* 2019;39(4):521-533. doi:10.1016/j.iac.2019.07.006
45. Nguyen HLT, Trujillo-Paez JV, Umehara Y, et al. Role of antimicrobial peptides in skin barrier repair in individuals with atopic dermatitis. *Int J Mol Sci.* 2020;21(20):1-18. doi:10.3390/ijms21207607
46. Inserm. Dermatite atopique (eczéma atopique). <https://www.inserm.fr/dossier/dermatite-atopique-eczema-atopique>. Published 2017. Accessed October 29, 2021.
47. Sies Helmut. Oxidative Stress: Introductory Remarks. In: *Oxidative Stress*. London: Academic Press Inc.; 1985:1-8. doi:10.1016/b978-0-12-642760-8.50005-3
48. Dean P. J. Redefining Oxidative Stress. *Antioxid Redox Signal.* 2006;8:1865-1879.

49. Halliwell B. Reactive oxygen species in living systems: Source, biochemistry, and role in human disease. *Am J Med.* 1991;91(3 Suppl. 3):14S-22S. doi:10.1016/0002-9343(91)90279-7
50. Schieber M, Chandel NS. ROS function in redox signaling and oxidative stress. *Curr Biol.* 2014;24(10):R453-R462. doi:10.1016/j.cub.2014.03.034
51. Nemoto S, Takeda K, Yu Z-X, Ferrans VJ, Finkel T. Role for Mitochondrial Oxidants as Regulators of Cellular Metabolism. *Mol Cell Biol.* 2000;20(19):7311-7318. doi:10.1128/mcb.20.19.7311-7318.2000
52. Finkel T. Oxygen radicals and signaling. *Curr Opin Cell Biol.* 1998;10:248-253.
53. Han D, Antunes F, Canali R, Rettori D, Cadenas E. Voltage-dependent anion channels control the release of the superoxide anion from mitochondria to cytosol. *J Biol Chem.* 2003;278(8):5557-5563. doi:10.1074/jbc.M210269200
54. Ayala A, Muñoz MF, Argüelles S. Lipid peroxidation: Production, metabolism, and signaling mechanisms of malondialdehyde and 4-hydroxy-2-nonenal. *Oxid Med Cell Longev.* 2014;2014:1-31. doi:10.1155/2014/360438
55. Szabadkai G, Duchon MR. Mitochondria: The hub of cellular Ca<sup>2+</sup> signaling. *Physiology.* 2008;23(2):84-94. doi:10.1152/physiol.00046.2007
56. Kurz T, Eaton JW, Brunk UT. Redox activity within the lysosomal compartment: Implications for aging and apoptosis. *Antioxidants Redox Signal.* 2010;13(4):511-523. doi:10.1089/ars.2009.3005
57. Kruszewski M. Labile iron pool: The main determinant of cellular response to oxidative stress. *Mutat Res - Fundam Mol Mech Mutagen.* 2003;531(1-2):81-92. doi:10.1016/j.mrfmmm.2003.08.004
58. Radisky DC, Kaplan J. Iron in cytosolic ferritin can be recycled through lysosomal degradation in human fibroblasts. *Biochem J.* 1998;336(1):201-205. doi:10.1042/bj3360201
59. Nilsson E, Ghassemifar R, Brunk UT. Lysosomal heterogeneity between and within cells with respect to resistance against oxidative stress. *Histochem J.* 1997;29(11-12):857-865. doi:10.1023/A:1026441907803
60. Brunk UT, Neuzil J, Eaton JW. Lysosomal involvement in apoptosis. *Redox Rep.* 2001;6(2):91-97. doi:10.1179/135100001101536094
61. Bhattacharyya A, Chattopadhyay R, Mitra S, Crowe SE. Oxidative stress: An essential factor in the pathogenesis of gastrointestinal mucosal diseases. *Physiol Rev.* 2014;94(2):329-354. doi:10.1152/physrev.00040.2012
62. Panday A, Sahoo MK, Osorio D, Batra S. NADPH oxidases: An overview from structure to innate immunity-associated pathologies. *Cell Mol Immunol.* 2015;12(1):5-23. doi:10.1038/cmi.2014.89
63. Al-Gubory KH. Environmental pollutants and lifestyle factors induce oxidative stress and poor prenatal development. *Reprod Biomed Online.* 2014;29(1):17-31. doi:10.1016/j.rbmo.2014.03.002
64. Lodovici M, Bigagli E. Oxidative stress and air pollution exposure. *J Toxicol.* 2011;2011. doi:10.1155/2011/487074

65. Riley PA. Free radicals in biology: Oxidative stress and the effects of ionizing radiation. *Int J Radiat Biol.* 1994;65(1):27-33. doi:10.1080/09553009414550041
66. Okado-Matsumoto A, Fridovich I. Subcellular distribution of superoxide dismutases (SOD) in rat liver. Cu,Zn-SOD in mitochondria. *J Biol Chem.* 2001;276(42):38388-38393. doi:10.1074/jbc.M105395200
67. Toppo S, Vanin S, Bosello V, Tosatto SCE. Evolutionary and structural insights into the multifaceted glutathione peroxidase (Gpx) superfamily. *Antioxid Redox Signal.* 2008;10(9):1501-1513. doi:10.1089/ars.2008.2057
68. Gloire G, Legrand-Poels S, Piette J. NF- $\kappa$ B activation by reactive oxygen species: Fifteen years later. *Biochem Pharmacol.* 2006;72(11):1493-1505. doi:10.1016/j.bcp.2006.04.011
69. Aggarwal BB. Signalling pathways of the TNF superfamily: A double-edged sword. *Nat Rev Immunol.* 2003;3(9):745-756. doi:10.1038/nri1184
70. Holmström KM, Finkel T. Cellular mechanisms and physiological consequences of redox-dependent signalling. *Nat Rev Mol Cell Biol.* 2014;15(6):411-421. doi:10.1038/nrm3801
71. Ray PD, Huang BW, Tsuji Y. Reactive oxygen species (ROS) homeostasis and redox regulation in cellular signaling. *Cell Signal.* 2012;24(5):981-990. doi:10.1016/j.cellsig.2012.01.008
72. Kalia YN, Guy RH. Modeling transdermal drug release. *Adv Drug Deliv Rev.* 2001;48(2-3):159-172. doi:10.1016/S0169-409X(01)00113-2
73. Kammerau B, Klebe U, Zesch A, Schaefer H. Penetration, Permeation and Resorption of 8-Methoxypsoralen. *Arch Dermatol Res.* 1976;255:31-42. doi:10.1007/BF00581675
74. Singh AK. Nanoparticle Pharmacokinetics and Toxicokinetics. In: *Engineered Nanoparticles.* San Diego: Elsevier Inc.; 2016:229-293. doi:10.1016/b978-0-12-801406-6.00006-6
75. Kim B, Cho H-E, Moon SH, et al. Transdermal delivery systems in cosmetics. *Biomed Dermatology.* 2020;4(1):1-12. doi:10.1186/s41702-020-0058-7
76. Moser K, Kriwet K, Naik A, Kalia YN, Guy RH. Passive skin penetration enhancement and its quantification in vitro. *Eur J Pharm Biopharm.* 2001;52(2):103-112. doi:10.1016/S0939-6411(01)00166-7
77. Ellison CA, Tankersley KO, Obringer CM, et al. Partition coefficient and diffusion coefficient determinations of 50 compounds in human intact skin, isolated skin layers and isolated stratum corneum lipids. *Toxicol Vitro.* 2020;69(August):104990. doi:10.1016/j.tiv.2020.104990
78. Barbero A, Frasch F. Transcellular Route of Diffusion through Stratum Corneum: Results from Finite Element Models. *J Pharm Sci.* 2006;10(5):2186-2194. doi:10.1002/jps
79. Williams AC, Cornwell PA, Barry BW. On the non-Gaussian distribution of human skin permeabilities. *Int J Pharm.* 1992;86(1):69-77. doi:10.1016/0378-5173(92)90032-W
80. Bolzinger M-A, Briançon S, Chevalier Y, Puel F. Formulation des systèmes pâteux ou préparations semi-solides. *Tech l'Ingenieur.* 2015;33(PHA2016 V1):1-23.



81. Pavlou P, Siamidi A, Varvaresou A, Vlachou M. Skin care formulations and lipid carriers as skin moisturizing agents. *Cosmetics*. 2021;8(3). doi:10.3390/cosmetics8030089
82. Phalippou J, Kocon L. Élaboration Des Gels Et Des Aérogels. *Tech l'ingénieur*. 2004;J2230(0):1-21.
83. Rowe R, Sheskey P, Quinn M. *Handbook of Pharmaceutical Excipients*. 6th ed. (Pharmaceutical Press and American Pharmacists Association, ed.). Washington: RPS Publishing; 2009.
84. Michniak-Kohn B. Skin: Physiology and Penetration Pathways. In: *Delivery System Handbook for Personal Care and Cosmetic Products-Technology, Applications, and Formulations*. Duxford: Elsevier Ltd.; 2020:701-718.
85. Działo M, Mierziak J, Korzun U, Preisner M, Szopa J, Kulma A. The potential of plant phenolics in prevention and therapy of skin disorders. *Int J Mol Sci*. 2016;17(2):1-41. doi:10.3390/ijms17020160
86. Davinelli S, Nielsen ME, Scapagnini G. Astaxanthin in skin health, repair, and disease: A comprehensive review. *Nutrients*. 2018;10(4):1-12. doi:10.3390/nu10040522
87. Zhang J, Li X, Wei J, et al. Gallic acid inhibits the expression of keratin 16 and keratin 17 through Nrf2 in psoriasis-like skin disease. *Int Immunopharmacol*. 2018;65(September):84-95. doi:10.1016/j.intimp.2018.09.048
88. Thangapazham RL, Sharad S, Maheshwari RK. Skin regenerative potentials of curcumin. *BioFactors*. 2013;39(1):141-149. doi:10.1002/biof.1078
89. Brown MB, Martin GP, Jones SA, Akomeah FK. Dermal and transdermal drug delivery systems: Current and future prospects. *Drug Deliv J Deliv Target Ther Agents*. 2006;13(3):175-187. doi:10.1080/10717540500455975
90. Barbosa NS, Kalaaji AN. CAM use in dermatology. Is there a potential role for honey, green tea, and vitamin C? *Complement Ther Clin Pract*. 2014;20(1):11-15. doi:10.1016/j.ctcp.2013.11.003
91. Kluth D, Banning A, Paur I, Blomhoff R, Brigelius-Flohé R. Modulation of pregnane X receptor-and electrophile responsive element-mediated gene expression by dietary polyphenolic compounds. *Free Radic Biol Med*. 2007;42(3):315-325. doi:10.1016/j.freeradbiomed.2006.09.028
92. Chun KS, Surh YJ. Signal transduction pathways regulating cyclooxygenase-2 expression: Potential molecular targets for chemoprevention. *Biochem Pharmacol*. 2004;68(6):1089-1100. doi:10.1016/j.bcp.2004.05.031
93. Aggarwal BB, Shishodia S. Molecular targets of dietary agents for prevention and therapy of cancer. *Biochem Pharmacol*. 2006;71(10):1397-1421. doi:10.1016/j.bcp.2006.02.009
94. K.P. Prabhakaran Nair. Turmeric: Origin and History. In: *The Agronomy and Economy of Turmeric and Ginger*. San Francisco: Elsevier Inc; 2013:1-5. doi:10.1016/B978-0-12-394801-4.00001-6
95. Carmen S. *Food Colorants-Chemical and Functional Properties*. First. New York: Taylor & Francis Group; 2008.
96. Nair KPP. The Chemistry of Turmeric. In: *The Agronomy and Economy of Turmeric and Ginger*. First.

- San Francisco: Elsevier Inc.; 2013:47-59. doi:10.1016/b978-0-12-394801-4.00004-1
97. Food and Agriculture Organization of the United Nations (FAO). Commission Directive 95/45/EC laying down specific purity criteria concerning colours for use in foodstuffs. *CELEX-EUR Off J L 226*. 2004;3(1):1-45.
  98. Goel A, Kunnumakkara AB, Aggarwal BB. Curcumin as 'Curecumin': From kitchen to clinic. *Biochem Pharmacol*. 2008;75(4):787-809. doi:10.1016/j.bcp.2007.08.016
  99. Priyadarsini KI. The chemistry of curcumin: From extraction to therapeutic agent. *Molecules*. 2014;19(12):20091-20112. doi:10.3390/molecules191220091
  100. Pabon HJJ. A synthesis of curcumin and related compounds. *Recl des Trav Chim des Pays-Bas*. 1964;83(4):379-386. doi:10.1002/recl.19640830407
  101. U.S. Food and Drug Administration (FDA). Summary of Color Additives for Use in the United States in Foods, Drugs, Cosmetics, and Medical Devices. <https://www.fda.gov/industry/color-additive-inventories/summary-color-additives-use-united-states-foods-drugs-cosmetics-and-medical-devices>. Published 2021. Accessed November 8, 2021.
  102. Nair KPP. Turmeric in Ayurveda. In: *The Agronomy and Economy of Turmeric and Ginger*. First. San Francisco: Elsevier Inc.; 2013:217-224. doi:10.1016/b978-0-12-394801-4.00014-4
  103. Dulbecco P, Savarino V. Therapeutic potential of curcumin in digestive diseases. *World J Gastroenterol*. 2013;19(48):9256-9270. doi:10.3748/wjg.v19.i48.9256
  104. Fan Z, Li J, Liu J, Jiao H, Liu B. Anti-Inflammation and Joint Lubrication Dual Effects of a Novel Hyaluronic Acid/Curcumin Nanomicelle Improve the Efficacy of Rheumatoid Arthritis Therapy. *ACS Appl Mater Interfaces*. 2018;10(28):23595-23604. doi:10.1021/acsami.8b06236
  105. Makuch S, Więcek K, Woźniak M. The immunomodulatory and anti-inflammatory effect of curcumin on immune cell populations, cytokines, and in vivo models of rheumatoid arthritis. *Pharmaceuticals*. 2021;14(4). doi:10.3390/ph14040309
  106. Goozee KG, Shah TM, Sohrabi HR, et al. Examining the potential clinical value of curcumin in the prevention and diagnosis of Alzheimer's disease. *Br J Nutr*. 2016;115(3):449-465. doi:10.1017/S0007114515004687
  107. Nair KPP. Nutraceutical Properties of Turmeric. In: *The Agronomy and Economy of Turmeric and Ginger*. First. San Francisco: Elsevier Inc.; 2013:179-204. doi:10.1016/b978-0-12-394801-4.00012-0
  108. Lu Y, Lin M, Zong J, et al. Highly bioavailable curcumin preparation with a co-grinding and solvent-free process. *Food Sci Nutr*. 2020;8(12):6415-6425. doi:10.1002/fsn3.1930
  109. Péret-Almeida L, Cherubino APF, Alves RJ, Dufossé L, Glória MBA. Separation and determination of the physico-chemical characteristics of curcumin, demethoxycurcumin and bisdemethoxycurcumin. *Food Res Int*. 2005;38(8-9):1039-1044. doi:10.1016/j.foodres.2005.02.021
  110. Shen L, Ji HF. The pharmacology of curcumin: Is it the degradation products? *Trends Mol Med*.

- 2012;18(3):138-144. doi:10.1016/j.molmed.2012.01.004
111. Priyadarsini K. The Chemistry of Curcumin: From Extraction to Therapeutic Agent. *Molecules*. 2014;19(12):20091-20112. doi:10.3390/molecules191220091
112. Esatbeyoglu T, Huebbe P, Ernst IMA, Chin D, Wagner AE, Rimbach G. Curcumin-from molecule to biological function. *Angew Chemie - Int Ed*. 2012;51(22):5308-5332. doi:10.1002/anie.201107724
113. Tønnesen HH, Karlsen J. Studies on curcumin and curcuminoids - V. Alkaline Degradation of Curcumin. *Z Lebensm Unters Forsch*. 1985;180(2):402-404. doi:10.1007/BF01042637
114. Rouco H, Diaz-Rodriguez P, Remuñán-López C, Landin M. *Recent Advances in Solid Lipid Nanoparticles Formulation and Clinical Applications*. INC; 2020. doi:10.1016/b978-0-12-816705-2.00007-2
115. Jankun J, Wyganowska-Swiatkowska M, Dettlaff K, et al. Determining whether curcumin degradation/condensation is actually bioactivation (Review). *Int J Mol Med*. 2016;37(5):1151-1158. doi:10.3892/ijmm.2016.2524
116. Price LC, Buescher RW. Decomposition of turmeric curcuminoids as affected by light, solvent and oxygen. *J Food Biochem*. 1996;20(5):125-133. doi:10.1111/j.1745-4514.1996.tb00577.x
117. Chen Z, Xia Y, Liao S, et al. Thermal degradation kinetics study of curcumin with nonlinear methods. *Food Chem*. 2014;155:81-86. doi:10.1016/j.foodchem.2014.01.034
118. Szente L, Mikuni K, Hashimoto H, Szejtli J. Stabilization and solubilization of lipophilic natural colorants with cyclodextrins. *J Incl Phenom Mol Recognit Chem*. 1998;32(1):81-89. doi:10.1023/A:1007970501916
119. Tønnesen HH, Másson M, Loftsson T. Studies of curcumin and curcuminoids. XXVII. Cyclodextrin complexation: Solubility, chemical and photochemical stability. *Int J Pharm*. 2002;244(1-2):127-135. doi:10.1016/S0378-5173(02)00323-X
120. Barzegar A. The role of electron-transfer and H-atom donation on the superb antioxidant activity and free radical reaction of curcumin. *Food Chem*. 2012. doi:10.1016/j.foodchem.2012.05.070
121. Apak R, Gorinstein S, Bohm V, Karen M S, Ozyurek, Mustafa Guclu K. Methods of measurement and evaluation of natural antioxidant capacity/activity (IUPAC Technical Report). *Pure Appl Chem*. 2010;85(5):957-998. doi:10.1109/ICHR.2010.5686322
122. Flory S, Frank J. Uptake and time-dependent subcellular localization of native and micellar curcumin in intestinal cells. *Biofactors*. 2022;(December 2021):1-11. doi:10.1002/biof.1828
123. Singh R, Kristensen S, Berg K. The influence of Pluronics® on dark cytotoxicity, photocytotoxicity, localization and uptake of curcumin in cancer cells: studies of curcumin and curcuminoids XLIX. *Photochem Photobiol Sci*. 2013;12:559-575. doi:10.1039/c2pp25249j
124. Kunwar A, Barik A, Mishra B, Rathinasamy K, Pandey R, Priyadarsini KI. Quantitative cellular uptake, localization and cytotoxicity of curcumin in normal and tumor cells. *Biochim Biophys Acta*.

- 2008;1780(4):673-679. doi:10.1016/j.bbagen.2007.11.016
125. Sala de Oyanguren F, Rainey N, Moustapha A, et al. Highlighting Curcumin-Induced Crosstalk between Autophagy and Apoptosis as Supported by Its Specific Subcellular Localization. *Cells*. 2020;9(361):1-24.
  126. Moustapha A, Pérétout P, Rainey N, et al. Curcumin induces crosstalk between autophagy and apoptosis mediated by calcium release from the endoplasmic reticulum lysosomal destabilization and mitochondrial events. *Cell Death Discov*. 2015;1(15017):1-14. doi:10.1038/cddiscovery.2015.17
  127. Ghosh M, Ryan R. Curcumin homing to the nucleus: mechanism for initiation of an apoptotic program. *J Nutr Biochem*. 2014;25(11):1117-1123. doi:10.1016/j.jnutbio.2014.06.009. Curcumin
  128. Ghosh M, Ryan R. ApoE enhances nanodisk-mediated curcumin delivery to glioblastoma multiforme cells. *Nanomedicine*. 2014;9(6):763-771. doi:10.2217/nnm.13.35. ApoE
  129. Zeng Z, Shen ZL, Zhai S, et al. Transport of curcumin derivatives in Caco-2 cell monolayers. *Eur J Pharm Biopharm*. 2017;117:123-131. doi:10.1016/j.ejpb.2017.04.004
  130. Yu H, Huang Q. Investigation of the absorption mechanism of solubilized curcumin using caco-2 cell monolayers. *J Agric Food Chem*. 2011;59(17):9120-9126. doi:10.1021/jf201451m
  131. Zhang X, Chen Q, Wang Y, Peng W, Cai H. Effects of curcumin on ion channels and transporters. *Front Physiol*. 2014;5(March):1-6. doi:10.3389/fphys.2014.00094
  132. Hillaireau H, Couvreur P. Nanocarriers' entry into the cell: Relevance to drug delivery. *Cell Mol Life Sci*. 2009;66(17):2873-2896. doi:10.1007/s00018-009-0053-z
  133. Männle R, Frank J. The Inhibitory Activity of Curcumin on P-Glycoprotein and Its Uptake by and Efflux from LS180 Cells Is Not Affected by Its Galenic Formulation. *Antioxidants*. 2021;10(1826):1-13.
  134. Meech R, MacKenzie PI. Determinants of UDP glucuronosyltransferase membrane association and residency in the endoplasmic reticulum. *Arch Biochem Biophys*. 1998;356(1):77-85. doi:10.1006/abbi.1998.0750
  135. Hashimoto N, Nakamichi N, Yamazaki E, et al. P-Glycoprotein in skin contributes to transdermal absorption of topical corticosteroids. *Int J Pharm*. 2017;521(1-2):365-373. doi:10.1016/j.ijpharm.2017.02.064
  136. Sleeman MA, Watson JD, Murison JG. Neonatal Murine Epidermal Cells Express a Functional Multidrug-Resistant Pump. *J Invest Dermatol*. 2000;115(1):19-23. doi:10.1046/j.1523-1747.2000.00033.x
  137. Baron JM, Ho D, Schiffer R, et al. Expression of Multiple Cytochrome P450 Enzymes and Multidrug Resistance-Associated Transport Proteins in Human Skin Keratinocytes. *J Invest Dermatol*. 2001;116(4):541-548. doi:10.1046/j.1523-1747.2001.01298.x
  138. Triel C, Vestergaard ME, Bolund L, Jensen TG, Jensen UB. Side population cells in human and mouse epidermis lack stem cell characteristics. *Exp Cell Res*. 2004;295:79-90. doi:10.1016/j.yexcr.2003.11.032

139. Mann GE. Nrf2-mediated redox signalling in vascular health and disease. *Free Radic Biol Med.* 2014;75:S1. doi:10.1016/j.freeradbiomed.2014.10.595
140. Liu T, Zhang L, Joo D, Sun S. NF- $\kappa$ B signaling in inflammation. *Signal Transduct Target Ther.* 2017;2(e17023):1-9. doi:10.1038/sigtrans.2017.23
141. Mohanty C, Sahoo SK. Curcumin and its topical formulations for wound healing applications. *Drug Discov Today.* 2017;22(10):1582-1592. doi:10.1016/j.drudis.2017.07.001
142. Hussain Z, Thu HE, Ng SF, Khan S, Katas H. Nanoencapsulation, an efficient and promising approach to maximize wound healing efficacy of curcumin: A review of new trends and state-of-the-art. *Colloids Surfaces B Biointerfaces.* 2017;150:223-241. doi:10.1016/j.colsurfb.2016.11.036
143. Shah BR, Zhang C, Li Y, Li B. Bioaccessibility and antioxidant activity of curcumin after encapsulated by nano and Pickering emulsion based on chitosan-tripolyphosphate nanoparticles. *Food Res Int.* 2016;89:399-407. doi:10.1016/j.foodres.2016.08.022
144. Phan TT, Sun L, Bay BH, Chan SY, Lee ST. Dietary compounds inhibit proliferation and contraction of keloid and hypertrophic scar-derived fibroblasts in vitro: Therapeutic implication for excessive scarring. *J Trauma Inj Infection Crit Care.* 2003;54(6):1212-1224. doi:10.1097/01.TA.0000030630.72836.32
145. Hsu Y-C, Chen M-J, Yu Y-M, Ko S-Y, Chang C-C. Suppression of TGF- $\beta$ 1/SMAD pathway and extracellular matrix production in primary keloid fibroblasts by curcuminoids: its potential therapeutic use in the chemoprevention of keloid. *Arch Dermatol Res.* 2010;302(396):717-724. doi:10.1007/s00403-010-1075-y
146. Gopinath D, Ahmed MR, Gomathi K, Chitra K, Sehgal PK, Jayakumar R. Dermal wound healing processes with curcumin incorporated collagen films. *Biomaterials.* 2004;25:1911-1917. doi:10.1016/S0142-9612(03)00625-2
147. Orsu P, Haider HY, Koyyada A. Bioengineering for curcumin loaded carboxymethyl guar gum / reduced graphene oxide nanocomposites for chronic wound healing applications. *Int J Pharm.* 2021;606(May):120928. doi:10.1016/j.ijpharm.2021.120928
148. Yang BY, Hu CH, Huang WC, Ho CY, Yao CH, Huang CH. Effects of bilayer nanofibrous scaffolds containing curcumin/lithospermi radix extract on wound healing in streptozotocin-induced diabetic rats. *Polymers (Basel).* 2019;11(11):1-17. doi:10.3390/polym11111745
149. Lee H-J, Jeong M, Na Y-G, Kim S-J, Lee H-K, Cho C-W. An EGF-and Curcumin-Co-Encapsulated Nanostructured Lipid Carrier Accelerates Chronic-Wound Healing in Diabetic Rats. *Molecules.* 2020;25:1-14. doi:10.3390/molecules25204610
150. Bahraini P, Rajabi M, Mansouri P, Sarafian G, Chalangari R, Azizian Z. Turmeric tonic as a treatment in scalp psoriasis: A randomized placebo-control clinical trial. *J Cosmet Dermatol.* 2018;17(3):461-466. doi:10.1111/jocd.12513

151. Heng MCY, Song MK, Harker J, Heng MK. Drug-induced suppression of phosphorylase kinase activity correlates with resolution of psoriasis as assessed by clinical, histological and immunohistochemical parameters. *Br J Dermatol*. 2000;143(5):937-949. doi:10.1046/j.1365-2133.2000.03767.x
152. Sun J, Zhao Y, Hu J. Curcumin Inhibits Imiquimod-Induced Psoriasis-Like Inflammation by Inhibiting IL-1beta and IL-6 Production in Mice. *PLoS One*. 2013;8(6). doi:10.1371/journal.pone.0067078
153. Algahtani MS, Ahmad MZ, Nourain IH, Ahmad J. Co-Delivery of Imiquimod and Curcumin by Nanoemugel for Improved Topical Delivery and Reduced Psoriasis-Like Skin Lesions. *Biomolecules*. 2020;10(968):1-18.
154. Terzopoulou Z, Michopoulou A, Palamidi A, Koliakou E, Bikiaris D. Preparation and evaluation of collagen-based patches as curcumin carriers. *Polymers (Basel)*. 2020;12(10):1-18. doi:10.3390/polym12102393
155. Jain A, Doppalapudi S, Domb AJ, Khan W. Tacrolimus and curcumin co-loaded liposphere gel: Synergistic combination towards management of psoriasis. *J Control Release*. 2016;243:132-145. doi:10.1016/j.jconrel.2016.10.004
156. Algahtani MS, Ahmad MZ, Ahmad J. Nanoemulsion loaded polymeric hydrogel for topical delivery of curcumin in psoriasis. *J Drug Deliv Sci Technol*. 2020;59(February):101847. doi:10.1016/j.jddst.2020.101847
157. Filippone A, Consoli GML, Granata G, et al. Topical delivery of curcumin by choline-calix[4]arene-based nanohydrogel improves its therapeutic effect on a psoriasis mouse model. *Int J Mol Sci*. 2020;21(14):1-15. doi:10.3390/ijms21145053
158. Mao KL, Fan ZL, Yuan JD, et al. Skin-penetrating polymeric nanoparticles incorporated in silk fibroin hydrogel for topical delivery of curcumin to improve its therapeutic effect on psoriasis mouse model. *Colloids Surfaces B Biointerfaces*. 2017;160:704-714. doi:10.1016/j.colsurfb.2017.10.029
159. Sun L, Liu Z, Wang L, et al. Enhanced topical penetration, system exposure and anti-psoriasis activity of two particle-sized, curcumin-loaded PLGA nanoparticles in hydrogel. *J Control Release*. 2017;254:44-54. doi:10.1016/j.jconrel.2017.03.385
160. Zhou F, Song Z, Wen Y, Xu H, Zhu L, Feng R. Transdermal delivery of curcumin-loaded supramolecular hydrogels for dermatitis treatment. *J Mater Sci Mater Med*. 2019;30(1). doi:10.1007/s10856-018-6215-5
161. Shrotriya S, Ranpise N, Satpute P, Vidhate B. Skin targeting of curcumin solid lipid nanoparticles-encapsulated topical gel for the treatment of pigmentation and irritant contact dermatitis. *Artif Cells, Nanomedicine Biotechnol*. 2018;46(7):1471-1482. doi:10.1080/21691401.2017.1373659
162. Sakai H, Sato K, Sato F, et al. Curcumin inhibits epigen and amphiregulin upregulated by 2,4,6-trinitrochlorobenzene associated with attenuation of skin swelling. *Inflamm Res*. 2017;66(8):663-678. doi:10.1007/s00011-017-1048-0

163. Ishizaki C, Oguro T, Yoshida T, Wen C, Sueki H, Iijima M. Enhancing Effect of Ultraviolet A on Ornithine Decarboxylase Induction and Dermatitis Evoked by 12-o-Tetradecanoylphorbol-13-Acetate and Its Inhibition by Curcumin in Mouse Skin. *Dermatology*. 1996;193:311-317.
164. Brannon-Peppas L. Recent advances on the use of biodegradable microparticles and nanoparticles in controlled drug delivery. *Int J Pharm*. 1995;116(1):1-9. doi:10.1016/0378-5173(94)00324-X
165. Ghezzi M, Pescina S, Padula C, et al. Polymeric micelles in drug delivery: An insight of the techniques for their characterization and assessment in biorelevant conditions. *J Control Release*. 2021;332(February):312-336. doi:10.1016/j.jconrel.2021.02.031
166. Astray G, Gonzalez-Barreiro C, Mejuto JC, Rial-Otero R, Simal-Gándara J. A review on the use of cyclodextrins in foods. *Food Hydrocoll*. 2009;23(7):1631-1640. doi:10.1016/j.foodhyd.2009.01.001
167. The European Joint Commission. Commission Recommendation of 18 October 2011 on the definition of nanomaterial. *Off J Eur Union*. 2011;275(20):38-40. doi:10.7748/ns.24.26.6.s4
168. Pita R, Ehmann F, Papaluca M. Nanomedicines in the EU—Regulatory Overview. *AAPS J*. 2016;18(6):1576-1582. doi:10.1208/s12248-016-9967-1
169. Halamoda-Kenzaoui B, Box H, van Elk M, et al. *Anticipation of Regulatory Needs for Nanotechnology-Enabled Health Products, EUR 29919 EN*. Luxembourg; 2019. doi:10.2760/596822
170. U.S. Food and Drug Administration (FDA). *Guidance for Industry Considering Whether an FDA-Regulated Product Involves the Application of Nanotechnology*. Vol 30.; 2011. doi:10.1089/blr.2011.9814
171. Wennerström H, Balogh J, Olsson U. Interfacial tensions in microemulsions. *Colloids Surfaces A Physicochem Eng Asp*. 2006;291:69-77. doi:10.1016/j.colsurfa.2006.09.027
172. McClements DJ. Nanoemulsions versus microemulsions: Terminology, differences, and similarities. *Soft Matter*. 2012;8(6):1719-1729. doi:10.1039/c2sm06903b
173. Bangham AD. Liposomes: the Babraham connection. *Chem Phys Lipids*. 1993;64(1-3):275-285. doi:10.1016/0009-3084(93)90071-A
174. Bangham AD, Standish MM, Watkins JC. Diffusion of univalent ions across the lamellae of swollen phospholipids. *J Mol Biol*. 1965;13(1):238-252. doi:10.1016/S0022-2836(65)80093-6
175. Elsayed MMA, Abdallah OY, Naggar VF, Khalafallah NM. Deformable liposomes and ethosomes: Mechanism of enhanced skin delivery. *Int J Pharm*. 2006;322(1-2):60-66. doi:10.1016/j.ijpharm.2006.05.027
176. Mehnert W, Mader K. Solid lipid nanoparticles-Production, characterization and applications. *Adv Drug Deliv Rev*. 2001;47:165-196. doi:10.7551/mitpress/4945.003.0031
177. Müller RH, Radtke M, Wissing SA. Solid lipid nanoparticles (SLN) and nanostructured lipid carriers (NLC) in cosmetic and dermatological preparations. *Adv Drug Deliv Rev*. 2002;54(Suppl. 1):S131-S155. doi:10.1016/S0169-409X(02)00118-7

178. Jennings V, Thünemann AF, Gohla SH. Characterisation of a novel solid lipid nanoparticle carrier system based on binary mixtures of liquid and solid lipids. *Int J Pharm.* 2000;199(2):167-177. doi:10.1016/S0378-5173(00)00378-1
179. Wolf M, Klang V, Stojic T, Fuchs C, Wolzt M, Valenta C. NLC versus nanoemulsions: Effect on physiological skin parameters during regular in vivo application and impact on drug penetration. *Int J Pharm.* 2018;549(1-2):343-351. doi:10.1016/j.ijpharm.2018.08.007
180. Elgart A, Cherniakov I, Aldouby Y, Domb AJ, Hoffman A. Lipospheres and pro-nano lipospheres for delivery of poorly water soluble compounds. *Chem Phys Lipids.* 2012;165(4):438-453. doi:10.1016/j.chemphyslip.2012.01.007
181. Irby D, Du C, Li F. Lipid-Drug Conjugate for Enhancing Drug Delivery. *Mol Pharm.* 2017;14(5):1325-1338. doi:10.1021/acs.molpharmaceut.6b01027
182. Müller RH, Petersen RD, Hommoss A, Pardeike J. Nanostructured lipid carriers (NLC) in cosmetic dermal products. *Adv Drug Deliv Rev.* 2007;59(6):522-530. doi:10.1016/j.addr.2007.04.012
183. Dolatabadi S, Karimi M, Nasirizadeh S, Hatamipour M, Golmohammadzadeh S, Jaafari MR. Preparation, characterization and in vivo pharmacokinetic evaluation of curcuminoids-loaded solid lipid nanoparticles (SLNs) and nanostructured lipid carriers (NLCs). *J Drug Deliv Sci Technol.* 2021;62(January):102352. doi:10.1016/j.jddst.2021.102352
184. Neves AR, van der Putten L, Queiroz JF, Pinheiro M, Reis S. Transferrin-functionalized lipid nanoparticles for curcumin brain delivery. *J Biotechnol.* 2021;331(January 2020):108-117. doi:10.1016/j.jbiotec.2021.03.010
185. Souto EB, Müller RH. The use of SLN® and NLC® as topical particulate carriers for imidazole antifungal agents. *Pharmazie.* 2006;61(5):431-437.
186. Tamjidi F, Shahedi M, Varshosaz J, Nasirpour A. Nanostructured lipid carriers (NLC): A potential delivery system for bioactive food molecules. *Innov Food Sci Emerg Technol.* 2013;19:29-43. doi:10.1016/j.ifset.2013.03.002
187. Borges A, de Freitas V, Mateus N, Fernandes I, Oliveira J. Solid lipid nanoparticles as carriers of natural phenolic compounds. *Antioxidants.* 2020;9(10):1-24. doi:10.3390/antiox9100998
188. Pardeike J, Hommoss A, Müller RH. Lipid nanoparticles (SLN, NLC) in cosmetic and pharmaceutical dermal products. *Int J Pharm.* 2009;366(1-2):170-184. doi:10.1016/j.ijpharm.2008.10.003
189. Müller RH, Alexiev U, Sinambela P, Keck CM. Nanostructured lipid carriers (NLC): The second generation of solid lipid nanoparticles. In: *Percutaneous Penetration Enhancers Chemical Methods in Penetration Enhancement: Nanocarriers.* Springer Berlin Heidelberg; 2016:161-185. doi:10.1007/978-3-662-47862-2\_11
190. Schubert MA, Müller-Goymann CC. Characterisation of surface-modified solid lipid nanoparticles (SLN): Influence of lecithin and nonionic emulsifier. *Eur J Pharm Biopharm.* 2005;61(1-2):77-86.



- doi:10.1016/j.ejpb.2005.03.006
191. Ganesan P, Narayanasamy D. Lipid nanoparticles: Different preparation techniques, characterization, hurdles, and strategies for the production of solid lipid nanoparticles and nanostructured lipid carriers for oral drug delivery. *Sustain Chem Pharm.* 2017;6(August):37-56. doi:10.1016/j.scp.2017.07.002
  192. Poux M, Canselier J-P. Procédés d'émulsification-Techniques et appareillage. *Tech l'Ingénieur.* 2004;33(J2153 V1):2-14.
  193. Souto EB, Almeida AJ, Müller RH. Lipid nanoparticles (SLN®, NLC®) for cutaneous drug delivery: Structure, protection and skin effects. *J Biomed Nanotechnol.* 2007;3(4):317-331. doi:10.1166/jbn.2007.049
  194. Håkansson A. Rotor-stator mixers: From batch to continuous mode of operation-A review. *Processes.* 2018;6(4):1-17. doi:10.3390/pr6040032
  195. Müller RH, Mäder K, Gohla S. Solid lipid nanoparticles (SLN) for controlled drug delivery - A review of the state of the art. *Eur J Pharm Biopharm.* 2000;50(1):161-177. doi:10.1016/S0939-6411(00)00087-4
  196. Pedersen N, Hansen S, Heydenreich A V., Kristensen HG, Poulsen HS. Solid lipid nanoparticles can effectively bind DNA, streptavidin and biotinylated ligands. *Eur J Pharm Biopharm.* 2006;62(2):155-162. doi:10.1016/j.ejpb.2005.09.003
  197. Battaglia L, Trotta M, Gallarate M, Carlotti ME, Zara GP, Bargoni A. Solid lipid nanoparticles formed by solvent-in-water emulsion-diffusion technique: Development and influence on insulin stability. *J Microencapsul.* 2007;24(7):672-684. doi:10.1080/02652040701532981
  198. Shah R, Eldridge D, Palombo E, Harding I. Production Techniques. In: Shah R, Eldridge D, Palombo E, Harding I, eds. *Lipid Nanoparticles: Production, Characterization and Stability.* Zürich: Springer; 2015:23-43. doi:10.1007/978-3-319-10711-0\_3
  199. Gasco MR. Method for producing solid lipid microspheres having a narrow size distribution. 1993;(19).
  200. Svilenov H, Tzachev C. Solid Lipid Nanoparticles: a Promising Drug Delivery System. *Nanomedicine.* 2014;12:187-237.
  201. U.S. Food and Drug Administration (FDA). Inactive Ingredient Search for Approved Drug Products. <https://www.accessdata.fda.gov/scripts/cder/iig/index.cfm>. Published 2021. Accessed January 8, 2022.
  202. U.S. Food and Drug Administration (FDA). Generally Recognized as Safe (GRAS). <https://www.fda.gov/food/food-ingredients-packaging/generally-recognized-safe-gras>. Published 2019. Accessed January 8, 2022.
  203. U.S. Food and Drug Administration (FDA). GRAS Substances (SCOGS) Database.

<https://www.fda.gov/food/generally-recognized-safe-gras/gras-substances-scogs-database>.

Published 2018. Accessed January 8, 2022.

204. Fang C-L, Al-Suwayeh S, Fang J-Y. Nanostructured Lipid Carriers (NLCs) for Drug Delivery and Targeting. *Recent Pat Nanotechnol.* 2013;7(1):41-55. doi:10.2174/18722105130105
205. Mishra D, Dhote V, Mishra P. Solid Lipid Nanoparticles: A Promising Colloidal Carrier. In: Chourasia MK, Chaurasia M, Jain NK, eds. *Novel Carriers for Drug Delivery*. Hyderabad: PharmaMed Press; 2015:278-301. doi:10.1007/978-3-030-34544-0\_13
206. Kang NW, Kim MH, Sohn SY, et al. Curcumin-loaded lipid-hybridized cellulose nanofiber film ameliorates imiquimod-induced psoriasis-like dermatitis in mice. *Biomaterials.* 2018;182(May):245-258. doi:10.1016/j.biomaterials.2018.08.030
207. Rapalli VK, Kaul V, Waghule T, et al. Curcumin loaded nanostructured lipid carriers for enhanced skin retained topical delivery: optimization, scale-up, in-vitro characterization and assessment of ex-vivo skin deposition. *Eur J Pharm Sci.* 2020;152. doi:10.1016/j.ejps.2020.105438
208. Espinosa-Olivares MA, Delgado-Buenrostro NL, Chirino YI, Trejo-Márquez MA, Pascual-Bustamante S, Ganem-Rondero A. Nanostructured lipid carriers loaded with curcuminoids: Physicochemical characterization, in vitro release, ex vivo skin penetration, stability and antioxidant activity. *Eur J Pharm Sci.* 2020;155(1-12):105533. doi:10.1016/j.ejps.2020.105533
209. Liakopoulou A, Mourelatou E, Hatziantoniou S. Exploitation of traditional healing properties, using the nanotechnology's advantages: The case of curcumin. *Toxicol Reports.* 2021;8:1143-1155. doi:10.1016/j.toxrep.2021.05.012
210. Chen P, Zhang H, Cheng S, Zhai G, Shen C. Development of curcumin loaded nanostructured lipid carrier based thermosensitive in situ gel for dermal delivery. *Colloids Surfaces A Physicochem Eng Asp.* 2016;506:356-362. doi:10.1016/j.colsurfa.2016.06.054
211. Riaz A, Ahmed N, Khan MI, Haq I ul, Rehman A ur, Khan GM. Formulation of topical NLCs to target macrophages for cutaneous leishmaniasis. *J Drug Deliv Sci Technol.* 2019;54(August):101232. doi:10.1016/j.jddst.2019.101232
212. Kesharwani P, Jain A, Srivastava AK, Keshari MK. Systematic development and characterization of curcumin-loaded nanogel for topical application. *Drug Dev Ind Pharm.* 2020;9045:1443-1457. doi:10.1080/03639045.2020.1793998
213. Iriverenti P, Gupta NV. Topical Delivery of Curcumin and Caffeine Mixture-Loaded Nanostructured Lipid Carriers for Effective Treatment of Psoriasis. *Pharmacogn Mag.* 2020;16:S206-17. doi:10.4103/pm.pm
214. Garcês A, Amaral MH, Sousa Lobo JM, Silva AC. Formulations based on solid lipid nanoparticles (SLN) and nanostructured lipid carriers (NLC) for cutaneous use: A review. *Eur J Pharm Sci.* 2017;112:159-167. doi:10.1016/j.ejps.2017.11.023
215. Almdal K, Dyre J, Hvidt S, Kramer O. Towards a phenomenological definition of the term 'gel'. *Polym*

- Gels Networks*. 1993;1(1):5-17. doi:10.1016/0966-7822(93)90020-I
216. Djabourov M, Leblond J, Papon P. Gelation of aqueous gelatin solutions. I. Structural investigation. *J Phys*. 1988;49:319-332.
217. Papon P, Leblond J, Meijer PHE. *The Physics of Phase Transitions: Concepts and Applications*. Second. Paris: Springer; 2006. doi:10.1007/3-540-33390-8
218. Hamidi M, Azadi A, Rafiei P. Hydrogel nanoparticles in drug delivery. *Adv Drug Deliv Rev*. 2008;60(15):1638-1649. doi:10.1016/j.addr.2008.08.002
219. Buwalda SJ, Boere KWM, Dijkstra PJ, Feijen J, Vermonden T, Hennink WE. Hydrogels in a historical perspective: From simple networks to smart materials. *J Control Release*. 2014;190:254-273. doi:10.1016/j.jconrel.2014.03.052
220. Wichterle O, Lim D. Hydrophilic Gels for Biological Use. *Nature*. 1960;185(4706):63-64. doi:10.1038/185063a0
221. Low ZWK, Li Z, Owh C, et al. Recent innovations in artificial skin. *Biomater Sci*. 2020;8(3):776-797. doi:10.1039/c9bm01445d
222. Fu R, Tu L, Zhou Y, et al. A Tough and Self-Powered Hydrogel for Artificial Skin. *Chem Mater*. 2019;31(23):9850-9860. doi:10.1021/acs.chemmater.9b04041
223. Sikdar P, Uddin MM, Dip TM, et al. Recent advances in the synthesis of smart hydrogels. *Mater Adv*. 2021;2(14):4532-4573. doi:10.1039/d1ma00193k
224. Ferreira NN, Ferreira LMB, Cardoso VMO, Boni FI, Souza ALR, Gremião MPD. Recent advances in smart hydrogels for biomedical applications: From self-assembly to functional approaches. *Eur Polym J*. 2018;99:117-133. doi:10.1016/j.eurpolymj.2017.12.004
225. Lim HL, Hwang Y, Kar M, Varghese S. Smart hydrogels as functional biomimetic systems. *Biomater Sci*. 2014;2(5):603-618. doi:10.1039/c3bm60288e
226. Winter GD. Formation of the scab and the rate of epithelization of superficial wounds in skin of the young domestic pig. *Nature*. 1962;4812:293-294. doi:https://doi.org/10.1038/1961048b0
227. Olmos D, González-benito J. Polymeric materials with antibacterial activity: A review. *Polymers (Basel)*. 2021;13(4):1-30. doi:10.3390/polym13040613
228. Harrison IP, Spada F. Hydrogels for atopic dermatitis and wound management: A superior drug delivery vehicle. *Pharmaceutics*. 2018;10(2). doi:10.3390/pharmaceutics10020071
229. Esposito CL, Kirilov P, Roullin VG. Organogels, promising drug delivery systems: an update of state-of-the-art and recent applications. *J Control Release*. 2018;271(October 2017):1-20. doi:10.1016/j.jconrel.2017.12.019
230. Wittemberg D, Blasco L. Gels. In: Pensé-Lhéritier A-M, Masson C, Roulleaux F, eds. *Conception Des Produits Cosmétiques*. Chartres: Cosmetic Valley Editions; 2018:103-139.
231. INCI Beauty. Ingredients used in cosmetics. <https://incibeauty.com/en/ingredients>. Published 2021.

- Accessed November 19, 2021.
232. Fiume M, Bergfeld W, Belsito D, et al. *Amended Safety Assessment of Acrylates Copolymers as Used in Cosmetics*. Washin; 2018.
  233. Singh VK, Anis A, Banerjee I, Pramanik K, Bhattacharya MK, Pal K. Preparation and characterization of novel carbopol based bigels for topical delivery of metronidazole for the treatment of bacterial vaginosis. *Mater Sci Eng C*. 2014;44:151-158. doi:10.1016/j.msec.2014.08.026
  234. Tang C, Yin L, Yu J, Yin C, Pei Y. Swelling Behaviour and Biocompatibility of Carbopol-Containing Superporous Hydrogel Composites. *J Appl Polym Sci*. 2006;104(5):2785-2791. doi:10.1002/app
  235. The Lubrizol Corporation. Carbopol® Polymer Products. <https://www.lubrizol.com/Health/Pharmaceuticals/Excipients/Carbopol-Polymer-Products>. Published 2021. Accessed November 18, 2021.
  236. Lubrizol Advanced Materials. *Compendial Specifications Applicable to Pharmaceutical Polymers;* 2013.
  237. Jaworski Z, Szychaj T, Story A, Story G. Carbomer microgels as model yield-stress fluids. *Rev Chem Eng*. 2021. doi:10.1515/revce-2020-0016
  238. Davies GA, Stokes JR. Thin film and high shear rheology of multiphase complex fluids. *J Nonnewton Fluid Mech*. 2008;148(1-3):73-87. doi:10.1016/j.jnnfm.2007.04.013
  239. Lefrançois P, Ibarboure E, Payré B, Gontier E, Le Meins JF, Schatz C. Insights into Carbopol gel formulations: Microscopy analysis of the microstructure and the influence of polyol additives. *J Appl Polym Sci*. 2015;132(46):1-7. doi:10.1002/app.42761
  240. Dobrynin A V. Theory and simulations of charged polymers: From solution properties to polymeric nanomaterials. *Curr Opin Colloid Interface Sci*. 2008;13(6):376-388. doi:10.1016/j.cocis.2008.03.006
  241. Lubrizol. Neutralization Procedures. *Pharm Bull*. 2011:1-5.
  242. Lubrizol. Flow and Suspension Properties. *Pharm Bull*. 2008;7:1-14.
  243. Oh KT, Bronich TK, Kabanov A V. Micellar formulations for drug delivery based on mixtures of hydrophobic and hydrophilic PluronicR block copolymers. doi:10.1016/j.jconrel.2003.10.018
  244. Bochot A, Fattal E, Gulik A, Couarraze G, Couvreur P. Liposomes dispersed within a thermosensitive gel of block polymers. *Pharm Res*. 1998;15(9):1364-1369.
  245. Lubrizol Advanced Materials. *Product Specification-Carbopol 980 NF Polymer*. Ohio; 2019.
  246. Lubrizol Advanced Materials. Carbopol 980 Polymer. Lubrizol - Beauty & Personal Care. <https://www.lubrizol.com/Personal-Care/Products/Product-Finder/Products-Data/Carbopol-980-polymer#>. Published 2021. Accessed April 14, 2022.
  247. Curtis G, Netherton E. Cutaneous hypersensitivity to triethanolamine. *Arch Derm Syphilol*. 1940;41(4):729-731. doi:10.1136/bmj.2.4308.148-b
  248. Toxicology J of the AC of. *Final Report on the Safety Assessment of Triethanolamine, Diethanolamine*

- and Monoethanolamine*. Vol 2.; 1983. doi:10.1080/10915810601163962
249. Rodriguez-Ruiz V, Salatti-Dorado J, Barzegari A, et al. Astaxanthin-Loaded Nanostructured Lipid Carriers for Preservation of Antioxidant Activity. *Molecules*. 2018;23(10):2601. doi:10.3390/molecules23102601
  250. Perkin-Elmer. Differential Scanning Calorimetry (DSC) A Beginner's Guide. [https://resources.perkinelmer.com/corporate/cmsresources/images/46-74542gde\\_dscbeginnersguide.pdf](https://resources.perkinelmer.com/corporate/cmsresources/images/46-74542gde_dscbeginnersguide.pdf). Published 2010.
  251. Montenegro L, Parenti C, Turnaturi R, Pasquinucci L. Resveratrol-Loaded Lipid Nanocarriers: Correlation between In Vitro Occlusion Factor and In Vivo Skin Hydrating Effect. *Pharmaceutics*. 2017;9(4):58. doi:10.3390/pharmaceutics9040058
  252. Radomska-Soukharev A. Stability of lipid excipients in solid lipid nanoparticles. *Adv Drug Deliv Rev*. 2007;59:411-418. doi:10.1016/j.addr.2007.04.004
  253. Bio-Rad Laboratories. Bio-Gel® P- Polyacrylamide Gel Instruction Manual. <https://www.bio-rad.com/webroot/web/pdf/lsr/literature/LIT-174B.pdf>. Published 2000. Accessed December 12, 2021.
  254. Ltd. MI. Zetasizer Nano Series User Manual: Issue 2.1. 2004;(1).
  255. Bhattacharjee S. DLS and zeta potential-What they are and what they are not? *J Control Release*. 2016;235:337-351. doi:10.1016/j.jconrel.2016.06.017
  256. Sonia TA, Sharma CP. *Experimental Techniques Involved in the Development of Oral Insulin Carriers*; 2014. doi:10.1533/9781908818683.169
  257. Re R, Pellegrini N, Proteggente A, Pannala A, Yang M, Rice-Evans C. Antioxidant activity applying an improved ABTS radical cation decolorization assay. *Free Radic Biol Med*. 1999;26(9-10):1231-1237. doi:10.1016/S0891-5849(98)00315-3
  258. Lien EJ, Ren S, Bui HH, Wang R. Quantitative structure-activity relationship analysis of phenolic antioxidants. *Free Radic Biol Med*. 1999;26(3-4):285-294. doi:10.1016/S0891-5849(98)00190-7
  259. Marin M, René F. Lyophilisation. *Tech l'Ingenieur*. 2000;33(F3240 V1):1-9.
  260. Hedoux A. Lyophilisation de produits pharmaceutiques et biopharmaceutiques. *Tech l'Ingénieur*. 2013;33(PHA2026 V1):1-14. doi:10.51257/a-v1-pha2026
  261. OECD. Test No. 428: Skin Absorption: In Vitro Method. *OECD Guidel Test Chem Sect 4*. 2004;OECD Publi. doi:10.1787/9789264071087-en
  262. Uchida T, Kadhum WR, Kanai S, Todo H, Oshizaka T, Sugibayashi K. Prediction of skin permeation by chemical compounds using the artificial membrane, Strat-M™. *Eur J Pharm Sci*. 2015;67:113-118. doi:10.1016/j.ejps.2014.11.002
  263. Haq A, Goodyear B, Ameen D, Joshi V, Michniak-Kohn B. Strat-M® synthetic membrane: Permeability comparison to human cadaver skin. *Int J Pharm*. 2018;547(1-2):432-437.

- doi:10.1016/j.ijpharm.2018.06.012
264. Ponmozhi J, Dhinakaran S, Varga-medveczky Z, et al. Development of skin-on-a-chip platforms for different utilizations: Factors to be considered. *Micromachines*. 2021;12(3):1-25. doi:10.3390/mi12030294
265. Di Prima G, Angellotti G, Scarpaci AG, et al. Improvement of resveratrol permeation through sublingual mucosa: Chemical permeation enhancers versus spray drying technique to obtain fast-disintegrating sublingual mini-tablets. *Pharmaceutics*. 2021;13(9). doi:10.3390/pharmaceutics13091370
266. Wojcik M, Kazimierczak P, Benko A, Palka K, Vivcharenko V, Przekora A. Superabsorbent curdlan-based foam dressings with typical hydrocolloids properties for highly exuding wound management. *Mater Sci Eng C*. 2021;124(March):112068. doi:10.1016/j.msec.2021.112068
267. Xiong ZM, Mao X, Trappio M, Arya C, Kordi J el, Cao K. Ultraviolet radiation protection potentials of Methylene Blue for human skin and coral reef health. *Sci Rep*. 2021;11(1):1-9. doi:10.1038/s41598-021-89970-2
268. Soonthornchai W, Tangtanatakul P, Meesilpavikkai K, Dalm V, Kueanjinda P, Wongpiyabovorn J. MicroRNA-378a-3p is overexpressed in psoriasis and modulates cell cycle arrest in keratinocytes via targeting BMP2 gene. *Sci Rep*. 2021;11(1):1-16. doi:10.1038/s41598-021-93616-8
269. Stockert JC, Horobin RW, Colombo LL, Blázquez-Castro A. Tetrazolium salts and formazan products in Cell Biology: Viability assessment, fluorescence imaging, and labeling perspectives. *Acta Histochem*. 2018;120(3):159-167. doi:10.1016/j.acthis.2018.02.005
270. Strober W. Trypan Blue Exclusion Test of Cell Viability. *Curr Protoc Immunol*. 2015;111(1):A3.B.1-A3.B.3. doi:10.1002/0471142735.ima03bs111
271. Wang H, Joseph JA. Quantifying cellular oxidative stress by dichlorofluorescein assay using microplate reader. *Free Radic Biol Med*. 1999;27(5-6):612-616. doi:10.1016/S0891-5849(99)00107-0
272. Wojtala A, Bonora M, Malinska D, Pinton P, Duszynski J, Wieckowski MR. *Methods to Monitor ROS Production by Fluorescence Microscopy and Fluorometry*. Vol 542. 1st ed. Elsevier Inc.; 2014. doi:10.1016/B978-0-12-416618-9.00013-3
273. Nawar WW. Thermal degradation of lipids. A review. *J Agric Food Chem*. 1969;17(1):18-21. doi:10.1021/jf60161a012
274. Rapalli VK, Kaul V, Waghule T, et al. Curcumin loaded nanostructured lipid carriers for enhanced skin retained topical delivery: optimization, scale-up, in-vitro characterization and assessment of ex-vivo skin deposition. *Eur J Pharm Sci*. 2020;152:1-12. doi:10.1016/j.ejps.2020.105438
275. Araujo VHS, da Silva PB, Szlachetka IO, et al. The influence of NLC composition on curcumin loading under a physicochemical perspective and in vitro evaluation. *Colloids Surfaces A Physicochem Eng Asp*. 2020;602(May). doi:10.1016/j.colsurfa.2020.125070

276. Corzo C, Meindl C, Lochmann D, Reyer S, Salar-Behzadi S. Novel approach for overcoming the stability challenges of lipid-based excipients. Part 3: Application of polyglycerol esters of fatty acids for the next generation of solid lipid nanoparticles. *Eur J Pharm Biopharm.* 2020;152:44-55. doi:10.1016/j.ejpb.2020.04.027
277. Paula Badan Ribeiro A, Helen Masuchi M, Koji Miyasaki E, et al. Crystallization modifiers in lipid systems. *J Food Sci.* 2015;52(7):3925-3946. doi:10.1007/s13197-014-1587-0
278. Araiza-Calahorra A, Akhtar M, Sarkar A. Recent advances in emulsion-based delivery approaches for curcumin: From encapsulation to bioaccessibility. *Trends Food Sci Technol.* 2018;71:155-169. doi:10.1016/j.tifs.2017.11.009
279. Ma P, Zeng Q, Tai K, et al. Preparation of curcumin-loaded emulsion using high pressure homogenization: Impact of oil phase and concentration on physicochemical stability. *LWT - Food Sci Technol.* 2017;84:34-46. doi:10.1016/j.lwt.2017.04.074
280. Xue J, Wang T, Hu Q, Zhou M, Luo Y. Insight into natural biopolymer-emulsified solid lipid nanoparticles for encapsulation of curcumin: Effect of loading methods. 2017. doi:10.1016/j.foodhyd.2017.12.018
281. Li J, Liu D, Tan G, Zhao Z, Yang X, Pan W. A comparative study on the efficiency of chitosan-N-acetylcysteine, chitosan oligosaccharides or carboxymethyl chitosan surface modified nanostructured lipid carrier for ophthalmic delivery of curcumin. *Carbohydr Polym.* 2016;146:435-444. doi:10.1016/j.carbpol.2016.03.079
282. Meng F, Asghar S, Xu Y, et al. Design and evaluation of lipoprotein resembling curcumin-encapsulated protein-free nanostructured lipid carrier for brain targeting. *Int J Pharm.* 2016;506(1-2):46-56. doi:10.1016/j.ijpharm.2016.04.033
283. Vishnu S, Rompicharla K, Bhatt H, et al. Formulation optimization, characterization, and evaluation of in vitro cytotoxic potential of curcumin loaded solid lipid nanoparticles for improved anticancer activity. *Chem Phys Lipids.* 2017;208:10-18. doi:10.1016/j.chemphyslip.2017.08.009
284. Baek J-S, Cho C-W. Surface modification of solid lipid nanoparticles for oral delivery of curcumin: Improvement of bioavailability through enhanced cellular uptake, and lymphatic uptake. *Eur J Pharm Biopharm.* 2017;117:132-140. doi:10.1016/j.ejpb.2017.04.013
285. Chen P, Zhang H, Cheng S, Zhai G, Shen C. Development of curcumin loaded nanostructured lipid carrier based thermosensitive in situ gel for dermal delivery. *Colloids Surfaces A Physicochem Eng Asp.* 2016;506:356-362. doi:10.1016/j.colsurfa.2016.06.054
286. Keck CM, Müller RH. Short review (expert opinion) Nanotoxicological classification system (NCS)-A guide for the risk-benefit assessment of nanoparticulate drug delivery systems. 2013. doi:10.1016/j.ejpb.2013.01.001
287. Karimi N, Ghanbarzadeh B, Hamishehkar H, Mehramuz B, Kafil HS. Antioxidant, Antimicrobial and

- Physicochemical Properties of Turmeric Extract-Loaded Nanostructured Lipid Carrier (NLC). *Colloids Interface Sci Commun*. 2018;22:18-24. doi:10.1016/j.colcom.2017.11.006
288. Wu L, Zhang J, Watanabe W. Physical and chemical stability of drug nanoparticles. *Adv Drug Deliv Rev*. 2011;63(6):456-469. doi:10.1016/j.addr.2011.02.001
289. Erickson HP. Size and shape of protein molecules at the nanometer level determined by sedimentation, gel filtration, and electron microscopy. *Biol Proced Online*. 2009;11(1):32-51. doi:10.1007/s12575-009-9008-x
290. Jores K, Mehnert W, Drechsler M, Bunjes H, Johann C, Mäder K. Investigations on the structure of solid lipid nanoparticles (SLN) and oil-loaded solid lipid nanoparticles by photon correlation spectroscopy, field-flow fractionation and transmission electron microscopy. *J Control Release*. 2004;95(2):217-227. doi:10.1016/j.jconrel.2003.11.012
291. Esposito E, Fantin M, Marti M, et al. Solid lipid nanoparticles as delivery systems for bromocriptine. *Pharm Res*. 2008;25(7):1521-1530. doi:10.1007/s11095-007-9514-y
292. Esposito E, Ravani L, Contado C, et al. Clotrimazole nanoparticle gel for mucosal administration. *Mater Sci Eng C*. 2013;33(1):411-418. doi:10.1016/j.msec.2012.09.007
293. Bunjes H. Structural properties of solid lipid based colloidal drug delivery systems. *Curr Opin Colloid Interface Sci*. 2011;16(5):405-411. doi:10.1016/j.cocis.2011.06.007
294. Bunjes H, Unruh T. Characterization of lipid nanoparticles by differential scanning calorimetry , X-ray and neutron scattering. *Adv Drug Deliv Re*. 2007;59:379-402. doi:10.1016/j.addr.2007.04.013
295. Salminen H, Helgason T, Kristinsson B, Kristbergsson K, Weiss J. Formation of solid shell nanoparticles with liquid  $\alpha$ -3 fatty acid core. *Food Chem*. 2013;141(3):2934-2943. doi:10.1016/j.foodchem.2013.05.120
296. Santos S, Brito B, Ávila A, et al. Nanostructured lipid carriers loaded with free phytosterols for food applications. *Food Chem*. 2019;298(June):125053. doi:10.1016/j.foodchem.2019.125053
297. Chevalier Y, Bolzinger M-A, Puel F. Émulsions. In: *Concéption Des Produits Cosmétiques*. 2nd ed. Chartres: Cosmetic Valley Editions; 2018:141-146.
298. Kato S, Shimizu N, Hanzawa Y, et al. Determination of triacylglycerol oxidation mechanisms in canola oil using liquid chromatography–tandem mass spectrometry. *npj Sci Food*. 2018;2(1). doi:10.1038/s41538-017-0009-x
299. Shajari M, Rostamizadeh K, Shapouri R, Taghavi L. Eco-friendly curcumin-loaded nanostructured lipid carrier as an efficient antibacterial for hospital wastewater treatment. *Environ Technol Innov*. 2020;18:100703. doi:10.1016/j.eti.2020.100703
300. Ak T, Ilhami G. Antioxidant and radical scavenging properties of curcumin. *Chem Biol Interact*. 2008;174:27-37. doi:10.1016/j.cbi.2008.05.003
301. Park SJ, Garcia C V., Shin GH, Kim JT. Improvement of curcuminoid bioaccessibility from turmeric by



- a nanostructured lipid carrier system. *Food Chem.* 2018;251(August 2017):51-57. doi:10.1016/j.foodchem.2018.01.071
302. Montanari E, Di Meo C, Coviello T, Gueguen V, Pavon-Djavid G, Matricardi P. Intracellular Delivery of Natural Antioxidants via Hyaluronan Nanohydrogels. *Pharmaceutics.* 2019;11(10). doi:10.3390/pharmaceutics11100532
303. Kharat M, Du Z, Zhang G, McClements DJ. Physical and Chemical Stability of Curcumin in Aqueous Solutions and Emulsions: Impact of pH, Temperature, and Molecular Environment. *J Agric Food Chem.* 2017;65(8):1525-1532. doi:10.1021/acs.jafc.6b04815
304. Wang Y-J, Pan M-H, Cheng A-L, et al. *PHARMACEUTICAL AND BIOMEDICAL ANALYSIS Stability of Curcumin in Buffer Solutions and Characterization of Its Degradation Products.* Vol 15.; 1997.
305. Chen C-C, Tsai T-H, Huang Z-R, Fang J-Y. Effects of lipophilic emulsifiers on the oral administration of lovastatin from nanostructured lipid carriers: Physicochemical characterization and pharmacokinetics. *Eur J Pharm Biopharm.* 2010;74:474-482. doi:10.1016/j.ejpb.2009.12.008
306. Tamjidi F, Shahedi M, Varhosaz J, Nasirpour A. Stability of astaxanthin-loaded nanostructured lipid carriers as affected by pH, ionic strength, heat treatment, simulated gastric juice and freeze-thawing. *J Food Sci Technol.* 2017;10(54):2017. doi:10.1007/s13197-017-2749-7
307. Pisarello ML, Querini CA. Catalyst consumption during one and two steps transesterification of crude soybean oils. *Chem Eng J.* 2013;234:276-283. doi:10.1016/j.cej.2013.08.109
308. Chanakaewsomboon I, Tongurai C, Photaworn S, Kungsanant S, Nikhom R. Investigation of saponification mechanisms in biodiesel production: Microscopic visualization of the effects of FFA, water and the amount of alkaline catalyst. *J Environ Chem Eng.* 2020;8(2):103538. doi:10.1016/j.jece.2019.103538
309. Santiago RR, Gyselle de Holanda e Silva K, Dantas dos Santos N, et al. Nanostructured lipid carriers containing Amphotericin B: Development, in vitro release assay, and storage stability. *J Drug Deliv Sci Technol.* 2018;48(April):372-382. doi:10.1016/j.jddst.2018.10.003
310. Blasi P, Schoubben A, Romano GV, Giovagnoli S, Di Michele A, Ricci M. Lipid nanoparticles for brain targeting II. Technological characterization. *Colloids Surfaces B Biointerfaces.* 2013;110:130-137. doi:10.1016/j.colsurfb.2013.04.021
311. Schwarz C, Mehnert W. Freeze-drying of drug-free and drug-loaded solid lipid nanoparticles (SLN). *Int J Pharm.* 1997;157(2):171-179. doi:10.1016/S0378-5173(97)00222-6
312. Kamel AE, Fadel M, Louis D. Curcumin-loaded nanostructured lipid carriers prepared using Peceol™ and olive oil in photodynamic therapy: development and application in breast cancer cell line. *Int J Nanomedicine.* 2019;14:5073. doi:10.2147/IJN.S210484
313. International Organization for Standardization (ISO). ISO 10993-1:2018 - Biological evaluation of medical devices - Part 1: Evaluation and testing within a risk management process. Online Browsing

- Platform (OBP). <https://www.iso.org/obp/ui#iso:std:iso:10993:-1:ed-5:v2:en>. Published 2018. Accessed March 10, 2022.
314. Kloesch B, Gober L, Loebisch S, Vcelar B, Helson L, Steiner G. In Vitro Study of a Liposomal Curcumin Formulation (Lipocurc): Toxicity and Biological Activity in Synovial Fibroblasts and Macrophages. *In Vivo (Brooklyn)*. 2016;30:413-420.
315. Lundvig DMS, Pennings SWC, Brouwer KM, et al. Curcumin induces differential expression of cytoprotective enzymes but similar apoptotic responses in fibroblasts and myofibroblasts. *Exp Cell Res*. 2015;330(2):429-441. doi:10.1016/j.yexcr.2014.10.006
316. Lundvig DMS, Pennings SWC, Brouwer KM, et al. Cytoprotective responses in HaCaT keratinocytes exposed to high doses of curcumin. *Exp Cell Res*. 2015;336(2):298-307. doi:10.1016/j.yexcr.2015.06.002
317. Doktorovova S, Souto EB, Silva AM. Nanotoxicology applied to solid lipid nanoparticles and nanostructured lipid carriers - A systematic review of in vitro data. *Eur J Pharm Biopharm*. 2014;87(1):1-18. doi:10.1016/j.ejpb.2014.02.005
318. de Campos PS, Matte BF, Diel LF, et al. Low Doses of Curcuma longa Modulates Cell Migration and Cell–Cell Adhesion. *Phyther Res*. 2017;31(9):1433-1440. doi:10.1002/ptr.5872
319. Saraste A. Morphologic Criteria and Detection of Apoptosis. *Herz*. 1999;95(3):189-195.
320. Pirkmajer S, Chibalin A V. Serum starvation: Caveat emptor. *Am J Physiol - Cell Physiol*. 2011;301(2):272-279. doi:10.1152/ajpcell.00091.2011
321. ibidi GmbH. *Ibidi Application Guide: Wound Healing and Migration Assays*. Gräfelfing; 2019. doi:10.1016/j
322. Block ER, Matela AR, SundarRaj N, Iszkula ER, Klarlund JK. Wounding induces motility in sheets of corneal epithelial cells through loss of spatial constraints. Role of heparin-binding epidermal growth factor-like growth factor signaling. *J Biol Chem*. 2004;279(23):24307-24312. doi:10.1074/jbc.M401058200
323. Sammak PJ, Hinman LE, Tran POT, Sjaastad MD, Machen TE. How do injured cells communicate with the surviving cell monolayer? *J Cell Sci*. 1997;110(4):465-475. doi:10.1242/jcs.110.4.465
324. Phan TT, Sun L, Bay BH, Chan SY, Lee ST. Dietary compounds inhibit proliferation and contraction of keloid and hypertrophic scar-derived fibroblasts in vitro: Therapeutic implication for excessive scarring. *J Trauma*. 2003;54(6):1212-1224. doi:10.1097/01.TA.0000030630.72836.32
325. Zhang J, Song M, Li W, Zhao F, Li Y. Curcumin inhibits proliferation and soluble collagen synthesis of NIH/3T3 cell line by modulation of miR-29a and via ERK1/2 and  $\beta$ -catenin pathways. *Mol Immunol*. 2019;116:191-198. doi:10.1016/J.MOLIMM.2019.10.018
326. Bindschadler M, McGrath JL. Sheet migration by wounded monolayers as an emergent property of single-cell dynamics. *J Cell Sci*. 2007;120(5):876-884. doi:10.1242/jcs.03395

327. Manca ML, Castangia I, Zaru M, et al. Development of curcumin loaded sodium hyaluronate immobilized vesicles (hyalurosomes) and their potential on skin inflammation and wound restoring. *Biomaterials*. 2015;71:100-109. doi:10.1016/j.biomaterials.2015.08.034
328. Alía M, Ramos S, Mateos R, Bravo L, Goya L. Response of the antioxidant defense system to tert-butyl hydroperoxide and hydrogen peroxide in a human hepatoma cell line (HepG2). *J Biochem Mol Toxicol*. 2005;19(2):119-128. doi:10.1002/jbt.20061
329. Goya L, Martin M, Ramos S, Mateos R, Bravo L. A Cell Culture Model for the Assessment of the Chemopreventive Potential of Dietary Compounds. *Curr Nutr Food Sci*. 2009;5(1):56-64. doi:10.2174/157340109787314721
330. Miyoshi H. Inhibitors of mitochondrial respiratory enzymes. *J Pestic Sci*. 2005;30(2):120-121. doi:10.1584/jpestics.30.120
331. Hofer T, Eriksen TE, Hansen E, et al. Cellular and Chemical Assays for Discovery of Novel Antioxidants in Marine Organisms. *Oxidative Stress Appl basic Res Clin Pract*. 2011:637-657. doi:10.1007/978-1-60761-956-7
332. Fahr A. *Voigt's Pharmaceutical Technology*. 1st ed. (Scherphof G, ed.). West Sussex: John Wiley and Sons Inc.; 2018.
333. Heilig ML. Carboxylic Polymers. *ACM SIGGRAPH Comput Graph*. 1994;28(2):131-134. doi:10.1145/178951.178972
334. Lubrizol Advanced Materials. Neutralization Procedures. <https://www.lubrizol.com/-/media/Lubrizol/Life-Sciences/Documents/Literature/Bulletin-05---Neutralization-Procedures.pdf>. Published 2011. Accessed June 15, 2020.
335. Lubrizol Advanced Materials. Pharmaceutical Bulletin-Neutralization Procedures. [https://www.lubrizol.com/-/media/Lubrizol/Life-Sciences/Documents/TDS/TDS-237\\_Neutralizing\\_Carbopol\\_Pemulen\\_in\\_Aqueous\\_Hydroalcoholic\\_Systems--PH.pdf](https://www.lubrizol.com/-/media/Lubrizol/Life-Sciences/Documents/TDS/TDS-237_Neutralizing_Carbopol_Pemulen_in_Aqueous_Hydroalcoholic_Systems--PH.pdf). Published 2009. Accessed June 15, 2020.
336. Waghule T, Rapalli VK, Singhvi G, et al. Voriconazole loaded nanostructured lipid carriers based topical delivery system: QbD based designing, characterization, in-vitro and ex-vivo evaluation. *J Drug Deliv Sci Technol*. 2019;52(April):303-315. doi:10.1016/j.jddst.2019.04.026
337. Takalkar D, Desai N. Nanolipid Gel of an Antimycotic Drug for Treating Vulvovaginal Candidiasis—Development and Evaluation. *AAPS PharmSciTech*. 2018;19(3):1297-1307. doi:10.1208/s12249-017-0918-7
338. Kang Q, Liu J, Zhao Y, et al. Transdermal delivery system of nanostructured lipid carriers loaded with Celastrol and Indomethacin: optimization, characterization and efficacy evaluation for rheumatoid arthritis. *Artif Cells, Nanomedicine Biotechnol*. 2018;46(sup3):S585-S597. doi:10.1080/21691401.2018.1503599

339. Sonawane R, Harde H, Katariya M, Agrawal S, Jain S. Solid lipid nanoparticles-loaded topical gel containing combination drugs: An approach to offset psoriasis. *Expert Opin Drug Deliv.* 2014;11(12):1833-1847. doi:10.1517/17425247.2014.938634
340. Marques AC, Rocha AI, Leal P, Estanqueiro M, Lobo JMS. Development and characterization of mucoadhesive buccal gels containing lipid nanoparticles of ibuprofen. *Int J Pharm.* 2017;533(2):455-462. doi:10.1016/j.ijpharm.2017.04.025
341. Kang Q, Liu J, Liu XY, et al. Application of quality by design approach to formulate and optimize tripterine loaded in nanostructured lipid carriers for transdermal delivery. *J Drug Deliv Sci Technol.* 2019;52(June):1032-1041. doi:10.1016/j.jddst.2019.06.006
342. Cosmetic Ingredient Review (CIR). *Report on Safety Assessment of Inorganic Hydroxides as Used in Cosmetics*; 2016.
343. Sarfaraz K N. *Handbook of Pharmaceutical Manufacturing Formulations*. 2nd ed. New York: Informa Healthcare USA, Inc.; 2009.
344. Fiume MM, Heldreth B, Bergfeld WF, et al. Safety Assessment of Triethanolamine and Triethanolamine-Containing Ingredients as Used in Cosmetics. *Int J Toxicol.* 2013;32:60S-83S. doi:10.1177/1091581813488804
345. Lubrizol Advanced Materials. Technical Data Sheet-Molecular Weight of Carbopol® and Pemulen™ Polymers. Technical Data Sheet-222. [https://www.lubrizol.com/-/media/Lubrizol/Life-Sciences/Documents/TDS/TDS-222\\_Molecular\\_Weight\\_Carbopol\\_-Polymers.pdf](https://www.lubrizol.com/-/media/Lubrizol/Life-Sciences/Documents/TDS/TDS-222_Molecular_Weight_Carbopol_-Polymers.pdf). Published 2008.
346. Oppong FK, Rubatat L, Frisken BJ, Bailey AE, De Bruyn JR. Microrheology and structure of a yield-stress polymer gel. *Phys Rev E - Stat Nonlinear, Soft Matter Phys.* 2006;73(4):1-9. doi:10.1103/PhysRevE.73.041405
347. Kowalczyk A, Oelschlaeger C, Willenbacher N. Visualization of micro-scale inhomogeneities in acrylic thickener solutions: A multiple particle tracking study. *Polymer (Guildf).* 2015;58:170-179. doi:10.1016/j.polymer.2014.12.041
348. Flaten GE, Palac Z, Engesland A, Filipović-Grčić J, Vanić Ž, Škalko-Basnet N. In vitro skin models as a tool in optimization of drug formulation. *Eur J Pharm Sci.* 2015;75:10-24. doi:10.1016/j.ejps.2015.02.018
349. Bergfeld WF, Donald V, Hill RA, et al. Safety Assessment of Polysorbates as Used in Cosmetics. *Cosmet Ingred Rev.* 2015.
350. Bide Y, Fashapoyeh MA, Shokrollahzadeh S. Structural investigation and application of Tween 80-choline chloride self-assemblies as osmotic agent for water desalination. *Sci Rep.* 2021;11(1):1-11. doi:10.1038/s41598-021-96199-6
351. Bommannan D, Potts RO, Guy RH. Examination of the effect of ethanol on human stratum corneum in vivo using infrared spectroscopy. *J Control Release.* 1991;16(3):299-304. doi:10.1016/0168-

3659(91)90006-Y

352. Kwak S, Brief E, Langlais D, Kitson N, Lafleur M, Thewalt J. Ethanol perturbs lipid organization in models of stratum corneum membranes: An investigation combining differential scanning calorimetry, infrared and <sup>2</sup>H NMR spectroscopy. *Biochim Biophys Acta - Biomembr.* 2012;1818(5):1410-1419. doi:10.1016/j.bbamem.2012.02.013
353. Nair RS, Morris A, Billa N, Leong CO. An Evaluation of Curcumin-Encapsulated Chitosan Nanoparticles for Transdermal Delivery. *AAPS PharmSciTech.* 2019;20(2):1-13. doi:10.1208/s12249-018-1279-6
354. Vigato AA, Querobino SM, De Faria NC, et al. Physico-chemical characterization and biopharmaceutical evaluation of lipid-poloxamer-based organogels for curcumin skin delivery. *Front Pharmacol.* 2019;10(September):1-11. doi:10.3389/fphar.2019.01006

## List of communications and publications

---

### Oral Communications:

R. Calderon-Jacinto, P. Matricardi, V. Rodriguez-Ruiz, E. Pauthe. **Development of a curcumin loaded-NLCs hydrogel system for topical applications.** *31<sup>st</sup> Annual Conference of the European Society for Biomaterials (ESB)*. 5-9 September 2021. Porto-Portugal. (Virtual conference)

R. Calderon-Jacinto, D. Lopez, M. Gentili, S. Abraham, S. Sandhu, F. Schoenstein, V. Gueguen, G. Pavon-Djavid, P. Matricardi, E. Pauthe, V. Rodriguez-Ruiz. **Formulation of a multiscale fluid gel based on nanostructured lipid carriers (NLCs) for wound-healing applications.** *3<sup>rd</sup> BIOMAT-Materials for Health Congress*. 03-07 June 2019. La Grande Motte-France.

### Poster Presentation:

R. Calderon-Jacinto, P. Matricardi, G. Pavon-Djavid, V. Gueguen, E. Pauthe, V. Rodriguez-Ruiz. **Development of a curcumin loaded-NLCs hydrogel system for dermal applications.** *4<sup>th</sup> BIOMAT-Materials for Health Congress*. 18-22 October 2021. Bourg Saint Maurice-France.

### Article:

R. Calderon-Jacinto, P. Matricardi, V. Gueguen, G. Pavon-Djavid, E. Pauthe, V. Rodriguez-Ruiz. **Dual Nanostructured Lipid Carriers/Hydrogel System for Delivery of Curcumin for Topical Skin Applications.** *Biomolecules*. 2022; 12(6):780. <https://doi.org/10.3390/biom12060780>



## Article

# Dual Nanostructured Lipid Carriers/Hydrogel System for Delivery of Curcumin for Topical Skin Applications

Rosa Calderon-Jacinto <sup>1</sup>, Pietro Matricardi <sup>2</sup>, Virginie Gueguen <sup>3</sup>, Graciela Pavon-Djavid <sup>3</sup>, Emmanuel Pauthe <sup>1,†</sup> and Violeta Rodriguez-Ruiz <sup>1,\*,†</sup>

- <sup>1</sup> ERRMECe Laboratory, Biomaterials for Health Group, CY Cergy Paris Université, Maison Internationale de la Recherche, I MAT, 1 rue Descartes, 95031 Neuville sur Oise, France; rosa.calderon-jacinto@cyu.fr (R.C.-J.); emmanuel.pauthe@cyu.fr (E.P.)
- <sup>2</sup> Department of Drug Chemistry and Technologies, Sapienza University of Rome, P.le Aldo Moro 5, 00185 Rome, Italy; pietro.matricardi@uniroma1.it
- <sup>3</sup> INSERM U1148, Laboratory for Vascular Translational Science, Cardiovascular Bioengineering, Université Sorbonne Paris Nord, 99 Av. Jean-Baptiste Clément, 93430 Villetaneuse, France; virginie.gueguen@univ-paris13.fr (V.G.); graciela.pavon@univ-paris13.fr (G.P.-D.)
- \* Correspondence: violeta.rodriguez-ruiz@cyu.fr; Tel.: +33-01-3425-2830
- † These authors contributed equally to this work.

**Abstract:** This work focuses on the development and evaluation of a dual nanostructured lipid carrier (NLC)/Carbopol<sup>®</sup>-based hydrogel system as a potential transporter for the topical delivery of curcumin to the skin. Two populations of different sized negatively charged NLCs (P1, 70–90 nm and P2, 300–350 nm) were prepared and characterized by means of dynamic light scattering. NLCs presented an ovoid platelet shape confirmed by transmission electron microscopy techniques. Curcumin NLC entrapment efficiency and release profiles were assessed by HPLC (high pressure liquid chromatography) and spectrophotometric methods. Preservation and enhancement of curcumin (CUR) antioxidant activity in NLCs (up to 7-fold) was established and cell viability assays on fibroblasts and keratinocytes indicated that CUR-NLCs are non-cytotoxic for concentrations up to 10  $\mu$ M and exhibited a moderate anti-migration/proliferation effect (20% gap reduction). CUR-NLCs were then embedded in a Carbopol<sup>®</sup>-based hydrogel without disturbing the mechanical properties of the gel. Penetration studies on Franz diffusion cells over 24 h in CUR-NLCs and CUR-NLCs/gels demonstrated an accumulation of CUR in Strat-M<sup>®</sup> membranes of 22% and 5%, respectively. All presented data support the use of this new dual CUR-NLC/hydrogel system as a promising candidate for adjuvant treatment in topical dermal applications.

**Keywords:** nanostructured lipid carriers; curcumin; hydrogel; oxidative stress; skin applications; topical; drug delivery; fibroblasts; keratinocytes; antioxidants



**Citation:** Calderon-Jacinto, R.; Matricardi, P.; Gueguen, V.; Pavon-Djavid, G.; Pauthe, E.; Rodriguez-Ruiz, V. Dual Nanostructured Lipid Carriers/Hydrogel System for Delivery of Curcumin for Topical Skin Applications. *Biomolecules* **2022**, *12*, 780. <https://doi.org/10.3390/biom12060780>

Academic Editor: Piergiorgio Gentile

Received: 27 April 2022

Accepted: 1 June 2022

Published: 3 June 2022

**Publisher's Note:** MDPI stays neutral with regard to jurisdictional claims in published maps and institutional affiliations.



**Copyright:** © 2022 by the authors. Licensee MDPI, Basel, Switzerland. This article is an open access article distributed under the terms and conditions of the Creative Commons Attribution (CC BY) license (<https://creativecommons.org/licenses/by/4.0/>).

## 1. Introduction

Skin diseases are classified as the fourth leading cause of non-fatal morbidity worldwide and are recognized to disturb the well-being of patients, having, in some cases, consequences for the patient's mental health and social life [1,2]. Some of these dermatological disorders, such as psoriasis [3] or atopic dermatitis [4], are directly related to chronic inflammatory processes and to prooxidant–antioxidant imbalance leading to oxidative stress.

Natural bioactive compounds (NBC) presenting anti-inflammatory and antioxidant properties, can contribute to stopping inflammation and restoring the redox balance necessary to reestablish normal dermal conditions [5]. In this regard, the topical use of NBC such as astaxanthin [6], gallic acid [7] or curcumin [8], has been described for the treatment of some skin pathologies.



Dermal topical therapy is a simple and non-invasive route of administration, which allows local delivery of high amounts of active ingredient at the site of action, improves compliance and limits some of the side effects related with systemic routes [9]. NBC are usually administered as adjuvant therapies to conventional treatments and their natural origin is usually associated with a low toxicity and a high biological activity [10]. In particular, the use of curcumin as adjuvant therapy for the topical treatment of psoriasis [11,12] has been reported. Curcumin (1,7-bis-(4-hydroxy-3-methoxyphenyl)-hepta-1,6-diene-3,5-dione) is the main active ingredient of the yellow-orange spice, *Curcuma longa*. It is a hydrophobic polyphenol recognized as safe by the Food and Drug Administration (FDA), with a wide range of biological activities, including anti-inflammatory and antioxidant properties [13]. At the molecular level, the multiple properties of curcumin (CUR) are based on its ability to interact with many molecules due to its special chemical structure, which confers to CUR, H-bond donating/accepting capacities and multivalent cation binding properties [14]. In particular, CUR's potent antioxidant capacity has been widely established through its ability to interact with several reactive oxygen species (ROS) (hydroxyl radical, superoxide anion, peroxy radicals, hydrogen peroxide and singlet oxygen) [15]. In the same way, the anti-inflammatory properties of CUR have also been widely demonstrated and appear to be related to its ability to modulate several molecules in cell signaling pathways. CUR has been shown to modulate signal transducers and transcription activators like JAK-STAT, Nrf2, Notch-1 and nuclear factor kappa B (NF- $\kappa$ B) as well as the protein kinases Akt and MAPK [16,17]. The anti-inflammatory effects of CUR are used to target and control skin inflammation in different skin diseases; its mechanism of action involves reducing the expression of cytokines released by immune cells [18].

The efficiency of CUR in humans has been evaluated in preclinical studies and in clinical trials [19]. From 263 currently listed as completed or ongoing in "[clinical-trials.gov](https://clinicaltrials.gov)" (accessed on 26 April 2022) only 5 are related to the topical route, where CUR was administered in conventional formulations such as gelatin capsules, solutions, gels and creams. The low number of topical studies could be related to the physicochemical characteristics of CUR such as its lipophilic character and oxygen and light instability, which limit its efficacy and clinical applications. To circumvent these limitations, CUR has been formulated in advanced delivery systems such as hydrogels [20], nanofibers [21], microsponges [22], emulsions [23], nanoparticles [24] and lipid-based nanoparticles [25], used alone or combined. In particular, a growing interest has recently been developed for nanostructured lipid carrier (NLC) formulations, which are composed of a mixture of solid and liquid lipids with a structural arrangement allowing high entrapping efficiency. Interesting curcumin–NLC delivery systems were designed for several applications. For example, optimized formulations for an intranasal administration were designed for the treatment of Alzheimer's disease [26] showing a high drug entrapment, a sustained release profile and a good stability. For an in situ administration, Murgia et al. prepared curcumin–NLCs and placed them in the dental alveoli to prevent alveolar bone resorption following dental extractions [27]. The possibility of associating several carriers of different nature and size (nano-, micro- and bulk-scale) in a more complex system allows the accumulation of the specific properties of each carrier, the ability to obtain longer sustained release kinetics and to protect and preserve the activity of therapeutic loaded agents [28]. The combination of nanostructured lipid carriers (NLCs) and hydrogels represents a promising strategy as a dual delivery system [29]. NLCs are lipidic nanoparticles with a solid/liquid mixed core able to improve stability, entrapment efficiencies and skin penetration of hydrophobic active compounds [30]. By entrapping CUR in such nanocarriers, high entrapment efficiencies (70–85%) have been reported, increasing its apparent water solubility ~60-fold [31] and its skin penetration capability more than 3-fold [25]. In the same way, hydrogels, and especially those based in Carbopol<sup>®</sup> (Lubrizol, Rouen, France), are greatly employed in the pharmaceutical and cosmetics industries. Carbopol<sup>®</sup> is a polymer of acrylic acid crosslinked with allyl pentaerythritol. This gelling agent endows formulations with a transparent appearance, good suspending ability, and good sensorial and adhesion properties. Moreover, it has been reported to

have low potential for skin irritation and sensitization [32] and to be biocompatible with dermal cells [33,34]. Thus, Carbopol<sup>®</sup> is a good candidate for constituting the matrix of a dual system.

The current work focuses on the development and evaluation of a dual CUR-NLC/Carbopol<sup>®</sup>-based hydrogel delivery system for its potential use as adjuvant therapy in topical skin applications. First, entrapment of CUR into the lipid nanocarrier was studied as well as its release from it and the preservation of CUR's antioxidant properties. Cell viability and dermal cell migration in presence of CUR-NLCs were also assessed. Next, CUR-NLCs were embedded into a Carbopol<sup>®</sup>-based hydrogel and its rheological properties were studied. Finally, penetration studies in Strat-M<sup>®</sup> membranes were carried out with both CUR-NLCs and CUR-NLCs/Carbopol<sup>®</sup>-based hydrogel delivery systems.

## 2. Materials and Methods

### 2.1. Chemicals

Precirol<sup>®</sup> ATO5 (glyceryl palmitostearate) and Labrafac<sup>®</sup> lipophile WL 1349 (caprylic/capric triglycerides) were kindly provided by Gattefosse (Nanterre, France). Curcumin (CUR, purity  $\geq 75\%$  HPLC), Tween<sup>®</sup> 80 (polyoxyethylene 20 sorbitan monooleate), poloxamer 407 (polyoxyethylene-polyoxypropylene copolymer), ( $\pm$ )- $\alpha$ -tocopherol (purity  $\geq 75\%$  HPLC), 2,2'-azino-bis (3-ethylbenzothiazoline-6-sulfonic acid) diammonium salt (ABTS), potassium persulfate ( $K_2S_2O_8$ , purity  $\geq 99\%$ ), triethanolamine (TEA, purity  $\geq 99\%$ ), 3-(4,5-dimethyl-2-thiazolyl)-2,5-diphenyl-2H-tetrazolium bromide (MTT), tert-butyl hydroperoxide (Luperox<sup>®</sup>), 2',7'-dichlorofluorescein diacetate (DCFH-DA) and Trolox (purity  $\geq 98\%$ ) were purchased from Sigma-Aldrich (Saint-Quentin-Fallavier, France). Acetonitrile (ACN) and trifluoroacetic acid (TFA, purity  $\geq 99\%$ ) were purchased from Sigma-Aldrich (Milan, Italy). Dichloromethane (DCM, purity  $\geq 99.8\%$ ), ethanol (EtOH, purity  $\geq 99.8\%$ ) and isopropanol (purity  $\geq 98\%$ ) were purchased from VWR Chemicals (Fontenay-sous-Bois, France). Carbopol<sup>®</sup> 980 NF (polyacrylic acid polymer crosslinked with allyl pentaerythritol) was kindly provided by Lubrizol (Rouen, France).

All aqueous solutions were made with ultrapure water obtained with the Milli-Q<sup>®</sup> Direct Water Purification System (Merck KGaA, Darmstadt, Germany).

### 2.2. Biological Reagents

Dulbecco's Modified Eagle Medium (DMEM), fetal bovine serum (FBS), trypan blue (TB), penicillin/streptomycin and phosphate-buffered saline (PBS) were obtained from Gibco-Fisher Scientific (Illkirch, France). Dermal Basal Medium (DBM), Keratinocyte Growth Kit (containing: bovine pituitary extract, rh TGF- $\alpha$ , L-glutamine, hydrocortisone hemisuccinate, rh insulin, epinephrine, and apo-transferrin), phenol red, BJ fibroblast (CRL-2522<sup>TM</sup>) primary cell line and the HEK293T (PCS-200-010<sup>TM</sup>) primary cell line were purchased from ATCC<sup>®</sup> (Manassas, VA, USA).

### 2.3. CUR Samples Preparation

The CUR used was a mixture of curcumin (MW 368.38 g/mol,  $>75\%$  HPLC), demethoxycurcumin (MW 338.4 g/mol), and bisdemethoxycurcumin (MW 308.3 g/mol). A mean molecular weight for CUR was calculated based on the different proportions of the three individual components of CUR (see Section 3.1). The mean MW was used in all experiments for the conversion of mass concentration to molar concentration.

CUR sample solutions for physicochemical analyses were prepared in a binary solvent composed of EtOH/DCM (60/40%, *v/v*) [35] or in ACN when specified. Calibration curves were constructed by spectrophotometric and HPLC methods. Spectrophotometric analyses were obtained using a UVIKON-XS double beam ultraviolet-visible (UV-VIS) spectrophotometer (Secomam-Aqualabo, Champigny sur Marne, France). A UV-VIS calibration curve of CUR (1–7  $\mu\text{g/mL}$ ) in EtOH/DCM (60/40%, *v/v*) was obtained at  $\lambda = 427 \text{ nm}$ , presenting a slope of  $y = (0.143 \pm 0.002)x$ ;  $R^2 = 0.999$ . Method was tested in the range of 0.5–0.7 AU. Chromatographic analyses were performed using an Azura HPLC (Knauer,

Berlin, Germany) equipped with an Azura Pump P6.1L, a KnauerEurospher II C18 column (250 × 4 mm) and a UV-VIS Azura detector DAD 2.1L, controlled by ClarityChrom<sup>®</sup> software version 6.1.0. The detection wavelength was fixed at  $\lambda = 425$  nm. The mobile phase consisted in a 13 min-gradient from 50:50 to 0:100 (water (+0.1% TFA)/ACN (+0.1% TFA)) at a flow rate of 1 mL.min<sup>-1</sup>. The injection volume was 20  $\mu$ L. All samples were diluted in acetonitrile (ACN) and filtrated (PTFE, 0.45  $\mu$ m). An HPLC calibration curve for CUR (0.31–50  $\mu$ g/mL) in ACN was performed, presenting a slope of  $y = (228.85 \pm 3.35) x$ ;  $R^2 = 0.999$ . Method was tested in the range of 650–4300 mAU.s.

CUR samples for biological tests were prepared by adding 30 mg of CUR to 4.5 mL of cell culture media (DMEM 10%FBS or DBM) and stirring for 4 h at room temperature. Then samples were centrifuged at 5000 rpm for 30 min at 20 °C (Sigma 3K30 centrifuge, Sigma, Osterode am Harz, Germany). Supernatant containing dissolved CUR was separated from the pellet (undissolved CUR). Concentration of dissolved CUR was determined by dilution (1:100) in EtOH/DCM (60/40%, *v/v*), centrifuging the mixture for 3 min at 13,000 rpm, reading the absorbance of the supernatant at 427 nm and calculating the CUR concentration from it according to the previously established calibration curve.

#### 2.4. NLCs Preparation

Unloaded NLCs (Blank-NLCs) and CUR loaded NLCs (CUR-NLCs) were prepared according to the hot homogenization method by modifying some procedures and parameters when necessary [35,36]. The general protocol was as follows. Two phases were prepared. An oil phase composed of 450 mg of Precirol<sup>®</sup> ATO 5, 100 mg of Labrafac<sup>®</sup> lipophile WL 1349 and 60 mg of Tween<sup>®</sup> 80. For CUR-NLCs, 15 mg of CUR was added. Separately, an aqueous phase was prepared with 450 mg of poloxamer 407 dissolved in 15 mL of ultrapure water.

First, both phases were heated at 70 °C for 10 min. Secondly, the oil phase was homogenized at 10,000 rpm at 70 °C for 2 min (Polytron<sup>®</sup> system, PT3100 homogenizer with a dispersing aggregate of 7 mm of diameter, Kinematica AG, Luzern, Switzerland). During this time the aqueous phase was maintained at 70 °C. Then, the aqueous phase was added to the oil phase during 1 min while the homogenization speed was increased to 20,000 rpm. Once all the aqueous phase was added and the speed reached, the homogenization was maintained for 30 min at 70 °C. Afterwards, the preparation was cooled down to 20 °C for 20 min and stored overnight at 4–8 °C. One day after preparation, the CUR loaded NLC suspension was centrifuged at 4000 rpm for 30 min at 20 °C. Pellets (corresponding to excess CUR) were separated from supernatants (CUR-NLCs). In order to remove any free molecules (lipid or surfactant) that might not have been eliminated by the centrifugation step, Blank-NLC and CUR-NLC samples were passed through a size exclusion chromatography (SEC) column. Briefly, 1 mL of the sample was deposited in a Bio-Gel<sup>®</sup> P-10 polyacrylamide gel column (Bio-Rad, Marnes-la-Coquette, France). Ultrapure water was used as eluent. Dead volume was 1 mL and subsequent collected fractions were 500  $\mu$ L. Fraction numbers 3, 4 and 5 were pooled for further analysis.

For Blank-NLCs, CUR was not added to the oil phase. Then, the same procedure as described above was followed.

#### 2.5. NLCs Physicochemical Characterization

##### 2.5.1. Particle Size Analysis and Zeta Potential (ZP) Measurements

Particle size analysis and ZP measurements were performed using a Zetasizer Nano ZS (Malvern Instruments Ltd., Worcestershire, UK) equipped with a He-Ne laser ( $\lambda = 633$  nm) at a scattering angle of 173°.

Particle size and polydispersity index (PDI) were determined by dynamic light scattering (DLS). NLC samples were diluted (1:100) in ultrapure water and placed in polystyrene cuvettes semi-micro (Brand GmbH + Co KG, Wertheim, Germany). Particle size was described in terms of the hydrodynamic diameter (Dh). Results were expressed as size distribution by intensity and by number. Zeta potential (ZP) was calculated from the

electrophoretic mobility obtained from laser Doppler microelectrophoresis. Samples were diluted (1:10) in 1 mM KCl and measurements were performed using a folded capillary zeta cuvette (DTS1070).

In order to measure the stability of NLCs samples, DLS measurements were carried out at 1 and 7 days on NLC samples before and after the SEC column. For NLC samples before the SEC column complementary DLS, PDI and ZP measurements were carried out at 1, 7, 14, 30 and 45 days. Samples were stored at 4 °C between measurements. Each experiment was carried out at 25 °C and in triplicate ( $n = 3$ ).

### 2.5.2. Morphological Analysis by Transmission Electron Microscopy (TEM) Techniques

Fresh NLC samples before and after the SEC column were analyzed by transmission electron microscopy (TEM) using the negative stain method and cryo technique.

For the negative stain method, 3  $\mu$ L of the NLC sample (55 mg/mL) was deposited on an air glow-discharged Quantifoil<sup>®</sup> R2/2 carbon-coated grid (Quantifoil Micro Tools GmbH, Großlobichau, Germany) for 1 min. The excess liquid was blotted, and the grid stained with 2% *w/v* aqueous uranyl acetate. The grids were visualized at 100 kV with a Tecnai 12 Spirit transmission electron microscope (ThermoFisher, New York, NY, USA) equipped with a K2 Base 4 k  $\times$  4 k camera (Gatan, Pleasanton, CA, USA). Magnification was at 14.700 X at the level of the camera, corresponding to a pixel size at the level of the specimen of 0.34 nm.

For the cryo technique, 3  $\mu$ L of the NLC sample (~60 mg/mL) was deposited on an air glow-discharged Quantifoil<sup>®</sup> R2/2 carbon-coated grid (Quantifoil Micro Tools GmbH, Großlobichau, Germany) for 1 min. The sample excess was blotted with a filter paper, and the grid plunged into liquid-nitrogen-cooled ethane. The grid was rapidly transferred and kept under liquid nitrogen. For observation, the grids were mounted in a 626 Gatan holder using its cryo-transfer device. The observations were made in a Tecnai 200 equipped with a field-emission gun (ThermoFisher, New York, NY, USA). Images of the samples were recorded with a direct detection camera K2 Summit (Gatan, Pleasanton, CA, USA) operated in movie mode. The images were aligned and summed as recommended by the manufacturer. They were recorded at 19.800X magnification (pixel size 0.26 nm at the specimen level), using a total dose less than 20 electrons/ $\text{Å}^2$ .

### 2.5.3. Quantification of Loaded CUR in NLCs

Quantification of loaded CUR was calculated by two different approaches: the direct method and the indirect method.

For the direct method, CUR-NLC supernatants (see 2.4 NLC preparation) were dissolved and diluted (1:200) in EtOH/DCM (60/40%, *v/v*) and transferred to 10 mm quartz cuvettes. Complete dissolution and lack of absorption of any component of the NLCs was monitored by obtaining the absorbance spectra of Blank-NLCs and setting this as the baseline for all measurements. CUR concentration in all samples was calculated ( $n = 3$ ) using the calibration curve of CUR in EtOH/DCM (60/40%, *v/v*) at  $\lambda = 427$  nm as described in Section 2.3.

Encapsulation efficiency (%EE) of CUR-NLCs refers to the concentration of CUR incorporated into NLCs over the initial CUR concentration (1 mg/mL). The %EE was calculated using the following equation:

$$\%EE = (\text{loaded} - \text{CUR}) / (\text{total} - \text{CUR}) \times 100$$

where total-CUR is the initial CUR mass concentration introduced (1 mg/mL) and loaded-CUR represents the mass concentration of CUR loaded into the NLCs determined at the end of preparation (for a final volume of 15 mL).

Drug loading (%DL) of CUR-NLCs refers to the amount of CUR incorporated into NLCs per weight of lipids (*w/w*). Drug loading (%DL) was calculated using the following equation:

$$\%DL = (\text{loaded} - \text{CUR}) / \text{Lipids} \times 100$$

where Lipids represent the total amount of lipids used for the preparation of NLCs, including liquid (Labrafac<sup>®</sup> lipophile WL 1349) and solid (Precirol<sup>®</sup> ATO 5) lipids.

For the indirect method, pellets (containing excess CUR) were dissolved in ACN. Concentration of CUR in excess CUR was determined using an HPLC calibration curve of CUR as described in Section 2.3.

Encapsulation efficiency (%EE) and drug loading (%DL) of CUR-NLCs were calculated using the following equations:

$$\%EE = ((\text{total} - \text{CUR}) - (\text{excess} - \text{CUR})) / (\text{total} - \text{CUR}) \times 100$$

$$\%DL = ((\text{total} - \text{CUR}) - (\text{excess} - \text{CUR})) / \text{Lipid} \times 100$$

where excess-CUR is the quantity of CUR not loaded into the NLCs and present in the pellet. All other parameters are described in the direct method section.

#### 2.5.4. Release Studies

CUR release from CUR-NLCs was studied in PBS, DMEM (supplemented with 10% FBS) and DBM (without 10% FBS but supplemented with Keratinocyte Growth Kit, see Section 2.2 for detailed components) media in static conditions. Released CUR was indirectly determined by measurement of remaining CUR in the CUR-NLC suspension. Briefly, CUR-NLC samples (containing 20  $\mu\text{M}$  of loaded CUR) prepared in the different media (4 mL) were placed in sterile conditions at 37  $^{\circ}\text{C}$  for 0, 24, 48 or 72 h incubation times. At the end of each incubation time, samples were centrifuged at 4000 rpm, 20  $^{\circ}\text{C}$  for 30 min. After centrifugation, supernatants (3 mL, containing CUR-NLCs) were freeze-dried for 24 h, then dissolved using EtOH/DCM (60/40%, *v/v*) and centrifuged at 9000 rpm, 4  $^{\circ}\text{C}$  for 5 min. Remaining CUR was calculated from the calibration curve after measurement of absorbance at 427 nm of these last supernatants. Released CUR was then calculated using the following equations:

$$\text{Released CUR (\%)} = 100 - \text{Remaining CUR}$$

$$\text{Remaining CUR (\%)} = (\text{CUR}_t / \text{CUR}_0) \times 100$$

CUR<sub>t</sub>: remaining CUR concentration in CUR-NLC solution at each incubation time.

CUR<sub>0</sub>: remaining CUR concentration in CUR-NLC solution before incubation at 37  $^{\circ}\text{C}$  (t = 0).

#### 2.6. Study of NLCs Antioxidant Activity

An ABTS assay was performed on CUR, Blank-NLCs and CUR-NLCs.  $\alpha$ -Tocopherol was used as a reference antioxidant. The procedure was adapted from previously established methodologies [35,36].

Briefly, ABTS (14 mM) and K<sub>2</sub>S<sub>2</sub>O<sub>8</sub> aqueous solutions (4.9 mM) were mixed (50/50%, *v/v*) and placed for 24 h in the dark and at room temperature to obtain a radical cation ABTS<sup>•+</sup> solution (7 mM). In order to reach an absorbance of ~0.8 at 734 nm, this ABTS<sup>•+</sup> solution was diluted (1:70) in ultrapure water.

NLC samples were dissolved in EtOH/DCM (60/40%, *v/v*). CUR-NLCs solutions were prepared at different CUR concentrations (0–40  $\mu\text{M}$ ). Blank-NLC solutions were prepared at the same mass concentrations as CUR-NLCs. Solutions of CUR (0 to 277  $\mu\text{M}$ ) and  $\alpha$ -tocopherol (0 to 100  $\mu\text{M}$ ) were prepared in the same solvent and used as controls.

Afterwards, 300  $\mu\text{L}$  of these solutions was added to 1000  $\mu\text{L}$  of the diluted ABTS<sup>•+</sup> solution (absorbance ~0.8) and mixed for 45 min at room temperature and in the dark. Samples were centrifuged (13,000 rpm, 3 min at 4  $^{\circ}\text{C}$ ) and the absorbance spectra of the aqueous phase was immediately monitored from 600 to 800 nm. Experiments were carried out in triplicate (*n* = 3).

Antioxidant activity was defined in terms of the percentage (%) of ABTS<sup>•+</sup> inhibited by each sample. This was calculated using the maximal absorbance of ABTS<sup>•+</sup> at 734 nm, according to the following equation:

$$\% \text{ inhibition ABTS}^{\bullet+} = (\text{Abs}_{734\text{nm}} \text{ ABTS}^{\bullet+} - \text{Abs}_{734\text{nm}} \text{ sample}) / \text{Abs}_{734\text{nm}} \text{ ABTS}^{\bullet+} \times 100$$

$\alpha$ -Tocopherol equivalent antioxidant capacity ( $\alpha$ -TEAC) was calculated from the slope ratios of the percentage of inhibition–concentration curves of respective samples and  $\alpha$ -tocopherol ( $\mu\text{M}$  CUR/ $\mu\text{M}$   $\alpha$ -tocopherol).

## 2.7. Cell Culture

Human neonatal BJ fibroblasts and human epidermal keratinocytes neonatal (HEK<sub>n</sub>) primary cell lines from human foreskin were used for this study. BJ fibroblasts were cultured in DMEM supplemented with GlutaMAX already containing phenol red, complemented with FBS (10%), penicillin/streptomycin (417 U/mL) and NaHCO<sub>3</sub> (0.625%). Cells were cultured in DMEM until 90–100% confluence, passages between 4 and 9 were used.

HEK<sub>n</sub> were cultured in DBM supplemented with bovine pituitary extract (0.4%), rh TGF- $\alpha$  (0.5 ng/mL), L-glutamine (6 mM), hydrocortisone hemisuccinate (100 ng/mL), rh insulin (5 mg/mL), epinephrine (1.0 mM), apo-transferrin (5 mg/mL), penicillin (10 U/mL) and streptomycin (10  $\mu\text{g}/\text{mL}$ ). Phenol red (33  $\mu\text{M}$ ) was added for cell culture routine procedures. For experiments where curcumin quantification was needed, phenol red was eliminated. Cells were maintained in DBM until 80% confluence, passages between 3 and 7 were used.

## 2.8. Cell Viability Evaluation

### 2.8.1. MTT and TB Assays

The MTT assay and the trypan blue (TB) exclusion assay were used to study the *in vitro* effect of CUR, CUR-NLCs and Blank-NLCs on BJ fibroblasts and HEK<sub>n</sub> cell lines.

For the MTT test 50,000 cells/well were seeded in a Corning<sup>®</sup> 96-well plate with a clear bottom (New York, NY, USA) and incubated for 24 h (37 °C and 5% CO<sub>2</sub>). Then, the medium was removed, cells were washed (PBS) and treated (24 h) with 10% FBS DMEM or DBM with or without samples: CUR (1–20  $\mu\text{M}$ ), CUR-NLCs (1–20  $\mu\text{M}$  of loaded CUR corresponding to 0.05–1.10 g/L of NLCs suspension) or Blank-NLCs (0.05–1.10 g/L). After washing, MTT (200  $\mu\text{L}$ , 0.5 g/L in PBS) was added and incubated for 2 h 30 min at 37 °C and 5% CO<sub>2</sub>. MTT was then removed and isopropanol (200  $\mu\text{L}$ ) was added to each well for 40 min. Absorbance at 570 nm was measured using a microplate reader (Xenius XM, Safas, Monaco). Metabolic activity (%) of cells treated with the samples (experimental cells) was reported compared with the metabolic activity of those treated with only 10% FBS DMEM or DBM (control cells, 100% metabolic activity). Experiments were performed in triplicate. The following equation was used:

$$\% \text{ metabolic activity} = (\text{Abs}_{570\text{nm}} \text{ experimental cells} / \text{Abs}_{570\text{nm}} \text{ control cells}) \times 100$$

For the TB exclusion assay, cells were seeded in a Corning<sup>®</sup> 24-well plate with a clear bottom (New York, NY, USA) and cultured 24 h. Then, cells were incubated without samples (control) or with samples (24 h) at the same concentration as described for the MTT test. Cells were detached, stained with TB (25  $\mu\text{L}$  at 0.04% *v/v* in PBS) and live/dead cells counted in a Malassez chamber using a DMi1 inverted microscope (Leica Microsystems, Wetzlar, Germany). Blue cells were counted as dead. Control cells represented 100% viability. Experiments were performed in triplicate.

### 2.8.2. Evaluation of BJ Fibroblasts under Oxidative Stress

For oxidative cell stress induction evaluation different Luperox<sup>®</sup> (stressor) concentrations were used to induce ROS production. ROS generation was demonstrated using the fluorogenic probe DCFH-DA. For this, 50,000 cells/well (156,000 cells/cm<sup>2</sup>) were

seeded in a 96-well plate in 10% FBS DMEM medium for 48 h. Medium was removed and cells were incubated with 100  $\mu$ L of DCFH-DA 20  $\mu$ M for 1 h. Next, cells were washed with PBS and 100  $\mu$ L of Luperox<sup>®</sup> at 50, 100 and 200  $\mu$ M was added. Fluorescence (at  $\lambda$ excitation = 485 nm/ $\lambda$ emission = 530 nm) was recorded during 180 min using a Synergy HTX Multi-Mode Reader (BioTek<sup>®</sup> Instruments, Vermont, USA) set at 37 °C. Samples without probe, either with or without stressor were used as blanks.

For cell viability under stress conditions: cells were seeded in a 96-well plate at a concentration of 50,000 cells/well (156,000 cells/cm<sup>2</sup>) in 10% FBS DMEM medium. Plates were incubated for 24 h at 37 °C and 5% CO<sub>2</sub>. Medium was taken off and cells were washed with 200  $\mu$ L of PBS. Then, cells were treated with Luperox<sup>®</sup> at 50, 100, 200 or 300  $\mu$ M for 1 h. After induction of stress, Luperox<sup>®</sup> was removed and the MTT test was performed as follows: 200  $\mu$ L of MTT 0.5 g/L in PBS was added to experimental wells, then incubated for 2 h 30 min at 37 °C and 5% CO<sub>2</sub>. MTT was then removed and isopropanol (200  $\mu$ L) was added to each well for 40 min. Absorbance at 570 nm was measured using a microplate reader (Xenius XM, Safas, Monaco). The % Metabolic activity was calculated as described in Section 2.8.1. Experiments were performed in triplicate. Photos were taken after incubation with MTT using a DMi1 inverted microscope (Leica Microsystems, Wetzlar, Germany). Obtained RGB images were converted to grayscale images using Fiji software (ImageJ, NIH, USA, version 2.0.0.).

### 2.8.3. Effect of NLCs on BJ Fibroblasts under Stress Conditions

The influence of NLCs on cell viability was also studied under stress conditions for BJ fibroblasts. They were seeded in a 96-well plate at a concentration of 50,000 cells/well (156,000 cells/cm<sup>2</sup>) in 10% FBS DMEM medium. Plates were incubated for 24 h at 37 °C and 5% CO<sub>2</sub>. Medium was taken off and cells were washed with 200  $\mu$ L of PBS. After 24 h incubation with 10  $\mu$ M CUR-NLCs, 0.54 g/L Blank-NLCs or Trolox at 10  $\mu$ M in 10% FBS DMEM, medium was removed and cells were washed with 200  $\mu$ L of PBS. Then, cells were treated with Luperox<sup>®</sup> at 100  $\mu$ M for 1 h. Afterwards, Luperox<sup>®</sup> was removed and the MTT test was performed as in no stress conditions: 200  $\mu$ L of 0.5 g/L MTT in PBS was added to experimental wells and then plates were incubated for 2 h 30 min (37 °C and 5% CO<sub>2</sub>). After incubation, photos were taken using a DMi1 inverted microscope (Leica Microsystems, Wetzlar, Germany). Obtained RGB images were converted to grayscale images using Fiji software (ImageJ, NIH, USA). MTT was then removed and 200  $\mu$ L of isopropanol was added to each well. Plates were gently stirred and stored at room temperature in the dark for 40 min. The percentage of viable cells was calculated as in no stress conditions through absorbance readings at 570 nm as described in Section 2.8.1 with a microplate reader (Xenius XM, Safas, Monaco).

### 2.9. Cell Migration/Proliferation Assay

Silicone culture inserts (Ibidi, Martinsried, Germany) were used to evaluate the migration/proliferation of dermal cell lines. The protocol was carried out as reported in the literature, with some modifications when needed [37]. Briefly, cells were seeded at a density of 159,000 cells/cm<sup>2</sup> (35,000 cells per well) for BJ fibroblasts and 95,500 cells/cm<sup>2</sup> (21,000 cells per well) for HEK293T in the 2-well culture inserts that were previously attached to the wells of a 12-well plate. After 24 h, inserts were taken off, leaving a cell-free gap. Cells were washed twice with 2 mL of PBS. Then, 2 mL of 10% FBS DMEM or DBM containing CUR (0–20  $\mu$ M) or CUR-NLCs (1–20  $\mu$ M of loaded CUR in 0.05–1.10 g/L of NLC suspension) or Blank-NLCs (0.05–1.10 g/L) was added to the cells. Phase-contrast images of the gap were taken immediately after adding the treatment using a DMi1 inverted microscope (Leica Microsystems, Wetzlar, Germany). Cells were incubated for 24 h and photos were taken again in the same place. For each photo, the areas were measured using the manual area measurement tool in the Fiji software (ImageJ, NIH, USA). For each sample, 5 images corresponding to different places along the gap were analyzed. Experiments were repeated twice. Pixel size at the specimen level was 0.235  $\mu$ m.

For controls, cell medium (10% FBS DMEM or DBM, for BJ fibroblasts and HEK293T, respectively), was used without CUR, Blank-NLCs or CUR-NLCs.

Reduction in the gap area was determined by comparing the areas in the photos at 0 h with the ones at 24 h with the following equation:

$$\% \text{ Reduction of gap area} = 100 - [(\text{Area at 24 h} / \text{Area at 0 h}) \times 100]$$

#### 2.10. Preparation of NLCs Loaded Gel

Carbopol® 980 NF was dispersed at 0.69%, *w/v* in ultrapure water by overnight stirring at room temperature. A total of 25 µL of TEA 20%, *v/v* was added for each mL of the final volume of the gel to be prepared and mixed until obtaining a homogenous mixture. The pH was ensured to be around 7. Then, Blank-NLCs (to form Blank-NLC gels) or CUR-NLCs (to form CUR-NLC gels) were added at 25% *v/v* of the final target volume of gel. The mixture was stirred and the final pH was checked to be around 6.4. To prepare the unloaded gel, NLCs were replaced by ultrapure water. The final Carbopol® 980 NF concentration in the gel was 0.50% *w/v*.

#### 2.11. Rheological Characterization of NLCs Loaded Gel

All characterization was performed using a stress-controlled rheometer (Discovery HR-1, TA Instruments, New Castle, DE, USA) joined to a cone-plane geometry (diameter: 40 mm, truncation gap: 27 µm and cone angle: 1.005°). Results were obtained with Trios V4.7 software (TA Instruments, New Castle, DE, USA). Every analysis was performed at 32 °C (the temperature on the surface of the skin). For each condition, experiments were repeated three times (*n* = 3).

In order to determine the linear viscoelastic region (LVE), strain sweep experiments were carried out at 1 Hz. To study the behavior of the formulations when applied and rubbed on the surface of the skin, flow curves of the viscosity in function of the shear rate (from 0.001 s<sup>-1</sup> to 1000 s<sup>-1</sup>) were constructed.

A strain recovery test was performed in order to mimic the behavior of the formulations during application. For this, viscosity of the sample was continuously monitored while applying intercalated low and high shear cycles. Starting with a low shear cycle, a total of five cycles were applied during each single test. The three low shear cycles were performed at 0.1 s<sup>-1</sup> for 150 s and the two high shear cycles at 100 s<sup>-1</sup> for 30 s.

#### 2.12. Penetration Studies with CUR-NLCs and CUR-NLCs/Gel

Strat-M® membranes (25 mm) were obtained from Merck KGaA (Darmstadt, Germany). Due to their multi-layer composition, they have proven to be good at mimicking intact skin barrier properties [38,39]. Immediately after unpacking, each membrane was clamped between the donor and the receptor compartment of a vertical Franz diffusion cell of 9 mm diameter. The donor and receptor compartments were filled with 5 and 1 mL PBS at pH 5.5 (pH regulated with HCl 1 M), respectively, and placed in a water bath at 32 °C, to mimic the temperature at the surface of skin, and under stirring at 290 rpm. After 10 min, PBS was removed from the donor compartment and replaced with either 1 mL of CUR-NLC suspension in ultrapure water containing 122 ± 4 µg of CUR, or 1 g of CUR-NLCs/gel containing 125 ± 4 µg of CUR, prepared as described in Section 2.10. After 15 min, 30 min, 1 h and 24 h of incubation, membranes were removed, excess CUR-NLCs and gel materials were removed with a clean paper and membranes were washed 3 times with ultrapure water. Excess water was removed by blotting, membranes were cut into small pieces and kept overnight under magnetic stirring in determined volumes of ACN/H<sub>2</sub>O (50/50%, *v/v*) in order to extract penetrated CUR: 2 mL for CUR-NLCs/gel samples and CUR-NLC samples after 15 min; 3 mL for CUR-NLC samples after 30 min; 5 mL for CUR-NLC samples after 1 h and 9 mL for CUR-NLC samples after 24 h. Samples were then centrifuged at 4000 rpm for 10 min and supernatant was analyzed using HPLC for determining the amount of CUR penetrated into the membranes (Q<sub>T</sub>). Throughout the diffusion experiments 1 mL was



removed from the receptor compartment every 1 h and analyzed by DLS as specified in Section 2.5.1. Volume taken off was replaced by an equal volume of PBS at pH 5.5.

The amount of CUR remaining in the donor compartment was determined at the end of each timepoint. For that, CUR-NLC suspension (0.5 mL) or CUR-NLCs/gel (500 mg) were collected from the donor compartment. Samples were freeze-dried, dissolved in 4 mL of EtOH/DCM (60/40%, *v/v*) and then centrifuged at 4000 rpm for 15 min. Absorbance was measured by UV-VIS spectrophotometry. All experiments were performed in triplicate ( $n = 3$ ).

From the amount of CUR penetrated into membranes ( $Q_T$ ), the amount of drug entrapped per unit area ( $De$ ) was calculated as follows [40]:

$$De = Q_T / A$$

where  $A$  is the area available for penetration ( $2.54 \text{ cm}^2$ )

The accumulation ( $Ac$ ) was then calculated by:

$$Ac = De / C_d$$

where  $C_d$  is the starting CUR mass concentration loaded in the donor compartment

### 2.13. Statistical Analysis

The software OriginPro 2018 (Northampton, MA, USA, version 9.5) was used. All results are presented as mean  $\pm$  standard deviation (SD). For the MTT test, the analysis of statistical significance was performed using one-way analysis of variance (ANOVA) followed by Tukey's multiple comparison HSD (honestly significant difference) post hoc test. For penetration studies, analysis of the statistical significance was performed using two sample Student's *t*-test.

## 3. Results

### 3.1. Preparation and Quantification of CUR-NLCs

The oil phase, composed of the solid (Precirol<sup>®</sup> ATO 5) and the liquid (Labrafac<sup>®</sup> lipophile WL 1349) lipids into which the CUR and the co-surfactant (Tween<sup>®</sup> 80) are introduced, is mixed with the aqueous solution that contains the surfactant (poloxamer) (Figure 1A).

NLC aqueous suspensions were obtained by the hot homogenization method (see Section 2.4). For CUR-NLCs, total CUR introduced into the preparation is distributed between the NLCs (Loaded-CUR) and the pellets (Excess-CUR) (Figure 1B). NLCs remain in the supernatant after centrifugation. For the direct quantification method, the supernatant is diluted with a binary solvent composed of EtOH/DCM (60/40%, *v/v*). This binary solvent was chosen for its high solubility power for lipids [35] and used for all spectrophotometric measurements. The standard CUR and loaded CUR show the same absorption spectra with a  $\lambda_{\text{max}} = 427 \text{ nm}$ . The CUR calibration curve gives an extinction coefficient of  $\epsilon_{427 \text{ nm}} = 0.143 \text{ } \mu\text{g}^{-1} \cdot \text{mL}$  (Figure 2, direct method). For the indirect quantification method, the pellet was dissolved in ACN for HPLC analysis. The standard CUR and Excess-CUR chromatograms present the same peaks corresponding to the three components of CUR: bisdemethoxycurcumin (retention time,  $R_t$  of 7.55 min), demethoxycurcumin ( $R_t$  7.79 min) and curcumin ( $R_t$  8.04 min). The percentages of these three components of CUR were determined from relative area peaks: curcumin (79%), demethoxycurcumin (19%) and bisdemethoxycurcumin (2%). These results confirm the purity given by the supplier and allow us to calculate a mean molecular weight for CUR: MW 361.4 g/mol. Chromatograms and CUR calibration curves based on the three peaks integration is presented in Figure 2, indirect method.

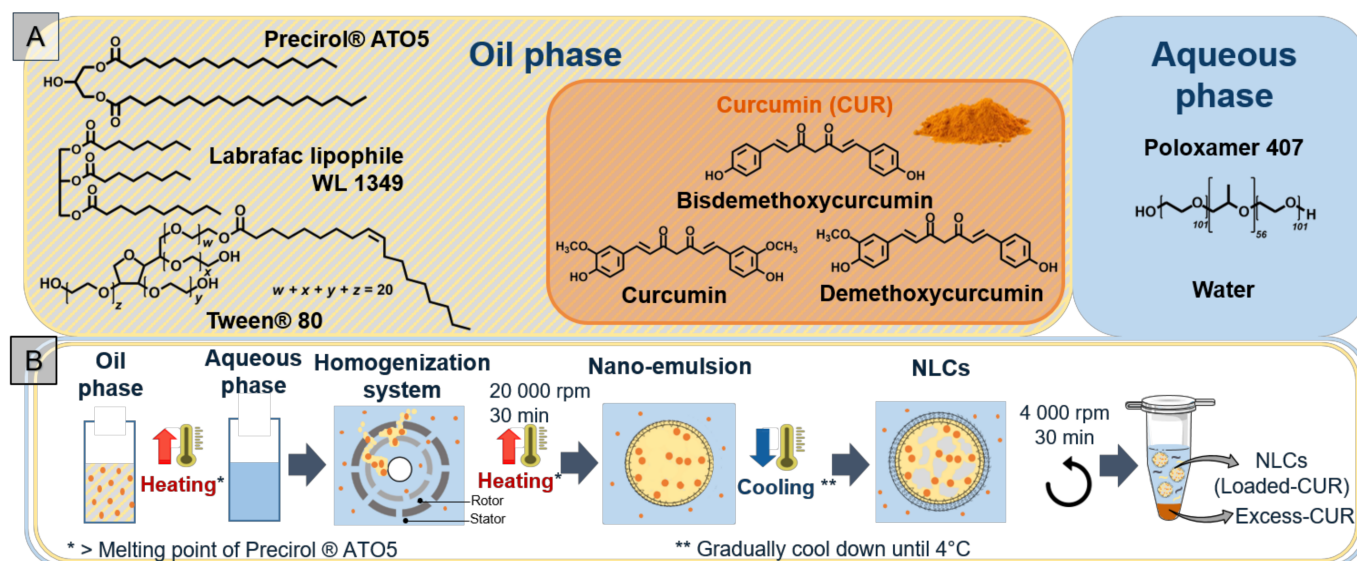


**Figure 1.** (A) Components of NLCs: in yellow and grey striped box, lipids (solid and liquid), co-surfactant and CUR, composed of three curcuminoids (orange box); in blue box, aqueous phase containing the surfactant. (B) NLCs preparation by hot homogenization method at heating temperature of 70 °C and separation of non-loaded CUR (Excess-CUR) by centrifugation. (Created with BioRender.com (accessed on 26 April 2022)).

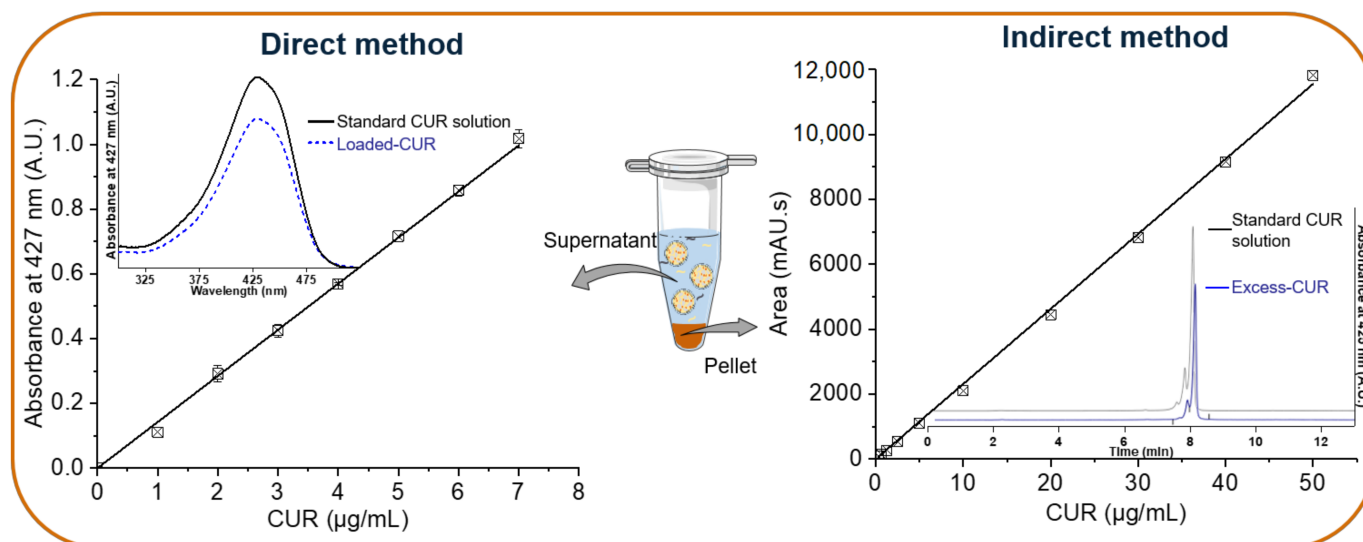


**Figure 2.** Quantification of loaded CUR in NLCs by the direct and indirect methods. For direct method NLCs were dissolved in a binary solvent composed of EtOH/DCM (60/40% *v/v*) before spectrophotometric analysis. For indirect method excess CUR was dissolved in ACN and determined by HPLC-DAD. (Created with BioRender.com (accessed on 26 April 2022)).

Table 1 shows results of CUR quantification in NLCs obtained before the SEC column step. Similar results for loaded CUR were obtained with the direct and indirect methods (0.85 mg/mL and 0.83 mg/mL, respectively), showing the accuracy of the UV-VIS spectrophotometry method. After preparation of CUR-NLCs, nearly 85% of CUR was encapsulated (%EE, Table 1). A CUR drug loading (%DL) of approximately 2.3% indicates the predominance of lipid nature in CUR-NLCs. This highlights the importance of taking unloaded Blank-NLCs as a control group for antioxidant and biological experiments in order to get an accurate understanding of the effects of the loaded drug. Results of CUR quantification in NLCs obtained by the direct method (UV-VIS) before and after

SEC column purification are compared in Table 2. When comparing CUR quantification (loaded CUR and EE%) in NLCs before and after the SEC column, a ratio of ~1.5–2 is found (0.85 mg/mL vs. 0.44 mg/mL, for loaded CUR and 84.56% vs. 54.79%, for EE%). These results could be explained in part by the fact that only fraction numbers 3, 4 and 5 were pooled (see Section 2.4).

**Table 1.** CUR content of NLCs before SEC column step.

	Direct Method	Indirect Method
Loaded CUR (mg/mL) <sup>1</sup>	0.85 ± 0.04	0.83 ± 0.03
%EE <sup>2</sup>	84.56 ± 4.48	83.40 ± 3.63
%DL <sup>3</sup>	2.33 ± 0.10	2.23 ± 0.12

<sup>1</sup> Loaded-CUR in NLCs refers to the mass concentration of CUR loaded in NLCs after preparation. <sup>2</sup> Encapsulation efficiency (%EE) of CUR-NLCs refers to the concentration of CUR incorporated into NLCs over the initial CUR concentration (1 mg/mL). <sup>3</sup> Drug loading (%DL) of CUR-NLCs refers to the amount of CUR incorporated into NLCs per weight of lipids (*w/w*). All values were obtained by direct and indirect method measurements. CUR determination in each batch was performed in triplicate (*n* = 3).

**Table 2.** CUR content of NLCs before and after SEC column obtained by direct method.

	Before SEC Column	After SEC Column
Loaded CUR (mg/mL) <sup>1</sup>	0.85 ± 0.04	0.44 ± 0.04
%EE <sup>2</sup>	84.56 ± 4.48	54.79 ± 6.09

<sup>1</sup> Loaded-CUR in NLCs refers to the mass concentration of CUR loaded in NLCs. <sup>2</sup> Encapsulation efficiency (%EE) of CUR-NLCs refers to the mass concentration of CUR in fractions 3–5 after SEC (mg/mL), over CUR mass concentration before SEC (mg/mL). CUR determination in each batch was performed in triplicate (*n* = 3).

### 3.2. Physicochemical Characterization

NLCs samples were characterized after 1 day and before and after the SEC column (Table 3, values of day 1). Particle size analysis, expressed as % of intensity or number, evidenced two populations of NLCs: a small-size-NLC population (P1, 70–90 nm) and a large-size-NLC population (P2, 300–350 nm). Distribution of these two populations was ~20% (P1) and ~80% (P2) expressed as % of intensity. However, when NLC size was expressed as % of number, the small-size-NLC population, P1, represented the principal peak (Figure 3). In all cases PDI was between 0.34–0.44. Blank-NLCs and CUR-NLCs present similar size and distribution profiles. ZP measurements showed a slight difference in the NLC surface charge before and after the SEC column (~−9 mV and ~−17 mV, respectively).

**Table 3.** Sizes (expressed as % of intensity) of CUR- and Blank-NLCs at 1 and 7 days before and after SEC column.

Day		Before SEC Column				After SEC Column			
		Blank-NLCs		CUR-NLCs		Blank-NLCs		CUR-NLCs	
		P1	P2	P1	P2	P1	P2	P1	P2
1	Size (nm)	77 ± 8	313 ± 37	72 ± 11	308 ± 36	89 ± 1	350 ± 16	72 ± 18	310 ± 24
7	Size (nm)	77 ± 10	318 ± 38	76 ± 15	362 ± 84	73 ± 23	329 ± 30	79 ± 18	348 ± 6

Results were done by duplicate (*n* = 2).

Ovoid shape NLCs were observed by cryo-TEM and negative-stain-TEM analyses (Figure 4A,C and Figure 4B,D, respectively). Observations confirmed the polydispersity and the presence of two size populations in Blank-NLCs and CUR-NLCs. Analyses by the cryo-TEM technique showed that small-size NLCs adopt two preferential conformations: an ovoid shape conformation when observed by the top view and a rod shape when NLCs are observed by the side view (yellow arrows in Figure 4A,C). Only ovoid shape conformation was observed for large-size NLCs (red arrows in Figure 4A,C). These results

point to a main ovoid platelet shape in NLCs. Some particles are surrounded by a darker edge, in both the top and the side view (red and yellow arrows on Blank-NLCs after the SEC column, in Figure 4C). A small compartment seems to be present inside or at the surface of some particles (Figure 4B,D).

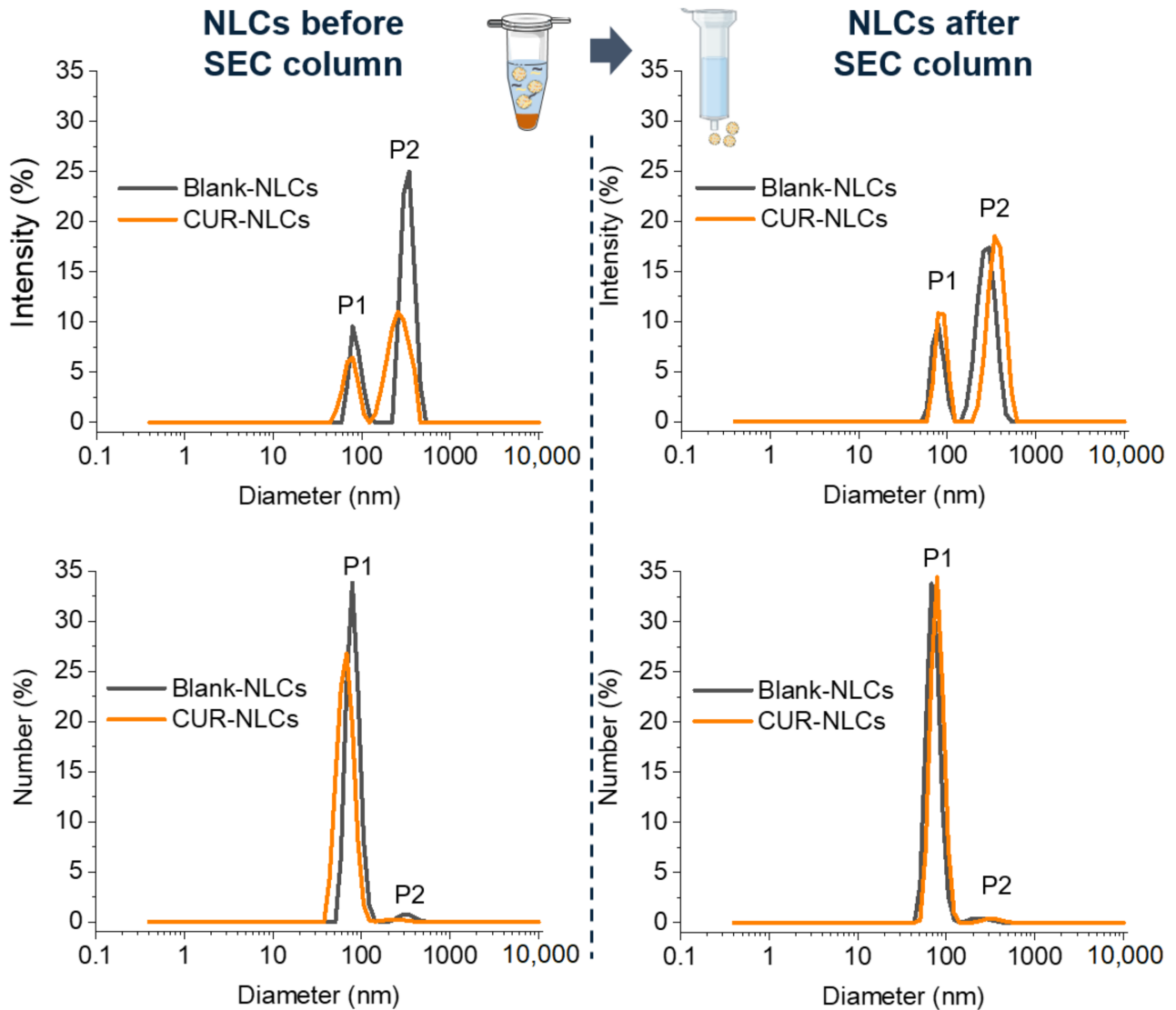


**Figure 3.** Particle size analysis in % intensity and in % number of Blank-NLC and CUR-NLC suspensions before and after passing through the SEC column. (Created with [BioRender.com](https://www.biorender.com) (accessed on 26 April 2022)).

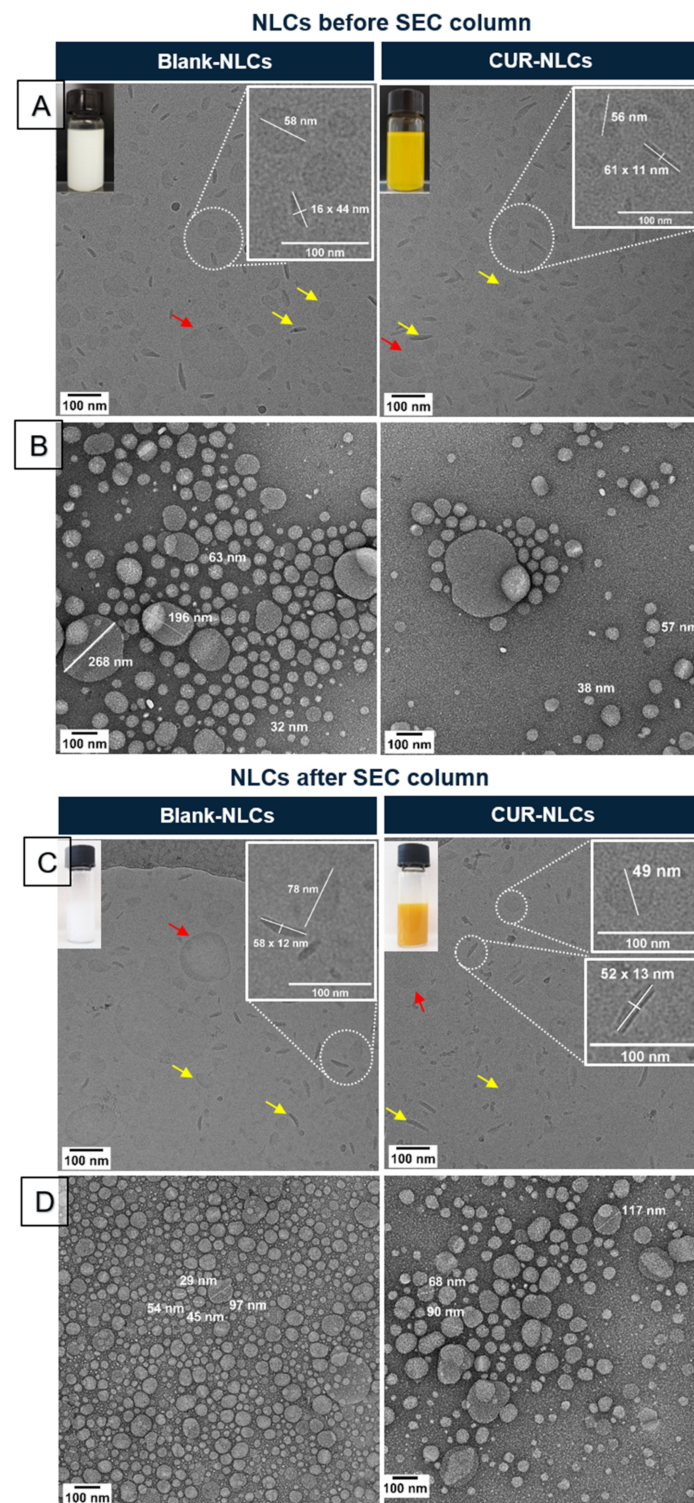


**Figure 4.** Morphological characterization of Blank-NLC and CUR-NLC suspensions. (A) Visual aspect and cryo-TEM images of samples before passing through the SEC column. (B) TEM images of samples before passing through the SEC column and after negative staining with uranyl acetate 2% *v/v* in water. (C) Visual aspect and cryo-TEM images of samples after passing through the SEC column. (D) TEM images of samples after passing through the SEC column and after negative staining with uranyl acetate 2% *v/v* in water. Yellow arrows show the ovoid platelet (top view) or rod (side view) shapes of small-size-NLC population. Red arrow shows the top view of large-size-NLC population.

Stability studies of NLC samples were carried out after 7 days on both NLC samples before and after the SEC column (Table 3, values of day 7). DLS measurements show that size did not significantly change over this period of time for Blank-NLCs or CUR-NLCs (Table 3). Considering the possibility of storing NLC samples until their SEC column purification, further studies about the stability of NLC samples before the SEC column were carried out. DLS measurements were carried out at 1, 7, 14, 30 and 45 days after preparation of NLC samples before the SEC column. Results show that size and distribution do not significantly change over time (Figure 5A).

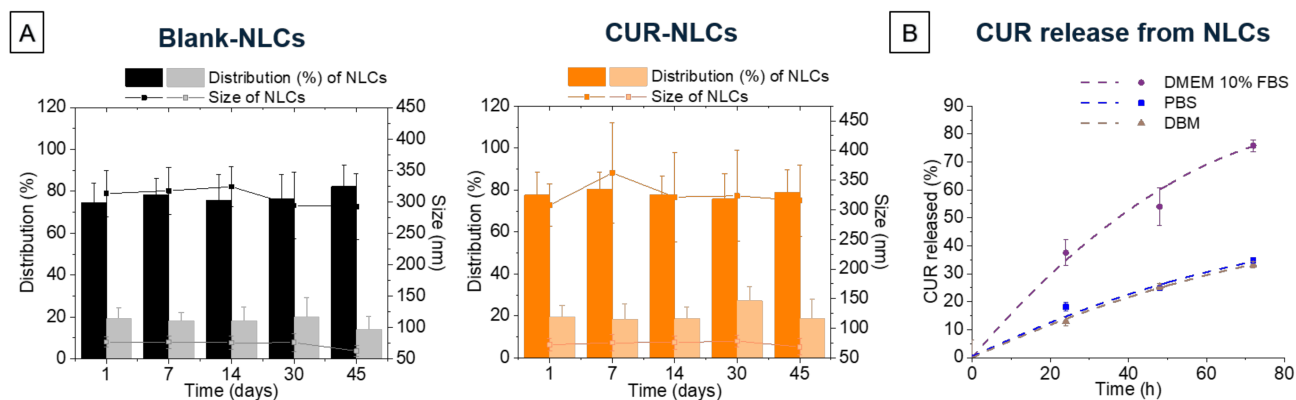


**Figure 5.** NLCs stability and CUR release. (A) Stability of Blank-NLCs and CUR-NLCs before SEC column at 1, 7, 14, 30 and 45 days. Bar graphs indicate the distribution in % intensity of NLCs, while line and dot graphs indicate the size of each NLC population in terms of their diameter. (B) CUR release from NLCs (after SEC column) in different biological media.

Figure 5B represents CUR release from NLCs (after SEC column) in different biological media without proteins (PBS) and with proteins (10% FBS DMEM and supplemented DBM). Delivery kinetics are the same for PBS and DBM, with a 35% CUR release after 72 h. In 10% FBS DMEM, release is slightly more than two times higher (75% after 72 h).

### 3.3. Study of NLCs Antioxidant Activity

Inhibition curves for CUR (Figure 6A) and CUR-NLCs before (Figure 6C) and after the SEC column (Figure 6D) were obtained by plotting the ABTS<sup>•+</sup> inhibition % vs. the concentration of CUR.  $\alpha$ -Tocopherol (Figure 6B) was used as an antioxidant standard. A background activity was observed for Blank-NLCs, which was subtracted from the activity of CUR-NLCs in order to only take into account the antioxidant activity of CUR.

The inhibition % of ABTS<sup>•+</sup> was proportional to the CUR concentration in NLCs up to 50  $\mu$ M (Figure 6C). For higher CUR concentrations in NLCs before the SEC column a saturation activity was observed with an inhibition plateau (data not shown). This saturation effect was not observed at the same range concentrations for the other formulations (CUR, CUR-NLCs after the SEC column and  $\alpha$ -tocopherol).

Figure 6A shows the antioxidant activity of CUR and has a slope of 0.28. Higher slopes of CUR-NLCs before and after the SEC column were found when compared with CUR (1.12 and 1.95, respectively, Figure 6C,D). Table 4 shows the  $\alpha$ -TEAC scores, calculated as  $\alpha$ -tocopherol equivalents ( $\mu$ M CUR/ $\mu$ M  $\alpha$ -tocopherol).

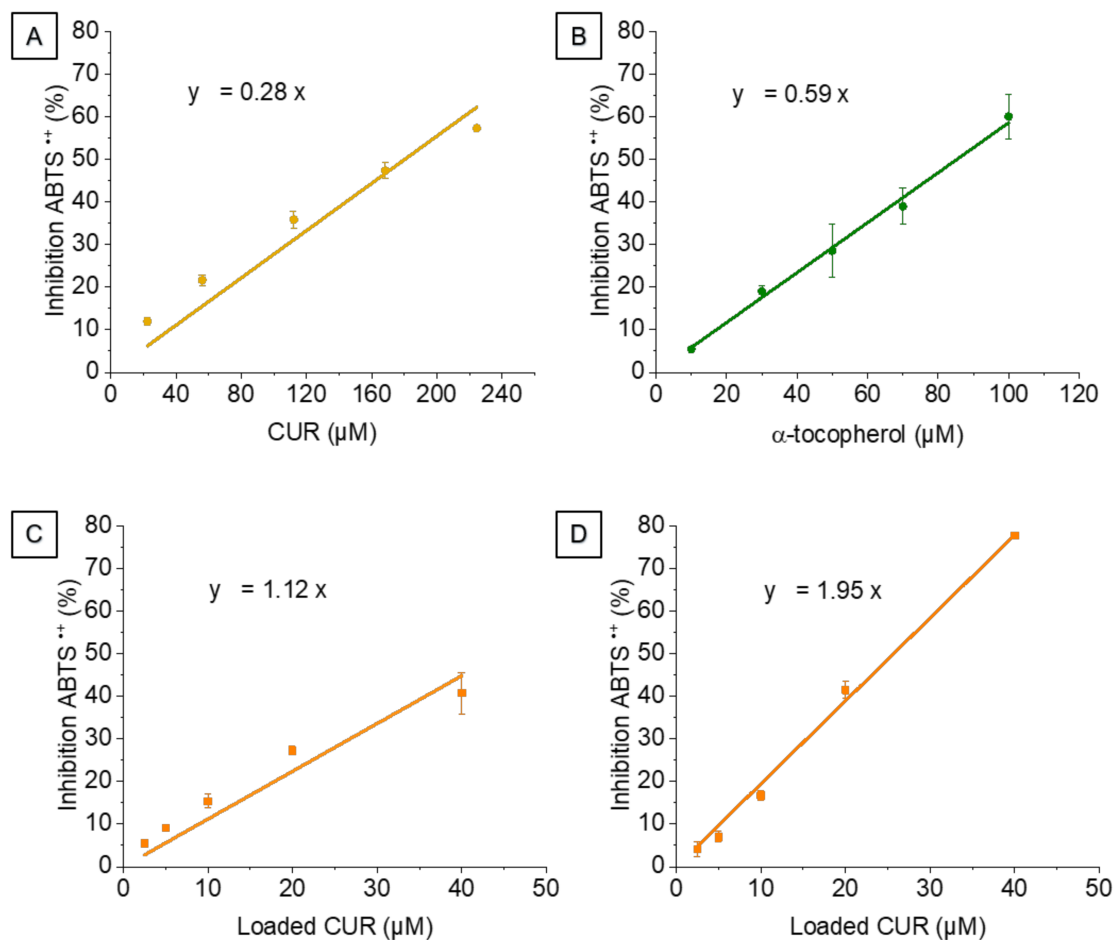


**Figure 6.** Inhibition of ABTS<sup>•+</sup> at different antioxidant concentrations. (A) CUR. (B) α-Tocopherol, antioxidant standard. (C) Loaded CUR in CUR-NLCs before SEC column. (D) Loaded CUR in CUR-NLCs after SEC column.

**Table 4.** Antioxidant activity measured by lipophilic ABTS assay.

	α-TEAC <sup>1</sup>
CUR	0.47
CUR-NLCs before SEC	1.90
CUR-NLCs after SEC	3.31

<sup>1</sup> α-TEAC is expressed as μM CUR/μM α-tocopherol. Each sample was analyzed in triplicate.

### 3.4. NLCs Biological Characterization

#### 3.4.1. Cell Viability Evaluation—MTT and TB Assays

The evaluation of the effects of CUR, CUR-NLCs and Blank-NLCs on cellular metabolism and viability was performed on BJ fibroblasts (Figure 7) and HEK293T cells (Figure 8) using the MTT and TB methods. In the MTT test, a tetrazolium salt is reduced mainly by mitochondrial dehydrogenases in metabolically active cells, giving rise to a purple formazan product whose concentration can be quantified through absorbance measurements [41]. The TB test is based on the principle that the membranes of living cells do not allow the passage of certain compounds, including dyes such as trypan blue. Incubated with the dye, living cells therefore remain colourless, while the weakening of the membrane in dead cells allows the passage of the dye and the cells therefore become blue.

## BJ Fibroblasts in basal conditions

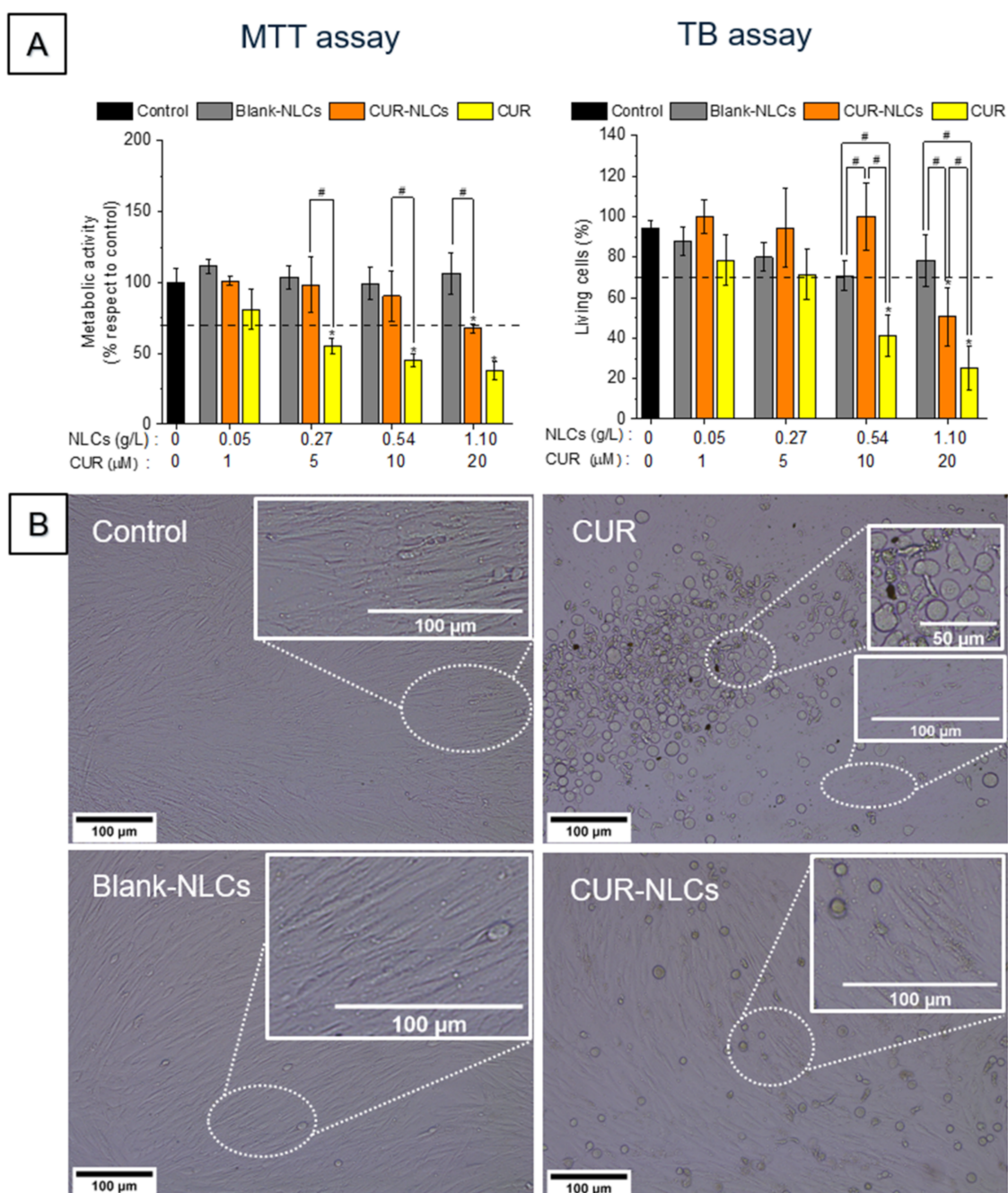


**Figure 7.** Cell viability assays on the BJ fibroblast cell line in basal conditions after 24 h treatment with CUR, CUR-NLCs or Blank-NLCs. **(A)** MTT and TB assays on BJ fibroblasts. **(B)** Phase contrast images of BJ fibroblasts after 24 h treatment with 10% FBS DMEM alone as control; CUR at 20  $\mu\text{M}$ ; Blank-NLCs at 1.1 g/L; or CUR-NLCs at 1.1 g/L containing 20  $\mu\text{M}$  of loaded CUR. Asterisks denote statistically significant differences between an experimental group and the control group, while hashes denote statistically significant differences between two experimental groups. One-way analysis of variance (ANOVA) followed by Tukey's multiple comparison HSD post hoc test were carried out and statistically significant differences were identified when  $p$ -values were lower than 0.05 (\*  $p < 0.05$  or #  $p < 0.05$ ).

In the case of BJ fibroblasts (Figure 7), after 24 h treatment with CUR ( $\geq 5 \mu\text{M}$  of CUR), cells showed a loss of metabolic activity and an important diminution in the number of



living cells compared with the control group ( $p < 0.05$ ). Treatment of BJ fibroblasts with CUR-NLCs or Blank-NLCs did not induce cellular behavior changes compared with the control group. However, cells cultured with 20  $\mu\text{M}$  CUR-NLCs showed a diminution in their metabolic activity and viability ( $p < 0.05$ ).

## HEKn in basal conditions

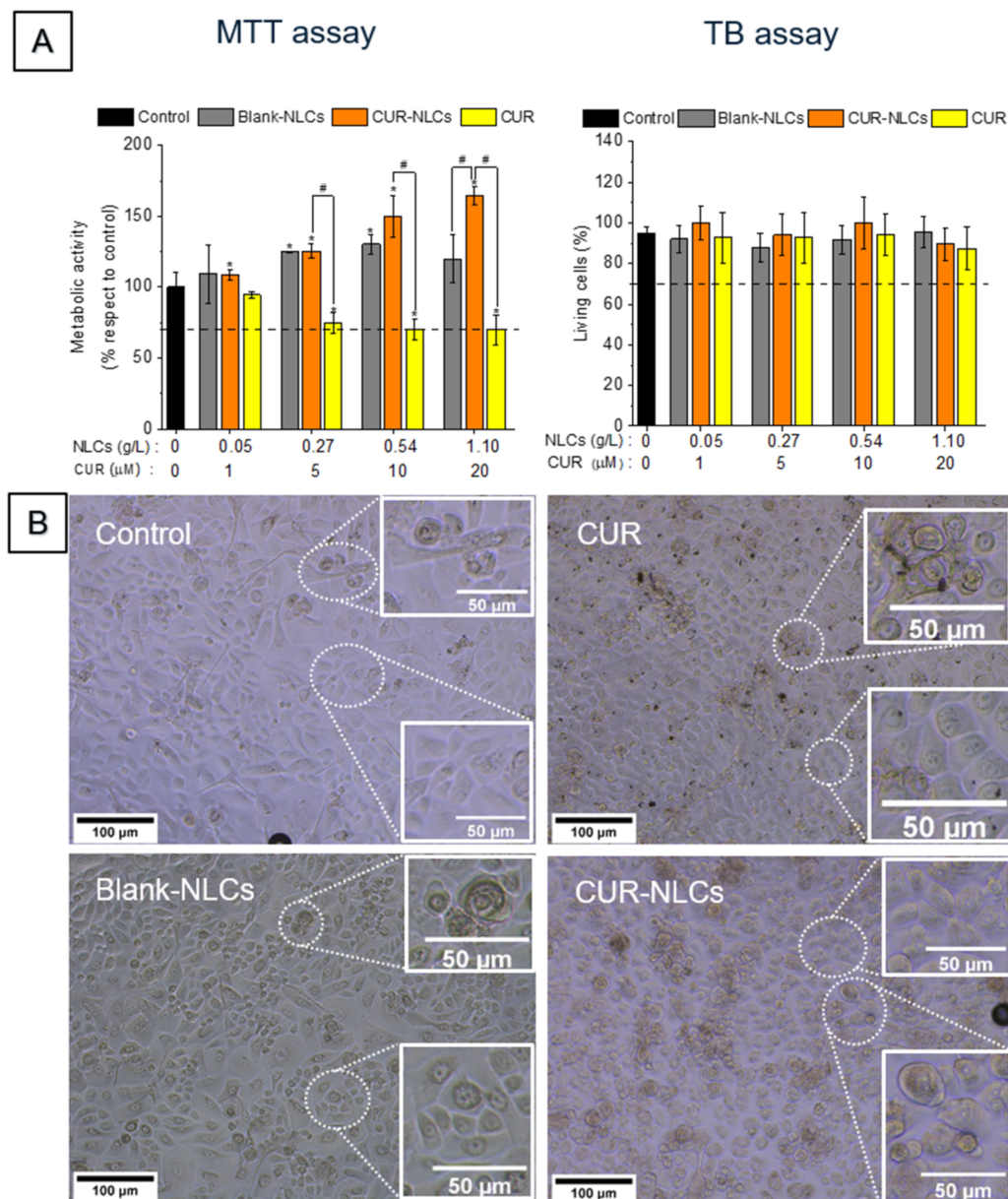


**Figure 8.** Cell viability assays on the HEKn cell line in basal conditions after 24 h treatment with CUR, CUR-NLCs or Blank-NLCs. **(A)** MTT and TB assays on HEKn. **(B)** Phase contrast images of HEKn after 24 h treatment with 10% FBS DMEM alone as control; CUR at 20  $\mu\text{M}$ ; Blank-NLCs at 1.1 g/L; or CUR-NLCs at 1.1 g/L containing 20  $\mu\text{M}$  of Loaded CUR. Asterisks denote statistically significant differences between an experimental group and the control group, while hashes denote statistically significant differences between two experimental groups. One-way analysis of variance (ANOVA) followed by Tukey's multiple comparison HSD post hoc test were carried out and statistically significant differences were identified when  $p$ -values were lower than 0.05 (\*  $p < 0.05$  or #  $p < 0.05$ ).

Treating HEK293 cells with CUR ( $\geq 5 \mu\text{M}$  of CUR) induced a loss of metabolic activity, which was visible after 24 h (Figure 8, MTT assay) ( $p < 0.05$ ). However, the TB test showed a number of living cells (Figure 8, TB assay) comparable to the control cells. Surprisingly, the treatment of HEK293 cells with CUR-NLCs or Blank-NLCs induced an increase in cellular metabolism compared with the control group. The cellular viability was found comparable to the control.

Taking into account the ISO 10993–1:2018 norm criteria regarding the evaluation of medical devices, Blank-NLCs have no toxic effect up to 1 g/L (20  $\mu\text{M}$  of CUR) on both studied dermal cell lines. CUR-NLCs present no cytotoxicity at concentrations  $\leq 20 \mu\text{M}$  of CUR on HEK293 cells and  $\leq 10 \mu\text{M}$  of CUR on BJ fibroblasts. In contrast, the tested CUR concentrations ( $\geq 5 \mu\text{M}$ ) might be classified as cytotoxic as the cell viability is  $\leq 70\%$  compared with the control.

### 3.4.2. BJ Fibroblasts under Stress Viability Evaluation

Oxidative stress can be induced in cells and tissues by different types of stressors that trigger different levels of toxicity in cells according to their chemical composition but also according to their concentration. In this work, we chose to evaluate the induction of oxidative stress by tert-butylhydroperoxide (Luperox®). In order to find the optimal concentrations of Luperox® that do not affect the morphology or metabolic activity of the cells, increasing concentrations of the stressor were added to the cells. Then, the intracellular kinetics of ROS production was evaluated by measuring the fluorescence responsiveness of the probe, DCFH-DA, for 180 min (Figure 9A). Results show that the concentration of 100  $\mu\text{M}$  Luperox® induced a significant fluorescent signal (Figure 9B), corresponding to the ROS production by cells. In parallel, the viability of BJ fibroblasts under the same Luperox® concentration was confirmed by an MTT assay (Figures 9C and 10B (control)).

#### Oxidative stress induction and evaluation on BJ Fibroblasts

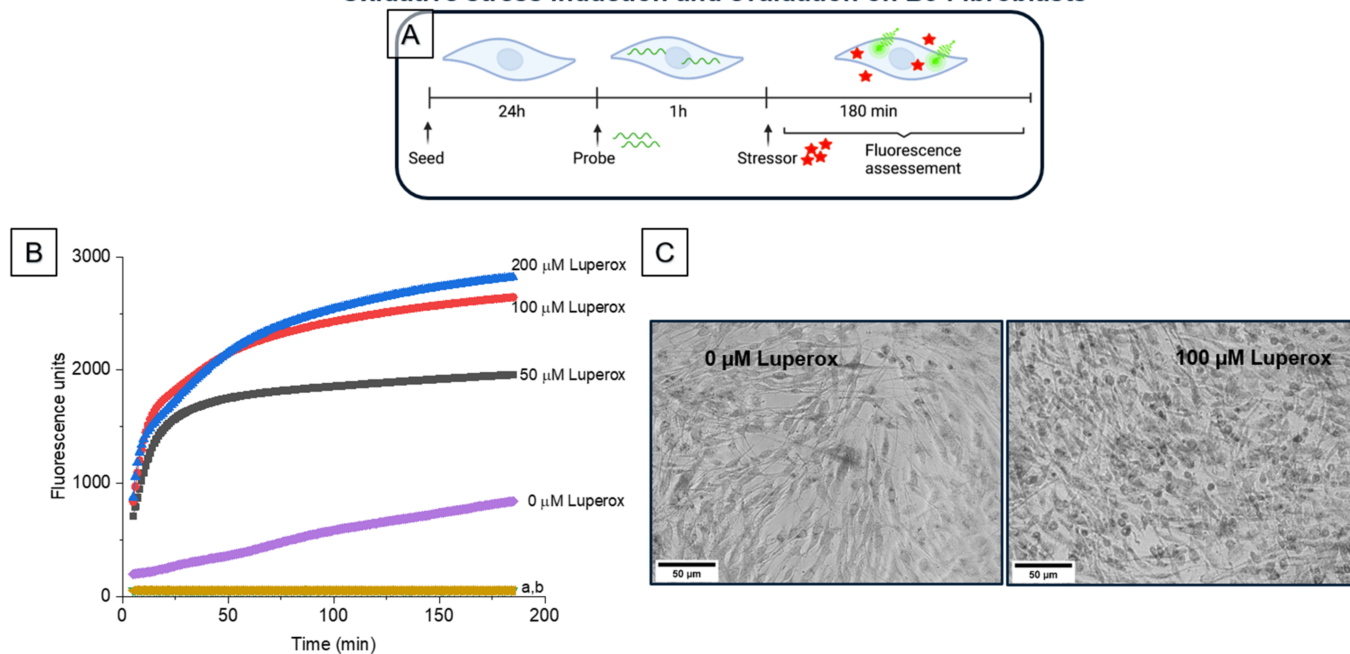


**Figure 9.** Evaluation BJ fibroblasts under oxidative stress. (A) In vitro stress model for the induction and the evaluation of oxidative stress. (B) Evaluation of oxidative stress induced by different concentrations of the stressor (Luperox). a: Cells exposed to the probe but not the stressor. b: Cells exposed to neither the probe nor the stressor. (C) Phase contrast images of BJ fibroblasts after 1 h treatment with 0  $\mu\text{M}$  or 100  $\mu\text{M}$  of stressor and subsequently incubated with MTT for 2 h 30 min. (Created with [BioRender.com](https://www.biorender.com) (accessed on 26 April 2022)).

With the aim of evaluating BJ fibroblasts metabolism under stress conditions in response to the presence of NLCs loaded or not with CUR, we assessed the fluorescence reactivity of the probe to Luperox<sup>®</sup> at 100  $\mu$ M. The cells were pretreated with Blank-NLCs or CUR-NLCs (24 h) before the stress induction; for the positive control we treated the cells with a reference antioxidant, Trolox; for the negative control the cells did not receive any antioxidant treatment (Figure 10A). Results show that the exposure of cells to NLCs (0.54 g/L or 10  $\mu$ M of CUR) does not induce significant changes in metabolism or cell morphology (Figure 10B,C).

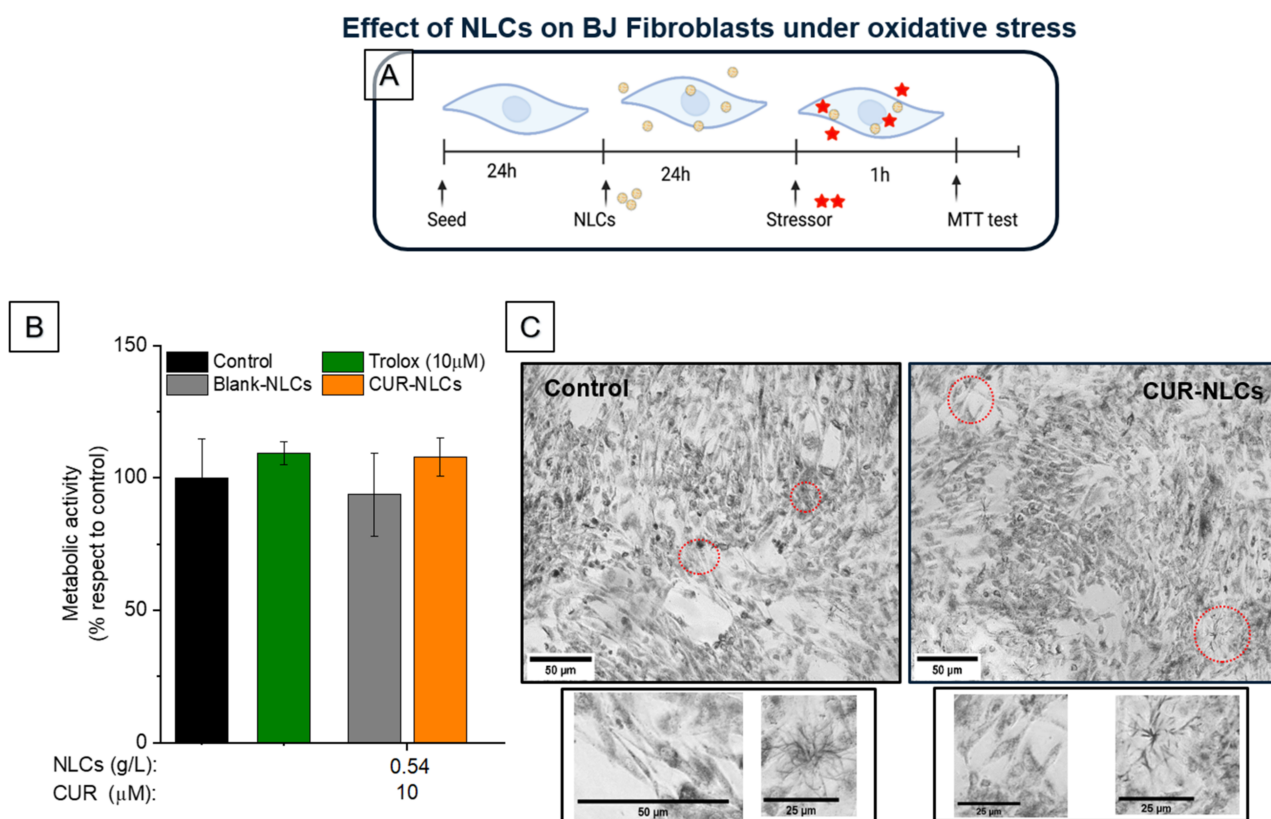


**Figure 10.** Effects of NLCs on BJ fibroblasts under oxidative stress. (A) In vitro model for the evaluation of the effect of NLCs on BJ fibroblast metabolic activity after undergoing oxidative stress for 1 h. (B) Impact of Blank-NLCs and CUR-NLCs on the metabolic activity of BJ fibroblasts undergoing oxidative stress; Trolox 10  $\mu$ M was used as an antioxidant standard. (C) Phase contrast images of BJ fibroblasts after treatment with 10% FBS DMEM alone as control, or 0.54 g/L of CUR-NLCs containing 10  $\mu$ M of CUR for 24 h prior to exposure to 100  $\mu$ M of stressor for 1 h and subsequent incubation with MTT for 2 h 30 min. Images in the lower panel correspond to magnifications of the indicated zones in the upper part of the images (red circles). Extended morphology of fibroblasts as well as the formation of formazan crystals can be distinguished, evidencing metabolically active cells. (Created with [BioRender.com](https://www.biorender.com) (accessed on 26 April 2022)).

### 3.4.3. Cell Migration/Proliferation Studies

The capacity of BJ fibroblasts (Figure 11A) and HEK293T cells (Figure 11B) to migrate and or proliferate after 24 h of culture were evaluated using an in vitro model [37]. Cell motility and proliferation were evaluated by image analysis according to the capacity of cells to migrate and fill the cell-empty gap initially created. Results were expressed as gap reduction (%) after 24 h.

Effects of CUR (5  $\mu$ M), CUR-NLCs (5  $\mu$ M) and Blank-NLCs (0.27 mg/mL, corresponding to the same lipid content of that in CUR-NLCs at 5  $\mu$ M) were studied and compared with the controls (cell medium without CUR or NLCs) (Figure 11).

Figure 11A shows that after 24 h of culture (control conditions), BJ fibroblasts were able to migrate and reduce the empty zones in the culture plate ( $53 \pm 7\%$  of gap reduction). Similar results were found after 24 h of cell treatment with CUR or Blank-NLCs ( $52 \pm 5\%$  and  $50 \pm 9\%$  gap reduction, respectively), whereas with CUR-NLCs, a moderate reduction in cell motility was observed compared with the control ( $35 \pm 3\%$  of gap reduction). None of the treatments (CUR, Blank-NLCs or CUR-NLCs) seemed to affect the morphology of the BJ fibroblasts compared with the control.

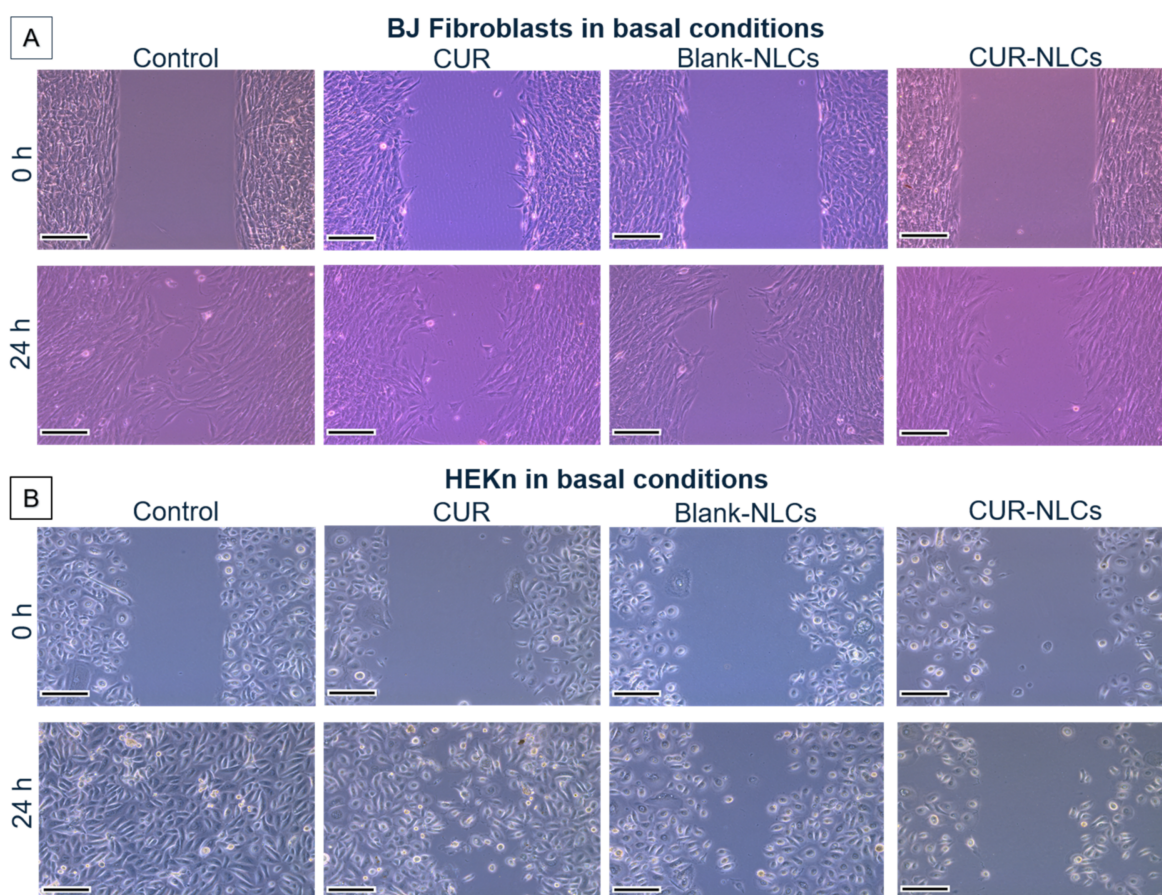


**Figure 11.** Cell migration/proliferation studies on BJ fibroblasts and on HEKn cell lines in basal conditions and under treatment with CUR ( $5 \mu\text{M}$ ), Blank-NLCs ( $0.27 \text{ g/L}$ ) or CUR-NLCs ( $0.27 \text{ g/L}$  containing  $5 \mu\text{M}$  of loaded CUR). (A) Phase contrast images of the gap at 0 h and after 24 h of treatment for BJ fibroblasts. Control group was treated with 10% FBS DMEM. (B) Phase contrast images of the gap at 0 h and after 24 h of treatment for HEKn cells. Control group was treated with DBM. Scale bar:  $100 \mu\text{m}$ .

For migration studies on HEKn cells (Figure 11B), an important cell migration/proliferation capacity with a complete reduction of the gap ( $100 \pm 3\%$  of gap reduction) under cell control conditions was observed. A similar result was obtained for cells treated for 24 h with CUR or Blank-NLCs ( $90 \pm 8\%$  and  $96 \pm 6\%$  of gap reduction, respectively). When CUR-NLCs were added to the medium and put in contact with the HEKn cells, a moderate decrease in cell migration capacity was observed ( $80 \pm 4\%$  of gap reduction). This represents a diminution of 20% in cell migration in the presence of CUR-NLCs for both the BJ fibroblast and HEKn cell lines.

However, in the case of HEK<sub>n</sub> cells, cell morphology is altered by the presence of CUR, Blank-NLCs and CUR-NLCs, displaying a rounder shape compared with the control in all cases. It should be noted that at these NLC concentrations (0.27 mg/mL, corresponding to 5  $\mu$ M of CUR) neither Blank-NLCs nor CUR-NLCs exhibit cell toxicity, as shown in Figure 8A. In the MTT assay, an increase in the metabolic activity due to NLCs is even observed.

### 3.5. Preparation and Rheological Characterization of NLCs Loaded Gel

CUR-NLCs after SEC column purification were incorporated in a Carbopol<sup>®</sup> 980 gel matrix in order to form a dual platform for CUR delivery to the skin (Figure 12).

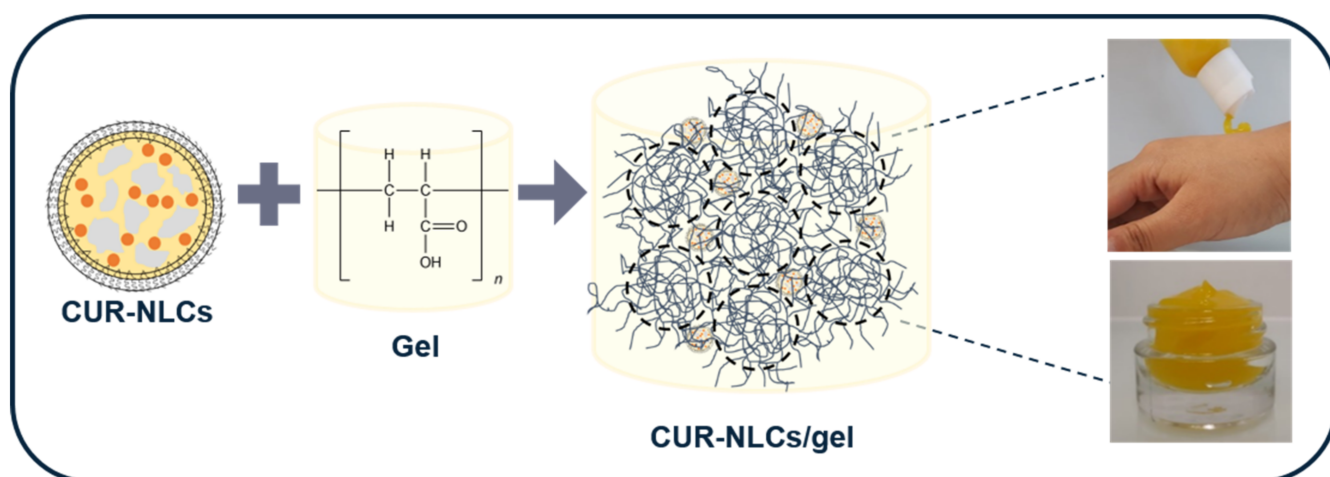


**Figure 12.** Formulation of the multiscale platform NLCs in gel.

As shown in Figure 13A, there were no statistically significant differences in the flow points of the gel alone or the gel containing NLCs (CUR or blank). In all cases, three regions could be distinguished in the graphs. At the beginning of the test, while  $G' > G''$  and their magnitudes remain constant, a consistent structure characteristic of the tridimensional network of a gel is observed. Thus, the addition of NLCs did not hinder the formation of the superstructure of the gel during the preparation. Then, while  $G' > G''$  is maintained but  $G''$  increases and  $G'$  decreases (roughly before  $\gamma = 2\%$ ), the gel superstructure starts to break until the crossover ( $G' = G''$ ). After this point, the viscous behavior prevails over the elastic behavior and there is no more a tridimensional structure. The formulation becomes fluid. Figure 13B indicates that the inclusion of NLCs in the formulation did not change the shear-thinning behavior of the gels. Even if for every sample viscosity decreases with an increasing shear rate, the gels rapidly recover their structure after undergoing a high-shear period of time, as depicted in Figure 13C. In the context of a topical application, this can be translated into easy squeezing from a tube, successfully staying in the skin, and finally, a good spreading during application.

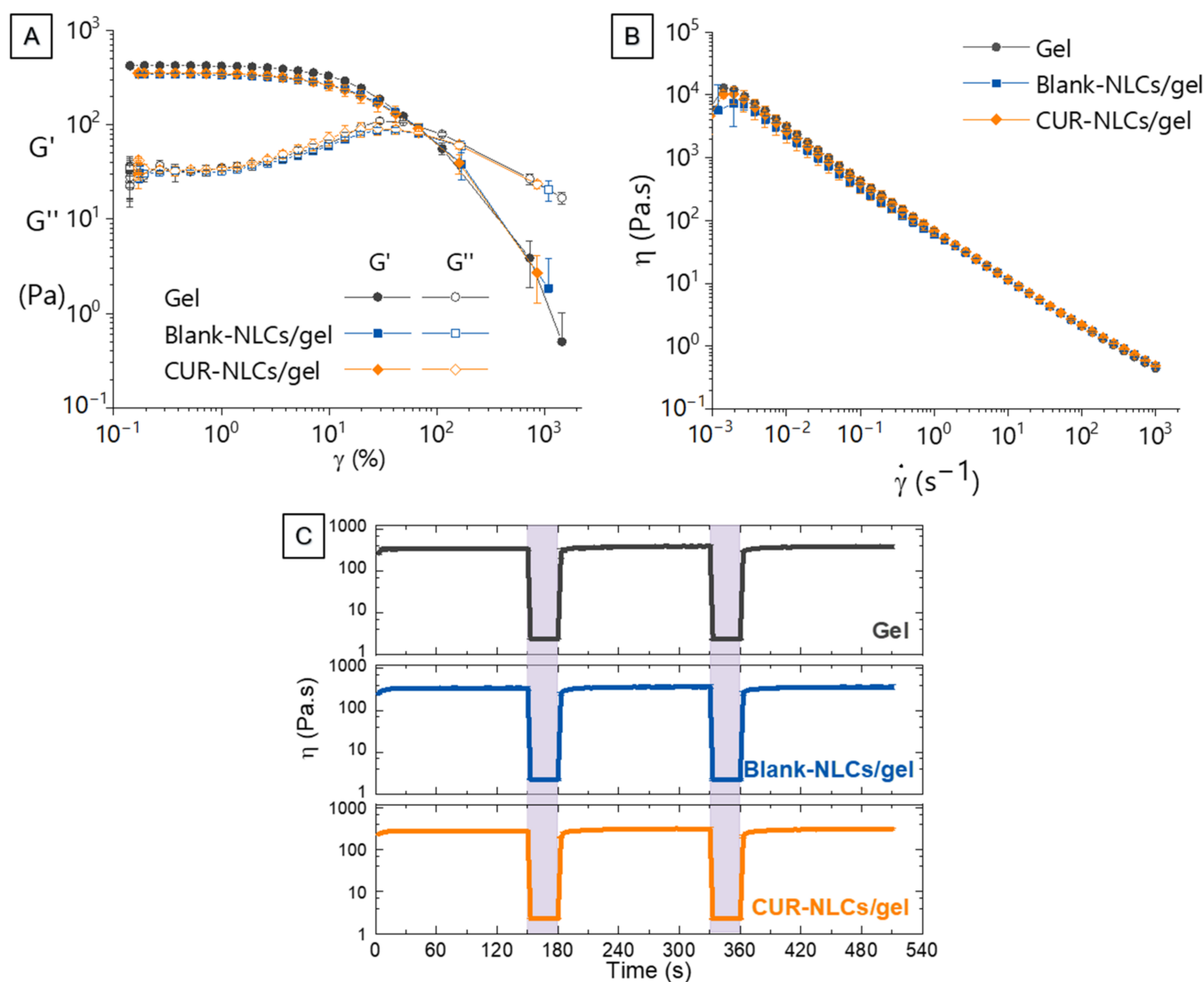


**Figure 13.** Rheological characterization of the multiscale platform NLCs in gel. (A) Strain ( $\gamma$ ) sweep for the Carbopol<sup>®</sup> gel alone, Carbopol<sup>®</sup> gel containing Blank-NLCs and Carbopol<sup>®</sup> gel containing CUR-NLCs. (B) Flow curves: viscosity ( $\eta$ ) in function of shear rate ( $\dot{\gamma}$ ) for Carbopol<sup>®</sup> gel alone, Carbopol<sup>®</sup> gel containing Blank-NLCs and Carbopol<sup>®</sup> gel containing CUR-NLCs. (C) Evaluation of time-dependent flow behavior (recovery test) for Carbopol<sup>®</sup> gel alone, Carbopol<sup>®</sup> gel containing Blank-NLCs and Carbopol<sup>®</sup> gel containing CUR-NLCs.

### 3.6. CUR Penetration from CUR-NLCs and CUR-NLCs/Gel

Penetration studies were performed on synthetic Strat-M<sup>®</sup> membranes. As described in Section 2.12, thanks to their multi-layer composition, this material is known to represent an intact skin barrier and is considered as a pertinent model in mimicking skin properties [38,39]. The timepoints assessed were 15 min, 30 min, 1 h and 24 h at pH = 5.5. The experimental temperature was set to 32 °C in order to simulate real-life topical application conditions.

Figure 14B shows the CUR penetration profiles for CUR-NLCs and CUR-NLCs/gel. For the formulations, the initial CUR concentration in the donor compartment of the Franz cell was  $122 \pm 4$   $\mu\text{g/mL}$  and  $125 \pm 4$   $\mu\text{g/g}$ , respectively. CUR penetration in Strat-M<sup>®</sup> membranes was time-dependent for both CUR-NLCs and CUR-NLCs/gel, but higher for CUR-NLCs at all timepoints. CUR penetration expressed as % from the initial amount in the donor compartment was  $1.97 \pm 0.76\%$  and  $0.78 \pm 0.06\%$  for CUR-NLCs and CUR-NLCs/gel after 15 min, respectively, and  $22.06 \pm 1.59\%$  and  $5.07 \pm 0.53\%$  for CUR-NLCs

and CUR-NLCs/gel at 24 h, respectively. Table 5 shows the biopharmaceutical parameters of the amount of CUR entrapped per unit area ( $De$ ) and the CUR accumulation ( $Ac$ ) at 15 min and 24 h for CUR-NLCs and CUR-NLCs/gel.

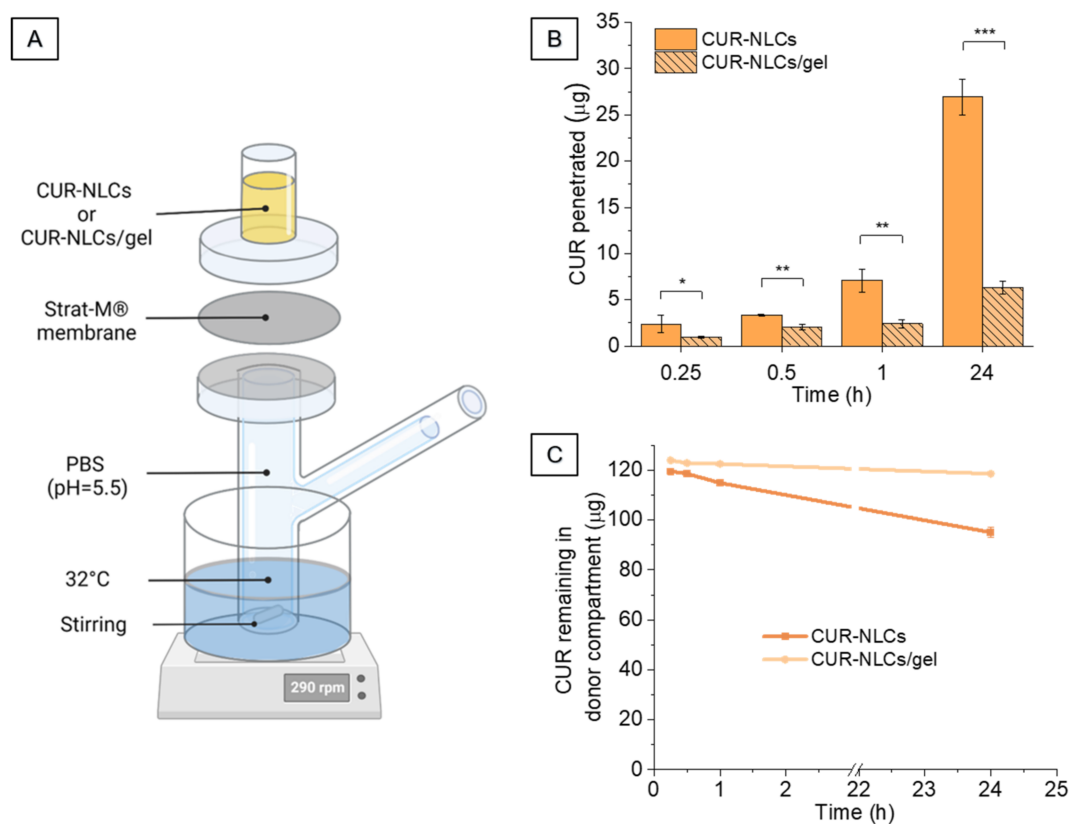


**Figure 14.** CUR penetration studies. (A) Experimental set-up of the Franz cell. (B) Penetration profiles of CUR into Strat-M<sup>®</sup> membranes from CUR-NLC suspensions and CUR-NLCs incorporated into gel. (C) Amount of CUR remaining in the donor compartment at the end of each timepoint. Asterisks denote statistically significant differences. Two-sample Student's *t*-test was carried out and statistically significant differences were identified when *p*-values were lower than 0.05 (\* *p* < 0.05), 0.01 (\*\* *p* < 0.01) or 0.001 (\*\*\*) *p* < 0.001). (Created with BioRender.com (accessed on 26 April 2022)).

**Table 5.** Biopharmaceutical parameters for CUR and CUR-NLCs/gel.

Time (h)	Sample	$Q_T$ (µg)	$De$ (µg/cm <sup>2</sup> )	$Ac$ (cm)
0.25	CUR-NLCs	2.40 ± 0.92	0.94 ± 0.36	0.0077 ± 0.0030
	CUR-NLCs/gel	0.97 ± 0.07	0.38 ± 0.03	0.0031 ± 0.0002
24	CUR-NLCs	26.92 ± 1.94	10.58 ± 0.76	0.0867 ± 0.0062
	CUR-NLCs/gel	6.33 ± 0.66	2.49 ± 0.26	0.0199 ± 0.0021

( $Q_T$ ) represents the amount of CUR penetrated into membranes. ( $De$ ) represents the amount of CUR entrapped per unit area, the area being available for penetration = 2.54 cm<sup>2</sup>. ( $Ac$ ) represents the CUR accumulation.

Neither CUR nor NLCs were able to permeate across the membranes. DLS measurements of receptor compartment samples over 24 h (data not shown) presented the same count rate as PBS, indicating that NLCs were retained by the membrane. It was not possible to quantify CUR in the receptor compartment by either HPLC or spectrophotometry; however, Figure 14C shows that the decrease in the amount of CUR in the donor compartment corresponds to the amount of CUR penetrated into the membrane (Figure 14B), demonstrating that CUR was not able to cross the membranes.

#### 4. Discussion

The combination of different carriers allows the attainment of advanced formulations. In this way, we proposed a biocompatible dual system composed of nanostructured lipid carriers (NLCs) and a Carbopol<sup>®</sup>-based hydrogel to locally deliver CUR in a controlled way while preserving its antioxidant properties.

NLCs were prepared by the hot homogenization method as described in previous works [35]. The lipids selected for NLC formulations are approved for pharmaceutical and/or cosmetic applications [42]. Precirol<sup>®</sup> ATO 5 (Glyceryl palmitostearate) was chosen as solid lipid (3% *w/w*) because of its relatively low melting point (~55 °C), which allows minimal exposure of CUR to heat while forming a homogeneous lipid melt. Labrafac<sup>®</sup> lipophile WL 1349 (Caprylic/capric triglyceride), also known as medium chain triglyceride (MTC), was used as liquid lipid (0.6 % *w/w*). As previously shown, the use of saturated lipids contributes to heat stability and limits the possibility of degradation [36]. Poloxamer 407 (3% *w/w*) and Tween<sup>®</sup> 80 (0.4% *w/w*) were used as surfactants in aqueous and lipid phases, respectively. The amounts used for preparing NLCs are in the range of those found in the literature for topical formulations (10–25% for Precirol<sup>®</sup> ATO 5 [43], 9% for Labrafac<sup>®</sup> lipophile WL 1349 (caprylic/capric triglyceride), 1.0–8.4% for Tween<sup>®</sup> 80 (<https://www.cir-safety.org> (accessed on 26 April 2022)) and 0.3–20% for Poloxamer 407) [44]. In these conditions, two populations of different sized negatively charged NLCs (P1, 70–90 nm and P2, 300–350 nm) were obtained. When results were expressed as % of number, P1 (70–90 nm) was the principal NLC peak found. Similar values have been reported by Tupal et al. (60–80 nm for mean size distribution and ~−11 mV for mean ZP) for NLCs containing similar lipid and surfactant compositions [45]. In addition, Singh et al. indicated a correlation between components of NLCs and their morphology, reporting a similar ovoid platelet shape and thickness values as our results [46]. CUR was successfully loaded into the optimized NLCs (DL% = 2.3%; EE% around 85%). These values are in accordance with those found in the literature (85–95% of EE% and around 3% of DL%) for CUR-NLCs [47–50]. A purification step was introduced to eliminate the “not particulate material” (low molecular weight substances or aggregates), which could interfere with the performance of the biological assays. After SEC column purification, CUR quantification in NLCs showed that the loaded CUR and EE% was halved. CUR concentrations in the prepared NLC aqueous suspensions before and after the SEC column were found to be higher (170-fold and 84-fold, respectively) than the solubility of CUR in water (0.005 mg/mL) reported by Chambure et al. An increase of the apparent water solubility of CUR in NLCs has already been reported by the same authors [31]. This could be partially explained by the selected lipid matrix, which has been shown to provide an environment favoring CUR incorporation into the NLCs and be capable of maximizing CUR solubility [51–53]. In addition, components (lipids and surfactants) and amounts used for NLC preparation are reported to stabilize nanoparticles and prevent them from agglomeration [54]. In particular, the use of non-ionic surfactants as poloxamer 407 and Tween<sup>®</sup> 80 has been associated with the formation of stable formulations through a steric repulsion phenomenon [55]. In this case, surfactant molecules present at the surface of nanoparticles could hinder the coalescence between them. This stability is supported by the homogeneous appearance of NLCs during the 45 days of observation after preparation.

In addition, our results show that NLCs preserve and improve the antioxidant activity of CUR (7-fold more after purification of the NLCs). This antioxidant activity enhancement by using NLCs has already been demonstrated in our previous work for other antioxidants (1.5-fold for astaxanthin-NLCs and 3-fold for supramolecular solvents-astaxanthin-NLCs) [33,36]. Concerning CUR, results are in accordance with those obtained by Ak and Gülçin [56], who tested the scavenging activity of various compounds, including CUR and  $\alpha$ -tocopherol by different methods and showed the same tendency.

The effect of CUR and CUR-NLCs on the viability and metabolism was evaluated in two representative skin cells, fibroblasts and keratinocytes. Culture media containing CUR induced a decrease of viability and metabolic activity of both cell types at concentrations



higher than 5  $\mu\text{M}$ . CUR-NLCs shown no toxic effects for concentrations up to 10  $\mu\text{M}$  for fibroblasts or keratinocytes. These results are in concordance with those described by Kloesch et al. [57], which showed a decrease in the toxicity of curcumin formulated in liposomes towards synovial fibroblasts and macrophages compared with non-encapsulated CUR. Furthermore, results suggested that the CUR-NLCs could preserve the metabolic activity of fibroblasts under stress conditions.

Additionally, in our work we observed that the treatment of both types of cells with CUR-NLCs leads to a reduction in their migration/proliferation ability after 24 h and to the keratinocytes morphology changes when compared with controls. In the same way, studies of CUR loaded on poly (lactic-co-glycolic acid)-nanoparticles showed strong inhibition of HaCaT human keratinocyte cell line activity [20]. Studies on mechanisms involved on the inhibition activity of CUR suggested a targeted action on the potassium channels of immune cells, which have a central role in chronic immune pathologies such as psoriasis [58]. For this reason, it has been suggested that CUR may be considered anti-psoriatic due to these anti-inflammatory effects [18,20].

All of the rheological results presented in this study may be explained by the nature of the interactions between NLCs and the microstructure of the Carbopol<sup>®</sup> gel. It could be hypothesized that the formulated NLCs are free to move together within the Carbopol<sup>®</sup> microparticles, which can reach diameters of 200  $\mu\text{m}$  after swelling and neutralization. In consequence, the measured viscosity is that of the surrounding media. By tracking fluorescent particle trajectories, Oppong et al. [59] suggested that when this happens two regions coexist. A region formed by the highly cross-linked cores of the microgels, and a more viscous region containing the polymer chains. If particles are found in the first region, they are trapped and will have limited movement. Taken with the experiments performed in this study, under flow conditions it is probable that they would interfere with the behavior of Carbopol<sup>®</sup> microgels. However, if they are found in the viscous region, the low density of entanglement in the polymer chains can form mesh sizes that will allow the particles to freely move. Thus, under flow conditions, the movement of the Carbopol<sup>®</sup> microgels are not hindered by the particles. Kowalczyk et al. [60] showed that an increase in the Carbopol<sup>®</sup> polymer concentration from 0.1% to 0.75% translated into a restriction in the movement of polystyrene particles of 510 nm diameter. This was due to the increased entanglement density at the viscous zones, which were responsible for diminishing the mesh size to below 500 nm. This might imply that the formulated NLCs could interfere with the flow behavior of the gel if higher Carbopol<sup>®</sup> concentrations are used.

In healthy skin (and Strat-M<sup>®</sup> membranes), the stratum corneum (or lipid coating for membranes) is the first barrier that NLCs would face in order to completely permeate. The fact that no NLC permeation was detected (thus, no risk of transdermal or systemic action in a real context) could be explained by their strong lipid nature, and thus strong affinity with the upper lipophilic layers in the Strat-M<sup>®</sup> membrane [61,62]. Our results are in line with those of Rapalli et al. [30], who did not detect CUR permeation after 24 h of contact of CUR-NLCs with goat ear skin. They demonstrated that CUR was preferentially accumulated in the stratum corneum rather than in the viable epidermis and dermis. Some other studies have concluded that NLCs could enhance CUR permeation through animal skin samples with reported flux between 0.092 and 2.45  $\mu\text{g}/\text{cm}^2/\text{h}$ . However, composition of the receptor media containing at least 20% *v/v* of EtOH [63,64] can change thinking of the possibility of disruption of the skin barrier function (by lipid disordering or lipid extraction) [65,66]. In any of these studies, identification of NLCs in the receptor compartment was performed. Thus, the curcumin detected could also be the result of the NLCs dissolution by EtOH and subsequent passage to the receptor chamber through the disordered/disintegrated lipid barrier of the skin. In both, CUR-NLCs and CUR-NLCs/gel, the increase of CUR penetration in the Strat-M<sup>®</sup> membrane with time could be explained by the ability of both formulations to increase the contact time with the membrane, which is important to have an effective transfer of NLCs. Lower CUR accumulation for CUR-NLCs/gel points to a decrease of NLC mobility due to the increase in the viscosity of the dispersant phase. This

seems to allow fewer CUR-NLCs to come into contact with the membrane, and thus, a decrease in their transfer into it.

## 5. Conclusions

In summary of this work, we designed and developed an innovative dual NLCs/hydrogel system able to deliver a natural bioactive compound of high interest, CUR. Antioxidant activity of CUR was preserved and enhanced when entrapped into the NLCs. Moreover, the non-cytotoxic CUR-NLCs presented a moderate anti-migration/proliferation effect onto dermal cell lines and allowed CUR penetration into a Strat-M<sup>®</sup> membrane. These results provide the proof of concept for considering this dual CUR delivery system as a potential candidate for specific skin applications and paves the way to offering new solutions to resolve challenging questions in existing critical dermal situations.

**Author Contributions:** Conceptualization, E.P., P.M., V.R.-R. and R.C.-J.; methodology, R.C.-J. and V.R.-R.; validation and writing—original draft preparation, R.C.-J., G.P.-D., V.G. and V.R.-R.; writing—review and editing, G.P.-D., E.P., P.M. and V.R.-R.; All authors have read and agreed to the published version of the manuscript.

**Funding:** This research was funded by CY Cergy Paris Université and Sapienza University of Rome.

**Institutional Review Board Statement:** Not applicable.

**Informed Consent Statement:** Not applicable.

**Data Availability Statement:** Not applicable.

**Acknowledgments:** Rosa Calderon-Jacinto thanks Doctoral School n<sup>o</sup> 417, Sciences and Engineering for the PhD grant and traveling funding. The authors are grateful to Gattefossé for the kind donation of Precirol<sup>®</sup> ATO 5 and Labrafac<sup>®</sup> lipophile WL 1349 and to Lubrizol for the kind donation of Carbopol<sup>®</sup> 980. Authors thank Ana-Andreea Arteni for TEM images from the platform of Cryo-EM of I2BC (supported by IBSA and by French Infrastructure for Integrated Structural Biology (FRISBI) (ANR-10-INBS-05). Authors are grateful to LPPI (EA2528) for the use of dynamic light scattering and Zetasizer Nano ZS equipment. Sapienza grant RM12117A81AEF242 is acknowledged by Pietro Matricardi.

**Conflicts of Interest:** The authors declare no conflict of interest.

## References

1. Seth, D.; Cheldize, K.; Brown, D.; Freeman, E.F. Global Burden of Skin Disease: Inequities and Innovations. *Curr. Dermatol. Rep.* **2017**, *6*, 204–210. [[CrossRef](#)] [[PubMed](#)]
2. Flohr, C.; Hay, R. Putting the Burden of Skin Diseases on the Global Map. *Br. J. Dermatol.* **2021**, *184*, 189–190. [[CrossRef](#)] [[PubMed](#)]
3. Guarneri, F.; Bertino, L.; Pioggia, G.; Casciaro, M.; Gangemi, S. Therapies with Antioxidant Potential in Psoriasis, Vitiligo, and Lichen Planus. *Antioxidants* **2021**, *10*, 1087. [[CrossRef](#)] [[PubMed](#)]
4. Bertino, L.; Guarneri, F.; Cannavò, S.P.; Casciaro, M.; Pioggia, G.; Gangemi, S. Oxidative Stress and Atopic Dermatitis. *Antioxidants* **2020**, *9*, 196. [[CrossRef](#)] [[PubMed](#)]
5. Działo, M.; Mierziak, J.; Korzun, U.; Preisner, M.; Szopa, J.; Kulma, A. The Potential of Plant Phenolics in Prevention and Therapy of Skin Disorders. *Int. J. Mol. Sci.* **2016**, *17*, 160. [[CrossRef](#)] [[PubMed](#)]
6. Davinelli, S.; Nielsen, M.E.; Scapagnini, G. Astaxanthin in Skin Health, Repair, and Disease: A Comprehensive Review. *Nutrients* **2018**, *10*, 522. [[CrossRef](#)] [[PubMed](#)]
7. Zhang, J.; Li, X.; Wei, J.; Chen, H.; Lu, Y.; Li, L.; Han, L.; Lu, C. Gallic Acid Inhibits the Expression of Keratin 16 and Keratin 17 through Nrf2 in Psoriasis-like Skin Disease. *Int. Immunopharmacol.* **2018**, *65*, 84–95. [[CrossRef](#)]
8. Thangapazham, R.L.; Sharad, S.; Maheshwari, R.K. Skin Regenerative Potentials of Curcumin. *Biofactors* **2013**, *39*, 141–149. [[CrossRef](#)]
9. Brown, M.B.; Martin, G.P.; Jones, S.A.; Akomeah, F.K. Dermal and Transdermal Drug Delivery Systems: Current and Future Prospects. *Drug Deliv.* **2006**, *13*, 175–187. [[CrossRef](#)]
10. Barbosa, N.S.; Kalaaji, A.N. CAM Use in Dermatology. Is There a Potential Role for Honey, Green Tea, and Vitamin C? *Complement. Ther. Clin. Pract.* **2014**, *20*, 11–15. [[CrossRef](#)]
11. Algahtani, M.S.; Ahmad, M.Z.; Nourein, I.H.; Ahmad, J. Co-Delivery of Imiquimod and Curcumin by Nanoemugel for Improved Topical Delivery and Reduced Psoriasis-Like Skin Lesions. *Biomolecules* **2020**, *10*, 968. [[CrossRef](#)] [[PubMed](#)]
12. Jain, A.; Doppalapudi, S.; Domb, A.J.; Khan, W. Tacrolimus and Curcumin Co-Loaded Liposphere Gel: Synergistic Combination towards Management of Psoriasis. *J. Control. Release* **2016**, *243*, 132–145. [[CrossRef](#)] [[PubMed](#)]

13. Gupta, S.C.; Prasad, S.; Kim, J.H.; Patchva, S.; Webb, L.J.; Priyadarsini, I.K.; Aggarwal, B.B. Multitargeting by Curcumin as Revealed by Molecular Interaction Studies. *Nat. Prod. Rep.* **2011**, *28*, 1937–1955. [[CrossRef](#)] [[PubMed](#)]
14. Priyadarsini, K.I. The Chemistry of Curcumin: From Extraction to Therapeutic Agent. *Molecules* **2014**, *19*, 20091. [[CrossRef](#)]
15. Barzegar, A.; Moosavi-Movahedi, A.A. Intracellular ROS Protection Efficiency and Free Radical-Scavenging Activity of Curcumin. *PLoS ONE* **2011**, *6*, e26012. [[CrossRef](#)]
16. Shehzad, A.; Lee, Y.S. Molecular Mechanisms of Curcumin Action: Signal Transduction. *BioFactors* **2013**, *39*, 27–36. [[CrossRef](#)]
17. He, Y.; Yue, Y.; Zheng, X.; Zhang, K.; Chen, S.; Du, Z. Curcumin, Inflammation, and Chronic Diseases: How Are They Linked? *Molecules* **2015**, *20*, 9183–9213. [[CrossRef](#)]
18. Panahi, Y.; Fazlollahzadeh, O.; Atkin, S.L.; Majeed, M.; Butler, A.E.; Johnston, T.P.; Sahebkar, A. Evidence of Curcumin and Curcumin Analogue Effects in Skin Diseases: A Narrative Review. *J. Cell Physiol.* **2019**, *234*, 1165–1178. [[CrossRef](#)]
19. Gupta, S.C.; Patchva, S.; Aggarwal, B.B. Therapeutic Roles of Curcumin: Lessons Learned from Clinical Trials. *AAPS J.* **2013**, *15*, 195–218. [[CrossRef](#)]
20. Sun, L.; Liu, Z.; Wang, L.; Cun, D.; Tong, H.H.Y.; Yan, R.; Chen, X.; Wang, R.; Zheng, Y. Enhanced Topical Penetration, System Exposure and Anti-Psoriasis Activity of Two Particle-Sized, Curcumin-Loaded PLGA Nanoparticles in Hydrogel. *J. Control. Release* **2017**, *254*, 44–54. [[CrossRef](#)]
21. Fereydouni, N.; Darroudi, M.; Movaffagh, J.; Shahroodi, A.; Butler, A.E.; Ganjali, S.; Sahebkar, A. Curcumin Nanofibers for the Purpose of Wound Healing. *J. Cell Physiol.* **2019**, *234*, 5537–5554. [[CrossRef](#)] [[PubMed](#)]
22. Bhatia, M.; Saini, M. Formulation and Evaluation of Curcumin Microsponges for Oral and Topical Drug Delivery. *Prog. Biomater.* **2018**, *7*, 239–248. [[CrossRef](#)] [[PubMed](#)]
23. Jeengar, M.K.; Rompicharla, S.V.K.; Shrivastava, S.; Chella, N.; Shastri, N.R.; Naidu, V.G.M.; Sistla, R. Emu Oil Based Nano-Emulgel for Topical Delivery of Curcumin. *Int. J. Pharm.* **2016**, *506*, 222–236. [[CrossRef](#)] [[PubMed](#)]
24. Terzopoulou, Z.; Michopoulou, A.; Palamidi, A.; Koliakou, E.; Bikiaris, D. Preparation and Evaluation of Collagen-Based Patches as Curcumin Carriers. *Polymers* **2020**, *12*, 2393. [[CrossRef](#)] [[PubMed](#)]
25. Rapalli, V.K.; Kaul, V.; Waghule, T.; Gorantla, S.; Sharma, S.; Roy, A.; Dubey, S.K.; Singhvi, G. Curcumin Loaded Nanostructured Lipid Carriers for Enhanced Skin Retained Topical Delivery: Optimization, Scale-up, in-Vitro Characterization and Assessment of Ex-Vivo Skin Deposition. *Eur. J. Pharm. Sci.* **2020**, *152*, 105438. [[CrossRef](#)] [[PubMed](#)]
26. Agrawal, Y.; Petkar, K.C.; Sawant, K.K. Development, Evaluation and Clinical Studies of Acitretin Loaded Nanostructured Lipid Carriers for Topical Treatment of Psoriasis. *Int. J. Pharm.* **2010**, *401*, 93–102. [[CrossRef](#)] [[PubMed](#)]
27. Murgia, D.; Angellotti, G.; Conigliaro, A.; Carfi Pavia, F.; D'Agostino, F.; Contardi, M.; Mauceri, R.; Alessandro, R.; Campisi, G.; De Caro, V. Development of a Multifunctional Bioerodible Nanocomposite Containing Metronidazole and Curcumin to Apply on L-PRF Clot to Promote Tissue Regeneration in Dentistry. *Biomedicines* **2020**, *8*, 425. [[CrossRef](#)]
28. Rojas, E.C.; Sahiner, N.; Lawson, L.B.; John, V.T.; Papadopoulos, K.D. Controlled Release from a Nanocarrier Entrapped within a Microcarrier. *J. Colloid Interface Sci.* **2006**, *301*, 617–623. [[CrossRef](#)]
29. Senna, J.P.; Barradas, T.N.; Cardoso, S.; Castiglione, T.C.; Serpe, M.J.; de Silva, K.G.H.E.; Mansur, C.R.E. Dual Alginate-Lipid Nanocarriers as Oral Delivery Systems for Amphotericin B. *Colloids Surf. B Biointerfaces* **2018**, *166*, 187–194. [[CrossRef](#)]
30. Sharma, G.; Thakur, K.; Raza, K.; Singh, B.; Katara, O.P. Nanostructured Lipid Carriers: A New Paradigm in Topical Delivery for Dermal and Transdermal Applications. *Crit. Rev. Ther. Drug Carr. Syst.* **2017**, *34*, 355–386. [[CrossRef](#)]
31. Chانبuree, S.; Tiyaboonchai, W. Enhanced Intestinal Absorption of Curcumin in Caco-2 Cell Monolayer Using Mucoadhesive Nanostructured Lipid Carriers. *J. Biomed. Mater. Res. B Appl. Biomater.* **2018**, *106*, 734–741. [[CrossRef](#)] [[PubMed](#)]
32. Monice, M.F. *Amended Safety Assessment of Acrylates Copolymers as Used in Cosmetics*; Cosmetic Ingredient Review: Washington, DC, USA, 2018.
33. Singh, V.K.; Anis, A.; Banerjee, I.; Pramanik, K.; Bhattacharya, M.K.; Pal, K. Preparation and Characterization of Novel Carbopol Based Bigels for Topical Delivery of Metronidazole for the Treatment of Bacterial Vaginosis. *Mater. Sci. Eng. C* **2014**, *44*, 151–158. [[CrossRef](#)] [[PubMed](#)]
34. Tang, C.; Yin, L.; Yu, J.; Yin, C.; Pei, Y. Swelling Behavior and Biocompatibility of Carbopol-Containing Superporous Hydrogel Composites. *J. Appl. Polym. Sci.* **2007**, *104*, 2785–2791. [[CrossRef](#)]
35. Rodriguez-Ruiz, V.; Salatti-Dorado, Á.J.; Barzegari, A.; Nicolas-Boluda, A.; Houaoui, A.; Caballo, C.; Caballero-Casero, N.; Sicilia, D.; Bastias Venegas, J.; Pauthe, E.; et al. Astaxanthin-Loaded Nanostructured Lipid Carriers for Preservation of Antioxidant Activity. *Molecules* **2018**, *23*, 2601. [[CrossRef](#)]
36. Salatti-Dorado, J.; Garcia-Gomez, D.; Rodriguez-Ruiz, V.; Gueguen, V.; Pavon-Djavid, G.; Rubio, S. Multifunctional Green Supramolecular Solvents for Cost-Effective Production of Highly Stable Astaxanthin-Rich Formulations from *Haematococcus Pluvialis*. *Food Chem.* **2019**, *279*, 294–302. [[CrossRef](#)]
37. Yan, T.; Zhang, J.; Tang, D.; Zhang, X.; Jiang, X.; Zhao, L.; Zhang, Q.; Zhang, D.; Huang, Y. Hypoxia Regulates MTORC1-Mediated Keratinocyte Motility and Migration via the AMPK Pathway. *PLoS ONE* **2017**, *12*, e0169155. [[CrossRef](#)]
38. Flaten, G.E.; Palac, Z.; Engesland, A.; Filipović-Grčić, J.; Vanić, Ž.; Škalko-Basnet, N. In Vitro Skin Models as a Tool in Optimization of Drug Formulation. *Eur. J. Pharm. Sci.* **2015**, *75*, 10–24. [[CrossRef](#)]
39. Uchida, T.; Kadhum, W.R.; Kanai, S.; Todo, H.; Oshizaka, T.; Sugibayashi, K. Prediction of Skin Permeation by Chemical Compounds Using the Artificial Membrane, Strat-M<sup>TM</sup>. *Eur. J. Pharm. Sci.* **2015**, *67*, 113–118. [[CrossRef](#)]

40. Di Prima, G.; Angellotti, G.; Scarpaci, A.G.; Murgia, D.; D'agostino, F.; Campisi, G.; De Caro, V. Improvement of Resveratrol Permeation through Sublingual Mucosa: Chemical Permeation Enhancers versus Spray Drying Technique to Obtain Fast-Disintegrating Sublingual Mini-Tablets. *Pharmaceutics* **2021**, *13*, 1370. [[CrossRef](#)]
41. Stockert, J.C.; Horobin, R.W.; Colombo, L.L.; Blázquez-Castro, A. Tetrazolium Salts and Formazan Products in Cell Biology: Viability Assessment, Fluorescence Imaging, and Labeling Perspectives. *Acta Histochem.* **2018**, *120*, 159–167. [[CrossRef](#)]
42. Belouqui, A.; Solinís, M.Á.; Rodríguez-Gascón, A.; Almeida, A.J.; Préat, V. Nanostructured Lipid Carriers: Promising Drug Delivery Systems for Future Clinics. *Nanomedicine* **2016**, *12*, 143–161. [[CrossRef](#)] [[PubMed](#)]
43. Rowe, R. *Handbook of Pharmaceutical Excipients*, 6th ed.; RPS Publishing: Washington, DC, USA, 2009.
44. Singh-Joy, S.D.; McLain, V.C. Safety Assessment of Poloxamers 101, 105, 108, 122, 123, 124, 181, 182, 183, 184, 185, 188, 212, 215, 217, 231, 234, 235, 237, 238, 282, 284, 288, 331, 333, 334, 335, 338, 401, 402, 403, and 407, Poloxamer 105 Benzoate, and Poloxamer 182 Dibenzoate as Used in Cosmetics. *Int. J. Toxicol.* **2008**, *27* (Suppl. S2), 93–128. [[CrossRef](#)] [[PubMed](#)]
45. Tupal, A.; Sabzichi, M.; Bazzaz, R.; Fathi Maroufi, N.; Mohammadi, M.; Pirouzpanah, S.M.; Ramezani, F. Application of  $\alpha$ -Tocotrienol-Loaded Biocompatible Precirol in Attenuation of Doxorubicin Dose-Dependent Behavior in HUH-7 Hepatocarcinoma Cell Line. *Nutr. Cancer* **2020**, *72*, 653–661. [[CrossRef](#)] [[PubMed](#)]
46. Hallan, S.S.; Sguizzato, M.; Esposito, E.; Cortesi, R. Challenges in the Physical Characterization of Lipid Nanoparticles. *Pharmaceutics* **2021**, *13*, 549. [[CrossRef](#)]
47. Li, J.; Liu, D.; Tan, G.; Zhao, Z.; Yang, X.; Pan, W. A Comparative Study on the Efficiency of Chitosan-N-Acetylcysteine, Chitosan Oligosaccharides or Carboxymethyl Chitosan Surface Modified Nanostructured Lipid Carrier for Ophthalmic Delivery of Curcumin. *Carbohydr. Polym.* **2016**, *146*, 435–444. [[CrossRef](#)]
48. Chen, P.; Zhang, H.; Cheng, S.; Zhai, G.; Shen, C. Development of Curcumin Loaded Nanostructured Lipid Carrier Based Thermosensitive in Situ Gel for Dermal Delivery. *Colloids Surf. A Physicochem. Eng. Asp.* **2016**, *506*, 356–362. [[CrossRef](#)]
49. Meng, F.; Asghar, S.; Xu, Y.; Wang, J.; Jin, X.; Wang, Z.; Wang, J.; Ping, Q.; Zhou, J.; Xiao, Y. Design and Evaluation of Lipoprotein Resembling Curcumin-Encapsulated Protein-Free Nanostructured Lipid Carrier for Brain Targeting. *Int. J. Pharm.* **2016**, *506*, 46–56. [[CrossRef](#)]
50. Kesharwani, P.; Jain, A.; Srivastava, A.K.; Keshari, M.K. Systematic Development and Characterization of Curcumin-Loaded Nanogel for Topical Application. *Drug Dev. Ind. Pharm.* **2020**, *46*, 1443–1457. [[CrossRef](#)]
51. Araiza-Calahorra, A.; Akhtar, M.; Sarkar, A. Recent Advances in Emulsion-Based Delivery Approaches for Curcumin: From Encapsulation to Bioaccessibility. *Trends Food Sci. Technol.* **2018**, *71*, 155–169. [[CrossRef](#)]
52. Ma, P.; Zeng, Q.; Tai, K.; He, X.; Yao, Y.; Hong, X.; Yuan, F. Preparation of Curcumin-Loaded Emulsion Using High Pressure Homogenization: Impact of Oil Phase and Concentration on Physicochemical Stability. *LWT* **2017**, *84*, 34–46. [[CrossRef](#)]
53. Kasongo, K.W.; Pardeike, J.; Müller, R.H.; Walker, R.B. Selection and Characterization of Suitable Lipid Excipients for Use in the Manufacture of Didanosine-Loaded Solid Lipid Nanoparticles and Nanostructured Lipid Carriers. *J. Pharm. Sci.* **2011**, *100*, 5185–5196. [[CrossRef](#)] [[PubMed](#)]
54. Mohammadi, M.; Pezeshki, A.; Mesgari Abbasi, M.; Ghanbarzadeh, B.; Hamishehkar, H. Vitamin D(3)-Loaded Nanostructured Lipid Carriers as a Potential Approach for Fortifying Food Beverages; in Vitro and in Vivo Evaluation. *Adv. Pharm. Bull.* **2017**, *7*, 61–71. [[CrossRef](#)] [[PubMed](#)]
55. Wu, L.; Zhang, J.; Watanabe, W. Physical and Chemical Stability of Drug Nanoparticles. *Adv. Drug Deliv. Rev.* **2011**, *63*, 456–469. [[CrossRef](#)] [[PubMed](#)]
56. Ak, T.; Gülçin, I. Antioxidant and Radical Scavenging Properties of Curcumin. *Chem. Biol. Interact.* **2008**, *174*, 27–37. [[CrossRef](#)] [[PubMed](#)]
57. Kloesch, B.; Gober, L.; Loebisch, S.; Vcelar, B.; Helson, L.; Steiner, G. In Vitro Study of a Liposomal Curcumin Formulation (Lipocurc<sup>TM</sup>): Toxicity and Biological Activity in Synovial Fibroblasts and Macrophages. *In Vivo* **2016**, *30*, 413–419.
58. Kang, D.; Li, B.; Luo, L.; Jiang, W.; Lu, Q.; Rong, M.; Lai, R. Curcumin Shows Excellent Therapeutic Effect on Psoriasis in Mouse Model. *Biochimie* **2016**, *123*, 73–80. [[CrossRef](#)]
59. Oppong, F.K.; Rubatat, L.; Frisken, B.J.; Bailey, A.E.; de Bruyn, J.R. Microrheology and Structure of a Yield-Stress Polymer Gel. *Phys. Rev. E* **2006**, *73*, 041405. [[CrossRef](#)]
60. Kowalczyk, A.; Oelschlaeger, C.; Willenbacher, N. Visualization of Micro-Scale Inhomogeneities in Acrylic Thickener Solutions: A Multiple Particle Tracking Study. *Polymer* **2015**, *58*, 170–179. [[CrossRef](#)]
61. Müller, R.H.; Petersen, R.D.; Hommoss, A.; Pardeike, J. Nanostructured Lipid Carriers (NLC) in Cosmetic Dermal Products. *Adv. Drug Deliv. Rev.* **2007**, *59*, 522–530. [[CrossRef](#)]
62. Müller, R.H.; Radtke, M.; Wissing, S.A. Solid Lipid Nanoparticles (SLN) and Nanostructured Lipid Carriers (NLC) in Cosmetic and Dermatological Preparations. *Adv. Drug Deliv. Rev.* **2002**, *54*, S131–S155. [[CrossRef](#)]
63. Espinosa-Olivares, M.A.; Delgado-Buenrostro, N.L.; Chirino, Y.I.; Trejo-Márquez, M.A.; Pascual-Bustamante, S.; Ganem-Rondero, A. Nanostructured Lipid Carriers Loaded with Curcuminoids: Physicochemical Characterization, In Vitro Release, Ex Vivo Skin Penetration, Stability and Antioxidant Activity. *Eur. J. Pharm. Sci.* **2020**, *155*, 105533. [[CrossRef](#)] [[PubMed](#)]
64. Riaz, A.; Ahmed, N.; Khan, M.I.; Haq, I.; Rehman, A.; Khan, G.M. Formulation of Topical NLCs to Target Macrophages for Cutaneous Leishmaniasis. *J. Drug Deliv. Sci. Technol.* **2019**, *54*, 101232. [[CrossRef](#)]

- 
65. Bommannan, D.; Potts, R.O.; Guy, R.H. Examination of the Effect of Ethanol on Human Stratum Corneum In Vivo Using Infrared Spectroscopy. *J. Control. Release* **1991**, *16*, 299–304. [[CrossRef](#)]
  66. Kwak, S.; Brief, E.; Langlais, D.; Kitson, N.; Lafleur, M.; Thewalt, J. Ethanol Perturbs Lipid Organization in Models of Stratum Corneum Membranes: An Investigation Combining Differential Scanning Calorimetry, Infrared and <sup>2</sup>H NMR Spectroscopy. *Biochim. Et Biophys. Acta (BBA) Biomembr.* **2012**, *1818*, 1410–1419. [[CrossRef](#)]



## **Development of a multiscale composite platform for delivery of natural active compounds: applications of curcumin toward skin**

Excess of reactive oxygen species produces oxidative stress in cells and is related to inflammatory process present in different skin conditions such as psoriasis, dermatitis or abnormal wound healing. Curcumin (CUR), a natural active molecule, has demonstrated to hold good antioxidant and anti-inflammatory properties as well as the ability to activate cytoprotective pathways in dermal cells. However, its topical administration is hindered by its low water solubility, as well as low stability in presence of heat and light. In this doctoral thesis, a multiscale composite delivery platform: a Carbopol® hydrogel matrix containing CUR-loaded nanostructured lipid carriers (CUR-NLCs), was developed. The system was evaluated in order to explore its potential for topical dermal uses.

We formulated stable CUR-NLCs and demonstrated that CUR antioxidant properties were preserved and even enhanced. Viability assays on fibroblasts and keratinocytes indicate that CUR-NLCs are non-cytotoxic for concentrations up to 10  $\mu$ M, even in cells undergoing oxidative stress and that they exhibit a slight-moderate anti-migration/proliferation effect. Then, CUR-NLCs were incorporated in a Carbopol® hydrogel (CUR-NLCs/gel) without disturbing its mechanical properties. CUR-NLCs and CUR-NLCs/gel proved to be able to differently contribute to CUR accumulation into synthetic membranes mimicking human skin. This manuscript provides evidence about the potential of the CUR-NLCs/gel system as a promising candidate for adjuvant therapy in topical skin applications.

Keywords: antioxidants, curcumin, lipid nanoparticles, topical dermal drug delivery, oxidative stress.

## **Développement d'une plateforme composite et multi-échelle pour la délivrance de composés actifs d'origine naturelle : application de la curcumine vers la peau**

L'excès d'espèces réactives de l'oxygène induit un état de stress oxydatif dans les cellules et est lié au processus inflammatoire présent dans différentes affections cutanées telles que le psoriasis, la dermatite ou encore pendant la cicatrisation anormale des plaies. La curcumine (CUR), une molécule active naturelle, a démontré de bonnes propriétés antioxydantes et anti-inflammatoires ainsi que la capacité d'activer les voies cytoprotectrices dans les cellules dermiques. Cependant, son administration topique est gênée par sa faible solubilité dans l'eau, ainsi que par sa faible stabilité en présence de la chaleur et de la lumière.

Dans cette thèse de doctorat, une plateforme d'administration composite et multi-échelle : une matrice hydrogel de Carbopol® contenant des transporteurs lipidiques nanostructurés chargés en CUR (CUR-NLCs), a été développée. Le système a été évalué afin d'explorer son potentiel pour des utilisations topiques cutanées.

Nous avons formulé des CUR-NLCs stables et démontré que les propriétés antioxydantes de la CUR étaient préservées et même améliorées. Des tests de viabilité sur des fibroblastes et des kératinocytes indiquent que les CUR-NLCs sont non cytotoxiques pour des concentrations allant jusqu'à 10  $\mu$ M, même dans des cellules sous stress oxydatif et qu'elles présentent un effet anti-migration/prolifération léger. Ensuite, les CUR-NLCs ont été incorporées dans un hydrogel de Carbopol® (CUR-NLCs/gel) sans perturber ses propriétés mécaniques. Les CUR-NLCs et les CUR-NLCs/gel se sont avérés capables de contribuer différemment à l'accumulation de CUR dans des membranes synthétiques imitant la peau humaine.

Ce manuscrit fournit des preuves sur le potentiel du système CUR-NLCs/gel en tant que candidat prometteur pour le traitement adjuvant dans les applications topiques cutanées.

Mots clés : antioxydants, curcumine, nanoparticules lipidiques, systèmes de délivrance topiques, stress oxydatif.